Electrokinetic Transport of Cr^{VI} and Integration with Zero-Valent Iron Nanoparticle and Microbial Fuel Cell Technologies for Aquifer Remediation

A Dissertation Presented to the
FACULTY OF THE USC GRADUATE SCHOOL
UNIVERSITY OF SOUTHERN CALIFORNIA
In Partial Fulfillment of the
Requirements for the Degree
DOCTOR OF PHILOSOPHY
(ENVIRONMENTAL ENGINEERING)

By
Ryan Thacher
August 2013

Acknowledgements

I remember receiving the acceptance letter from the USC School of Civil and Environmental Engineering in the spring of 2008, and being thrilled at the opportunity to study at a world-renowned university. At the time I was living in Santa Barbara, a city that loves Los Angeles sports teams yet has an extreme distaste for the City of Los Angeles. I remember telling friends, "a year-and-a-half Master's program in Los Angeles will fly by," and thinking I'd be back up north in the blink of an eye. Well, here we are five years later. Los Angeles gave me more than I could have asked for in terms of education, fun, friendships, and, of course, surf.

First and foremost I need to thank my advisor, Professor Massoud Pirbazari, who constantly inspired, motivated, and supported me throughout this journey. His novel ideas and unique approach to the field of environmental engineering were instrumental in my academic and professional development, and changed the way I observe the world. Additionally, I would like to thank Dr. Varadarajan Ravindran, a fellow Gaucho and Chemical Engineer, for generously sharing the contents of his amazing mind with me.

I would also like to extend my gratitude to the members of my defense committee, Professor Patrick Lynett, Professor Surya Prakash, and Professor Katherine Shing for their helpful suggestions and encouragement. Additionally, I would like to acknowledge the National Science Foundation for the financial support that partially funded this research (NSF grant No. 0826198).

I owe much of my success to countless friends and colleagues I have made throughout my time at USC, and they deserve many thanks as well. Dr. Lewis Hsu played an essential role in my development as a colleague and a friend. Lewis put his reputation on the line for me many times, for which I will always be grateful. I would also like to extend my appreciation to the undergraduate researchers I had the pleasure of mentoring over the years, namely Aditi Yokota-Joshi, Charlotte Chan, and Hannah Gray.

Lastly I extend the biggest thank you to my mom Susan, my dad Tom, and my brother Tyler for the unconditional support, and always being my biggest fans. I could write another dissertation about all they've done for me, yet it would still only scratch the surface.

Table of Contents

List of Tables

List of Figures

Abstract

Hexavalent chromium (Cr^{VI}) is a carcinogenic heavy metal that is a product of many industrial processes. In it's hexavalent state, chromium exists in the anionic form of chromate and dichromate, which are both stable and highly soluble in water. Once introduced to the environment, Cr^{VI} species can percolate through soils and reach the water table. From here Cr^{VI} can spread quickly throughout an aquifer as it moves naturally with the groundwater flow. Remediation of aquifers contaminated with Cr^{VI} is typically energy intensive, a slow process, and can be highly invasive. The study presented here investigates alternative remediation options for Cr^{VI} through the integration of effective contaminant transport and novel treatment technologies. It was determined that contaminant transport by electrokinetic technology can be used in conjunction with zero-valent iron nanoparticles (nZVI) for Cr^{VI} reduction, and also integrated with microbial reduction in a microbial fuel cell (MFC). NZVI have been proposed as an economic and effective *in situ* remediation technology, capable of rapidly reducing Cr^{VI} species to insoluble and non-toxic Cr^{III} species. MFC technology is capable of reducing Cr^{VI} through microbiological mechanisms, and is viewed as a potential renewable energy resource. Both of these technologies are environmentally conscious alternatives to many conventional remediation approaches.

Electrokinetic contaminant transport has been proposed to be effective for contaminated groundwater in soils of low hydraulic conductivity such as clay. Thus, initial electrokinetic investigations were performed using two different clay soils, EPK kaolin and kaolinite. Bench-scale isotherm and rate studies were performed to characterize the interaction between the two clay soils and Cr^{VI}. It was found that EPK kaolin had an extremely high capacity for reducing Cr^{VI} through chemical reduction and physical adsorption, resulting from natural organic matter (NOM) bound to the EPK kaolin particle surface. Comparisons between the soils indicated the importance of NOM on the fate and transport of Cr^{VI} in aquifers, and also highlighted the significance of surface bound NOM relative to dissolved NOM in the water matrix. Surface bound NOM was shown to rapidly interact with Cr^{VI} driving its reduction to Cr^{III} species, while dissolved NOM and Cr^{VI} formed complexes over relatively long time periods. Electrokinetic column studies with the two clay soils reflected these initial findings, and also highlighted transport inhibition due to pH gradient formation, as described in literature.

To circumvent inherent problems associated with electrokinetic transport through clay soils, a sandy soil was used for the continuous-flow column studies. This work focused on the integration of electrokinetic transport with nZVI addition for Cr^{VI} remediation, and evaluated the effects of NOM. Since transport of nZVI through subsurface formations has been shown to be difficult, it was decided that using electrokinetic transport to move contaminants to the point of nZVI injection could be effective. A series of adsorption/reduction studies and rate experiments determined the reduction capacity of nZVI to be nearly two times greater under anoxic conditions in comparison to oxygenated water containing naturally occurring groundwater constituents such as humic acid and calcium ion, and indicated rapid reaction kinetics. Electrokinetic transport experiments with nZVI injection showed that transporting Cr^{VI} to the site of nZVI injection was beneficial in terms of reducing the amount of nZVI required for treatment, and overall treatment time. Additionally, the continuous-flow system eliminated pH gradient formation, allowing for continual Cr^{VI} transport. The presence of humic acid in these studies did not effect electrokinetic transport of Cr^{VI}, however did lower its removal by nZVI. In a pilot- or full-scale nZVI treatment system, it seems appropriate to place a number of nZVI injection wells at strategic locations in the aquifer to optimize treatment, however for the sake of simplicity and ease of evaluation only one injection location was used in the experimental studies.

An alternate treatment approach using biological systems was evaluated following the work with nZVI, as bacteria have been shown to effectively reduce Cr^{VI}. This was conducted through the integration of electrokinetic transport with microbial treatment in an MFC - a green alternative to traditional pump-and-treat remediation systems. In a continuous-flow system, electrokinetic transport of Cr^{VI} was found to reduce the treatment time for a given volume of contaminated water, and improved power output from the MFC. The MFC proved to be a sustainable treatment approach as well, reducing an influent contaminant stream to non-detectable Cr^{VI} concentrations for 12 days. Introduction of humic acid to the system to represent NOM also resulted in an improvement in the reduction of Cr^{VI}. Humic acid extended the breakthrough time for Cr^{VI} by almost 2 days in the sustainability studies relative to a system without humic acid. In the MFC systems, humic acids were shown to serve the role of an electron shuttle, a terminal electron acceptor, and reduced the bioavailability of soluble Cr^{III} species, which are toxic to the microorganisms by complexation reactions.

Similar to the continuous-flow system with nZVI injection, the MFC-electrokinetic system did not experience pH gradient formation, resulting in effective Cr^{VI} transport for the duration of the study. Microbial reduction was effective in these studies, however a single culture of bacteria cannot reduce Cr^{VI} indefinitely. The toxic nature of Cr^{VI} and soluble Cr^{III} species to microorganisms is undeniable, however bacteria can be prepared as needed cost effectively. In the context of an MFC, as performance deterioration is observed one would simply replace the electrodes and introduce a new batch of bacteria to the cell, a renewable resource for remediation.

The MFC studies inspired an interest in *in situ* biological reduction of Cr^{VI} in the context of microbial injection. Injecting microbes specific for a remediation task directly to a contamination plume is a remediation approach currently practiced. A column charged with *Shewanella oneidensis* MR-1 biofilm growth in sand media to simulate *in situ* biological treatment (biotic column) was exposed to a continuous-flow Cr^{VI} solution with and without humic acid, and experimental breakthrough curves were developed. A similar experiment was conducted for an iron oxide coated sand (IOCS) media to simulate a permeable reactive barrier (abiotic column), another groundwater treatment approach currently utilized. Two separate predictive models were employed to investigate Cr^{VI} reduction by i) microbial biofilm (biotic column), and ii) IOCS adsorptive layer (abiotic column). The predictive models were shown to accurately describe the experimental breakthrough data. A series of sensitivity analyses provided further insight into the dynamics of both column systems, highlighted the degree of influence of each parameter to system dynamics. The model was run for the IOCS system using input flow rates comparable to those observed in groundwater systems to simulate the performance of IOCS as a permeable reactive barrier. The results reflected the high adsorptive capacity of IOCS, and highlighted the utility of such predictive models for design purposes.

Chapter 1 : Introduction

The decline of natural resources around the world is no longer an issue of debate, but that of fact. While the abundance and availability of natural resources declines at an alarming rate, consumption continues to increase. The fundamental requirement for consumption of fresh water is no exception to this paradox. Water is the most basic and yet essential natural resource on earth. It's an obvious requirement for sustaining life on the planet, but also an essential component of most industrial processes for the production of nearly everything we use, see, and touch. In the United States, the average water use per capita is on the order of 150 gallons per day. Many European countries including Germany, France, and the UK use approximately half of that quantity. Shifting focus to less developed countries, the water use per capita drops to just a couple gallons a day or less.[1] Most parts of the world are realizing shortages of clean, fresh water due to famine, disease, or cost. In the United States, we are momentarily removed from the bleak future that the majority of the world is facing. Our naivety to this issue reaches to the extent that the general public continues to consume water at an increasing rate.

Of the total water consumed in the United States, including that used domestically and for industrial purposes alike, nearly 50% comes from natural underground reserves known as aquifers.[2] The depth of aquifers and the groundwater they carry can range from the earth's surface, seen in the form of streams and springs, to over one thousand feet below the surface. However most groundwater used for domestic and industrial use is pumped from aquifers on the order of 100 feet deep. Aquifers are susceptible to contamination just as any other water source, as contaminants discharged to the ground above them can percolate through soils with water flow. While EPA regulations have curbed a significant amount of new contamination from discharge events, groundwater sources are still threatened by existing sources of contamination. In the United States, the EPA estimates there are 1.1 million federally regulated storage tanks buried underground that can corrode, crack, and develop leaks. Additionally, there are over 20-thousand known abandoned uncontrolled hazardous waste sites that threaten the underlying waters.[3] Once a contaminant is introduced to an aquifer, it can be very difficult to remove.

One of the EPA's target groundwater contaminants is hexavalent chromium (Cr^{VI}) due to its high toxicity and prevalence in natural waters. It is a known carcinogen, and can cause a variety of health issues from acute exposure, from non-allergenic skin irritation to chrome ulcers. A product of many anthropogenic activities such as chrome plating, leather tanning, stainless steel production, wood preservation, and widespread use as a corrosion inhibitor, Cr^{VI} has found its way into groundwater and soils around the world. Due to a series of potential interactions with natural constituents found in groundwater, remediation of Cr^{VI} can be challenging. Treatment is often limited to excavation or *ex situ* chemical or biological treatment, which is generally done through reduction of Cr^{VI} species to their most stable, non-toxic, and sparingly soluble Cr^{III} species.[4] However the pump-and-treat method is ineffective in soils of low hydraulic conductivity such as clay due to the difficulty and energy consumption in pumping through tightly packed soil. Additionally, treatment becomes increasingly difficult in aquifers that are difficult to reach such as below developed land. In situations such as these, it has been proposed that electrokinetic remediation can be effective in transporting contaminants by use of an applied electric field. With this technology, any contaminant in ionic form will migrate through groundwater independent of bulk fluid movement, effectively concentrating the contaminants in an optimal location dictated by the architecture of the treatment system.

Electrokinetic remediation has been explored as a means to transport Cr^{VI} and other heavy metals through aquifers.[5,6] The transport mechanisms include electromigration (the movement of ions), electroosmosis (the motion of liquid), and electrophoresis (the movement of particles). Strategic placement of electrodes surrounding a contaminated zone with low voltage application facilitates transport of both ions and particulate matter through aquifers. Commercial processes have been developed and applied in field tests to determine its effectiveness as an *in situ* remediation technique.[7] The ability of this technique to be applied over heterogeneous subsurface components and as a non-invasive *in situ* method is a promising aspect of this technology. It must be noted that known difficulties arise during electrokinetic treatment, which must be addressed during the design of an electrokinetic remediation system. These issues are derived from a pH change that evolves as a result of electrolysis reactions at the electrodes. Acid and base fronts form at each electrode and migrate under the applied electric potential.[5] These create local changes in precipitation and dissolution reactions occurring throughout the soil, which affects the fate and transport of the target contaminant(s). Additionally, the electrical conductivity becomes very low at the meeting point of these two fronts, which can substantially inhibit transport.

Electrokinetic remediation has shown potential for transporting contaminants through the subsurface, however once they reach their end destination treatment is still required. For the treatment of chromium, chemical addition to the concentrated contamination plume is usually required to reduce Cr^{VI} to Cr^{III}, or the contaminated groundwater must be pumped out for *ex situ* treatment. These options are far from ideal, as chemical addition to a drinking water supply has the potential to do more harm than good, and *ex situ* remediation efforts are often invasive and energy intensive. Recent advancements in nanoparticle technology offer the potential to meet this demand for an economic and effective method of *in situ* remediation.

Nanotechnology has risen to the forefront of water treatment technologies due to the size and behavioral advantages offered by materials on the nanoscale. Apart from the more conventional applications of nanotechnology such as in consumer products, electronics, and medical devices, nanoscale metals are currently being investigated for their ability to remove contaminants from water. Nanoparticles can be injected into deep aquifers, or into groundwater that would otherwise be difficult to access, such as under developed land. Nanoparticles have the capacity to travel with the groundwater flow through porous subsurface materials, and interact with contaminants, decontaminating as they move.[8] Zero-valent iron nanoparticles (nZVI) are an ideal candidate for groundwater remediation purposes, as they can be produced economically and won't further compromise water quality. These nanoparticles are a strong reducing agent, and have the capacity to rapidly reduce Cr^{VI} to Cr^{III}.

The integration of nZVI with an electrokinetic remediation system offers the advantage of controlling the transport of contaminants so nZVI can be injected in the optimal subsurface location(s) to minimize cost and maximize contaminant treatment. The reactivity of nZVI is exhausted on the order of hours, as the iron particles are rapidly oxidized to Fe^{2+} and Fe^{3+} upon contact with water containing oxidized species. Therefore, concentration of a contaminant plume prior to nZVI addition offers the most efficient and economic treatment.

Bioremediation is another method used for treatment of organic and inorganic pollutants alike, and has been shown to be effective in the reduction of Cr^{VI}. Bioremediation taps into the electron transport chain in natural microbiological systems to reduce chemical species to insoluble states that can be easily removed from water. A variety of aerobic as well as anaerobic bacteria have the capacity to reduce Cr^{VI} to Cr^{III}. This process can be optimized in a microbial fuel cell (MFC), which facilitates the reduction of Cr^{VI} as well as energy production by harnessing electrons produced by electrochemically active microorganisms.[9] While this is an *ex situ* treatment method, the energy produced can be used to reduce the overall energy requirements of the treatment system, making this a green option relative to conventional treatment technologies.

This research aims to optimize the reduction of hexavalent chromium in a simulated groundwater solution by integrating electrokinetic remediation technology with the application of zero-valent iron nanoparticles, and separately by integration with microbial fuel cell technology. Additionally, the effect of organic and inorganic natural groundwater constituents on Cr^{VI} treatment will be investigated for each integrated remediation system. An in-depth evaluation of the potential of each integrated system for Cr^{VI} remediation and how these results may vary in a natural system will help outline the advantages and limitations of these technologies.

This dissertation is structured in a manor to facilitate the understanding of the primary physical and chemical mechanisms that govern the integrated remediation systems investigated. Chapter 2 provides a background on some of the essential components of this research including chromium fate and transport in the subsurface, Cr^{VI} reduction by zero-valent iron in natural systems, and the mechanisms that drive microbial fuel cells. The fundamentals outlined here provide depth and understanding to the following four chapters.

Chapters 3 through 6 are stand-alone chapters and reflect the evolution of this dissertation. Chapter 3 is an investigation into electrokinetic transport of Cr^{VI} through clay soils, and evaluates the effects of natural organic matter on the transport. This chapter targets differentiating between surface bound natural organic matter on the soil media and dissolved natural organic matter dissolved in the pore fluid. The electrokinetic experiments were conducted as bench-scale systems, and the effect of nZVI addition for Cr^{VI} treatment was investigated. Initial studies encountered Cr^{VI} transport difficulties with the types of clay soils used, and thus they necessitated a shift to soils with a higher hydraulic conductivity. This transitioned into Chapter 4, which evaluates the integration of electrokinetic transport with nZVI injection in a sandy soil. Systems were tested with and without humic acid, and with different applied electric potentials to optimize Cr^{VI} transport and reduction. A thorough study into the effects of humic acid on the use of nZVI is also presented in this chapter.

It was shown that humic acid could inhibit Cr^{VI} reduction by nZVI, and thus effect the treatment of Cr^{VI} and its transport through groundwater. Chapter 5 also investigates the effect of humic acid on biological Cr^{VI} reduction in an MFC. Furthermore, electrokinetic transport was employed to concentrate Cr^{VI} before pumping it to the MFC.

In Chapter 6, Cr^{VI} transport through soil media was investigated through experimental work and by employment of a predictive model. Transport of Cr^{VI} through sandy soil containing *Shewanella oneidensis* MR-1 biofilm was performed experimentally by determining the Cr^{VI} breakthrough curve. In a parallel study, iron oxide coated sand was prepared and charged to a soil column representative of a permeable reactive barrier, and a continuous flow Cr^{VI} solution was fed through the column. A predictive model was used to describe the dynamics of Cr^{VI} removal in each system, and for modeling the performance of IOCS as a permeable reactive barrier under relevant flow rates and contaminant loads.

1.1 Chapter 1 References

1. Hoekstra, A.Y., A.K. Chapagain (2007). Water footprints of nations: water use by people as a function of their consumption pattern. *Water Resources Management* 21(1): 35-48.

2. Kenny, J.F., N.L. Barber, S.S. Hutson, K.S. Linsey, J.K. Lovelace, M.A. Maupin (2009). Estimated Use of Water in the United States in 2005. *USGS Circular:* 1344.

3. U.S. Environmental Protection Agency (2012). Tanks and Containment/Underground Storage Tanks. Last updated on June 27, 2012, http://www.epa.gov/agriculture/ttan.html.

4. Kotaś, J., & Stasicka, Z. (2000). Chromium occurrence in the environment and methods of its speciation. *Environmental pollution (Barking, Essex□: 1987)*, *107*(3), 263–83.

5. Acar, Y.B. and A.N. Alshawabkeh (1993). Principles of Electrokinetic Remediation. *Environmental Science and Technology*, 27(13): p. 2638.

6. Probstein, R.F. and R.E. Hicks (1993). Removal of Contaminants from Soils by Electric Fields. *Science*, 260(5107): p. 498-503.

7. Page, M. M., & Page, C. L. (2002). Electroremediation of Contaminated Soils. *Journal of Environmental Engineering*, *128*(3), 208.

8. Zhang, W. (2003). Nanoscale iron particles for environmental remediation: An overview. *Journal of nanoparticle Research*, *5*(3), 323–332.

9. Hsu, L. (2011), Evaluation of Chromium Remediation in Groundwater: Investigations Using Microbial Fuel Cells and Electrokinetic Systems, *Dissertation Document*, Chapter 3, pp. 48-50.

Chapter 2 : Background

2.1 Groundwater Movement in Aquifers

In the United States, approximately 50% of the drinking water consumed comes from groundwater sources, and groundwater makes up about 20% of the total potable water usage nationwide. The majority of this water is used for irrigation and public supply purposes, such as drinking water for the Nation's population. Groundwater makes up 99% of the water available to people who live in rural areas and supply their own water. California withdraws more groundwater than any other state, and is responsible for 13% of the total groundwater consumption of the United States.[4] This is due largely to the agricultural belt running through California's central valley region, which uses large volumes of water for irrigation year-round. Groundwater is an essential resource that many parts of the United States economy and overall well-being of the public depend on. Figure 2.1 is a typical schematic representing groundwater and aquifer flow through subsurface geological formations. An aquifer is defined as a subsurface layer consisting of an unconsolidated material such as rock, sand, or silt, containing groundwater that can be extracted by a water-well. Aquifers are recharged during precipitation events, as water percolates through soil until it reaches the water table. Groundwater, which makes up the water table, flows along hydraulic gradients through aquifers at rates dependent upon the aquifer material and associated hydraulic conductivity.

Contaminants can enter aquifers by two primary pathways: 1) the improper discharge of liquid waste that percolates through the soil and reaches the water table, and 2) from improper storage or discharge of solid waste on the ground, which can be solubilized by precipitation and leach through the underlying soil with water flow. Once introduced to groundwater, contaminants can spread quickly by traveling with groundwater flow. Transport in this manner can turn a localized spill or discharge event into and extensive contamination plume, which makes remediation much more difficult and costly.

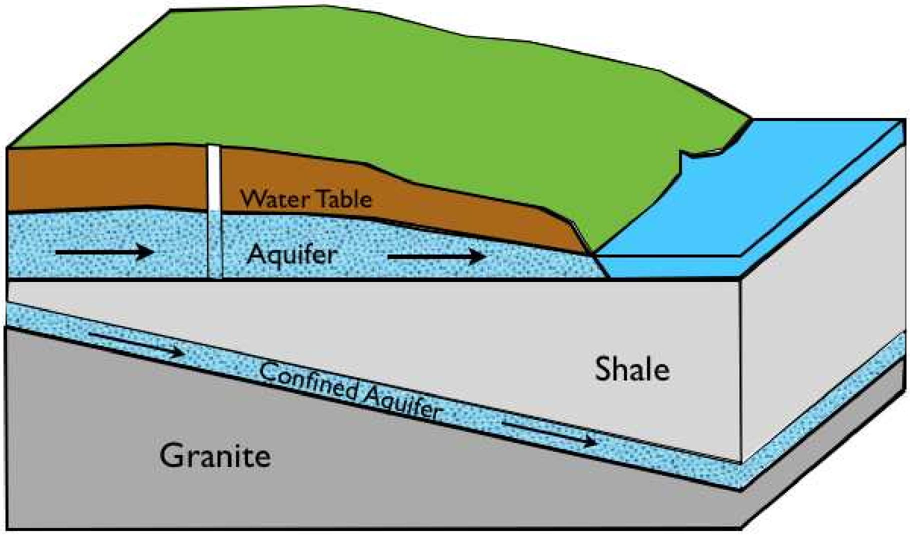

Figure 2.1 Schematic of a generic aquifer system.[5]

2.2 Hexavalent Chromium

Sources, Prevalence, and Regulations

Chromium occurs in nature as a result of anthropogenic activities, such as leather tanning, electroplating, pulp production, ore refining, and wood preservation. Another large source of chromium pollution is from its use as a corrosion inhibitor in power plant cooling water systems, and subsequent discharge to the environment. Once introduced to the environment, chromium can leach through soils and reach the underlying groundwater table.

Cr^{VI} is a strong oxidizing agent known to be carcinogenic, mutagenic, and teratogenic, and forms free radicals through its reduction to Cr^{III} within cells, making it toxic in biological systems.[6] Once introduced to the body, several mechanisms can reduce Cr^{VI} to Cr^{III}, which the body excretes. The Cr^{VI} not reduced by the body is transferred into cells by the same mechanisms responsible for the transfer of phosphates and sulfate. The strong oxidational properties of Cr^{VI} make it acutely toxic, and damage is generally observed in the kidneys, liver, and blood cells. This has been known to lead to hemolysis, renal, and liver failure, the effects of which can only be improved by aggressive dialysis. The dosage of Cr^{VI} at which at least 50% of humans would be expected to die (LD50) is between 50 and 150 mg/kg.

Recent studies by the Environmental Working Group have discovered hexavalent chromium in 31 out of 35 major cities tested in the United States. Out of these 35 cities, 25 were distributing tap water with Cr^{VI} concentrations higher than the recent proposition by California regulators. The U.S. EPA has set a maximum contaminant level (MCL) for total chromium of 100 ppb (μg/L), while the state of California has set an MCL of 50 ppb (μg/L). In 2009 however, California regulators proposed a new public health goal of 0.060 ppb (μg/L) for Cr^{VI} in tap water. This is estimated to have a "one in a million" lifetime cancer risk, meaning that for every million people who drink two liters of water with that level of Cr^{VI} for 70 years, no more than one person is expected to develop cancer from exposure.[7]

Fate and Speciation of Chromium in the Natural Environment

The fate and speciation of chromium is essential to understanding the implications of chromium contamination in the environment. Soil and groundwater conditions and constituents, as well as chromium oxidation state and concentration are all factors that determine extent of contamination. Once introduced into the environment chromium can exist in multiple oxidation states, however only two oxidation states occur under natural conditions: Cr^{VI} and Cr^{III}. Cr^{III} has a greater thermodynamic stability than Cr^{VI} in most natural systems, and conversion of Cr^{III} to higher or lower oxidation states requires high energies.[8]

Cr^{VI} species are highly soluble in water (~1680 g/L), and in the environment Cr^{VI} is found generally as chromate (CrO_4^{2-}), chromic acid ($HCrO_4^-$), and when present in high concentrations as dichromate ($Cr_2O_7^{2-}$). The following equilibrium expressions describe Cr^{VI} speciation relative to pH:

$$H_2CrO_4 \Leftrightarrow H^+ + HCrO_4^- \qquad K_1=10^{-0.75}$$

$$HCrO_4^- \Leftrightarrow H^+ + CrO_4^{2-} \qquad K_2 = 10^{-6.45}$$

$$2HCrO_4^- \Leftrightarrow Cr_2O_7^{2-} + H_2O \qquad K = 10^{2.2}$$

Cr^{VI} species in general are not strongly adsorbed to organic colloids and materials in natural waters, and this lack of interaction gives Cr^{VI} species the ability to travel long distances with groundwater flow. Alternatively, Cr^{III} species are known to chelate with organic molecules readily, and are much less soluble in water than Cr^{VI} species.[6] The primary aqueous Cr^{III} species found in natural waters are Cr^{3+}, $Cr(OH)^{2+}$, $Cr(OH)_3$, and $Cr(OH)_4^-$, however the concentrations of these species are typically low due complexation with organic matter and subsequent precipitation, as well as the solubility limitations of Cr^{III} hydroxides.

The speciation of chromium in water is well estimated by use of a Pourbaix diagram, which shows the possible equilibrium phases of an aqueous electrochemical system (Figure 2.2). This illustrates the conditions under which each species is thermodynamically stable in a dilute aqueous solution, in the absence of any complexing agent other than H_2O or OH^-. Pourbaix diagrams are a good reference for estimating speciation, however their application to a natural system is limited because of the variety of constituents found in natural waters.

In general, it is observed that speciation is dominated by the Cr^{III} oxidation state, however Cr^{VI} can remain stable with increasing redox potential conditions and increasing pH. For a low redox potential (< 1.0 V) and under acidic conditions, Cr^{VI} can be reduced to Cr^{III}. The redox potential of natural soil can vary from reducing conditions (0.2 to -0.4 V) to oxidizing conditions (0.8 to 0.3 V), depending the soil and water constituents.[9] Furthermore, the application of direct current in electrokinetic experiments alters the redox conditions significantly. In an electrokinetic remediation study by Pamucku and coworkers[10], redox potential was measured in kaolinite clay soil contaminated with Cr^{VI} containing soluble Fe^{II} species. The redox potential was measured between 0.3 - 0.6 V for different initial ratios of Cr^{VI} to Fe^{2+}. It was observed that due to slightly acidic conditions, Cr^{III} species were thermodynamically favored as $Cr(OH)^{+2}$, and Cr^{III} precipitates (Figure 2.3). Had this system been at pH 7, Cr^{VI} species would have been the dominant form of chromium as can be seen in the diagram. This illustrates how site-specific conditions play a significant role in the redox chemistry of chromium. Here, the addition of Fe^{II} lowered the solution pH and lowered the redox potential of the soil, which created conditions favorable for Cr^{III} formation. The presence of any readily oxidizable species such as natural organic matter will likely have the same impact of increasing redox potential, while readily reducible species present will have the opposite effect.

During electrokinetic remediation, the speciation of chromium is also impacted by pH changes that occur as a result of electrolysis reactions. In the anode reservoir, electron release occurs and results in an oxidative environment. At the cathode, the consumption of electrons creates a reducing environment. Electrolysis reactions at the electrodes also create acidic and basic fronts at the anode and cathode, respectively, which migrate under the electric potential towards the opposite electrode. This alters the solution pH, which ultimately affects the speciation of chromium and its fate in aqueous subsurface environments.

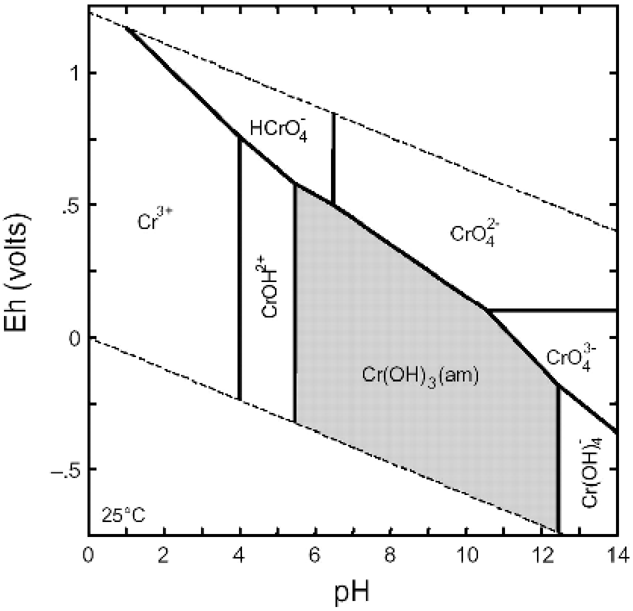

Figure 2.2 Pourbaix diagram for chromium in a dilute aqueous solution in the absence of any complexing agents.

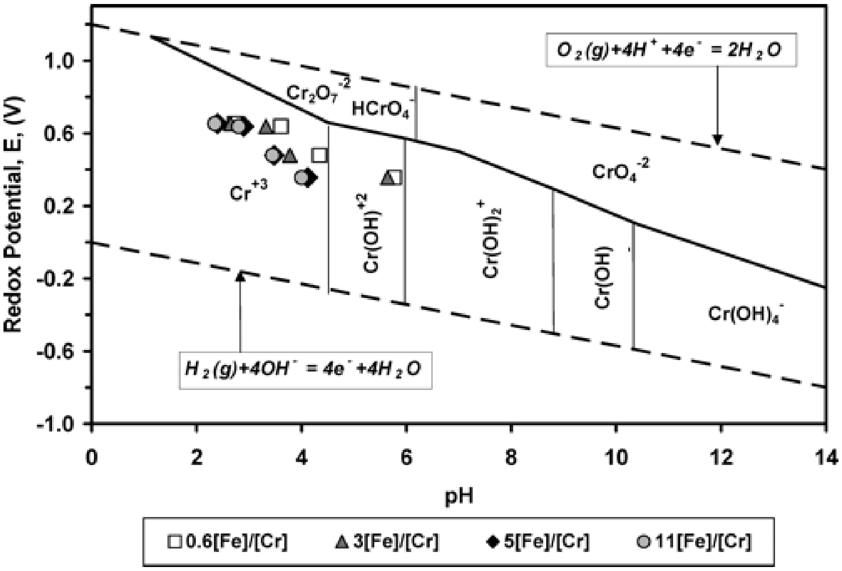

Figure 2.3 Pourbaix diagram for chromium with superimposed redox potential measurements taken after 24 hours of direct current application in an electrokinetic cell.[10]

The Effect of Background Organic Matter on Chromium Speciation

Chromium fate and speciation in groundwater and soils can be largely influenced by both surface bound and dissolved natural organic matter (NOM). NOM is a general term used to describe naturally occurring organic material in water, which is a decay product of plants and animals. NOM is derived from proteins, lipids, carbohydrates, as well as constituents such as cellulose, tannin, cutin, and lignin. It can be transported into groundwater with leachate through benthic sediment and soils in rivers, lakes, and marine systems. NOM can serve to transport nutrients to plants and animals, and can be a natural buffer in water systems. Groundwater is often responsible for distributing NOM throughout subsurface ecosystems, and in saturated soil undergoing shifts in chemical equilibria, NOM can transfer between the solid and liquid phases through adsorption-desorption processes.[11]

No single structure for NOM exists, as this is dependent primarily upon the parent material. It is known that NOM is heterogeneous and composed of many smaller fractions, with a composition along the lines of 45-55% carbon, 35-45% oxygen, 3-5% hydrogen, and 1-4% nitrogen.[12] A significant percentage of the carbon present is in the form of aromatic rings, adding both stability to these molecules as well as providing the foundation for polymerization, which can create larger molecules of NOM.

A significant fraction of NOM is made up of humic substances, which can be broken down into three primary subgroups; humic acid, fulvic acid, and humin. Humin has the largest molecular weight of these three, generally in the range of 100,000 – 300,000.[13] Humin is insoluble in water and in alkali solutions, and is excluded from this discussion. Humic acids are soluble above pH 2 and are a complex mixture of many different acids, however the phenolic and carboxylic constituents tend to dominate in terms of surface charge and reactivity. These functional groups give humic acid amphiphilic properties from the hydrophobicity of aliphatic and aromatic fractions, and the polar functional groups such as hydroxyls, phenols, and carbohydrate sub-units. In general, humic acids tend to behave as dibasic acids, with a pK_1 value near 4 representing the protonation of carboxylic acid groups, and a near 8 for the protonation of phenolic groups. These reactive functional groups facilitate humic acid complexation with ions such as Mg^{2+}, Ca^{2+}, Fe^{2+}, Fe^{3+}, and have been shown to complex heavy metals such as Cr^{VI} to varying degrees. The molecular weight of humic acid generally ranges from 10,000 – 100,000 (Stevenson, 1982). A typical humic acid molecule and its typical functional groups are shown in Figure 2.4, and Figure 2.5, respectively.

Fulvic acids are essentially humic acids of much lower molecular weight in the range of 2,000 – 10,000, and contain higher oxygen content.[13] They are yellow to brown in color and are soluble in water of all pH values. A typical fulvic acid molecule is shown in Figure 2.6.

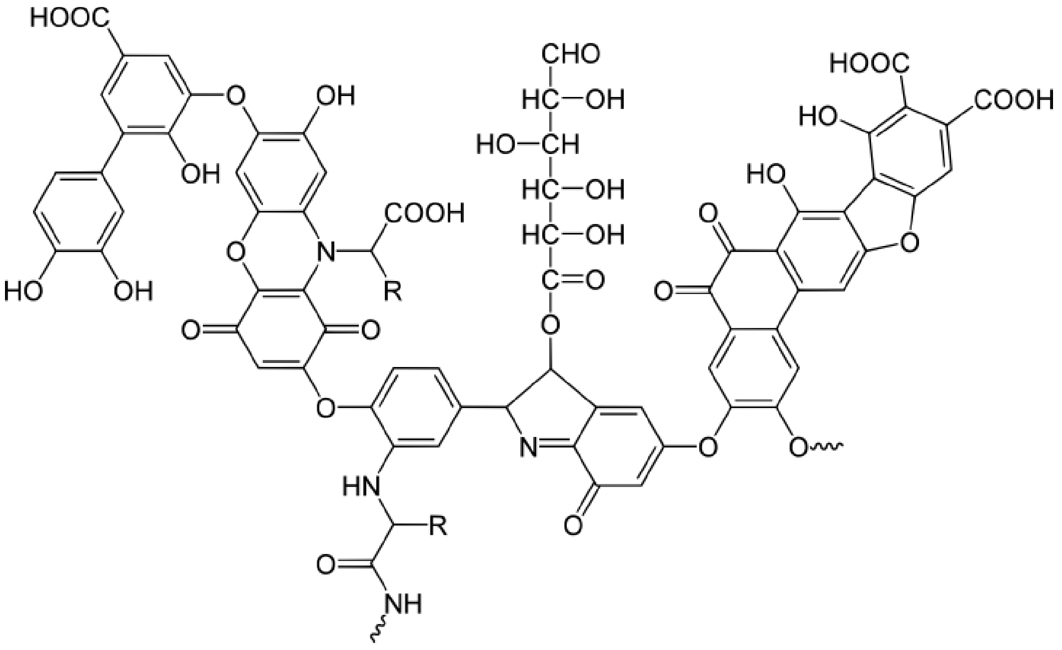

Figure 2.4 A typical humic acid molecule.[13]

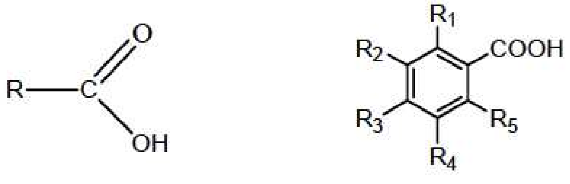

Aliphatic Carboxyl

Aromatic Carboxyl

Aliphatic-OH

Phenolic-OH

Carbonyl

Quinone

Figure 2.5 Functional groups typically found in humic substances.[14]

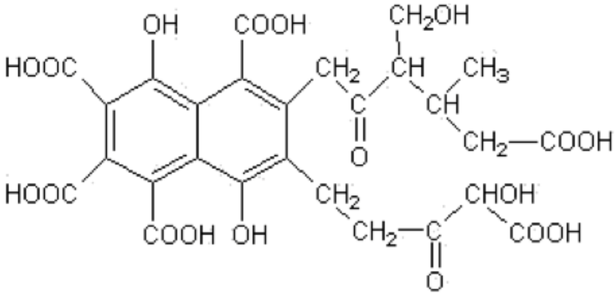

Figure 2.6 A typical fulvic acid molecule.[15]

The ability of humic substances to complex metal ions can lead to significant changes in the fate and transport of these ions in subsurface environments. Metal cations can form complexes with humic substances by a weak electrostatic attraction of counter ions. Humic substances nearly always carry a negative charge due to the dissociation of protons and their incomplete replacement by coordinated metal ions, and are therefore attracted to cationic species. Carboxyl and phenolic groups are largely responsible for cation complexation, and proposed reactions are shown in Figure 2.7. This process can affect the fate of cationic species in natural groundwater systems, as well as on redox processes associated with Cr^{VI}.

The fate and transport of Cr^{VI} through the subsurface in groundwater has been shown to be heavily influenced by the presence of NOM. Jardine and coworkers found that soils amended with natural organic matter slowed the breakthrough time of Cr^{VI} in a soil column by 1,200 hours relative to unamended soils.[16] Overall, the NOM amended soil reduced 46% of the total chromium, versus 24% in the unamended soils, indicating that NOM adsorbed to the soil is capable of complexation with Cr^{VI} and reduction to Cr^{III}. In the absence of a mineral solid however, Cr^{VI} complexation and reduction by humic acid was shown to occur at a much slower rate. Batch systems containing 0.145 mM Cr^{VI} and 25 mg/L humic acid noted a 35-time increase in reduction in the presence of a solid.[16]

These results were in agreement with complexation studies conducted by Fukushima *et al.*, who observed 40% reduction of a 12.4 mg/L Cr^{VI} solution by a 40-mg/L humic acid solution after 62 days under acidic conditions.[6] Of the 40% reduced, 30% existed as a Cr^{III}-HA complex, and 10% was present as inorganic Cr^{III}. These findings were corroborated through a series of adsorption studies of Cr^{VI} to kaolin with varying electrolyte and humic acid concentrations.[17] It was determined that the presence of humic acid increased adsorption significantly.

The following mullet-step process mechanism for the reduction of Cr^{VI} by humic acid was proposed[6]:

1. Rapid Cr^{VI} combination with humic acid to form a chromate ester.
2. Slow decomposition of the chromate ester to an unstable Cr^{V} intermediate.
3. Rapid reduction of the Cr^{V} intermediate to either Cr^{III}-HA complex or to inorganic Cr^{III}.

It has been reported that Cr^{VI} reduction by various humic substances is possible under acidic and anaerobic conditions (Figure 2.8), however reduction rates in this study were negligible at pH values above 7.[18] In their study, equilibrium was not achieved after over 300 hours of reaction time, however Cr^{VI} concentrations were shown to decline by as much as 95%. Similar results were obtained by an aerobic batch study with initial Cr^{VI} concentrations of 50µM in 40 mg/L humic acid at pH values of 5.1, 4.0, and 3.2.[6] Complexation of Cr^{VI} with humic acid was found to increase with decreasing pH. At pH 3.2, nearly 50% of the initial Cr^{VI} was complexed with humic acid after 1500 hours, and at pH 5.1 only about 20% of the Cr^{VI} had been complexed. Under acidic conditions ($pH < 5$), chromium exists as partially dissociated chromic acid, $HCrO_4^-$, whereas above that it exists primarily as the chromate ion, CrO_4^{2-}. As the pH increases and reactive functional groups deprotonate, it is likely that repulsive forces between chromate and humic acid limit the amount of interaction in dilute solutions.

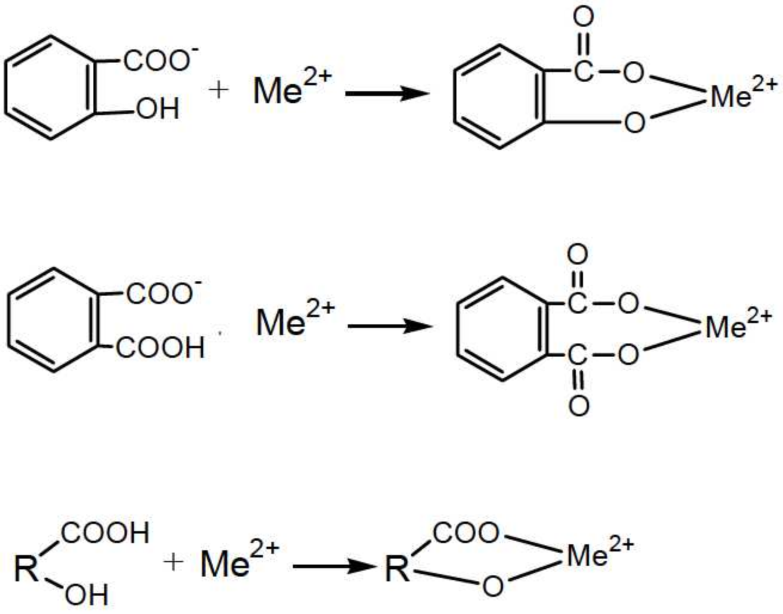

Figure 2.7 Metal cation binding by humic substances.[11]

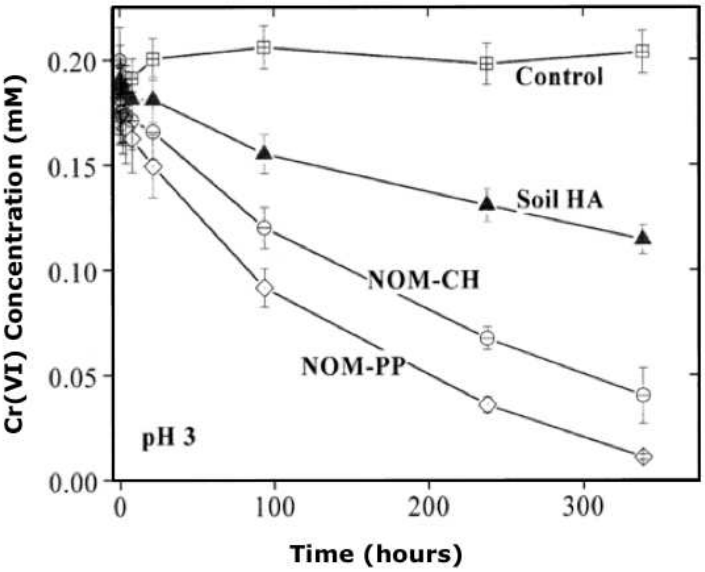

Figure 2.8 Reduction of Cr^{VI} by various humic acid fractions at pH 3.[18]

Adsorption of Cr^{VI} to Clay Soils

When contaminants are released into the environment, they are commonly transported through soils by a number of different mechanisms. Chemicals can continue to leach vertically through soils until they reach either a confining subsurface layer, or reach the water table where they will move with groundwater. Factors such as the concentration of the released chemical, its oxidation state and speciation, the solution pH, the receiving soil pH, soil particle structure and associated reactive functional groups, and constituents bound to the soil surface such as NOM, all affect adsorption. Adsorption can fix a given amount of contaminant to the solid phase thereby removing it from water, a term referred to as "natural attenuation."

Given its chemical properties, hexavalent chromium has the capacity to be reduced and immobilized in soil under reducing conditions. The reduction of Cr^{VI} can occur by reactions with many naturally occurring reductants such as natural organic matter, ions adsorbed to soils such as Fe^{2+}, mineral constituents, and any other aqueous reducing species. Depending on the availability of reducing species, natural attenuation of chromium can reduce the required amount of costly and invasive remedial action at a remediation site.

Adsorption of chromium to different soils is an essential component of remediation research as this is a significant factor in determining the extent of damage done by a discharge event. Extensive research has been conducted regarding the adsorption of heavy metals onto all types of soils, and in general results indicate that adsorption capacities and the associated mechanisms involved in the adsorption process can differ greatly from soil to soil. The clay mineral kaolin is a commonly used soil in adsorption studies involving heavy metals because it has been well characterized. Kaolinite soil consists primarily of the kaolin mineral (>95%), and is commonly used in soil adsorption studies. A schematic of the kaolinite structure is shown in Figure 2.9. Kaolinite is a 1:1 alumina silicate sheet comprised of a tetrahedral silica sheet bound to an octahedral alumina sheet by sharing oxygen atoms between adjacent silicon and aluminum sheets.[19] The linear chemical formula is $Al_2O_32SiO_22H_2O$. Hydrogen bonding or interstitial cations holds successive layers together, and substitution of Al^{3+} for Si^{4+} in the tetrahedral sheet of the mineral gives kaolin a negative surface charge in all aqueous solutions.[20] The charge held by the alumina octahedra and the crystal edges can change with pH from the protonation and deprotonation of hydroxyl groups.

While adsorption studies of countless combinations of metals and soils have been investigated, many discrepancies exist between various publications – even those investigating the same metal-soil combinations. These differences are due to factors such as soil pretreatments, and experimental conditions such as pH, presence of competing chemical species, soil to liquid ratio, and the concentration of the metal adsorbate. The results of a select number of adsorption studies are summarized in Table 2.1, and illustrate the variety in reported results. Adsorption capacities range from 0.037 mg Cr^{VI}/g kaolinite to 13.8 mg Cr^{VI}/g kaolinite.[21,22]

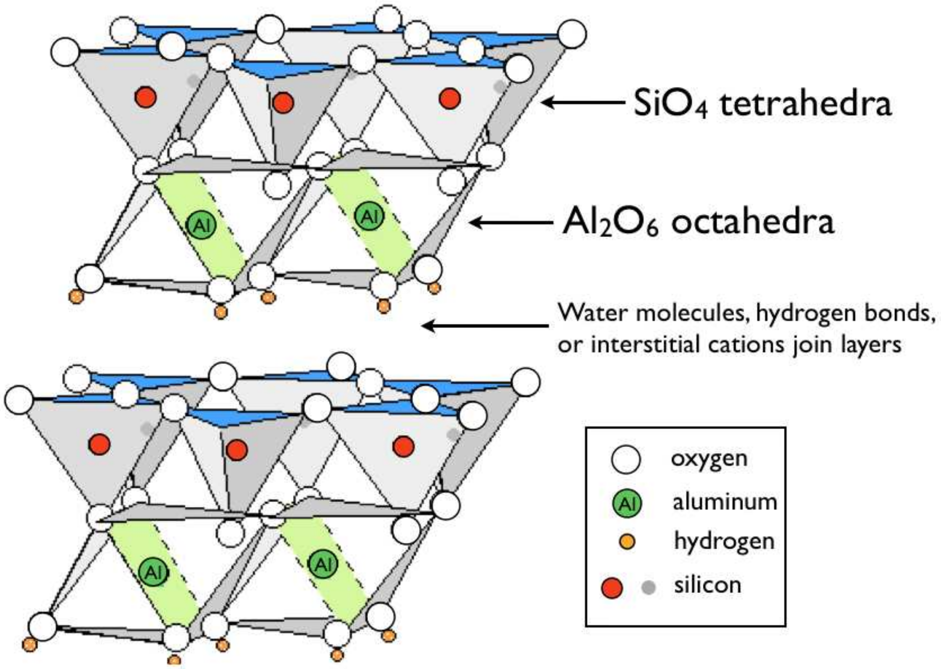

Figure 2.9 Chemical structure of kaolinite clay.[23]

Table 2.1 Summary of various heavy metal and clay soil adsorption studies, showing a wide range in reported values.

Author/Date	Adsorbant (clay type)	Clay Treatment	Adsorbate (metal contaminant)	Adsorbate Concentration	Soil/Solution Ratio (g/L)	pH	Isotherm Model	Adsorption Capacity (mg/g)	Notes
Angove 1996	Kaolinite	Raw and treated for oxide removal	Cd2+	5.6ppm	6.38, 3.34	5.5, 7.5	Langmuir (pH 5.5), two-series Langmuir (pH 7.5)	1.3 - 1.4	Adsorption increased with increasing pH.
Bhattacharyya 2006	Kaolinite	Three different washing techniques	CrO42-	10 - 250ppm	2.0 - 6	4.6	Langmuir/ Freundlich	10 - 13.8	Acid activated kaolinite had the largest adsorption capacity.
Heidmann 2004	Kaolinite	< 1.0um	Pb2+, Cu2+	NA	5	4, 6, 8	face-surface site adsorption	0.6 but never reached cap	Adsorption increased with fulvic acid addition.
Hizal and Apak 2006	Three kaolinite based clays	NA	Pb2+, Cu2+	10ppm	50	2.0 - 10	Langmuir	0.64 - 2.8	At low pH the presence of HA increased adsorption.
Li 2010	Kaolin	NA	CrO42-	1 - 20ppm	0.2	3.0 - 10	Langmuir	4.8	Addition of HA increased adsorption. Adsorption increased with pH to a degree (pH 6-7).
Reddy 1997	Glacial till, kaolin, Na-montmorillonite	NA	CrO42-	1 - 1000ppm	100, 50 (Na-mont.)	2.0 - 10	Langmuir	0.48 (pH 6)	Adsorption increased with decreasing pH. Adsorption follows surface complexation model.
Schmitt 2002	Kaolinite, monmorillonite	NA	Al, Fe, Zn2+, Pb2+	~ 0.5 - 1.0ppm	0.33	5, 7	NA	0.6 - 1.4	In general, humic acid decreased adsorption onto clay.
Zachara 1988	Kaolinite (Georgia)	Oxide and hydroxide surface coating removal	CrO42-	0.5 - 260 ppb as CrVI	10, 20	5.5	Two series Langmuir / Freundlich	0.037	Adsorption increased with decreasing pH.

2.3 Zeta Potential of Soils under an Applied Electric Potential

The surface charge carried by soil particles is a property that has a direct influence on its function as an adsorbent. Reaction rates and quantities of a chemical adsorbed are partially regulated by the surface charge of a sorbent, which controls electrostatic attraction or repulsion in solution. The surface charge of colloidal particles is often described by the zeta potential, a value that represents a measure of electrokinetic potential that exists across the interface of all solids and liquids. Electrokinetic potential is the electric potential in the interfacial double layer at the location of the slipping plane compared to a point in the bulk fluid away from the interface (Figure 2.10). This is essentially the electric potential difference between the bulk fluid and the layer of fluid attached to the dispersed particle. The zeta potential of particles in a suspension are a function of solution pH. With an increase in pH, an increase in negative surface charge density is typically observed as reactive functional surface groups deprotonate.[24] When the pH of a solution drops, the opposite effect occurs, reducing the negative surface charge. For clay soils, the zeta-potential is generally negative because of the net negative charge on clay particle surfaces. Hydrogen and hydroxyl ions are the potential determining ions, so a pH drop usually results in the decrease in the absolute value to zeta potential. The zeta potential may become zero at a specific pH, which is referred to as the isoelectric point, or the point of zero charge.

The measure of zeta potential is used to determine the stability of a colloidal dispersion. A higher absolute value of zeta potential indicates that colloidal particles have a higher net surface charge and will therefore repel one another in solution and remain suspended. Conversely, a low zeta potential indicates that particles carry a low net surface charge and can interact with other particles through van der Waals attractive forces, leading to agglomeration and eventual gravitational sedimentation.[25] At the point of zero change, particle stability in solution is at a minimum. Table 2.2 shows the relationship between zeta potential values and relative particle stability.

Soil Particle Surface Charges

The surface charge carried by particles originates from isomorphic substitutions among different ions of different valences in soil minerals, as well as from broken chemical bonds, and lastly from reactive functional groups on the particle surface. Four different surface charges make up the net total surface charge as described by Yeung:[25]

1) the permanent structural charge, σ_0, which is due to isomorphic substitutions and broken bonds;
2) the net proton charge, σ_H, which is the difference between the moles of protons and hydroxide ions complexed by surface functional groups;
3) the inner-sphere complex charge, σ_{IS}, which is the net charge from ions other than hydrogen or hydroxide that are bound into inner-sphere surface complexes;
4) and the outer-sphere complex charge, σ_{OS}, which is the net charge from ions other than hydrogen or hydroxide that are bound into outer-sphere surface complexes.

The intrinsic surface charge of soil depends largely on the degree of weathering of the minerals and organic matter associated with it, and this determines the contribution of σ_0 and σ_H to the overall charge. Soils that have undergone little to an intermediate degree of weathering carry the charge determined by the siloxane cavity, the primary source of permanent structural charge. These soils still contain primarily the characteristic minerals that comprise the soil, such as that of feldspars, illite, vermiculite, and chlorite. These soils are referred to as permanent-charge soils. Clay soils on the other hand are in the advanced stages of weathering and are enriched in minerals containing hydroxide reactive functional groups. This makes σ_H the dominant contributor to surface charge, and as a result pH changes strongly influence the surface charge. This category of soils including clay is referred to as variable-charge. The value of σ_0 is nearly always negative, however the other contributions to surface charge can be negative, zero, or positive. As a result, the net surface charge can therefore carry a negative, zero, or positive surface charge, due to pH and the relative extent of weathering.

These factors make zeta potential variable during electrokinetic remediation processes from pH and ionic concentration changes in the pore fluid. This can make parameter estimation such as electroosmotic velocity difficult because of the temporal and spatial distribution predictions in electroosmotic flow. Electric double layer properties such as fluid viscosity, dielectric constant, solute distribution, and electrical field can vary significantly from one point to another within soil cross sections in any direction.

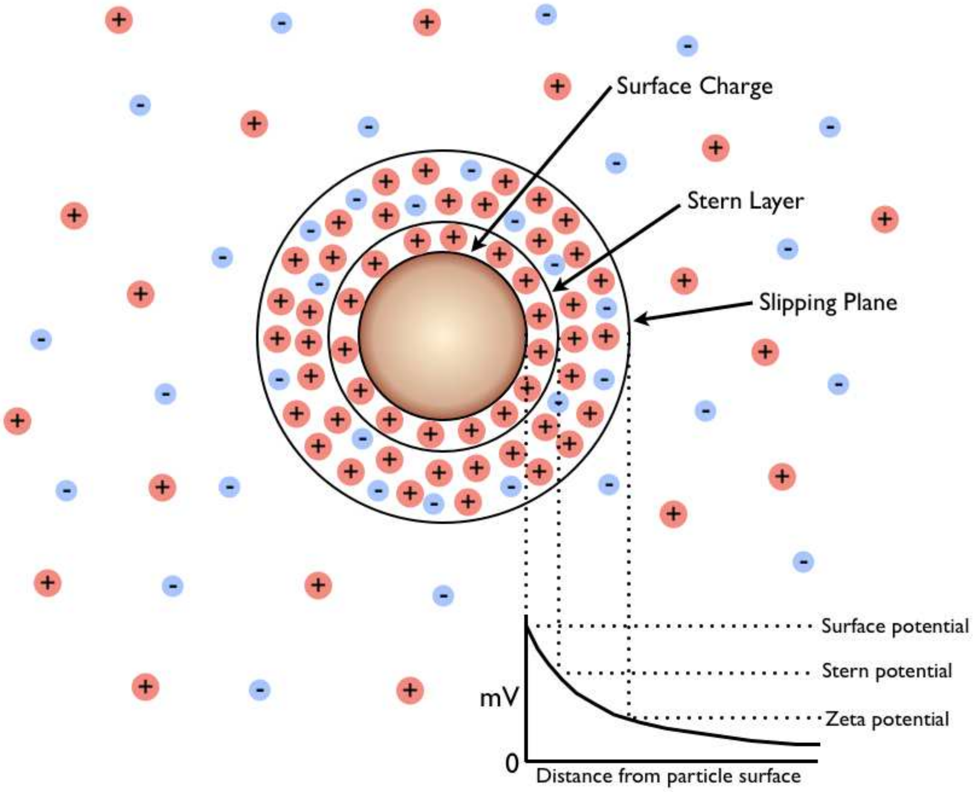

Figure 2.10 Schematic representing zeta potential (image adapted from Yukselen and Kaya).[25]

Table 2.2 Particle stability in aqueous solution in terms of zeta potential.

Zeta Potential (mV)	Stability
±0 – ±5	Rapid coagulation – very unstable
±10 – ±30	Incipient stability
±30 – ±40	Moderate stability
±40 – ±60	Good stability
±61 +	Excellent stability

2.4 Electrokinetic Remediation

Theory

Electrokinetic remediation is a technique used to transport contaminants through soils and groundwater with the use of an electric field. This is also termed electrokinetics, electroremediation, electrochemical remediation, and a host of similar names. In the last decade electrokinetic remediation has received a lot of attention from environmental professionals and academics alike due to the advantages it offers over conventional technologies. These advantages include:

- use as an *in situ* or *ex situ* remediation method;
- applicability to heterogeneous soils and soils of low hydraulic conductivity;
- effectiveness in both saturated and unsaturated soils;
- use for remediation of any ionic contaminant as well as mixtures of contaminants;
- the possibility of integration with conventional remediation technologies.

Electrokinetic remediation is performed by applying a low-voltage direct current to electrodes submerged in the ground surrounding a contaminated area (Figure 2.11), which generates an electric field between the electrodes. The ionic content of the pore water carries the current and forces the migration of ionic species towards either electrode, where they can ultimately be recovered. Ions can be carried through pore water by four primary mechanisms: electromigration, electroosmosis, advection, and electrophoresis (when bound to a solid). Electromigration is the most significant transport mechanism, as electroosmotic transport can be as much as 300 times slower, and diffusion rates are negligible in comparison as well. The direction of direct ion transport (electromigration) is dependent upon the charge of the ion; cations will travel toward the cathode, and anions will travel towards the anode. Ions will move along the electric field lines determined by the placement of the electrodes, allowing for good control of flow direction. Heavy metals present in ionic form are easily transported by electromigration through soil pore space towards the respective electrode where they will concentrate. Additionally, ions are transported with the movement of the bulk fluid as it moves towards the cathode from the transport of cations in the slipping plane (electroosmosis).

For effective transport the target contaminant must be dissolved in the pore fluid, however situations often arise where contaminants are not in the form of their soluble salts, but in the form of some less soluble chemical substance. Furthermore, contaminants can be adsorbed tightly to soil surfaces, in which case the contaminant must be desorbed or dissolved before it can be transported by electrokinetic phenomena.

The foundations of this technology have been well established by many research groups. Implementation of electrokinetic remediation in the field can be as simple as illustrated in Figure 2.11, however successful remediation requires a comprehensive understanding of the specific site and the dynamic transport, transfer, and transformation processes that will occur as a result of the applied electric potential. Some of the soil and groundwater characteristics of primary importance are the buffering capacity, mineralogy, and the natural organic matter content. These properties affect the geochemistry and electrochemistry of the system, and must be accounted for when engineering a remediation approach.

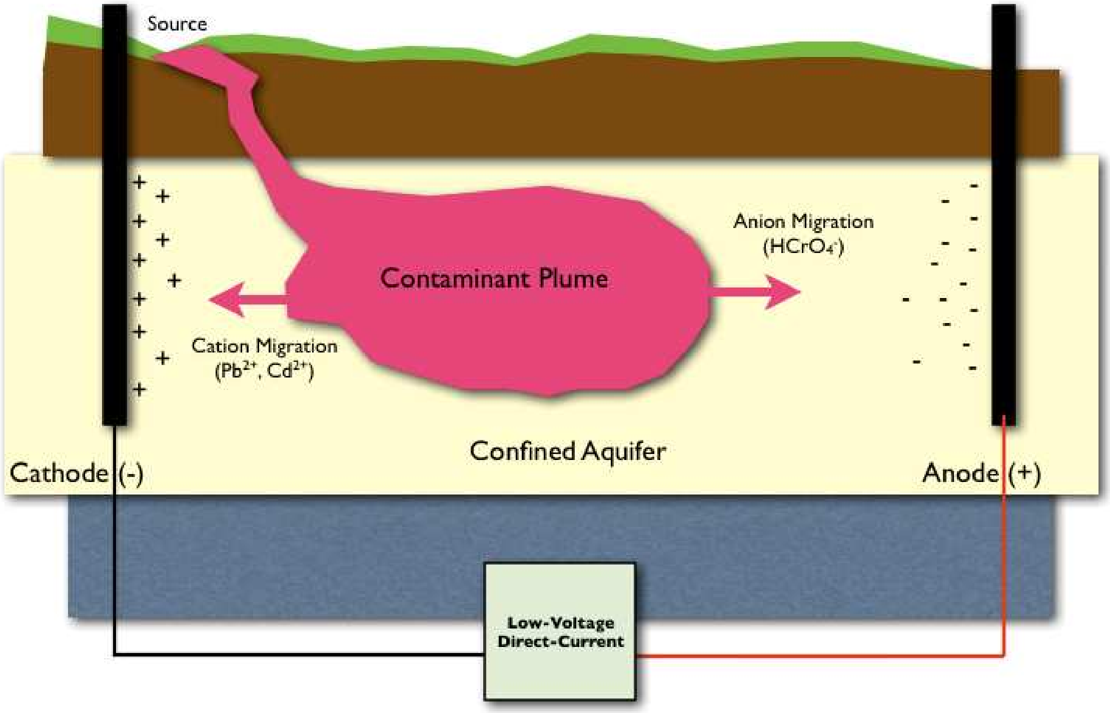

Figure 2.11 Conceptual rendition of electrokinetic remediation technology.

Electrokinetic Remediation of Cr^{VI}

Electrokinetic remediation of groundwater and soils contaminated with Cr^{VI} has been investigated in the past on the lab scale, pilot scale, and even some full-scale remediation projects. The results of some of these studies are summarized in Table 2.3. The removal percentage of Cr^{VI} varies greatly, from 3% removal in a lab scale investigation in a sand-soil column, to 90% removal in a full-scale investigation in a clay soil.[26,27] The disparity in results illustrates the need for further work on electrokinetic removal of Cr^{VI}, and the need for a consistent approach to electrokinetic remediation.

Table 2.3 Summary of various electrokinetic experiments for Cr^{VI} remediation in groundwater.

Soil Type	Scale	Current Density (mA/cm^2)	Voltage (V/cm)	Duration (days)	Concentration Initial/Final (mg/L)	Removal %	Reference
<1mm	Lab	0.02	1.2	46	25.3/24.5	**3**	Weng *et al*. (1994)
Clay (19%), Silt (64%)	Lab	unknown	2.3	59	890/744	**16**	Wieczorek *et al.* (2005)
Clay	Full	unknown	unknown	unknown	7300/755	**90**	Clarke *et al.* (1996)
Loamy Sand	Lab	0.2	unknown	85	880/700	**20**	Ribeiro (1994)
Loamy Sand	Lab	0.4	unknown	16	550/380	**31**	Ribeiro (1994)
Unknown	Lab	0.5	unknown	50	900/600	**33**	Gent *et al.* (2004)
Wastewater Sludge	Pilot	1	unknown	5	116/75	**35**	Kim *et al.* (2005)
Clay (67%), Silt (13%)	Lab	Unknown	2.3	59	1464/589	**60**	Wieczorek et al. (2005)
Sand (0.85-0.42mm)	Lab	0.015	0.9-1.2	9	14.2/5.1	**64**	Bibler *et al.* (1993)

pH Gradient Formation

During electrokinetic remediation, a pH change in the pore liquid is commonly observed as a product of electrolysis reactions occurring at the electrodes. As previously mentioned, pH change affects the adsorption-desorption, and precipitation-dissolution reactions of contaminants in the soil, and also changes the zeta potential of the soil.

At the anode and cathode, electrolysis reactions create highly acidic and highly basic conditions (respectively), according to the following reactions:

$$2H_2O - 4e^- \rightarrow O_{2(g)} + 4H^+ \quad E_o = -1.229 \text{ (anode)} \tag{1}$$

$$2H_2O + 2e^- \rightarrow H_{2(g)} + 2OH^- \quad E_o = -0.828 \text{ (cathode)} \tag{2}$$

where E_o is the standard electrochemical reduction potential required to drive each reaction from reactants in their standard states to products in their standard states. The hydrogen and hydroxide ions formed as a result of electrolysis are subject to the same electrokinetic transport as any other ion. Due to the relative mobility of the hydrogen ion to hydroxide ion based on size, the acid front at the anode migrates about twice as fast as the hydroxide front at the cathode. The acid front propagation process has been described by researchers using the advection-dispersion equation to model transport of hydrogen and hydroxide ions using measured ionic mobilities and diffusivities of these two ions.[1,28] Over time, a section of soil undergoing electrokinetic remediation will experience a pH drop, the extent of which is determined by the buffering capacity of the groundwater and soil.

The shift in pH during electrokinetic remediation processes can have detrimental effects on removal of the target contaminants. As the pH changes, physical and chemical changes occur affecting precipitation and dissolution reactions, speciation of chemical species, the cation exchange capacity of the soil, and adsorption and desorption processes. Additionally, one of the largest concerns regards the area where the acid and base fronts meet. At this intersection, the electrical conductivity significantly drops as hydroxide and hydrogen ions bond with electrolytes in solution. This can dramatically inhibit electrokinetic phenomena by insulating a space between the electrodes. Managing the pH shift is a key consideration in electrokinetic treatment, and many different enhancement techniques have been developed to accommodate this. These techniques include reagent addition to solubilize contaminants from soils, or mitigate pH changes through acid or base addition. Altering the redox reactions through reagent addition can also affect remediation by shifting the oxidation state of a particular contaminant, or through a change in oxidation state of a ligand that can form chemical bonds with the contaminant.[29] Additionally, enhancement techniques are used to shorten the overall remediation time. Transport rates of heavy metals through groundwater by electrokinetic phenomena are typically slow, which requires treatment times to be on the order of many months.[30]

Electrochemical Transport Processes

The electrochemical transport of charge through a system is an essential mechanism that regulates many natural processes, and can be utilized to drive chemical and physical phenomena in electrokinetic systems. The basis for many theories used to describe electrochemical transport phenomena are well over a century old, from noted scientists such as Quinke (1861), Helmholtz (1879), Nerst (1888), and Planck (1890). Today, electrochemistry plays a significant role in everything from energy storage and conversion, to semiconductor devices, to metallurgy, to water treatment. The fundamentals of electrochemical ionic transport of contaminants through soils are an extension of this century-old work. The fundamentals of electrokinetic transport are well described by Sibel Pamukcu in *Electrochemical Remediation Technologies for Polluted Soils, Sediments, and Groundwater* (pp. 29-48) as follows.[31]

The Nerst-Planck (Eq. 3) and Poisson (Eq. 4) equations are used in mass transport analysis of electrochemical systems. The Nerst-Planck equation is a conservation of mass equation used to describe the motion of ions under an ionic concentration gradient and an electric field. The Poisson equation considers the affects to local ion concentrations on electrostatic potential.

$$\frac{\delta C_i}{\delta t} = \nabla\left(D_i \nabla C_i + u_i z_i F C_i \nabla \phi\right) \tag{3}$$

$$-\varepsilon_s \nabla^2 \phi = \rho = \sum_i z_i F C_i \tag{4}$$

Here C_i is concentration, D_i is the diffusion coefficient, u_i is mobility, z_i is the charge number of species *i, F* is Faraday's constant, ϕ is the electrostatic potential, ε_s is the permittivity of the solvent, and ρ is the charge density. Solution permittivity (ε_s) is a measure of how an electric field interacts with a dielectric medium, describing of the flux generation per unit charge of the medium. A smaller electric flux exists in solutions with higher permittivity due to polarization effects.

In the description of many electrochemical systems the local electroneutrality condition is used to simplify Equation 4 by setting the right side to zero (zero charge density). This mathematically satisfies the Laplace equation ($\nabla^2\phi = 0$), and indicates that the concentration distribution and conductivity are uniform throughout the electrochemical cell. However a real system does have concentration gradients, where the current density can be affected to the point of current flow moving opposite to the electric field. By the electroneutrality condition and the PNP equations, it can be shown mathematically that concentration gradients exist and create spatial variations of conductivity. Here, diffusion potential arises and ensures ion movement at the same speed to overcome the charge separation and violation of electrical neutrality.

As mentioned, the Nernst-Planck equation, describes the movement of ions in a fluid medium based on concentration and electric field strength. Assumptions are required to make the Nernst-Planck equation a functional model for this application, including solutions are dilute, association-disassociation reactions are rapid, and the double-layer thickness is small. The total flux of species *i* in one-dimension to an electrode by advective and diffusive forces can be written in terms of the Nerst-Planck equation as:

$$J_{\mathrm{i}}(x) = -D_{\mathrm{i}}\frac{\delta C_{\mathrm{i}}(x)}{dx} - u_{\mathrm{i}} z_{\mathrm{i}} F C_{\mathrm{i}} \frac{\delta \Phi(x)}{\delta x} - C_{\mathrm{i}} v(x) \tag{5}$$

where J_{i} is the total flux of species *i* ($Mt^{-1}l$), u_i is the mobility of species *i,* and $v(x)$ is the advective velocity. In an electric field of unit strength, the mobility of the ion (u_i) is defined as the limiting velocity. The minus sign is used to indicate the direction of flux is opposite to that of increasing C_i.

With the application of Fick's second law, the basic mass transfer equation for an electrochemical system under an electric field can be derived:

$$\frac{\delta C_i}{\delta t} = -\nabla J_i(x) \tag{6}$$

$$\frac{\delta C_i}{\delta t} = \nabla\left(D_i \nabla C_i + u_i z_i F C_i \nabla \phi\right) + \left(u_i z_i F \nabla \phi + v\right) \nabla C_i \tag{7}$$

The first term in Equation 7 describes diffusive transport, the second term describes ion migration from the electric field, and the final term describes the contribution of advection to the total mass transport of the species *i*. In clay-groundwater systems, the advective term is neglected due to the extremely slow movement of groundwater through tightly packed soils. The velocity term in Equation 7 is given by:

$$v = -\kappa_h \nabla h - \kappa_e \nabla \Phi \tag{8}$$

where κ_h is the hydraulic conductivity of the soil, h is the hydraulic head, and κ_e is the electroosmotic permeability. The first term in Equation 8 is Darcy's law, and the second term represents contributions from electroosmosis. The hydraulic conductivity is dependent on the soil particle size and the pore size distribution, as well as on the tortuosity path of the flowing fluid.

The electroosmotic permeability has a more complex relationship with some fundamental variables of the system such as soil porosity and the zeta potential of the soil particles. The Helmholtz–Smoluchowski model is the primary model used to describe electrokinetic transport of pore fluid in saturated soils:

$$v_e = \frac{\varepsilon_s \zeta}{\eta} \bullet \frac{\delta \Phi}{\delta x} = \kappa_e E \tag{9}$$

Here E is the electric field applied to the system, η is the viscosity of the pore fluid, κ_e is the electroosmotic conductivity coefficient, ε_s is the permittivity of the pore fluid, ζ is the zeta potential, and υ_e is the resultant electroosmotic velocity. The foundations of this model are illustrated in Figure 2.12. The interface between the soil and the fluid is treated like a capacitor with ions of a single charge lining the particle surface and ions of opposite charge arranged in a line adjacent to them in the bulk fluid. Due to the negative surface charge on soil particles, an excess of cations forms a mobile shell surrounding the particle. The mobile cation layer that defines the slipping plane will move in an electrokinetic system in the direction of the cathode, which is the basis for electroosmosis.

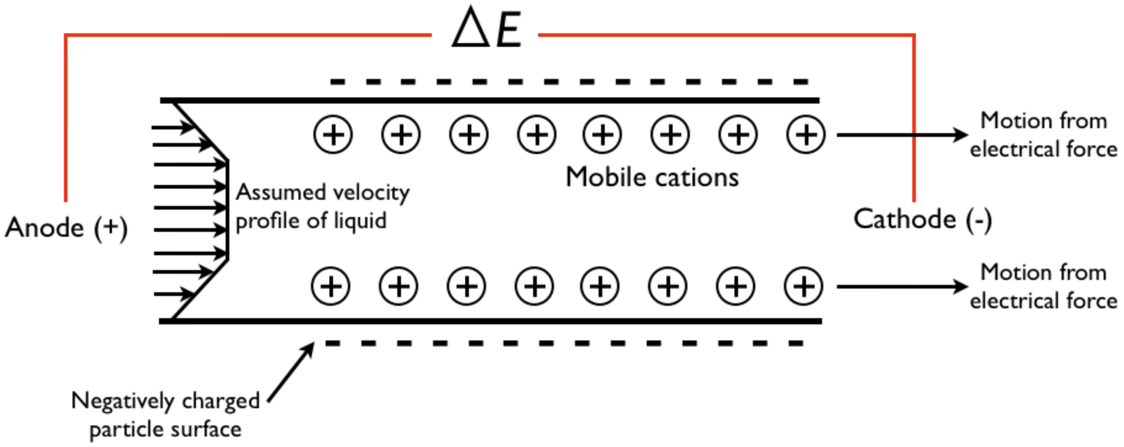

Figure 2.12 Schematic of the Helmholtz-Smoluchowski model used in modeling electroosmotic flow (Image adapted from Yeung).[25]

The mass transfer equation (Equation 7) described in terms of the charge flux, J_i, is defined as the molar concentration flow of charge through a unit cross-sectional area. This number fluctuates with time at different locations within an electrokinetic system due to the relative contributions of diffusion, electromigration, and advection at different locations and times. In most cases though, the flux from electroosmotic transport is orders of magnitude smaller than flux from electromigration, so electroosmotic transport is neglected from transport equations.[1] Additionally, as previously mentioned the contributions of ion transport by advection from pore liquid flow can be neglected for very low groundwater flow rates, comparable to those observed in clay soils. Therefore, in soils of low hydraulic conductivity, electromigration is the primary driving force behind ion transport in electrokinetic systems.

The flow of current in an electrochemical system is achieved through ionic conduction in the liquid phase and electronic conduction through the solid phase and the interface layer. The solid phase and bulk fluid interface, termed the electric double layer, is what drives ion transport by electromigration and electroosmosis. The electric double layer couples ion motion and fluid flow, and connects the solid and liquid phases. This mediates the relative movement between the two phases by accumulation of charge density, the transport of ions and charge across the solid surface, and by passing charge to electrolytes in the bulk fluid.

The current measured during electrokinetic remediation is a product of ion movement and can be related to the ionic flux by:

$$I = F\sum z_i J_i \tag{10}$$

When this expression is combined with Equation 7 and simplified, the current can be expressed as:

$$I = F\sum -z_i D_i C_i - \sigma\nabla\Phi \tag{11}$$

where

$$\sigma = F\sum z_i C_i u_i \tag{12}$$

The quantity σ represents the effective electrical conductivity of the bulk fluid in the soil and is dependent on the ionic mobility of all the species in solution. Equation 11 assumes that electroneutrality holds at all points within the bulk fluid, which is not a safe assumption to make in complex natural systems, however is justifiable in dilute homogeneous solutions.

These expressions have been shown to provide adequate predictions for simple systems, with homogeneous soils. Field scale studies however are much more difficult to model with these expressions due primarily to the heterogeneity of natural systems.

Electrokinetic Modeling Considerations

Mathematical models are a powerful tool in the investigation of reactions and processes that occur during electrokinetic remediation. Many lab-scale studies on contaminant transport by electrokinetics have been attempted, however relatively few attempts to model electrokinetic phenomena have been done due to the complexity of even the simplest systems. An electrokinetic remediation model should consider contaminant transport and transfer, physical and chemical transformations, dynamic changes in electrical conductivity, dynamic pH changes, and geochemical reactions. The modeling of the two primary transport processes, electromigration and electroosmosis, have been reported to adequately model ion transport assuming dilute solutions, rapid dissociation-association chemical reactions, and small electric double layer thickness. The aforementioned transport of ions changes the local concentration distributions, and therefore temporal and spatial fluctuations in electrical conductivity are experienced. These fluctuations change the electric potential at different locations within the system, and as a result the transport rates change as well. Modeling the migration of ions in the bulk fluid requires considering the changing electric field, as well as other affects that may inhibit mobility.

The concentration and mobility of each ion in the pore water at each point in time must be known to determine the evolution of electrical resistance and the electric potential distribution. This calculation requires a set of conservation equations for each ion in solution, which must be integrated simultaneously. Due to the complexity of this calculation, a solution can generally only be found through numerical methods.

For a simplified approach, a one-dimensional model can be derived by treating the electrokinetic system as an electrical circuit, as described by Wilson, Rodriguez-Maroto, and Gomez-Lahoz, and summarize in the following section.[32]

The one-dimensional system is divided into $N_i + 2$ gridblocks, as shown in Figure 2.13.

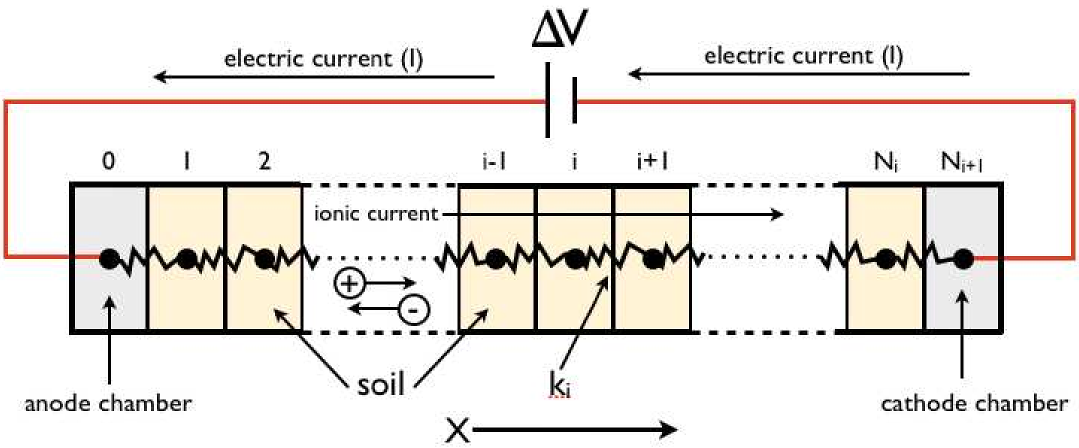

Figure 2.13 Schematic illustrating the foundations of a 1-dimensional model for contaminant transport by electrokinetic phenomena.[32]

A series of assumptions are required for this one-dimensional model, including:

- The soil is completely saturated with water.
- Electromigration is the only significant transport mechanism.
- The potential drop in the electrode compartments is considered negligible.
- Electrolysis reactions occurring at the anode and cathode are water oxidation and reduction, respectively.
- Chemical reaction rates are greater than transport rates such that local equilibrium conditions can be assumed.
- The electrokinetic system is electrically insulated.
- The current density is maintained at a constant value.

These assumptions can limit the model by ignoring synergistic effects of multiple chemical species, not considering temperature effects, and not considering the effect of pH and ionic strength on adsorption equilibria.

Voltage Drop

The electrical resistance of the soil and the electrode processes create two distinct voltage drops in series in an electrokinetic system. The resistance of a soil to ionic current flow can be determined through Ohm's law for a single volume element then applied to each element of the gridblock system. The total electrical resistance is the sum of the resistance of each of the N_i volume elements:

$$R = \sum_{i=1}^{N_i} R_i \tag{13}$$

and the resistance of the *i*th volume element is given by

$$R_i = \frac{\Delta x \tau}{A \omega} * \frac{1}{\sum_{k=1}^{N_k} \lambda_k C_{ik}} \tag{14}$$

where Δx is equal to the thickness of the volume element, τ is the tortuosity of the soil, A is the cross-sectional area, ω is the porosity of the soil, N_k is the number of ions in the pore water, λ_k is the molar conductivity of the *k*th ion, and C_{ik} is the concentration of the *k*th ion in the *i*th volume element.

The voltage drop due to electrode activity can be determined through the standard reduction potentials of the half reactions occurring at the electrodes and the Nerst equation. This assumes the partial pressure of gases to be 1 atm, and the temperature to be 25°C.

$$\text{Cathode: } 4H_2O + 4e^- \leftrightarrow 4OH\text{-}_{(aq)} + 2H_{2(gas)} \quad E^0 = -0.828\ V \tag{15}$$

$$\text{Anode: } 2H_2O \leftrightarrow 4H^+_{(aq)} + O2_{(gas)} + 4e^- \quad E^0 = -1.229\ V \tag{16}$$

$$E = (-0.828V - 1.229V) - \frac{RT}{F}(\ln [OH^-]_{cathode} + \ln [H^+]_{anode}) \tag{17}$$

$$E = -1.23 - 0.059\,(pH_{cathode} - pH_{anode}) \tag{18}$$

The potential difference between electrodes is described as the sum of these two voltage drops:

$$\Delta V = |\,E\,| + IR \tag{19}$$

$$\Delta V = |- 1.23 - 0.059\,(pH_{cathode} - pH_{anode})\,| + I\sum_{i=1}^{N_i}\frac{\Delta x\tau}{A\omega} * \frac{1}{\sum_{k=1}^{N_k}\lambda_k C_{ik}} \tag{20}$$

Equation 2.20 can be used to calculate the electric current flowing between electrodes in an electrokinetic system, assuming a constant electric potential drop.

Modeling Transport by Electromigration

Based on the assumption that electromigration is the only significant transport phenomenon, a mass conservation equation for a single volume element can be described as:

$$(\Delta x A\omega)\frac{dC_{ik}}{dt} = \dot{n}_{ik} - \dot{n}_{i-1k} \quad for\ k = 1, 2, 3 \ldots N_k \tag{21}$$

where $\dot{n}_{ik}$ is the molar flow of the *k*th ions from the $(i+1)$th volume element toward the inside of the *i*th volume element. This is proportional to the electric current according to the expression:

$$\dot{n}_{ik} = \frac{-I}{z_k F} t_{ik} \tag{22}$$

where the product of z_k and F is Faraday's constant. The current density due to the *k*th ions divided by the sum of the current densities of all the ions in the electrolyte determines t_{ik}, the transport number of the *k*th ions. The negative sign is a convention used to indicate that the flow of cations is through the right face of the *i*th cell, and therefore anions move in the opposite direction (Figure 2.14).

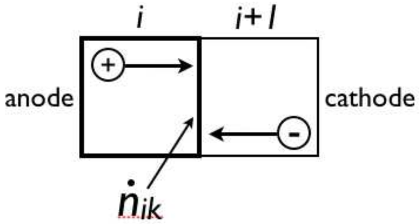

Figure 2.14 Molar flows of cations and anions through the right side of the *i*th volume element.

The total conductivity between the *i*th and *(i+1)*th volume elements, k_i, can be described by the sum of the contribution to the conductivity of the cations moving to the right and the anions moving to the left. This can be expressed as:

$$k_i = \sum_{k=1}^{N_k} \lambda_k [C_{ik} S(z_k) + C_{i+1} S(-z_k)] \tag{23}$$

where *S(x)* is a function to differentiate between the directional movement of anions and cations. It has a value of 0 if *x* is lower than or equal to zero, and a value of 1 if *x* is greater than zero.

$$S(x) = \begin{cases} 0 & x \leq 0 \\ 1 & x > 0 \end{cases} \tag{24}$$

The fraction of the total current carried by the *k*th ions between the two volume units, t_{ik}, can be calculated as the ratio between the contribution of these ions to the conductivity and the total conductivity at the boundary face:

$$t_{ik} = \frac{m [C_{ik} S(z_k) + C_{i+1k} S(-z_k)]}{k_i} \tag{25}$$

The molar flow of the *k*th ions between the *i*th and *(i+1)*th volume elements can then be expressed as:

$$\dot{n}_{ik} = \frac{-I}{z_k F} \frac{\lambda_k [C_{ik} S(z_k) + C_{i+1k} S(-z_k)]}{k_i} \quad for\, k = 1, 2, 3 ... N_k \;\; and \;\; for\, 1 \leq i \leq N_i \tag{26}$$

Substituting this expression into the mass conservation equation yields:

$$(\Delta x A \omega) \frac{dC_{ik}}{dt} = \frac{-I\lambda_k}{z_k F} \left(\frac{[C_{ik} S(z_k) + C_{i+1k} S(-z_k)]}{k_i} - \frac{[C_{i-1k} S(z_k) + C_{i+1k} S(-z_k)]}{k_{i-1}} \right) \tag{27}$$

Lastly, the new values of the concentrations at the time $t+\Delta t$ can be calculated using a numerical solution of this ordinary differential equation. Euler's method is often used for its simplicity:

$$C^{*}_{ik}(t+\Delta t) = C_i(t) + \left.\frac{dC_{ik}}{dt}\right|_{t} \Delta t \tag{28}$$

$$C^{*}_{ik}(t+\Delta t) = C_i(t) + \frac{-I\lambda_k}{(\Delta x A\omega)\, z_k F}\left(\frac{[C_{ik}S(z_k) + C_{i+1k}S(-z_k)]}{k_i} - \frac{[C_{i-1k}S(z_k) + C_{i+1k}S(-z_k)]}{k_{i-1}}\right)\Delta t \tag{29}$$

These equations describe the contaminant concentrations at all of the inner volume elements however don't consider the electrode reservoirs, which are the system boundaries. The right-side boundary is assumed to be electrically insulated because molar flow through the right side of the cathode reservoir is not possible. Therefore molar flow needs only to be calculated through the N_ith cell and the cathode, which is already calculated by Equation 2.26. Additionally taking place in the cathode reservoir is the generation of hydroxyl ions (one mole of hydroxyl ions per one Faraday of circulating charge), which must be considered in the mass conservation equation.

For all ions in the cathode reservoir with the exception of hydroxyl ions,

$$V_{Ni+1}\frac{dC_{Ni+1k}}{dt} = -\dot{n}_{Nik} \tag{30}$$

where V_{Ni+1} is the volume of the cathode compartment:

$$V_{Ni+1}\frac{dC_{Ni+1k}}{dt} = \frac{I\lambda_k}{z_k F}\left(\frac{[C_{Nik}S(zk) + C_{Ni+1k}S(-zk)]}{\chi_{Nik}}\right) \tag{31}$$

For k = hydroxyl ions,

$$V_{Ni+1}\frac{dC_{Ni+1k}}{dt} = -\dot{n}_{Nik} + \frac{I}{F} \tag{32}$$

$$V_{Ni+1}\frac{dC_{Ni+1k}}{dt} = \frac{I\lambda_k}{z_k F}\left(\frac{[C_{Nik}S(zk) + C_{Ni+1k}S(-zk)]}{\chi_{Nik}}\right) + \frac{I}{F} \tag{33}$$

The concentration at each time point can be obtained similarly to the concentrations in the inner compartments using Euler's method.

The left side boundary extends to the left end of the anode compartment, and is electrically insulated as well. Therefore ionic flow only travels through the face on the right end of the anode compartment:

$$\dot{n}_{0k} = \frac{-I}{z_k F}\frac{\lambda_k\left[C_{0k}S(z_k) + C_{1k}S(-z_k)\right]}{\chi_0}\ for\ k = 1, 2, 3 \ldots N_k \tag{34}$$

In the anode compartment the constant production of protons must be considered in the mass conservation equation as well. For all ions except protons,

$$V_0\frac{dC_{0k}}{dt} = \dot{n}_{0k} \tag{35}$$

where V_0 is the volume of the anode compartment. Therefore,

$$V_0\frac{dC_{0k}}{dt} = \frac{-I\lambda_k}{z_k F}\left(\frac{\left[C_{0k}S(z_k) + C_{1k}S(-z_k)\right]}{\chi_0}\right) \tag{36}$$

For protons,

$$V_0\frac{dC_{0k}}{dt} = \dot{n}_{0k} + \frac{I}{F} \tag{37}$$

$$V_0\frac{dC_{0k}}{dt} = \frac{-I\lambda_k}{z_k F}\left(\frac{\left[C_{0k}S(z_k) + C_{1k}S(-z_k)\right]}{\chi_0}\right) + \frac{I}{F} \tag{38}$$

Once again the concentration can be solved for at each consecutive time point in the same manor as before. This series of equations describes the transport steps, however this doesn't consider sources and sinks in the system. The consumption or production of ions needs to be calculated independently from the transport model. By assuming that reaction rates are high, it can be considered that local equilibrium is rapidly reached. This means that the change in concentration of the various chemical species considered in the model can be calculated using the mass action equations of the involved chemical reactions. The transport calculation step will determine preliminary concentrations of species in each volume element, which are not at chemical equilibrium. The equilibrium concentrations can be determined from the solution in each volume element from the mass conservation equations, the electroneutrality condition of the aqueous phase, and constraints set of the nonlinear mass action equations. This is a common problem in modeling of environmental systems, and can be solved using a variety of available computer programs such as Visual MINTEQ and PHREEQC.

2.5. Zero-Valent Iron Nanoparticles

Basis for use in Groundwater Remediation

Zero-valent iron (ZVI) for use as a reactive sorbent for contaminant removal from water has been evaluated for many contaminants over the last few decades. Zero-valent-state metals serve as electron donors for reducing redox active metals to valence states that generally have lower solubility in water.[33] ZVI is a strong reductant, as can be seen from the negative standard potential of the Fe^{2+}/Fe^{0} couple.[34]

$$Fe^{0}_{(s)} \leftrightarrow Fe^{2+}_{(aq)} + 2e^{-} \qquad E^{0} = -\,0.44V \tag{39}$$

Due to the low electrode potential of the Fe^{0}/Fe^{2+}, electrons are given up by iron as a result of electrochemical corrosion in aqueous solution until all ZVI is depleted (Noubactep and Schoner, 2009). Oxidized species in solution will accept the excess of electrons and become reduced. In aerobic conditions, dissolved oxygen behaves as the primary electron acceptor by the reaction:[36]

$$2Fe^{0}_{(s)} + O_{2(g)} + 2H_2O_{(l)} \rightarrow 2Fe^{2+}_{(aq)} + 4OH^{-}_{(aq)} \tag{40}$$

In anaerobic conditions where oxidized species and dissolved oxygen are absent, water will serve as the electron acceptor under alkaline to slightly acidic conditions, and under acidic conditions protons will serve as electron acceptors.[34]

$$Fe^0_{(s)} + 2H_2O_{(l)} \rightarrow Fe^{2+}_{(aq)} + 2HO^-_{(aq)} + H_{2(g)} \quad (41)$$

$$Fe^0_{(s)} + 2H^+_{(aq)} \rightarrow Fe^{2+}_{(aq)} + H_{2(g)} \quad (42)$$

The anaerobic corrosion of iron is slow relative to the rapid corrosion in the presence of dissolved oxygen. In many groundwater remediation applications using ZVI, the dissolved oxygen content is very low and therefore the rate of ZVI dissolution is slow.

ZVI has been shown to be effective in the treatment of many target groundwater contaminants such as PCE, TCE, CT, energetic munitions (TNT) and RDX, many pesticides, and heavy metals.[37] ZVI was first used for groundwater remediation in the 1990s in the form of a permeable reactive barrier (PRB). A PRB is a barrier constructed out of a material specific for the treatment of a contaminant, which is then strategically placed in soil or a shallow aquifer to intercept contaminants as they move with the groundwater. Since their introduction, over 100 PRBs have been constructed in the United States, and many have been a success. PRBs can be effective for the right application, however they are limited in application and have many disadvantages. They require a very large amount of iron, and once placed in the ground they cannot be moved or adjusted. They cannot be applied to deep aquifers, and they come with high costs associated with the construction and placement in the ground. A promising alternative to the use of macro or even micro scale ZVI is zero-valent iron nanoparticles (nZVI). NZVI offer a significant increase in reductive capacity of contaminants per unit mass, and their nanoscale size enables them to move with water flow through aquifers. NZVI have a much higher density of reactive sites, as well as a higher intrinsic reactivity. Certain contaminants have been shown to be inert in the presence of micro-scale iron, but react rapidly with nZVI.[38] Other contaminants that are known to react with macro-scale ZVI will react with nZVI at much higher rates.

NZVI is a multipurpose environmental remediation tool, as it is reactive in water and is an excellent electron donor. The typical core-shell structure of an nZVI particle is shown in Figure 2.15. In the production of nZVI the particles are initially entirely Fe^0, however rapid oxidation of the exterior creates an iron oxide shell (FeOOH). The core remains as metallic, or zero-valent iron. The mixed valence iron oxide shell is effective at reducing heavy metals, as well in the reduction of chlorinated hydrocarbons. While nZVI are generally described as spherical in shape, they are typically extremely porous in structure, which greatly increases the ratio of reactive surface area to mass.

A concern regarding the use of nZVI in natural systems is their tendency to agglomerate and form larger particles and settle out of solution by gravity, or adsorb to soil particles. Many conditions affect the degree of agglomeration, such as pH, the presence of multi- or mono-valent cations, and natural organic matter. NOM in solution will quickly bind to the nZVI surface,[39] and pH and presence of cationic species will affect particle stability by influencing electric double layer interactions.[40] These factors reduce mobility and lifetime in the subsurface, in some cases rendering them inactive.

A strategy to counteract agglomeration is to coat nZVI with an organic polymer layer to increase the surface charge of the particle in solution. Strong repulsive forces between particles as a result of these surface coatings give nZVI colloidal properties, allowing them to stay suspended for long periods of time. Some commonly used dispersants are carboxylmethyl cellulose (CMC), polystyrene sulfonate (PSS), and polyacrylic acid (PAA).[41] Some research groups have attempted to use humic acids as a dispersant, however there are indications that humic acids can act as bridges between particles when present in high concentrations, increasing aggregation rates.[42]

The reduction of Cr^{VI} by a surface stabilized nZVI particle was investigated by using CMC as a dispersant.[43] CMC is a water-soluble carbohydrate chain that is environmentally friendly, biodegradable, and commercially available, making it a good candidate for groundwater remediation work as a nanoparticle stabilizer. SEM imagery showed that the CMC solution dispersed nanoparticles in solution and reduced aggregation significantly. Additionally, CMC-stabilized nanoparticles exhibited higher removal efficiency of Cr^{VI} relative to bare nanoparticles. A 10 mg/L Cr^{VI} solution was reduced by 94% over a 60-minute period in the presence of 0.1 g/L nZVI coated in a 0.5 g/L CMC solution, while only 52% removal was observed under the same conditions in the absence of CMC.[43]

In the same study, the presence of calcium was shown to affect Cr^{VI} removal by CMC-stabilized nZVI. In previous studies, a 10 mg/L Cr^{VI} solution was spiked with calcium for final concentrations of 0, 1, 2, and 5 mM Ca^{2+} and nZVI was added for a final concentration of 0.1 g/L. Cr^{VI} removal efficiencies were found to be 94, 47, 56, and 61% for 0, 1, 2, and 5 mM Ca^{2+} respectively. With increasing Ca^{2+} concentration (up to 1mM), monovalent ions are replaced by multivalent calcium ions resulting in CMC-metal precipitates, blocking Cr^{VI} precipitation. With increasing Ca^{2+} concentration (beyond 1 mM) the formation of $Ca(OH)_2$ can occur as well and the absorption of Cr^{VI} by $Ca(OH)_2$ can possibly take place.[43]

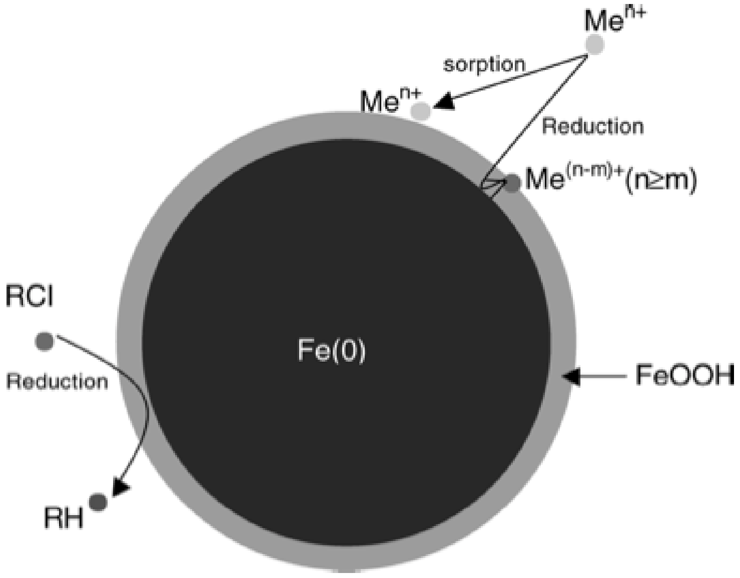

Figure 2.15 The core-shell structure of nZVI.[44]

Synthesis of nZVI

The synthesis of nZVI is a relatively simple process, making the use of nZVI on a large scale feasible and economically competitive. The most widely used procedure is a bottom-up approach referred to as the borohydride reduction method.[44] Borohydride is a strong reductant capable of reducing Fe^{III} and Fe^{II} to Fe^0 by the following reaction:

$$Fe(H_2O)_6^{2+} + 2BH_4^- \rightarrow Fe^0 + 2BH(OH)_3 + 7H_2 \qquad (43)$$

The process is performed under nitrogen gas, and begins with 0.25 M sodium borohydride ($NaBH_4$) added dropwise to 0.045 M ferric chloride until a 1:1 volume ratio is reached. The nanoscale Fe^0 precipitates form during the reaction described in Equation 2.43, and can be collected by vacuum filtration. The nZVI are rinsed repeatedly with deoxygenated water, or with a water-ethanol mixture, then dried and stored under nitrogen gas. Before use, the nZVI are added to water to make a slurry, or they can be mixed as a slurry with an aqueous solution containing a dispersant, enhancing particle stability. In either case the slurry is sonicated immediately before use to reduce the average particle size by breaking apart aggregates.

Cr^{VI} Reduction with nZVI

Numerous lab-scale and field-scale studies have shown the reduction of Cr^{VI} by nZVI to follow a reduction-precipitation process (Powell et al, 1995; Blowes et al., 1997: Alowitz and Scherer, 2002; Wilkin et al., 2005). The electrons released during nZVI corrosion are accepted by Cr^{VI}, which in turn becomes reduced to Cr^{III}. There are several Cr^{VI} reduction pathways that have been suggested for reaction with nZVI. The following pathway assumes a direct electron transfer from the nZVI surface to the Cr^{VI} oxidized species to cause direct reduction to Cr^{III} by the following equation:[45,46]

$$2HCrO_4^-{}_{(aq)} + 3Fe^0{}_{(s)} + 14H^+{}_{(aq)} \rightarrow 3Fe^{2+}{}_{(aq)} + 2Cr^{3+}{}_{(aq)} + 8H_2O_{(l)} \qquad (44)$$

This reduction process has been proposed to occur in aqueous solution through the following five steps:[47,48] 1) diffusion of Cr^{VI} from the bulk fluid through the electric double layer to the nZVI surface, 2) adsorption of Cr^{VI} onto the surface of unreacted nZVI, 3) reduction of Cr^{VI} at the nZVI surface through the formation of Fe^{III}-Cr^{III} precipitates, 4) desorption of the reduction products from the surface of the oxidized iron, 5) diffusive transport of the reduction product back into the bulk solution. Upon complete oxidation of the nZVI surface, Cr^{VI} reduction can still occur with slower rates at the particle surface, or can occur within the pores of nZVI by diffusion though the iron particle.[48]

An alternative Cr^{VI} reduction pathway is through an indirect mechanism where Cr^{VI} is reduced by Fe^{2+} ions formed in the oxidation of nZVI, which occurs through the mechanism previously described:[45,46]

$$HCrO_4^-{}_{(aq)} + 3Fe^{2+}{}_{(s)} + 7H^+{}_{(aq)} \rightarrow 3Fe^{3+}{}_{(aq)} + Cr^{3+}{}_{(aq)} + 4H_2O_{(l)} \quad (45)$$

The net Cr^{VI} reduction reaction with nZVI by indirect and direct mechanisms is:

$$HCrO_4^-{}_{(aq)} + Fe^0{}_{(s)} + 7H^+{}_{(aq)} \rightarrow Fe^{3+}{}_{(aq)} + Cr^{3+}{}_{(aq)} + 4H_2O_{(l)} \quad (46)$$

The reduction of Cr^{VI} by reduction-precipitation reaction with nZVI can in general be described by a pseudo first-order kinetic model:[49,50]

$$\frac{d[Cr(VI)]}{dt} = -k_{obs}[Cr(VI)] \quad (47)$$

where [Cr(VI)] is the Cr^{VI} concentration and k_{obs} is the observed Cr^{VI} reduction rate constant with units of inverse time. The kinetics of this reaction are dependent upon the type and size of nZVI, the solution chemistry, and how solution chemistry alters the nZVI surface. A schematic representing Cr^{VI} reduction pathways is illustrated in Figure 2.16.[51]

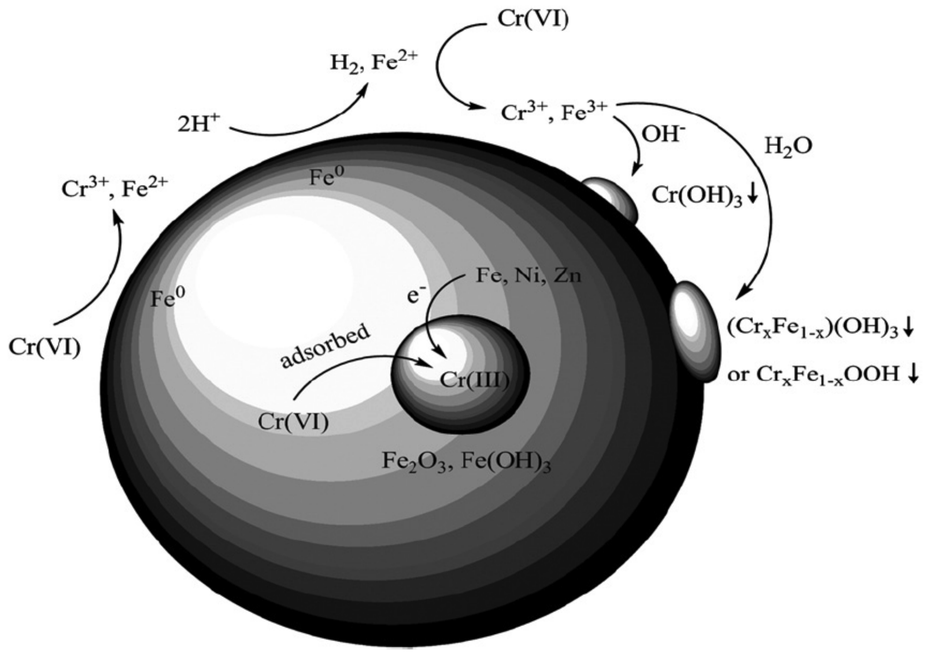

Figure 2.16 Theoretical schematic of Cr^{VI} reduction mechanisms by nZVI.[51]

Effect of Background Humic Substances on Cr^{VI} Remediation with nZVI

The presence of humic substances in an nZVI remediation system will create a series of complex interactions that have been shown to have the capacity to enhance or interfere with Cr^{VI} reduction. As previously discussed, humic substances can complex Cr^{VI} which influences the fate and transport of Cr^{VI} in the subsurface, and additionally humic substances have strong interactions with nZVI. When humic acids coat the surface of nZVI, the reactivity of the particle towards Cr^{VI} decreases dramatically as it's reductive capacity is largely exhausted by reaction with humic acid.

Multiple studies investigating macro-scale ZVI reduction of Cr^{VI} in the presence of humic acids have shown an insignificant decrease in ZVI reductive capacity, with this small inhibitory effect due to a coating of humic acid on the oxidized iron surface.[52-54] It is hypothesized that this effect could be enhanced in the presence of divalent metals such as Ca^{2+} and Mg^{2+}, as these can facilitate the aggregation of humic acids and the precipitation of these larger agglomerates on the iron surface.

Recently however, studies have determined that humic acids may enhance the reduction of Cr^{VI} by ZVI, possibly due to an increased amount of dissolved iron in the form of soluble Fe-humate complexes, suppressing the precipitation of iron corrosion products at the surface of ZVI.[55]

The presence of humic acids have a more significant effect on Cr^{VI} reduction by nanoscale ZVI relative to macro-scale ZVI. Humic acids were found to adsorb rapidly to nZVI in aqueous solution by a pseudo-first-order reaction, and a maximum adsorption capacity of 80 mg humic acid per g nZVI was achieved.[39] In this same study, the presence of humic acid at 20 mg/L was shown to decrease arsenic removal from aqueous solution by 43%. This decrease in efficiency was attributed largely to competitive adsorption of humic acids to reactive sites on the nZVI surface. Possible mechanisms of humic acid adsorption to oxidized iron are presented in Figure 2.17.[56]

A separate investigation of the effects of humic acid on Cr^{VI} treatment by non surface-stabilized nZVI concluded that humic acid inhibits Cr^{VI} reduction.[43] Humic acid coats nZVI surfaces, occupying reactive surface sites, and can also increase nanoparticle aggregation by forming particle bridges. The interactions between the nanoparticle and humic acid however will change when a surface-stabilizing agent is present. A dispersant such as CMC may repel humic acid due to the predominant negative charge it carries, reducing the previously reported adverse effects. Conversely, the opposite may occur as well if interactions between humic acid and nanoparticles are promoted by the presence of a surface-stabilizing agent.

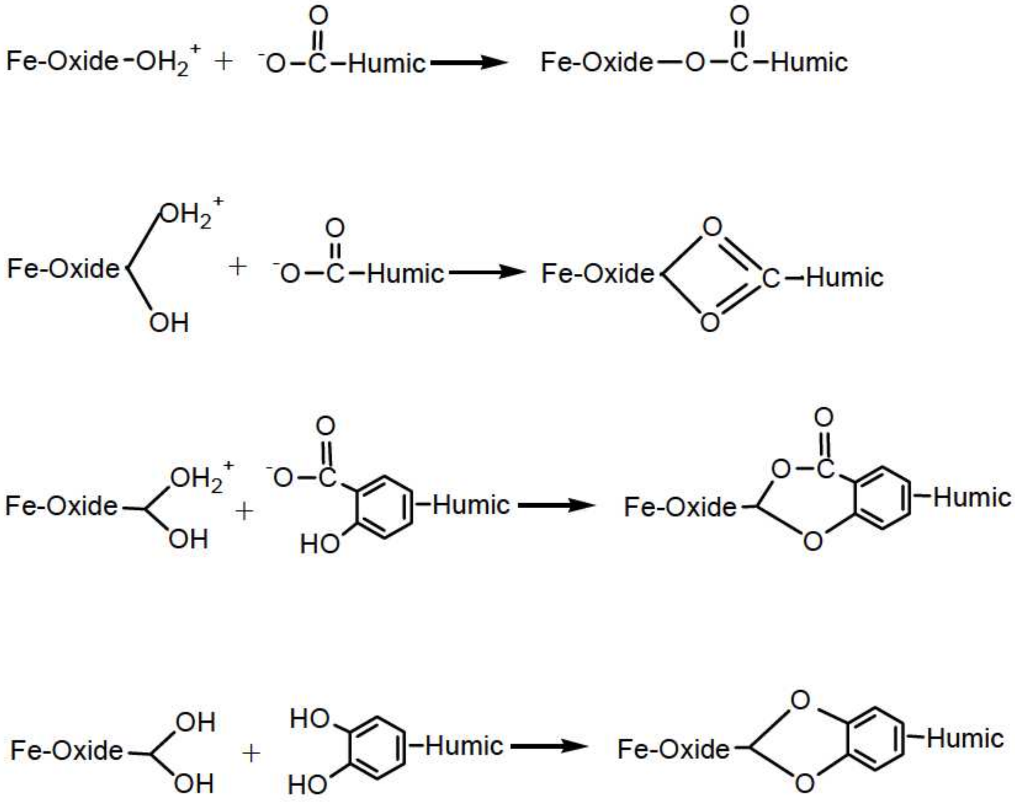

Figure 2.17 Possible mechanisms of humic acid adsorption to oxidized sites on iron nanoparticles.[56]

Transport of nZVI through soils by Electrokinetic Phenomena

A variety of surface modifications have been used in attempts to increase the stability of nanoparticles and enhance the migration potential of these particles through porous media. Surface-stabilizer solutions have been shown to be effective for these applications, however as the hydraulic conductivity of a soil decreases, the advective flux becomes smaller for a constant hydraulic head gradient, and nZVI delivery becomes more challenging.[57] Under typical aquifer conditions surface-stabilized nZVI carry a negative surface charge, and therefore application of electrokinetics has been proposed to transport nZVI by electrophoresis through soils of low hydraulic conductivity.

Electrokinetic studies have had some success in nZVI transport by electrophoresis. Jones and coworkers achieved breakthrough of nZVI through a 10-cm soil column loaded with a sand soil (300 μm particle size) after 25 hours of electric potential application at 1.3 V/cm.[58] However when the same study was conducted using the same sand but a smaller average particle size (90 μm), the breakthrough time increased significantly. A similar study corroborated these results with the transport of surface-stabilized nZVI through a 5.0 cm soil column packed with a silica sand with an average particle size of 195 μm.[57]

Transport through idealized sand soils has been shown as effective on the lab scale, however a very limited number of studies have evaluated the potential of nZVI transport through clay or silt soils. Furthermore, the influence of common groundwater constituents such as minerals and organic matter on the electrophoretic transport of nZVI have yet to be considered.

2.6. Microbial Fuel Cells and Cr^{VI} Reduction

Theory of Microbial Fuel Cell Operation

Microbial fuel cell (MFC) technology has been proposed as a source of renewable energy as well as a remediation tool. The applications of MFCs range from replacing batteries in electronic devices, to generating energy through wastewater degradation, to heavy metal treatment in water supplies. MFCs offer the capability to generate electricity by tapping into natural microbiological processes. The electrochemical reactions that occur during MFC operation provide reductive and oxidative environments in the cathode and anode compartments, respectively. These conditions can be optimized to drive redox reactions that either break down or remove toxic chemicals from water. This process works well in the reduction of many heavy metals, including Cr^{VI}, from soluble and highly toxic species to insoluble forms that can easily be removed. Numerous bacteria including *Pseudomonas dechromaticans, Escherichia coli, Desulfovibrio vulgaris, Shewanella oneidensis, and Enterobacter cloacae* among others have shown the capacity to reduce Cr^{VI} to insoluble Cr^{III} species.[59]

MFCs can be easily integrated with other process as can be seen in the wide variety of their application. In groundwater remediation applications for Cr^{VI} removal, contaminated water can be delivered directly to the cathode compartment accept electrons in the reduction to Cr^{III} species. Integration of this technology with electrokinetics can enhance the delivery of Cr^{VI} species to the cathode reservoir, which can decrease remediation time. The Cr^{VI} species can be transport through soil and concentrated near the anode reservoir of an electrokinetic system, and then pumped directly to an MFC for Cr^{VI} reduction. A schematic of this theory is illustrated in Figure 2.18, and shows how this cannot only be an effective integrated remediation system, but a green process as well. The use of a renewable energy resource such as solar power could be used to provide the energy required to run the electrokinetic transport system, which could be supplemented by the power output of the MFC.

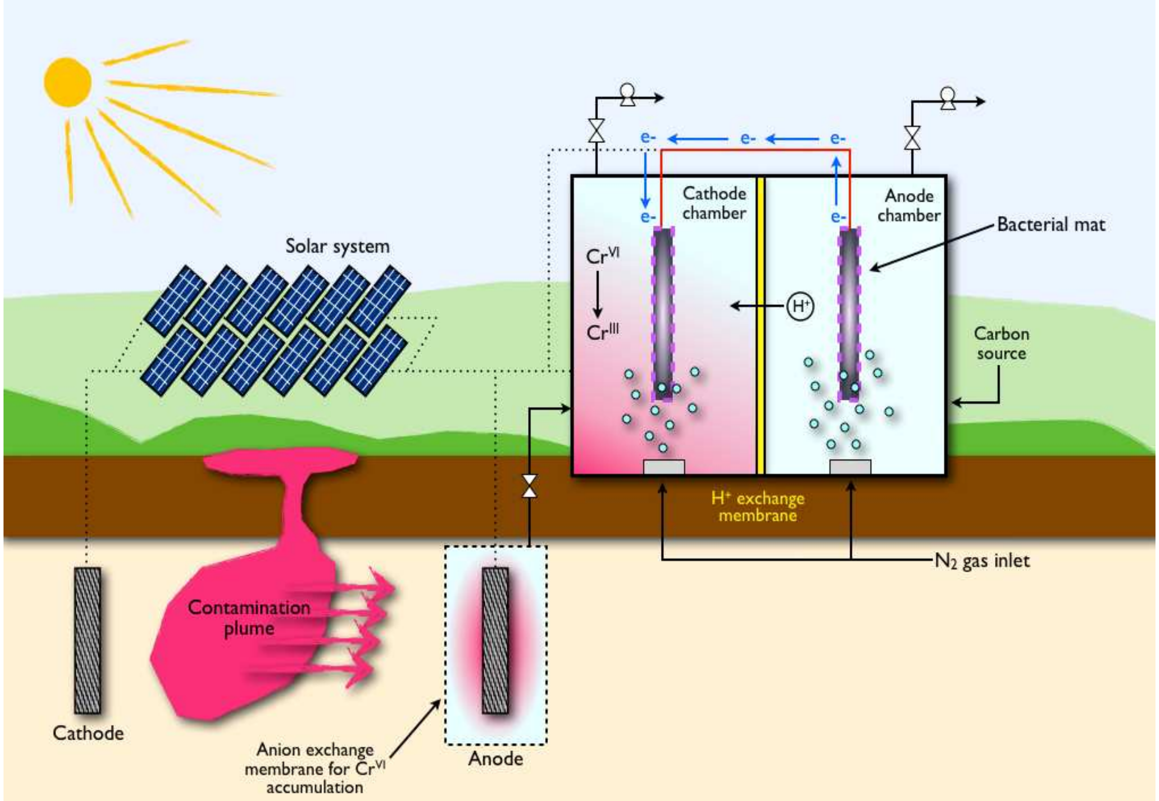

Figure 2.18 A conceptual rendering of MFC technology integrated with electrokinetic transport to enhance Cr^{VI} remediation in groundwater.

Bioelectricity was first realized by M.C. Potter in 1911, however not much evolved from this work until the mid to late 1900s. The potential of MFCs for energy generation was unveiled in the early 1990s by researchers like Allen and Bennetto. Their experiments were carried out using chemical mediators, or electron shuttles, to carry electrons from inside the bacterial cell to the electrodes. It was determined in a 1999 study that chemical mediators weren't actually necessary, as some bacteria can transfer electrons exogenously.[60]

In an MFC, microorganisms degrade organic matter, which produces electrons that travel through a series of respiratory enzymes in the cell and make energy for the cell in the form of ATP. The electrons are then released to a terminal electron acceptor, which becomes reduced by the electrons. Terminal electron acceptors such as oxygen, nitrate, and sulfate, diffuse into the cell and accept the electron, and the reduction product can diffuse out. Exoelectrogenic bacteria however are capable of transferring that electron to terminal electron acceptors outside of the cell, and it is these bacteria that can be used to power an MFC.

In an MFC the anode and cathode reservoirs are separated by a proton exchange membrane, which serves the purpose of maintaining anaerobic conditions in the anode compartment, as well as allowing the diffusion of H^+ ions to the cathode compartment. If oxygen is present in the anode reservoir, it will act as an electron acceptor and no electricity production will occur. The production of H^+ through the decomposition of organic matter can create acidic conditions in the anode compartment if the solution isn't well buffered, and H^+ needs to diffuse to the cathode compartment to react with electrons and form water. Nafion (Dupont Corp) is a cation exchange membrane designed to transfer protons, however in an MFC it preferentially conducts other positively charged species that are usually present in concentrations many orders of magnitude higher than protons. The MFC performance is adversely impacted by the competitive transport of other cations. If the proton transfer rate from the anode to the cathode is not sufficient, the pH will drop in the anode. This creates a harsh environment for bacterial respiration, which is what drives the current generation. In the cathode compartment the pH can rise if protons can't diffuse readily from the anode. This can lead to mass transfer limited proton transport to the biocatalyst.

Power Generation from Shewanella Species

Many bacteria are capable of transferring electrons to an electrode by using self-produced mediators, and some bacteria including *Geobacter* and *Shewanella* species are capable of producing conductive nanowires that can perform this function as well.[61] However it has not been determined to what degree if at all bacteria require the nanowires for electron transfer to a surface. *Shewanella oneidensis* grown anaerobically were shown to adhere to an iron surface with two to five times the force of those grown aerobically, which gives rise to the idea that the anaerobic conditions may allow closer contact for electron transfer from cell bound cytochromes without the use of nanowires. Chemical mediator electron transfer was supported by a variety of studies, including a finding that *Shewanella* could reduce iron encapsulated within a porous silica bead.[62] The specific mediators capable of accomplishing this task however were never isolated and identified. Upon finding that *Shewanella* produce nanowires, the theory of electron transfer shifted towards the possibility of using solely the nanowires. Studies have since shown nanowire penetration into silica beads, making reduction of the encapsulated iron possible from a distance.

Before the discovery of nanowires, chemical mediators were believed to be the sole route of electron transfer from bacteria to a surface. Some of the well-characterized exogenous mediators include neutral red, anthraquinone-2-6,disulfonate (AQDS), thionin, potassium ferricyanide, and methyl viologen.[63,64] It was later demonstrated that self-produced or endogenous chemical mediators such as pyocyanin and related compounds produced by *Pseudomonas aeruginosa* could shuttle electrons to a surface and produce electricity in an MFC.[65] Studies using mixed cultures have shown that many mediators produced in MFC reactors have characteristics like those of pyocyanin and can effectively transfer electrons to electrode surfaces.

Electricity production by *Shewanella* was demonstrated in the absence of an added chemical mediator, however cyclic voltammetry indicated that mediators were present in solution at the experiments end.[66] This implied that mediators were self-produced during MFC operation. In a 2002 study, Park and Zeikus[67] reached a power density of 10.2 mW/m^2 from an MFC using *Shewanella putrefacians* and lactate as a substrate. When the carbon source was switched to pyruvate, a small drop in power density was observed, and the power density dropped to 1.6 and 1.9 mW/m^2 using acetate and glucose, respectively. This finding was in agreement with previous work indicating that *Shewanella* are incapable of utilizing these substrates. When a chemical mediator was incorporated into the graphite electrode, the power density increased by about an order of magnitude.[68] A 2006 study increased power density drastically from previous work by growing a culture of *Shewanella oneidensis* in lactate and feeding into a small MFC (1.2 cm^3), with ferricyanide catholytes.[69] The power production peaked at 3 W/m^2, and upon addition of mediators the power production increased by 30-100%. These studies indicate that while the exact electron transfer mechanism from *Shewanella* to electrode surfaces are not fully understood, the addition of chemical mediators are not required, however they do enhance current generation. The development of the biocathode has been a recent breakthrough for MFC technology for groundwater remediation, as biofilm growth on the cathode catalyzes the reduction of Cr^{VI}, which is a very slow reaction under abiotic conditions.

Voltage and Power

The typical voltage range achieved by MFCs is between 0.3 and 0.7 V, and the current generated in a single MFC on the lab scale is generally so small that it is not measured but generally calculated. The voltage output, current, and external resistance on a circuit are summarized in the next section from Bruce Logan's, *Microbial Fuel Cells.*[70]

$$E = I\, R_{ext} \tag{48}$$

where E represents the voltage. The resistance and voltage are proportional to one another, and the maximum voltage production is the open circuit voltage where the resistance is infinite and the current is zero. In chemical fuel cells the voltage can be well predicted, however microbial fuel cells are much more complicated due to start-up times required for bacteria to colonize electrodes, and the dynamics of electron transfer from bacteria to the electrodes. In mixed cultures the power output is regulated by the specific species that grow, which makes potential prediction with any degree of accuracy very difficult, and even for pure cultures the power output cannot be predicted. What can be determined though is the upper limit of voltage generation that is possible for an electron donor and acceptor pair. The maximum electromotive force that can be created in a fuel cell is given by:

$$E_{\mathrm{emf}} = E^{0} - \frac{RT}{nF}\ln(\Pi) \qquad (49)$$

where E^0 is the standard cell potential based on hydrogen under standard conditions where $E^0(H_2) = 0$, R is the universal gas constant, T is the temperature, n is the number of electrons transferred, and F is Faraday's constant. The reaction quotient is given by:

$$\Pi = \frac{[products]^{\mathrm{p}}}{[reac\tan ts]^{\mathrm{r}}} \qquad (50)$$

where p and r are the respective stoichiometric coefficients.

The reported potentials in biological systems are usually adjusted to the pH value of the cytoplasm in most cells, which is about 7. The standard potential for hydrogen at 298 K can then be calculated to be -0.414V. In the laboratory however, temperatures are generally maintained at 303 K for the incubation of bacteria, which results in a hydrogen potential of -0.421 V. The standard potentials for various anodic and cathodic reactions will change depending on specific pH values, temperatures, and pressures and need to be adjusted to accommodate for these conditions.

For MFCs to be useful in power generation, the voltage output is the primary variable to optimize. Power is calculated from a voltage and current as $P = I\,E$, and in an MFC the power output is calculated from the measured voltage across the load as

$$P = I\,E_{MFC} \qquad (51)$$

In a laboratory scale MFC, the current can be calculated using $I = E_{MFC} / R_{ext}$ and the power output can then be calculated as

$$P = \frac{E^2_{\mathrm{MFC}}}{R_{\mathrm{ext}}} \tag{52}$$

Power output is generally normalized in terms of the surface area of the anode, A_{an}, to accommodate for the differences in MFC architecture. The power density of the MFC is then calculated as

$$P_{\mathrm{An}} = \frac{E^2_{\mathrm{MFC}}}{A_{\mathrm{An}} R_{\mathrm{ext}}} \tag{53}$$

Factors that Affect Cell Voltage

The power output for an MFC is always less than the theoretical maximum potential calculated for the cell. Cheng and Logan[71] obtained a maximum voltage of 0.83V using oxygen at the cathode for an air-cathode MFC. The theoretical maximum potential of the cell, E^0_{cell}, is calculate to be 1.1V. The differential between the two voltages is likely due to the maximum potentials that can be established by bacterial enzymes. In a typical MFC, there are three regions of voltage drop. The first is a rapid drop as current flows through the circuit, the second is a slow, linear decrease in voltage, and the last is a second rapid decrease at high current densities. At any specific current, the cell voltage produced is the result of voltage losses due to electrode overpotentials and ohmic losses, which can be written as

$$E_{emf} = E^0 - (\Sigma OP_{An} + |\Sigma OP_{\mathrm{Cat}}| + I\,R_{\Omega}) \tag{54}$$

where ΣOP_{An} and $|\Sigma OP_{Cat}|$ are the overpotentials of the anode and cathode respectively, and the ohmic losses (IR_{Ω}) are proportional to the current and the resistance of the system. The voltage losses between the electrodes are most obvious at low current densities, however the voltage losses continuously change with the specific current.

The three voltage drops are more specifically due to activation, bacterial metabolism, and mass transport. Activation losses are due to the energy lost as heat in oxidation-reduction reactions, as well as the energy lost through the transfer of an electron from the cell terminal protein or enzyme to the anode surface. These loses can be mitigated by using more efficient catalysts at the cathode, different bacteria at the anode, or enhancing electron transfer between bacteria and the anode.

Bacterial metabolism loses are unavoidable as they are a result of energy derivation by substrate oxidation. In theory, bacteria only need enough energy to push one electron across a membrane using the Krebs cycle, or to make one ATP by substrate phosphorylation. In actuality, most bacteria pump numerous protons across the membrane per NADH oxidized. Acetate oxidation by substrate fermenting bacteria results in the production of several ATP as well. To maximize MFC power output, electron transfer must still be possible at the most negative anode potential achievable.

Another loss of voltage is due to mass transfer of reactants to the electrode or the mass transfer of products from the electrode, which have the effect of slowing the rate of reaction. In theory this could largely inhibit power output, however this has not been shown to be significant problem in laboratory MFCs. Mass transfer across the MFC can be a problem though, if protons cannot easily diffuse from the anode. An accumulation of protons leads to acidic conditions in the anode, and potentially high pH conditions in the cathode, which can limit power generation.[72] These loses can be minimized through addition of a sufficient buffer to the solution, as well as by limiting biofilm and other material growth on the cathode that can hinder proton diffusion.

Lastly, ohmic losses occur within an MFC, which can be greatly mitigated through MFC design. Ohmic losses are a product of resistance of proton conduction due to the solution and the membrane, and the losses from electron transport through the electrodes to wires or other contact points. By minimizing the space between electrodes, choosing materials with low resistances, maintaining good contact points, and increasing conductivity and buffering capacity, these losses are limited. These different factors however can only help to a certain extent with increasing power. For example bacteria cannot grow under highly saline solutions, and if the electrodes are too close the power production decreases despite lowering the ohmic resistance.[73] Additionally, the cost of materials used in optimizing an MFC must be taken into consideration especially when scaling-up.

2.7 Chapter 2 References

1. Acar, Y.B. and A.N. Alshawabkeh (1993). Principles of Electrokinetic Remediation. *Environmental Science and Technology*, 27(13): p. 2638.

2. Probstein, R.F. and R.E. Hicks (1993). Removal of Contaminants from Soils by Electric Fields. *Science*, 260(5107): p. 498-503.

3. Page, M. M., & Page, C. L. (2002). Electroremediation of Contaminated Soils. *Journal of Environmental Engineering*, *128*(3), 208.

4. *USGS Water Science School,* USGS.gov. 29, Oct. 2010. *http://ga.water.usgs.gov/edu/wugw.html*

5. Waller, R. (2013). *Groundwater and the Rural Homeowner*. USGS.gov, http://pubs.usgs.gov/gip/gw_ruralhomeowner/.

6. Fukushima, M. A., Nakayasu, K., Tanaka, S., & Nakamura, H. (1997). Speciation analysis of chromium after reduction of chromium (VI) by humic acid. *Toxicological & Environmental Chemistry*, 62(1), 207–215.

7. OEHHA (2011). *Final Technical Support Document on Public Health Goal for Hexavalent Chromium in Drinking Water*, http://oehha.ca.gov/water/phg/072911Cr6PHG.html, Updated 7/29/11.

8. Kotaś, J., & Stasicka, Z. (2000). Chromium occurrence in the environment and methods of its speciation. *Environmental pollution (Barking, Essex□: 1987)*, *107*(3), 263–83.

9. Ponnamperuma, F.N. (1972). The Chemistry of Submerged Soils. *Advances in Agronomy,* 24:29-95.

10. Pamukcu, S., A. Weeks, J.K. Whittle (2004). Enhanced Reduction of Cr(VI) by Direct Electric Current in a Contaminated Clay. *Environ. Sci. Technol.* 38:1236-1241.

11. Tipping, E. *Cation Binding by Humic Substances;* Cambridge University Press: Cambridge, 2002.

12. Cabaniss, Steve, Greg Madey, Patricia Maurice, Yingping Zhou, Laura Leff, Olacheesy head Bob Wetzel, Jerry Leenheer, and Bob Wershaw, comps, Stochastic Synthesis of Natural Organic Matter, part II: molecular property distributions. *Biogeochemistry,* 86(3): 269-286.

13. Stevenson F.J., *Humus Chemistry: Genesis, Composition, Reactions*. Wiley, New York (1982)

14. Thurman, E.M., *Organic Geochemistry of Natural Waters*. Martnum Nijhoff/Dr. W. Junk. Publishers, Dordrecht (1985).

15. Buffle, J., Greter, F.L., Haerdi, W. (1977) Measurement of complexation properties of humic and fulvic acids in natural waters with lead and copper ion-selective electrodes. *Anal. Chem.*, 49:216-222.

16. Jardine, P. M., Fendorf, S. E., Mayes, M. a., Larsen, I. L., Brooks, S. C., & Bailey, W. B. (1999). Fate and Transport of Hexavalent Chromium in Undisturbed Heterogeneous Soil. *Environmental Science & Technology*, *33*(17), 2939–2944.

17. Li, Y., Yue, Q.-Y., & Gao, B.-Y. (2010). Effect of humic acid on the Cr(VI) adsorption onto Kaolin. *Applied Clay Science*, *48*(3), 481–484.

18. Gu, B., & Chen, J. (2003). Enhanced microbial reduction of Cr(VI) and U(VI) by different natural organic matter fractions. *Geochimica et Cosmochimica Acta*, *67*(19), 3575–3582.

19. Yukselen, Y. and Kaya, A. (2003). Zeta potential of kaolinite in the presence of alkali, alkaline earth and hydrolyzable metal ions. *Water, Air, & Soil Pollution*, 155-168.

20. Holtz, R.D. and Kovacs, W.D. (1981). *An Introduction to Geotechnical Engineering*, Prentice Hall. (Chapter 4).

21. Zachara, J.M., C.E. Cowan *et al.* (1988). "Chromate adsorption by kaolinite." *Clay and Clay Minerals.* 36(4): 317-326.

22. Bhattacharyya, K. G., & Sen Gupta, S. (2006). Adsorption of Chromium(VI) from Water by Clays. *Industrial & Engineering Chemistry Research*, *45*(21), 7232–7240.

23. Grim, RE. 1968. Clay minerology. New York: McGraw hill. 596 p.

24. Kaya, A., & Yukselen, Y. (2005). Zeta potential of soils with surfactants and its relevance to electrokinetic remediation. *Journal of hazardous materials*, *120*(1-3), 119–26.

25. Yeung AT. (1994). Electrokinetic flow processes in porous media and their applications. *Advances in Porous Media,* Vol. 2 (ed. MY Corapcioglu). Amsterdam, the Netherlands: Elsevier, pp. 309-395.

26. Weng CH, Takiyama LR, Huang CP. (1994). Electroosmosis for the in-situ treatment of chromium-contaminated soil. *Hazardous and Industrial Wastes* 26:496-505.

27. Clarke RL, Kimmel S, Lageman R, Smedley SI. (1996). Electrokinetic remediation of soils, sludges, and groundwater. *Proceedings of the American Power Conference 1996,* April 9-11, Chicago, pp. 347-352.

28. Eykholt GR, Daniel DE. (1994). Impact of system chemistry on electro-osmosis in contaminated soil. *ASCE Journal of Geotechnical Engineering* **120**(5):797-815.

29. Sposito G. (1989). *The Chemistry of Soils.* New York: Oxford University Press.

30. Ottosen LM, Christenson IV, Rorig-Dalgaard I, Jensen PE, Hansen HK. (2008). Ulitization of electromigration in civil and environmental engineering. Processes, transport rates and matrix changes. *Journal of Environmental Science and Health Part A* **43**(8):795-809.

31. Reddy, K.R., and Cameselle, C., *Electrochemical Remediation Technologies for Polluted Soils, Sediments and Groundwater*, John Wiley & Sons, Inc., Hoboken, New Jersey (2009), pp. 29-48.

32. Wilson DJ, Rodriguez-Maroto JM, Gomez-Lahoz C. (1995a). Electrokinetic remediation. I. Modeling of Simple Systems. *Separation Science and Technology* 30(15):2937-2961.

33. Gheju, M., & Balcu, I. (2010). Hexavaelnt chromium reduction with scrap iron in continuous-flow system. Part 2: Effect of scrap iron shape and size. *Journal of Hazardous Materials,* 182, 484-493.

34. Scherer, M. M., Richte. S., Valentine, R. L., Alvarez, P.J., 2000. Chemistry and microbiology of permeable reactive barrier for in situ groundwater clean up. *Crit. Rev. Environ. Sci. Technol.* 30, 363-411.

35. Noubactep, C., & Schoner, A. (2010). Metallic iron for environmental remediation: Learning from electrocoagulation. *Journal of Hazardous Materials,* 175, 1075-1080.

36. Ponder, S. M., Darab, J. G., & Mallouk, T. E. (2000). Remediation of Cr(VI) and Pb(II) aqueous solutions using supported, nanoscale zero-valent iron. *Environmental Science & Technology*, *34*(12), 2564–2569.

37. Zhang, W. (2003). Nanoscale iron particles for environmental remediation: An overview. *Journal of nanoparticle Research*, *5*(3), 323–332.

38. Keane, E. (2010). *Fate, Transport and Toxicity of Nanoscale Zero-Valent Iron (nZVI) Used During Superfund Remediation*. Duke University.

39. Giasuddin, A. B. M., Kanel, S. R., & Choi, H. (2007). Adsorption of humic acid onto nanoscale zerovalent iron and its effect on arsenic removal. *Environmental science & technology*, *41*(6), 2022–7.

40. Yang, G. C. C., Tu, H.-chuan, & Hung, C.-hsiung. (2007). Stability of nanoiron slurries and their transport in the subsurface environment. *Test*, *58*, 166-172.

41. Phenrat, T., & Saleh, N. (2007). Aggregation and Sedimentation of Aqueous Nanoscale Zerovalent Iron Dispersions. *Environmental Science & Technology*, *41*(1), 284–290.

42. Baalousha, M., Manciulea, A., Cumberland, S., Kendall, K., & Lead, J. R. (2008). Aggregation and surface properties of iron oxide nanoparticles: influence of pH and natural organic matter. *Environmental Toxicology and Chemistry*, *27*(9), 1875–1882. Wiley Online Library.

43. Wang, Q., Qian, H., Yang, Y., Zhang, Z., Naman, C., & Xu, X. (2010). Reduction of hexavalent chromium by carboxymethyl cellulose-stabilized zero-valent iron nanoparticles. *Journal of Contaminant Hydrology*, *114*(1-4), 35–42.

44. Li, X., Elliott, D. W., & Zhang, W. (2006). Zero-Valent Iron Nanoparticles for Abatement of Environmental Pollutants□: Materials and Engineering Aspects. *Critical Reviews in Solid State and Material Sciences, 31:* 111–122.

45. Bowers, A.R., C.A. Ortiz and R.J. Cardozo (1986). Iron processes for treatment of Cr(VI) wastewater. *Metal Finishing*, 84, 37-41.

46. El-Shazly, A.H., A.A. Mubarak, A.H. Konsowa (2005). Hexavalent chromium reduction using a fixed bed of scrap bearing iron spheres. *Desalination*, Volume 185, Issues 1–3, 1 November 2005, Pages 307-316.

47. Fiúza, A., A. Silva, G. Carvalho, A.V. de la Fuente, C. Delerue-Matos (2010). Heterogeneous kinetics of the reduction of chromium (VI) by elemental iron. *Journal of Hazardous Materials*, Volume 175, Issues 1–3, Pages 1042-1047.

48. Vega, A., Fiuza, A., & Guimarães, F. (2010). Insight into the Phenomenology of the Cr(VI) Reduction by Metallic Iron Using an Electron Probe Microanalyzer. *Langmuir*, *26*(14), 11980–11986.

49. Cantrell, K.J., Kaplan, D.I., Wietsma, T.W. (1995). Zero-valent iron for the in-situ remediation of selected metals in groundwater. *J. Hazard. Mat.* 42, 201-212.

50. Alowitz, M.J., Scherer, M.M. (2002) Kinetics of nitrate, nitrite, and Cr(VI) reduction by iron metal. *Environ. Sci. Technol.* 36, 299-306.

51. Fang, Z., Xiuqi Qiu, Ruixiong Huang, Xinhong Qiu, Mingyu Li (2011). Removal of chromium in electroplating wastewater by nanoscale zero-valent metal with synergistic effect of reduction and immobilization. *Desalination*, Volume 280, Issues 1–3, Pages 224-231.

52. Dries, J., L. Bastiaens, D. Springael, S. Kuypers, S.N. Agathos, and L. Diels (2005). Effect of humic acids on heavy metal removal by zero-valent iron in batch and continuous flow column systems. *Water Research,* 39:3531-3540.

53. Liu, T., & Tsang, D. (2008). Chromium (VI) reduction kinetics by zero-valent iron in moderately hard water with humic acid: Iron dissolution and humic acid adsorption. *Environmental science & technology*, *42*(6), 2092-2098.

54. Mak, Mark S.H., Irene M.C. Lo (2011). Influences of redox transformation, metal complexation and aggregation of fulvic acid and humic acid on Cr(VI) and As(V) removal by zero-valent iron. *Chemosphere*, Volume 84, Issue 2, Pages 234-240.

55. Liu, T., & Lo, I. M. C. (2010). Influences of Humic Acid on Cr(VI) Removal by Zero-Valent Iron From Groundwater with Various Constituents: Implication for Long-Term PRB Performance. *Water, Air, & Soil Pollution*, *216*(1-4), 473–483.

56. Gu, B., Schmitt, J., Chen, Z., Liang, L., & MaCarthy, J. F. (1994). Adsorption and desorption of natural organic matter on iron oxide mechanisms and models. Environ- mental Science & Technology, 28, 38–46.

57. Chowdhury, A.I.A., D.M. O'Carroll, Y. Xu, and B.E. Sleep (2012). Electrophoresis enhanced transport of nano-sclae valent iron, *Advances in Water Resources*, 40:71-82.

58. Jones, E. H., Reynolds, D. A., Wood, A. L., & Thomas, D. G. (2009). Use of Electrophoresis for Transporting Nano-Iron in Porous Media. *Ground Water*, 1-12.

59. Chen, J. M., & Hao, O. J. (1998). Microbial Chromium (VI) Reduction. *Critical Reviews in Environmental Science and Technology*, *28*(3), 219–251.

60. Kim, B.H., Kim, H.J., Hyun, M.S., Park, D.H., 1999. Direct electrode reaction of Fe(III)-reducing bacterium, Shewanella putrifaciens. *Microbiol. Biotechnol*. 9, 127–131.

61. Gorby, Y. A., Yanina, S., McLean, J. S., Rosso, K. M., Moyles, D., Dohnalkova, A., Beveridge, T. J., Chang, I. S., Kim, B. H. & other authors (2006). Electrically conductive bacterial nanowires produced by Shewanella oneidensis strain MR-1 and other microorganisms. *Proc Natl Acad Sci U S A* 103, 11358–11363.

62. Lies DP, et al. (2005) *Shewanella oneidensis* MR-1 uses overlapping pathways for iron reduction at a distance and by direct contact under conditions relevant for biofilms. *Appl Environ Microbiol* ,**71**:4414–4426

63. Park, D.H. and Zeikus, J.G. (1999) Utilization of electrically reduced neutral red by *Actinobacillus succinogenes:* physiological function of neutral red in membrane driven fumurate reduction and energy conservation. *Journal of Bacteriology* 181, 2403-2410.

64. Bond, D.R., Holmes, D.E., Tender, L.M., Lovley, D.R. (2002). Electrode- reducing microorganisms that harvest energy from marine sediments. Science 295 (5554), 483–485.

65. Rabaey, K., and Verstraete, W. (2005). Microbial fuel cells: novel biotechnology for energy generation. *Trends in Biotechnology* 23, 291-298.

66. Kim, B.H., Kim, H.J., Hyun, M.S., Park, D.H., 1999. Direct electrode reaction of Fe(III)-reducing bacterium, Shewanella putrifaciens. Microbiol. Biotechnol. 9, 127–131.

67. Park, D.H. and Zeikus, J.G. (2002) Impact of electrode composition on electricity generation in a single-compartment fuel cell using *Shewanella putrefaciens. Applied Microbiology and Biotechnology* 59, 58-61

68. Park, D.H. and Zeikus, J.G. (2003) Improved fuel cell and electrode designs for producing electricity from microbial degradation. *Biotechnology and Bioengineering* 81, 348-355.

69. Ringeisen, B. R., Henderson, E., Wu, P. K., Pietron, J., Ray, R., Little, B., Biffinger, J. C., et al. (2006). High Power Density from a Miniature Microbial Fuel Cell Using Shewanella oneidensis DSP10. *Environmental Science & Technology*, *40*(8), 2629–2634.

70. Logan, B.E. 2008. *Microbial Fuel Cells*. John Wiley & Sons, New York

71. Logan, B.E., S. Cheng, V. Watson, and G. Estadt. (2007). Graphite Fiber Brush Anodes for Increased Power Production in Air-Cathode Microbial Fuel Cells. *Environ. Sci. Technol.*, 41(9):3341-3346.

72. Kim, J.R., S.H. Jung, B.E. Logan, and J. Regan. (2007). Electricity generation and microbial community analysis of alcohol powered microbial fuel cells. *Bioresource Technol.* 98(13): 2568-2577.

73. Cheng, S., H. Liu and B.E. Logan. (2006). Increased performance of single-chamber microbial fuel cells using an improved cathode structure. *Electrochem. Comm.* 8:489-494.

Chapter 3 : Electrokinetic Transport of Cr^{VI} in Clay Soils: Differentiation and Effects of Surface Bound and Dissolved Natural Organic Matter

3.1 Introduction

Groundwater and soil contamination is a global issue resulting from the discharge of contaminants to the environment, either accidentally, or purposefully because of a lack of regulation or a lack of concern. Methods of remediating contaminated groundwater and soils are limited, what is feasible is often dictated by the environmental conditions at the site, and the type and extent of contamination. In soils of low hydraulic conductivity, such as clay, the difficulties of site cleanup are exacerbated and treatment options are severely restrained due to the lack of access to the contamination plume. Electrokinetic remediation has been proposed as a potential method for groundwater remediation in soils of low hydraulic conductivity, by transporting ionic contaminants through the soil pore water using an applied electric potential. As such, contaminants can be concentrated in a defined area and dealt with as required, either through a treatment approach or excavation.

Electrokinetic transport is not a new theory, and it has been investigated over the last few decades from lab scale to field scale demonstrations. A list summarizing many published electrokinetic research projects is presented in Chapter 2. The 1993 article, “Principles of Electrokinetic Remediation” by Yalcin Acar and Akram Alshawabkeh of Louisiana State University was a major publication that introduced this, at the time, “recently emerging technology.” Since then, research groups around the world have exhaustedly explored the range of applications and possibilities of electrokinetic remediation. Electrokinetic research has been highlighted by many publications from Acar and Alshawabkeh, as well as from Krishna Reddy and Usha Parupudi of the University of Illinois at Chicago, and Sibel Pamucku of Lehigh University, among many others.

Essential to the application of electrokinetic remediation is that contaminants can only be transported by electrokinetic phenomena if they exist in an ionic state, and exist freely in water. Thus, this technology is often applied to groundwater contaminated with heavy metals. Hexavalent chromium (Cr^{VI}) is an ideal contaminant for electrokinetic research for the following reasons: i) it is stable as the chromate ion ($HCrO_4^-$) in natural waters, ii) it is an EPA priority contaminants due to its toxicity, and iii) it is prevalent in natural waters around the United States. For a more detailed description of chromium, see Chapter 2.

Heavy metal contamination in clay soils, and interactions between the soil media and the toxic metal have been investigated through adsorption studies involving clays such as kaolin, kaolinite, glacial till, and montmorillonite.[1-9] Each clay differs in its physical and chemical properties, and as a result varying degrees of adsorption are observed for each metal-clay combination. Some of these studies have involved the addition of humic or fulvic acids, representing natural organic matter (NOM), to evaluate the effects on adsorptive capacity of the soil for toxic metals. NOM is ubiquitous in the environment, and can have significant effects on the fate and transport of contaminants in subsurface environments. Hizal et al. (2) investigated the dependence of pH on adsorption, and concluded that metal adsorption onto clay soils was enhanced in the presence of humic acid under acidic conditions. This was in accordance with a 2010 study by Li et al. (4), that illustrated the adsorption of chromate onto kaolin increased in the presence of humic acid. These findings were in contrast with a 2002 study by Schmitt et al. (6) investigating the adsorption of metals Al, Fe, Zn, and Pb, onto kaolinite and montmorillonite. They determined the presence of humic acid decreased the adsorption capacities of the clay soils for the various metals. The range in results provokes the conclusion that environmental conditions play a significant role in determining the fate of heavy metals, including Cr^{VI}, upon introduction the environments.

Cr^{VI} transport by electrokinetic phenomena through the aforementioned clay soils has been performed under a variety of simulated and natural conditions, and the reported results vary from soil to soil.[12-24] Common to most studies is the measurement of moisture content of the soil, conductivity and pH of the pore fluid, and contaminant distribution in the soil. A factor that hasn't received much attention is the effect of NOM on electrokinetic transport of chromium. NOM carries a predominant negative charge at neutral pH values, and similar to Cr^{VI} will migrate towards the anode electrode during electric potential application. Cr^{VI} and NOM have the capacity to complex and engage in redox reactions resulting in the reduction of Cr^{VI} to Cr^{III} species.[10,11] In some cases, natural organic matter is bound to soil particle surfaces as well. It has been shown that when bound to a mineral surface, NOM is significantly more active in redox chemisty, and will reduce Cr^{VI} at rates much higher than dissolved organic matter.[25]

The goals of this study are to make a clear distinction between dissolved NOM and surface bound NOM, and evaluate the effects of these different forms of organic matter on electrokinetic transport of Cr^{VI} through clay soils. These goals are achieved through a series of experiments comparing two clay soils: kaolinite, and EPK kaolin. These clays have the same base mineral composition, however EPK kaolin is natural soil and coated in a layer of surface bound NOM, and kaolinite is a commercially processed clay void of NOM. Adsorption studies were run first, and upon noting the differences in adsorption capacity of the two clays, the natural organic matter layer coating the EPK kaolin was extracted and analyzed by FTIR to identify functional groups capable of reducing or complexing Cr^{VI} species. A zeta-potential analysis on the two clays provided additional depth into the trends observed in the adsorption studies. Rate studies of Cr^{VI} reduction to Cr^{III} by the two clay soils were performed next, and dissolved humic acid was introduced to specific reaction vessels to serve as a proxy for natural organic matter. The effects of dissolved NOM relative to surface bound NOM could be evaluated through this comparison. Finally, the two clays were saturated with a simulated groundwater containing Cr^{VI} and charged to soil columns under an applied electric potential, also referred to in this study as electrokinetic cells. Frequent sampling from various locations throughout the electrokinetic cells compared Cr^{VI} transport by electrokinetic phenomena in the two systems. Knowledge gained through the experiments was used to formulate postulations describing observations during experimental electrokinetic studies.

3.2 Materials and Methods

Materials

Chemicals

All chromium stock solutions were prepared by dissolving 2.828 g of ACS reagent grade (≥99.0% purity) potassium dichromate in 1.0 L of distilled-deionized (DDI) water for a final Cr^{VI} concentration of 1000 mg Cr^{VI} /L. A 1.0 M stock bicarbonate buffer solution was prepared from ACS reagent grade (99.7-100.3% purity) $NaHCO_3$, and diluted as required for experiments. A calcium chloride stock solution of 1000 mg/L was made by dissolving 1.0 g of bioreagent grade (≥ 96%) $CaCl_2$ in 1.0 L of distilled deionized water. All solutions were refrigerated at 3°C until use.

The humic acid chosen for this study was technical grade Fluka humic acid. This is a well-characterized humic acid and is commonly used to represent natural organic matter in reserach. Dried humic acid was dissolved in DDI water at pH 12 for four hours under constant agitation for a concentration of 2.0 g/L, then filtered through a 0.45 μm pore size membrane to remove insoluble fractions.

The eluent solution required for Cr^{VI} determination by ion-exchange chromatography was prepared by dissolving 66.0 g of ammonium sulfate in about 1 L of DDI water with the addition of 13.0 mL of 29% ammonium hydroxide. The solution was then diluted to a volume of 2.0 L with DDI water.

A buffer solution was added to samples to stabilize Cr^{VI} while in storage before analysis. The buffer solution was prepared by dissolving 3.3 g of ammonium sulfate in about 75 mL of DDI water with the addition of 6.5 mL of 29% ammonium hydroxide, then diluting to a volume of 100 mL.

A post-column reagent solution was used for colorimetric determination of Cr^{VI} by absorption spectrophotometry at 530 nm. A specified volume of sulfuric acid (98% purity) was added to about 500 mL of DDI water, then set aside to cool. While cooling, 0.5 g of 1,5-diphenylcarbazide was added to about 75 mL of HPLC-grade methanol, and the 1,5-diphenylcarbazide was dissolved by sonication. Once dissolved, methanol was added to reach a final volume of 100 mL. This solution was added to the cooled sulfuric acid solution and brought to a volume of 1.0 L with DDI water.

A 1000 mg/L inorganic carbon (IC) standard solution was prepared by dissolving appropriate amounts of reagent grade sodium bicarbonate and sodium carbonate in 1.0 L of DDI water. Similarly, a 1000 mg/L organic carbon (TOC) standard solution for TOC calibration was prepared by adding an appropriate amount of reagent grade potassium hydrogen phthalate to 1.0 L of DDI water.

All pH adjustments were carried out using solutions of 0.1 – 10 M NaOH or HCl, and all chemicals were obtained from Sigma-Aldrich unless otherwise noted.

Materials

Soils

Kaolinite and EPK kaolin clays were used as model clay soils in this study. Kaolinite was purchased from Sigma-Aldrich (Fluka, natural grade), and used as delivered. Kaolinite is a kaolin-based clay mineral, used commonly as a clay soil in related research due to the low content of impurities and surface bound organic matter. It is white-gray in color, and contains an insignificant quantity of organic mater on its surface.

EPK kaolin was purchased from Edgar Minerals Inc., Florida, and used as delivered. EPK kaolin is naturally coated in a organic matter layer, which gives the kaolin-based clay a yellow-brown color.

Methods

Adsorption of Cr^{VI} to Soils

Adsorption isotherms were conducted for chromium adsorption to EKP kaolin and kaolinite clays. In 50 mL polypropylene centrifuge tubes (VWR), 5.0 grams of clay were mixed by vortex with 10.0 mL of Cr^{VI} solutions ranging in concentration from 0.01 mg/L – 10.0 mg/L, containing a 10^{-2} M carbonate buffer. The pH was adjusted to 7.0±0.05 with HCl, and the samples were shaken on a shake plate for 24 hours to ensure thorough mixing. All samples were prepared in duplicates. Samples were taken and prepared for analysis by centrifugation to separate the liquid phase, followed by filtration through a 0.2 μm membrane filter, then analyzed for Cr^{VI} by ion-chromatography.

Natural Organic Matter Extraction from Clay Soils

An extraction procedure was performed on the two clay soils to isolate the natural organic matter present on the particle surface. The extraction procedure as described by the International Humic Substance Society (Swift, R. 1996) follows:

Five grams of EPK kaolin and kaolinite clays were added individually to 50 mL centrifuge tubes. DDI water was added for a final solution volume of 50 mL and the pH was adjusted to the range of 1.0-2.0. The suspension was mixed thoroughly to make a homogeneous solution, followed by moderate shaking for 1 hour. The liquid phase was seperated by low-speed centrifugation from the clay and stored. This first extraction contained fulvic acid, as it is highly soluble under acidic conditions. Following the fulvic acid extraction, the soil residue was resuspended in 10 mL of DDI water, and the pH was adjusted to 7.0 with 1 M NaOH added dropwise. The entire experimental apparatus was then moved to a glovebox containing a nitrogen atmosphere. Under nitrogen, the solution was filled to a final volume of 50 mL with 0.1 M NaOH to start the humic acid extraction. The solution was shaken intermittently for four hours, then left to settle overnight. The following day, the solution was centrifuged and the supernatant was removed and filtered twice through the same 0.2μm membrane filter under pressure to remove any remaining particulates. The filtrate was collected and acidified with 6 M HCl to a pH of 1.0 and was left to sit for 12-16 hours, at which point it was centrifuged to isolate the precipitates (humic acid), and the supernatant was collected as the second fulvic acid extract. The humic acid precipitate was dissolved in DDI water adjusted to pH 12 and stirred continuously for four hours. The different components were stored at 3°C until analysis.

Analysis was performed by FTIR spectroscopy to collect spectral data over a large spectral range to determine the dominant reactive functional groups, and compare with spectra from other humic acids. Additionally, the total organic carbon content was measured by a TOC analyzer.

Zeta-Potential of EPK Kaolin and Kaolinite

Zeta-potential was determined for EPK kaolin and kaolinite clays over a pH range of 4 to 11. Electrophoretic mobility measurements were conducted using a Zeta Meter equipped with a microprocessor unit, allowing statistical calculations to be made immediately for each sample. Each clay was added individually to a 10 mmol carbonate buffered DDI solution for a final concentration of 100 mg/L, and the pH was adjusted and stabilized prior to analysis using concentrated HCl and NaOH. Twenty consecutive measurements of zeta potential were taken per sample, and averaged.

Cr^{VI} Reduction in Clay Soils by Humic Acid

In 50 mL centrifuge tubes, clay slurries with the appropriate amount of Cr^{VI} were prepared and adjusted to pH 7.0±0.05. Five sets of slurries were prepared in duplicates, as described in Table 3.1. The tubes were shaken continuously for six days to achieve equilibration. The tubes were then centrifuged to separate the liquid phase, and filtered through a 0.2 μm membrane filter (Membrane Solutions, LLC.; North Bend, Ohio), to remove remaining particulates, and analyzed by ion-exchange chromatography.

Table 3.1 List of samples used in Cr^{VI} reduction studies in clay soils and humic acid.

Sample Number	Clay Type and Mass	Chemical Constituents (10 mL total volume)
1	5.0 g Kaolinite	10^{-2} M HCO_3^-, 3 mg/L Cr^{VI}
2	5.0 g EPK kaolin	10^{-2} M HCO_3^-, 3 mg/L Cr^{VI}
3	5.0 g EPK kaolin	10^{-2} M HCO_3^-, 3 mg/L Cr^{VI}, 10 mg/L humic acid
4	5.0 g EPK kaolin	10^{-2} M HCO_3^-, 3 mg/L Cr^{VI}, 100 mg/L humic acid
5	5.0 g EPK kaolin	10^{-2} M HCO_3^-, 3 mg/L Cr^{VI}, 200 mg/L humic acid

Chromium Complexation with Dissolved Humic Acid

A 10 mmol carbonate buffered solution containing 5 mg/L of Cr^{VI} was divided into two separate containers, and the pH of the solutions were adjusted to 5.0 and 7.0. An equal aliquot of each solution was added to individual 50 mL centrifuge tubes, followed by addition of humic acid to achieve final humic acid concentrations of 5 mg/L, 10 mg/L, 20 mg/L, 30 mg/L, 50 mg/L, and 100 mg/L. The pH of individual samples were recorded to note fluctuations from humic acid addition, and adjusted if necessary to remain within ±0.1 of the target value. A control sample containing no humic acid was prepared at both pH 5 and 7 as well. The samples were shaken continuously with the exception of sampling events, and were analyzed for remaining Cr^{VI} by ion-exchange chromatography.

Batch Electrokinetic Column Studies with Clay Soils

Vertical electrokinetic columns (Figure 3.1) were constructed from acrylic pipe of dimensions 1.5” I.D. x 2” O.D. x 12”L. Each column was divided into three sections: the cathode reservoir, the soil compartment, and the anode reservoir. The reservoir compartments housed the electrodes, and were separated from the soil column by cellulose-fiberglass partitions. These partitions kept the fine clay soils from entering the electrode reservoirs.

Sampling ports were installed at 1 cm intervals along the soil column section with an additional port at each electrode reservoir. The cellulose-fiberglass partitions were assembled such that they would both allow water to pass freely and remain impermeable to suspended clay particles. The electrodes were prepared by machining 0.25” thick graphite plates into 1” diameter disks. A 0.8 mm diameter titanium wire was attached to the graphite inside the electrode reservoir and used to connect the electrode to the external power supply.

A clay-chromium suspension was prepared by mixing the clay (kaolinite or EPK kaolin) with a 3.0 mg/L Cr^{VI}, 10^{-2} M buffered solution to achieve a 40% (wt/wt) clay suspension. The pH was adjusted to 7.0 with NaOH or HCl. This suspension was used to fill the soil column of the electrokinetic apparatus.

A 3.0 mg/L Cr^{VI} solution was added to each of the electrode reservoirs. The ends of the columns were sealed and the column was left to equilibrate for 24 hours. After equilibration, a 10.0 V electric potential was applied across electrodes to maintain a voltage gradient of 0.5 $V\text{-}cm^{-1}$ using an external power supply (HQ Power, Gavere, Belguim). A valve at the top of the column was left open to allow the release of H_2 and O_2 gases formed during the experiment. Each experiment was run in duplicate. The electrode reservoirs and center of the clay column were sampled every 24 hours for five to seven days. Sample volumes of 1.5 mL were centrifuged at 17,000 g for ten minutes to remove clay particles followed by filtration through a 0.2 μm syringe filter tip. The pH was recorded, and the sample was analyzed for Cr^{VI} using ion-chromatography.

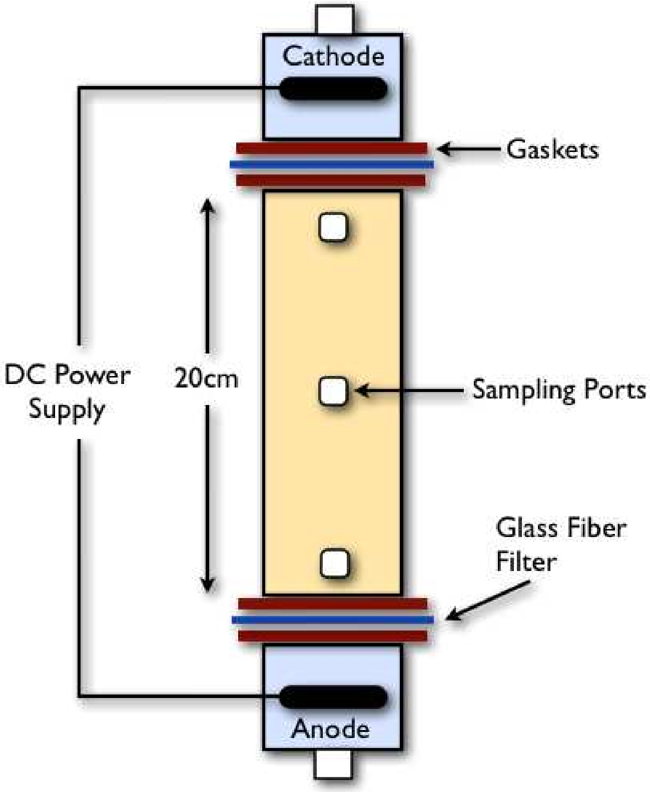

Figure 3.1 Experimental electrokinetic cell apparatus illustrating the key components.

Analytical Methods

Ion-Exchange Chromatography

Samples were analyzed for Cr^{VI} by ion-exchange chromatography (Dionex ICS-1000, Sunnyvale, CA) in accordance with EPA method 218.6. To enhance sensitivity a high-capacity IonPac® AS7 anion exchange column is employed to separate Cr^{III} from Cr^{VI} (Dionex Technical Note 26). The product of the postcolumn reaction between Cr^{VI} and diphenylcarbazide is detected by absorbance at 530 nm using a spectrophotometer, which yields a detection limit of 0.4 µg/L.

Total Organic Carbon

Total organic carbon analysis was performed using an organic carbon analyzer (Shimadzu TOC-V CSH; Shimadzu Corp., Kyoto, Japan), in accordance with EPA method 415.1. Samples were filtered to remove particulates before analysis.

Flame Atomic Absorption Spectroscopy

Flame atomic absorption spectroscopy was performed to measure total soluble chromium (Analytik novAA series, Analytik Corp., Jena, Germany). An air/acetylene flame was used in conjunction with a measurement line of 359.35 nm, and the samples and standards were diluted with a 1% HCl/KCl solution as recommended in literature.

Fourier-Transform Infrared Spectroscopy

Fourier-transform infrared spectroscopy was used in humic acid analysis to identify reactive functional groups. This was performed using a Nicolet iS10 FT-IR spectrometer (Thermo Scientific, USA).

Zeta Potential

Zeta potential measurements were taken using a Zeta Meter 3.0+ (Zeta Meter Inc., New York) equipped with a microprocessor unit, allowing statistical calculations to be made immediately for each sample. Clay or nZVI was added to 10^{-2} M carbonate buffered DDI water for a final concentration of 100 mg of solids/L, and the pH was adjusted and stabilized prior to analysis using concentrated HCl and NaOH.

Current Measurement

Current measurements within the electrokinetic cell were taken with a digital multimeter (Extech, EX430; Radioshack, Los Angeles, CA). Titanium wiring fixed within the anode and cathode reservoir were contacted with leads to obtain current readings.

3.3 Results and Discussion

Cr^{VI} Adsorption to Clay Soils

Preliminary adsorption experiments were conducted to establish the adsorption capacity of EPK kaolin and kaolinite clay for Cr^{VI}. Figure 3.2 shows a plot of the equilibrium concentration of Cr^{VI} in solution (C_e, mg/L) versus the quantity adsorbed to the solid phase (q_e, μg Cr^{VI}/gram clay) indicating that the adsorption capacity of EPK kaolin is significantly larger than that of kaolinite. The data were well described by the Langmuir adsorption isotherm model (Figure 3.3). By the Langmuir model, the adsorption capacity of EPK kaolin (Q^0) was predicted to be 1.75 μg Cr^{VI} per gram of clay, and Q^0 of kaolinite was predicted to be 1.25 μg Cr^{VI} per gram of clay.

These results are in relatively good agreement with those reported by several investigators (see Chapter 2, Table 2.1). The increase in adsorption capacity observed for EPK kaolin is likely a product of the soil's natural organic matter content. Natural organic matter can form complexes with Cr^{VI} species ($HCrO_4^-$, $CrO_4^=$), and the associated redox reactions oxidize the organic matter while reducing chromium from the hexavalent state to the trivalent state.[11, 27] Although the term "adsorption capacity" is used to describe Cr^{VI} removal is this study, it is important to note that in the EPK kaolin isotherm the removal mechanisms are more complex. Upon mixing EPK kaolin in water some of the surface bound NOM is dissolved into the liquid phase, which has the potential to complex and reduce Cr^{VI} species. Additionally, Cr^{VI} species may be engaging with NOM bound at the EPK kaolin surface and undergoing reduction reactions. The removal of Cr^{VI} by EPK kaolin is just as much a chemical process as a physical sorption process. For ease of comparison with kaolinite adsorption studies, these various reduction/removal mechanisms are clumped together.

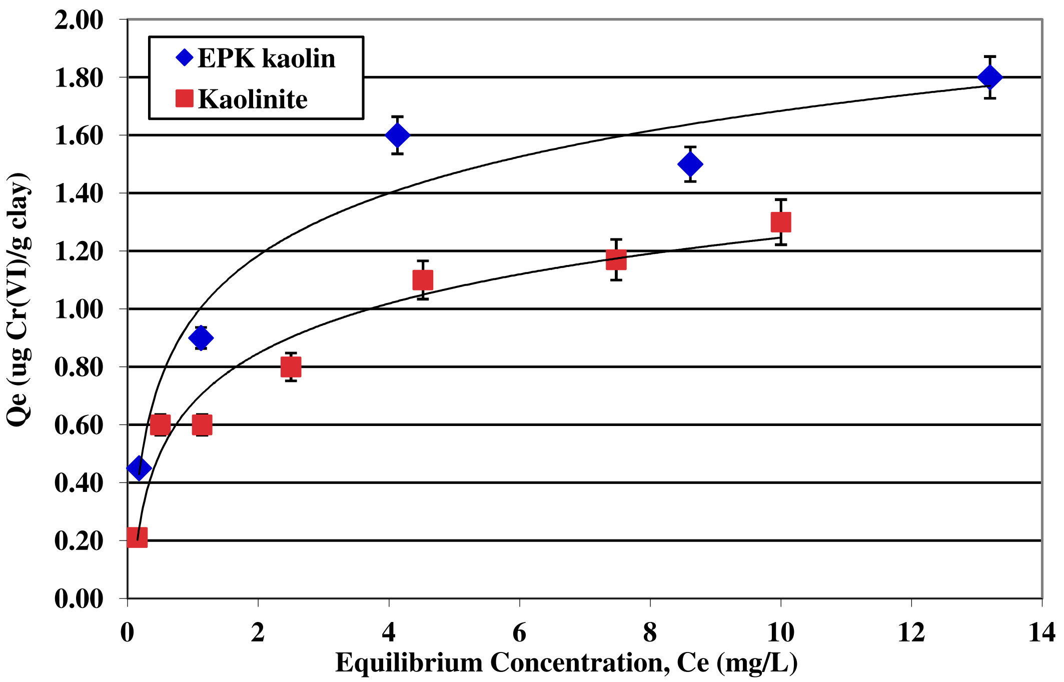

Figure 3.2 Adsorption of Cr^{VI} to EPK kaolin and kaolinite clays in a solution containing 10^{-2} M carbonate buffer.

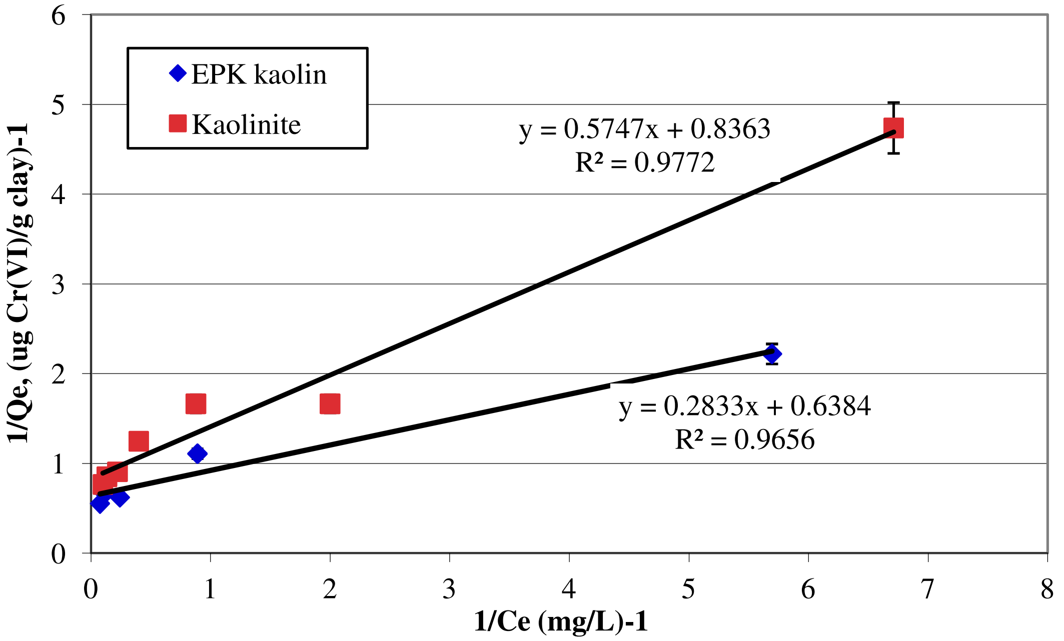

Figure 3.3 Adsorption equilibrium data of Cr^{VI} to EPK kaolin and kaolinite described by the Langmuir adsorption isotherm model.

Humic Acid Extraction from Clay Soils

The EPK kaolin clay was subjected to an extraction process to isolate the layer of organic matter coating its surface to determine the functional groups that are likely to contribute to the Cr^{VI} reduction observed in the adsorption experiments. Fourier-Transform Infrared (FTIR) spectroscopy was performed on the soil organic matter extract resulting in the spectrum shown in Figure 3.4. The FTIR spectrum provided the following band assignments:

The band at about 3301 cm^{-1} represents the –OH group of the carboxylic acid or the carbohydrate.[28] The other peaks in the vicinity are too small and insignificant for interpretation. The peak observed at wavenumbers of 1715-1716 cm^{-1} denotes the –C=O group of the carboxylic acid. The peaks corresponding to 1655 and 1540 cm^{-1} is characteristic of the peptide moiety of -CO-NH- in the soil-extracted humic acid. The peptide and carboxylic acid content of this humic acid is relatively low. The large band covering the spectrum of 1453 to 1376 cm^{-1} is characteristic of the lignin group, and the high intensity shows the dominance of lignin content in the humic acid. The band at around 1042 cm^{-1} represents C-O stretching of polysaccharides or polysaccharide-like substances, and the Si-O of silicate impurities, commonly found in soil-extracted humic substances. The small peaks seen at 1222 to 1233 cm^{-1} represent the –CO stretching and–OH deformation of the carboxylic acid groups.[28, 29] The peak commencing from 157 cm^{-1} to 980 cm^{-1} shows the –OH stretching of the carbohydrate group. It can be seen that this soil-extracted humic acid is high in carbohydrate content based on the intensity of the band. This is also confirmed by the large band at 3301 cm^{-1}.

These results are consistent with literature[30], and highlight the functional groups believed to be involved in Cr^{VI} reduction. The dominance of the lignin group in the humic acid likely gives EPK kaolin soil the superior Cr^{VI} reduction capacity. Lignin is comprised of numerous phenylpropane monomers groups joined by ether and carbon to carbon linkages. Polyphenyls have been shown to be the most effective Cr^{VI} reducing agent in humic substances.[25] Secondary to lignin is the carboxylic acid functional group, which has moderate significance in Cr^{VI} reduction.[31]

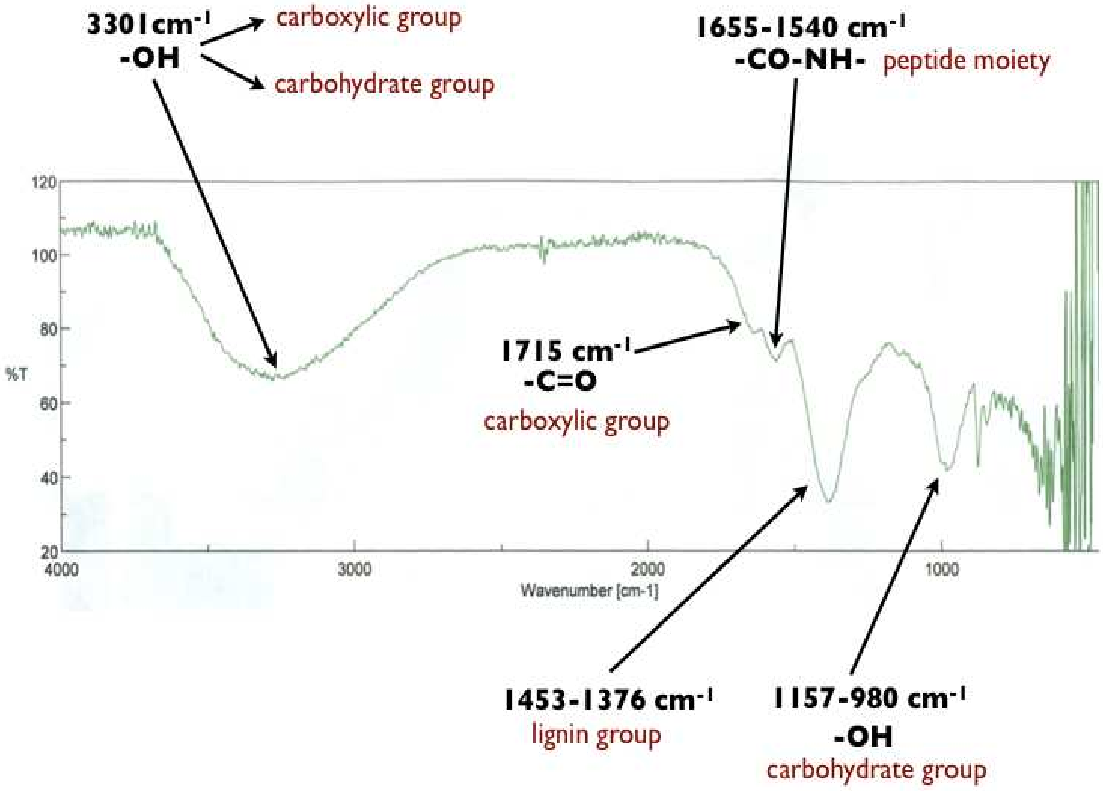

Figure 3.4 FTIR spectrum of the NOM extracted from EPK kaolin and noteworthy peaks associated with functional groups of humic acids.

Furthermore, the total organic carbon (TOC) content of the extracted soil organic matter was measured. This measurement was used to determine the soil organic matter content, which was calculated to be 0.8% by weight. However this is a gross underestimation of total organic matter content of the soil due to three primary factors: 1) the efficiency of the extraction process is not 100%, and 2) during the extraction process the initial fulvic acid fraction was collected separately and was not included in this measurement, 3) during the extraction process filtration is done to remove the insoluble organic matter fractions, which are not included in this soil organic matter calculation, and 4) the TOC analyzer is not capable of complete oxidation of high molecular weight fractions of NOM. The quantity of 0.8% organic matter by weight determined from the TOC analysis represents primarily the humic acid fraction of the NOM.

Zeta Potential of EPK Kaolin and Kaolinite

The zeta potential of the clay soils (EPK kaolin and kaolinite) was measured to evaluate the surface charge characteristics, and more importantly to investigate the changes of clay surface charge as a function of pH. Surface charge is a key parameter that influences adsorption because it dictates the degree of electrostatic forces between the particle surface and molecules in solution. The zeta potential of EPK kaolin and kaolinite between pH 3.5 and pH 11 is shown in Figure 3.5. A point of zero charge is observed for kaolinite at pH 5.2, which is consistent with literature values.[24,33] No point of zero charge was observed for EPK kaolin within the pH range used in this analysis, as EPK kaolin demonstrated a much higher stability in water than kaolinite. With an increase in pH, each of the clay soils increased in stability as seen by the increase in the absolute value of zeta potential. The surface charge of clay soils is dominated by the net proton charge, σ_H, as they are rich in minerals containing hydroxide functional groups.[34]

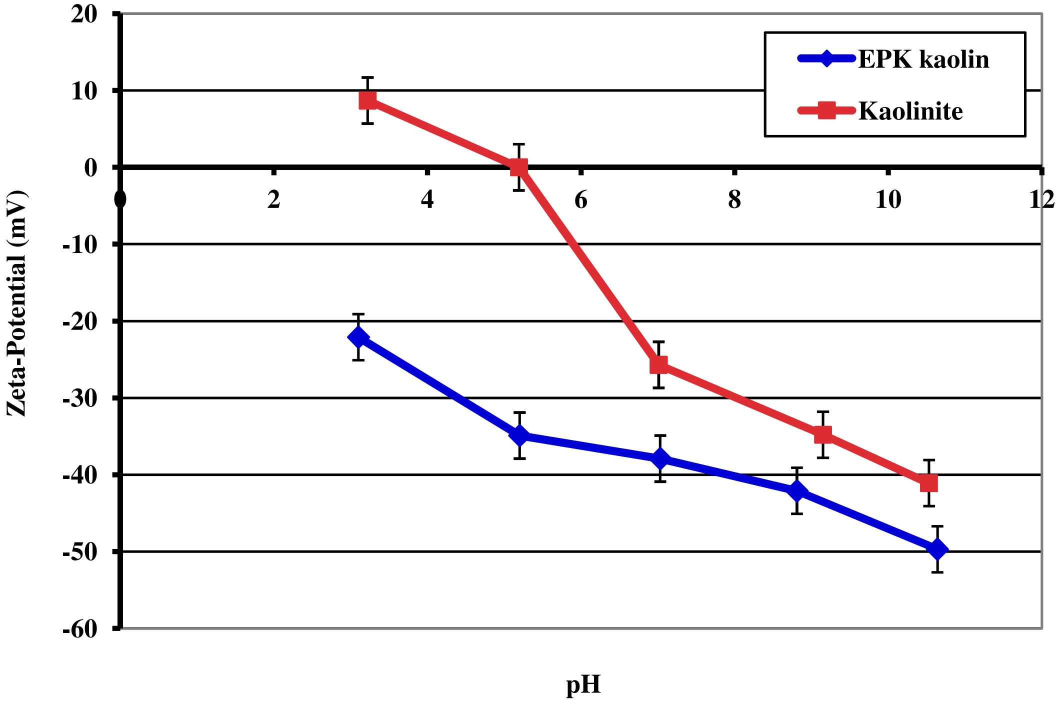

Figure 3.5 Zeta-potential of EKP kaolin and kaolinite clays in a 10^{-2} M carbonate buffered solution.

These results indicate the natural organic matter content of the EPK kaolin soil provides a higher density of negative surface charge. Above pH 5.2, both clay soils carry a negative surface charge, and so electrostatic repulsion between $CrO_4^{=}$ and $HCrO_4^{-}$ is anticipated. The repulsive forces will increase with pH due to the increase in negative surface charge density on the clay particle surface, and as a result adsorption rates and quantities will decrease.

Despite the increased negative surface charge carried by EPK kaolin relative to kaolinite, the adsorption capacity was still greater than that of kaolinite. The natural organic matter content substantially increased Cr^{VI} removal regardless of the electrostatic repulsive forces between these two predominantly-negatively charged chemical species. The affect of pH change on adsorption characteristics is a significant consideration in electrokinetic remediation. The pH gradient formed across a soil under an applied electric potential will drive local sorption and desorption reactions, causing a dynamic shift in chemical equilibria throughout the contaminated area.

Cr^{VI} Reduction by Surface Bound NOM

The surface bound NOM layer on EPK kaolin was shown to increase adsorption of Cr^{VI} species in comparison to kaolinite. This conclusion was drawn from experiments based on a 24-hour adsorption equilibration time. A similar adsorption study, described earlier, was performed to determine if additional adsorption or desorption processes were significant over a longer time scale, and to further investigate the affects of surface bound and dissolved NOM on Cr^{VI} reduction. The results show that no additional adsorption to the kaolinite surface occurs after 24 hours, however EPK kaolin reduced Cr^{VI} rapidly over a period of multiple days (Figure 3.6). Additionally, the Cr^{VI} reduction rate was found to increase in the presence of high concentrations of humic acid (>100 mg/L). The Cr^{VI} solution concentrations in the EPK kaolin slurry were negligible after six days of continuous mixing. The most rapid reduction of Cr^{VI} corresponded to the sample containing EPK kaolin and the highest quantity of added humic acid (200 mg/L).

The results indicate that surface bound organic plays a major role in Cr^{VI} reduction and is by far more significant that dissolved organic matter. This is in agreement with findings by Deng and Stone (1996) who proposed that the presence of a mineral surface catalyzes Cr^{VI} reduction by organic matter.

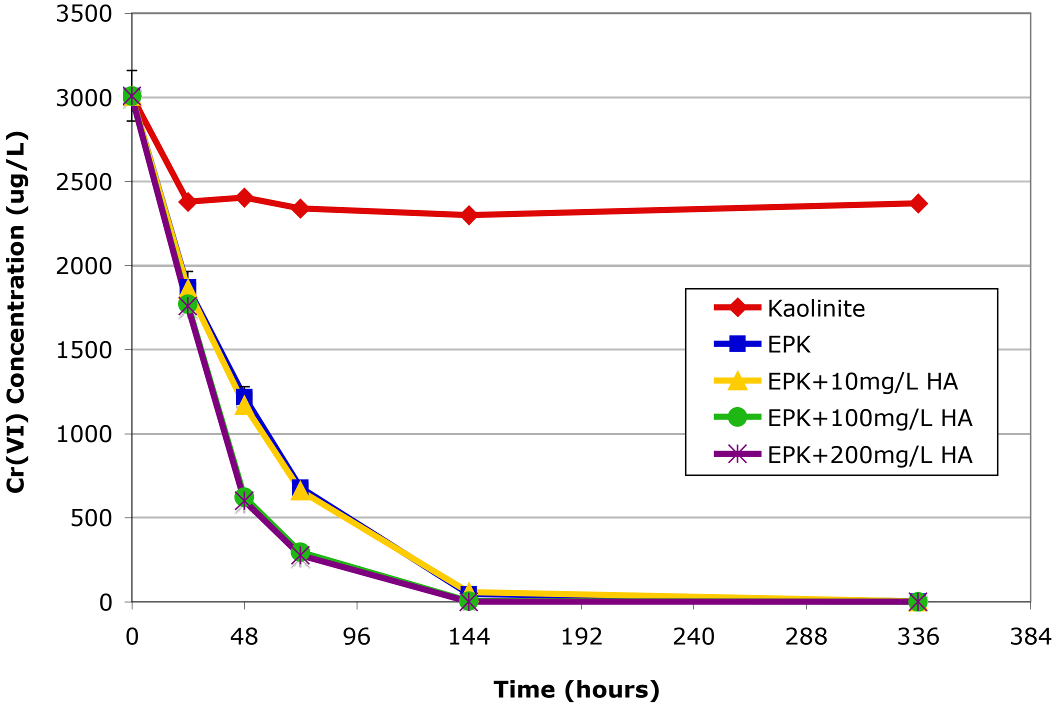

Figure 3.6 Cr^{VI} concentration in EPK kaolin and kaolinite clays, as well as in EPK kaolin with additional dissolved humic acid added.

Cr^{VI} Complexation with Dissolved Humic Acid

The extent of complexation between Cr^{VI} and dissolved organic matter was investigated to determine the significance of this interaction in aquifers. Solutions containing Cr^{VI} and varying humic acid concentrations were prepared at pH 5 as well as pH 7. The samples were mixed continuously and sampled routinely for 34 days. The results indicate a very slow complexation rate between humic acid and Cr^{VI} (Figure 3.7). At pH 7, the Cr^{VI} concentration was reduced by 2.35% with a 100 mg/L humic acid solution. At lower humic acid concentrations negligible reduction was observed at pH 7.0. The samples at pH 5 showed an increase in complexation, due to the decrease in repulsive forces at lower pH. The most concentrated humic acid solution (100 mg/L) at pH 5 reduced 14.2% of the Cr^{VI} after 34 days.

A mechanistic explanation for the above observation can be advanced, as follows. Hexavalent chromium as $HCrO_4^-$ can be treated as a dibasic acid with a pKa_1 near 1, and pKa_2 near 6. Therefore, as pH increases from 5 to 7, $HCrO_4^-$ deprotonates to become CrO_4^{2-}. Similarly, deprotonation occurs in the humic acid solution as the pH increases. The decrease in complexation between Cr^{VI} and humic acid with increasing pH can be explained as a product of the increased electrostatic repulsion between the two species. Furthermore, the results indicate that complexation is a slow process and does not make a substantial contribution to Cr^{VI} reduction in groundwater over relatively short time scales. A summary of the reduction percentages from complexation studies at different pH values can be seen in Table 3.2.

Longer equilibration times are expected to increase the amount of complexation between the two species until an eventual equilibration is reached. The amount of organic matter required to effectively reduce a substantial amount of Cr^{VI} in groundwater at neutral pH appears to be much greater than that found in natural systems.

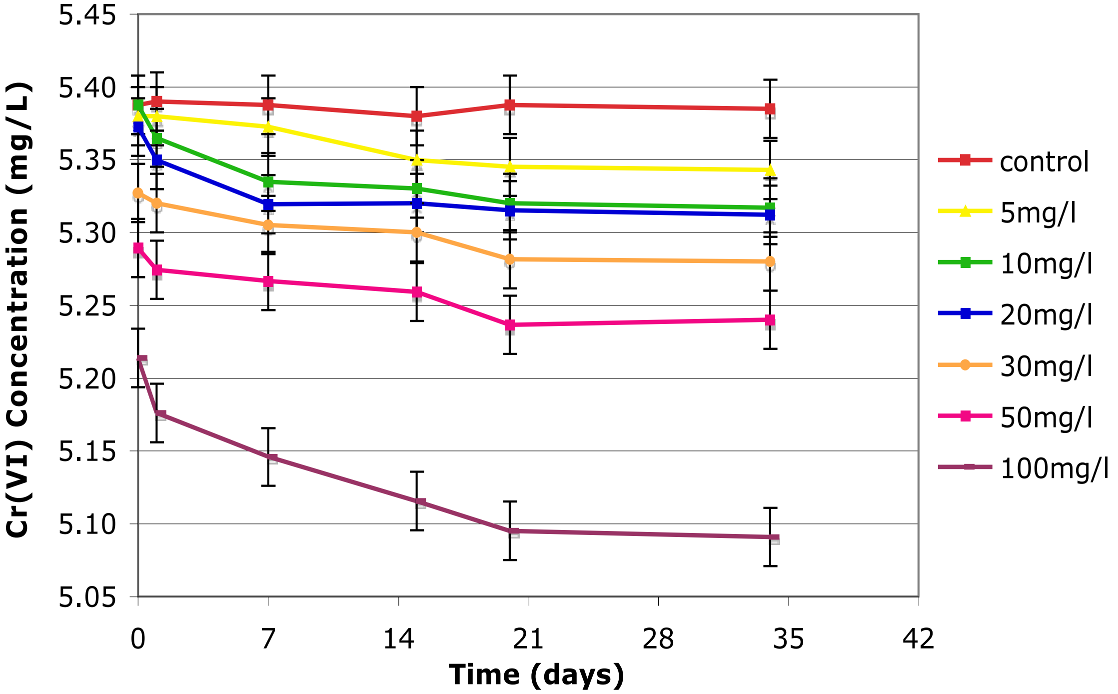

Figure 3.7 Cr^{VI} **concentration change with time in solution with dissolved humic acid ranging in concentration from 5 mg/L to 100 mg/L at pH 7.**

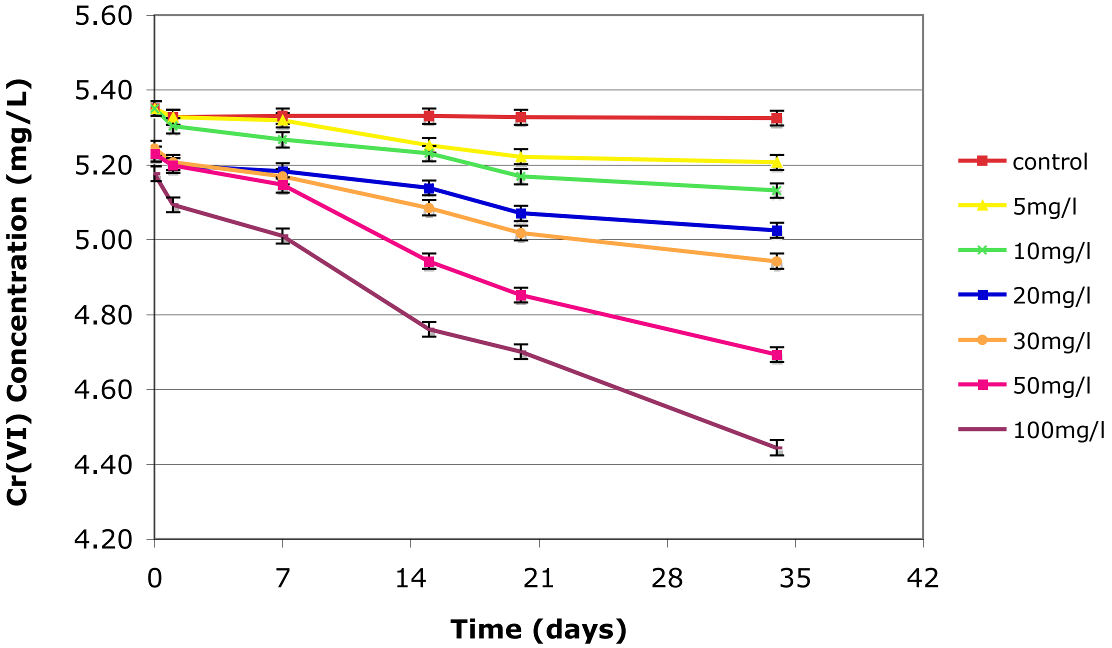

Figure 3.8 Cr^{VI} concentration change with time in solution with dissolved humic acid ranging in concentration from 5mg/L to 100mg/L at pH 5.

Table 3.2 Percent of chromium complexed with humic acid after 34 days of reaction time at pH 5 and pH 7.

HA Concentration (mg/L)	Percent Cr^{VI} Complexed (%) pH 7	Percent Cr^{VI} Complexed (%) pH 5
5	0.69	2.68
10	1.31	4.09
20	1.12	3.9
30	0.88	5.76
50	0.93	10.26
100	2.35	14.15

Batch Electrokinetic Column Studies with Clay Soils

Kaolinite

Electrokinetic column experiments were conducted using kaolinite clay. Upon application of an electric field, Cr^{VI} species (primarily $HCrO_4^-$) migrated towards the anode as anticipated. This is seen by the increase in Cr^{VI} concentration in the anode reservoir from about 3 mg/L to nearly 4.4 mg/L within 48 hours (Figure 3.9). Following this increase, Cr^{VI} concentrations rapidly declined in the anode reservoir to negligible concentrations by the 120-hour time point. At this time however, the concentration of total chromium was measured at 1.68 mg/L. After 168 hours (7 days), the total chromium concentration had dropped to 1.53 mg/L. The difference between total chromium and Cr^{VI} species is due to the reduction of Cr^{VI} to soluble Cr^{III} species. The subsequent precipitation of Cr^{III} species is reflected in the slow decline of total soluble chromium species. Reduction is mainly due to the low pH conditions that exist at the anode, which promote conversion to Cr^{III}. Also, an unspecified amount of reduction may be due to oxidation by minerals (iron or manganese) existing in trace amounts within the clay mixture.[22]

The pH change of the aqueous solution in the proximity of the electrodes is attributed to the production of H^+ at the anode and the production of OH^- ions at the cathode. Reduction of H^+ to H_2 occurring at the cathode decreases the proton concentration, contributing to the pH increase observed at the cathode. Oxidation of OH^- to O_2 contributes to the decrease in pH experienced at the anode. The effects of redox chemistry at the electrodes are clearly noticeable within the first 24 hours of the system start-up.

As can be seen in Figure 3.10, the concentration of Cr^{VI} and total chromium in the center of the clay compartment does not undergo any significant change. The initial concentration of Cr^{VI} is 0.438 mg/L less than the starting concentrations within the anode and cathode reservoirs due to Cr^{VI} adsorption to kaolinite. After seven days of electric potential application, a slight difference between Cr^{VI} and total chromium concentrations exists. This is likely due to the diffusive and electrokinetic transport of soluble Cr^{III} species from the anode reservoir into the column. Soluble Cr^{III} species generally carry a positive charge and will migrate towards the cathode. Figure 3.10 also shows the gradual pH change from 7.9 to 2.5 over the seven days indicating that the migration of H^+ from the anode towards the cathode slowly acidifies the column.

Changes in Cr^{VI} and total chromium concentration in the cathode reservoir are presented in Figure 3.11. As may be observed, Cr^{VI} concentrations decreased from 3.0 mg/L down to nearly 0.10 mg/L within the first 24 hours, where they stayed constant for the remainder of the experiment. Additionally, the pH in the cathode increased to 12.5 within 24 hours, indicating Cr^{VI} stability in its most mobile form, as CrO_4^{2-}. The lack of CrO_4^{2-} migration beyond this point is evidence that transport is being somewhat inhibited. The lack of removal from the clay column indicates that electrokinetic remediation was not effective for this system.

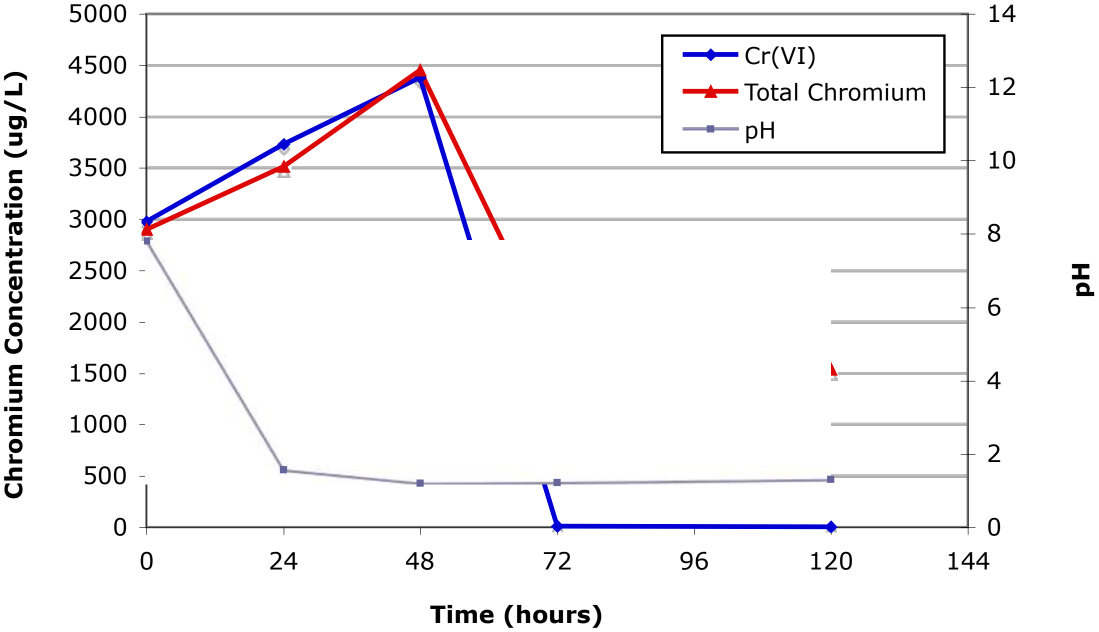

Figure 3.9 Cr^{VI} **and total chromium and concentrations in the anode reservoir during electric potential application for kaolinite clay.**

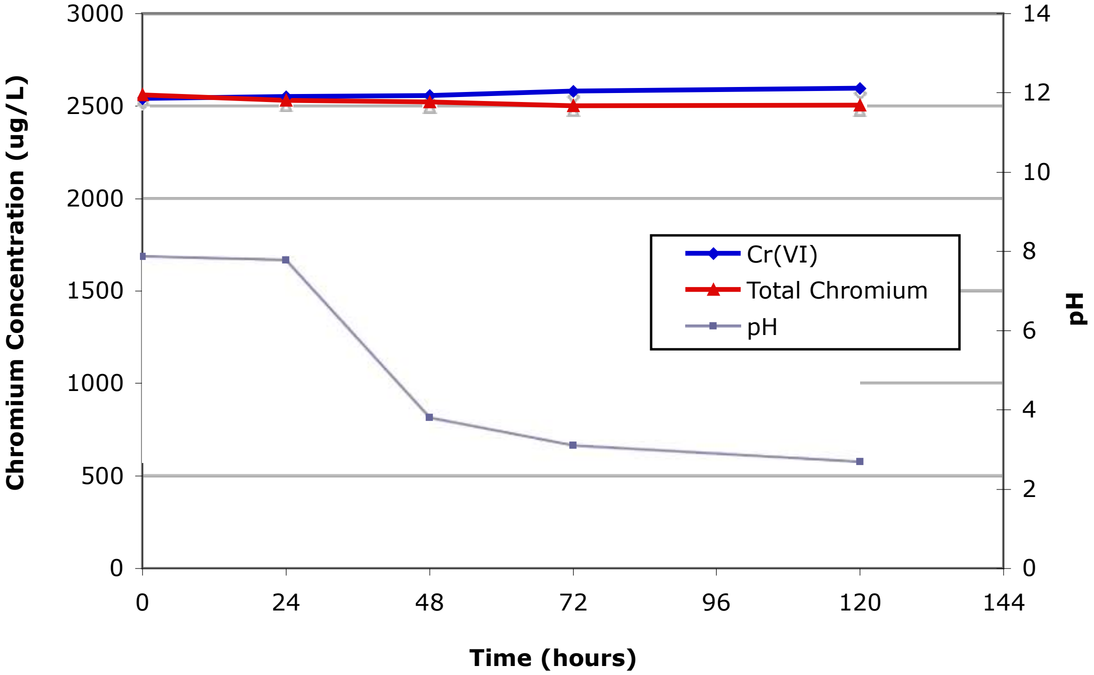

Figure 3.10 Cr^{VI} and total chromium concentrations in the center of the clay column during electric potential application for kaolinite clay.

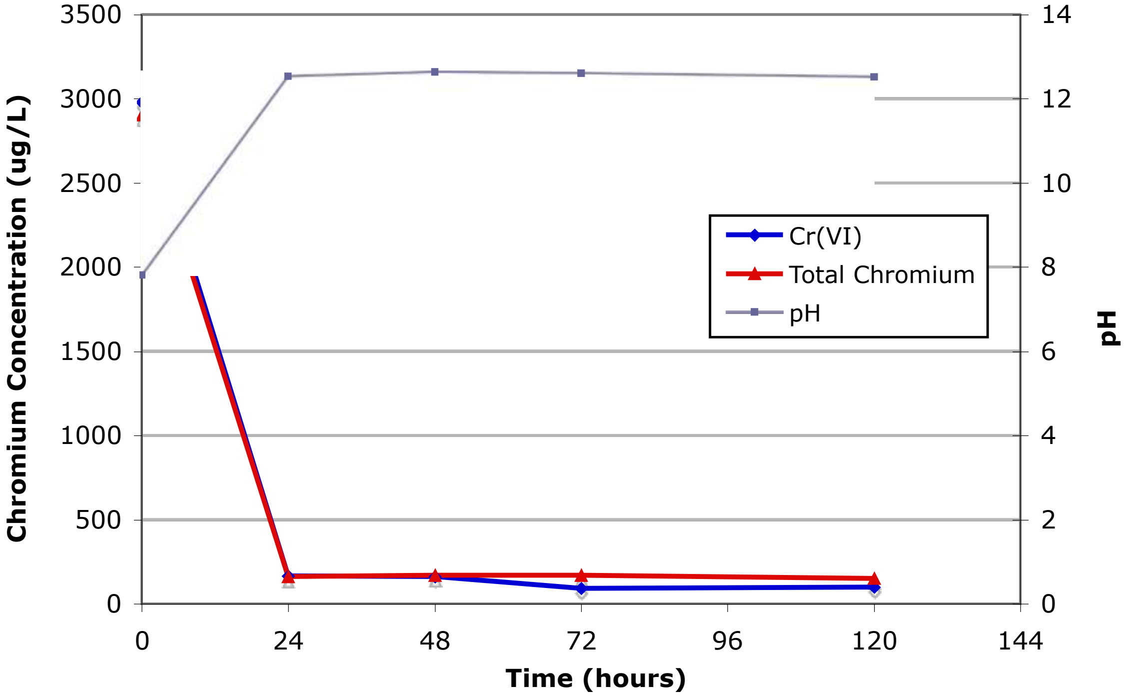

Figure 3.11 Cr^{VI} and total chromium concentrations in the cathode reservoir during electric potential application for kaolinite clay.

EPK Kaolin

Electrokinetic studies were conducted with EPK kaolin soil in similar mannor described for kaolinite. Unlike the results observed in the kaolinite studies, no chromium accumulation was observed within the clay column or in the anode reservoir. The Cr^{VI} concentration at each measured location within the electrokinetic cell decreased continuously with time (Figures 3.12, 3.13, and 3.14). It is difficult to conclude if transport is occurring due to the lack of accumulation in the anode reservoir, however the rapid initial decrease in concentration in the cathode reservoir is a good indication that chromium is migrating from the cathode towards the anode. The lack of accumulation in the anode reservoir (Figure 3.12) suggests that Cr^{VI} reduction to Cr^{III} is occurring at a faster rate than Cr^{VI} species can migrate to the anode. This observation may also indicate that transport from the clay compartment to the anode reservoir is not occurring as a result of complexation reactions between Cr^{VI} species and surface bound NOM. Similar to the kaolinite experiments, reduction may be occurring as a result of the low pH conditions in addition to oxidation by trace minerals (iron or manganese) present in the soil. The results observed in the previous studies however indicate that a significant fraction of Cr^{VI} reduction was a result of complexation reactions with the NOM content of EPK kaolin.

Unique to the EPK kaolin column experiments was a distinct yellow color to the pore liquid in cathode reservoir as well as in clay column adjacent to it. Samples taken after 24-hours were faintly yellow, however the color became more apparent with each consecutive day. This coloring was postulated to be a result of the humic acid fraction of the NOM associated with EPK kaolin, as it was slowly being solubilized under the basic conditions near the cathode. The TOC was measured throughout the column to determine the concentration of humic acid released from the soil, and it was determined that a TOC concentration gradient had developed. The TOC measured 93.2 mg TOC/L in the cathode reservoir, 67.74 mg TOC/L in the clay column 2-cm below the cathode reservoir, 50.7 mg TOC/L adjacent in the center of the clay column, and 16.3 mg TOC/L in the anode reservoir. A large fraction of the dissolved NOM likely consisted of humic acid due to its solubility under basic conditions, and its limited solubility at pH values below 3. It is likely that the solubilized NOM migrated by electrokinetic phenomena towards the anode, as NOM carries predominantly a negative charge in water. Transport of NOM however is likely very slow due to its large and complex molecular structure.

Similar to the experiments with kaolinite, the pH of the aqueous solution is dominated by the reduction of H^+ at the cathode and the oxidation of OH^- ions at the cathode. The pH in the cathode reservoir increased to 10.0 after 24 hours and slowly increased to 11.7 after 168 hours (seven days). The pH of the pore liquid in the clay column remained essentially constant over the seven-day period, and the pH in the anode reservoir decreased to 2.3 within 24 hours and remained nearly constant for the remainder of the experiment.

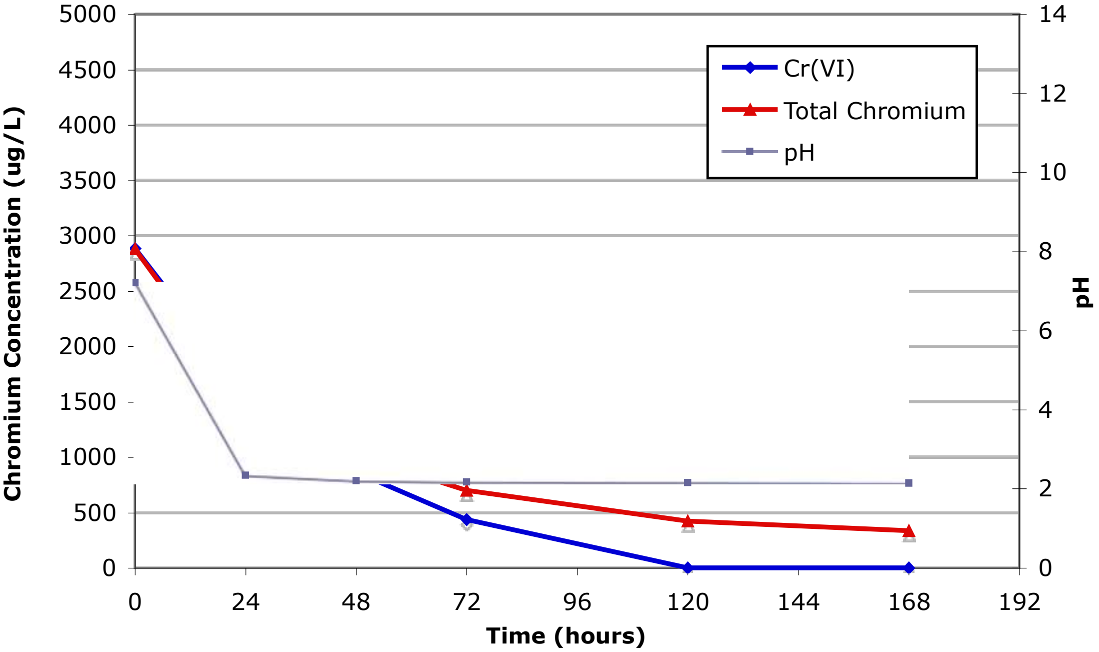

Figure 3.12 Cr^{VI} **and total chromium concentrations in the anode reservoir during electric potential application for EPK kaolin.**

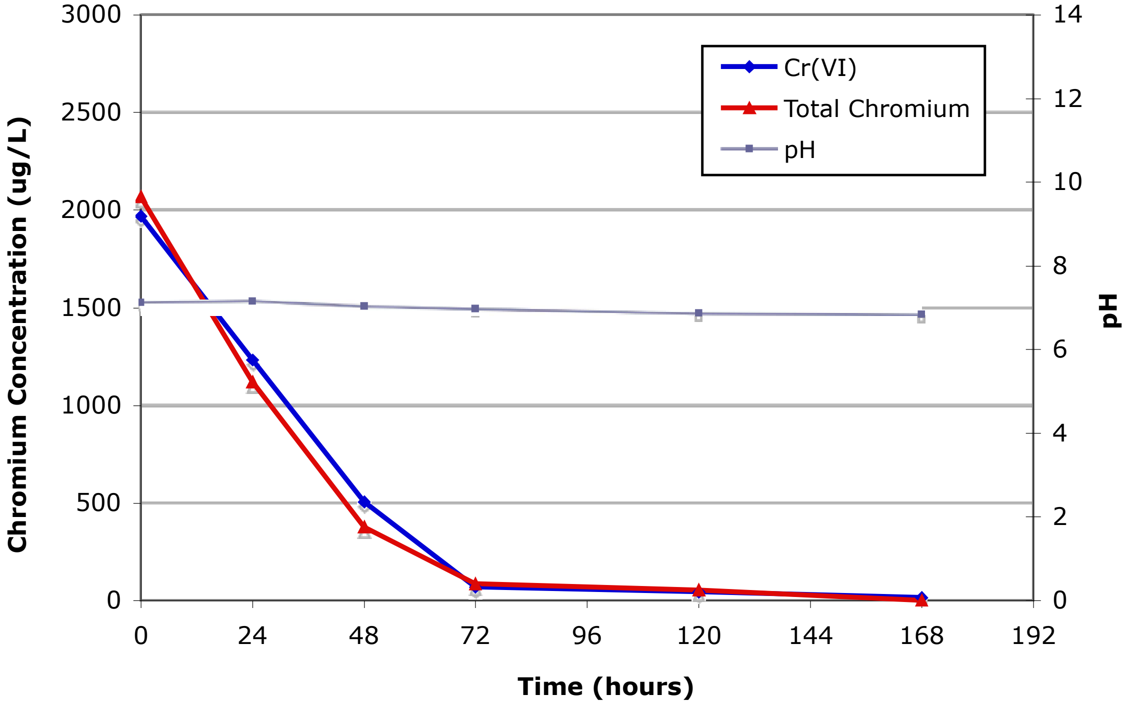

Figure 3.13 Cr^{VI} and total chromium concentrations in the center of the clay column during electric potential application for EPK kaolin

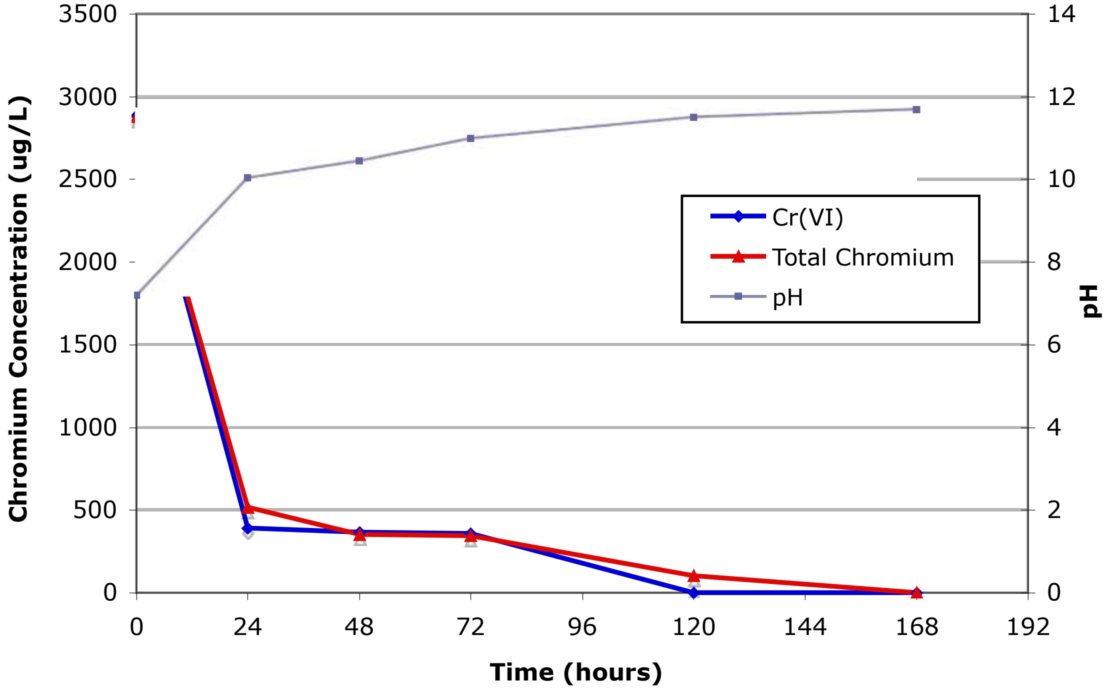

Figure 3.14 Cr^{VI} and total chromium concentrations in the cathode reservoir during electric potential application for EPK kaolin.

A comparison of chromium removal between the two clay shows that surface bound natural organic matter can reduce significant quantities of Cr^{VI} during electrokinetic remediation. This observation is based on the fact that Cr^{VI} concentration remained constant during electric potential application in the kaolinite clay column, however it dropped to negligible values after three days in EPK kaolin. EPK kaolin showed better Cr^{VI} removal due to reactions between surface bound NOM and Cr^{VI}, and to some extent from complexation between soluble NOM and Cr^{VI} near the anode reservoir. In the EPK kaolin studies, surface bound NOM was solubilized by the basic conditions at the cathode, and was slowly transported towards the anode by electromigration. This added to the buffer capacity of the pore liquid, slowing the development of the pH gradients.

The pH gradients formed during electrokinetic remediation in EPK kaolin and kaolinite are shown in Tables 3.3 and 3.4, respectively. The pH within the kaolinite column gradually decreased to 2.5, while only a slight pH decrease was seen within EPK kaolin column. It has been reported that the pH effects are what ultimately inhibit transport by influencing the direction of electroosmotic flow, the sorption and desorption of contaminants on and from soil surfaces, the extent of solubilization of NOM from soil, complexation reactions between contaminants and NOM, and dissolution and precipitation reactions of heavy metals.[26] Additionally, the pH gradient can cause areas of very low electrical conductivity near where the two fronts meet, disrupting the flow of current and obstructing contaminant transport.

Table 3.3 pH gradients in EPK kaolin columns during electric potential application.

Time (hours)	0	24	48	72	120	168
Anode pH	7.2	2.34	2.2	2.17	2.15	2.14
Clay Column pH	7.13	7.15	7.03	6.98	6.87	6.85
Cathode pH	7.2	10.03	10.44	10.98	11.5	11.69

Table 3.4 pH gradients in kaolinite columns during electric potential application.

Time (hours)	0	24	48	72	120	168
Anode pH	7.81	1.57	1.2	1.22	1.3	1.3
Clay Column pH	7.86	7.77	3.8	3.11	2.69	2.49
Cathode pH	7.81	12.53	12.63	12.61	12.52	12.54

An alternate set of electrokinetic column studies were performed specifically to monitor the current during electric potential application. The results presented in Figure 3.15 are consistent with findings from a similar study.[32] The current trends observed for the two clay soils are very similar, with an initial rapid increase followed by almost an equally rapid decrease in current around the 24-hour mark. The rapid increase is a result of electrolysis reactions involving water at the anode and cathode generating H^+ and OH^-, respectively. The production of these ions adds substantially to the ionic strength of the pore liquid and thus an increase in current as they are transported by electrokinetic phenomena.[26] Despite the transport phenomena, OH^- and H^+ slowly accumulate at the anode and cathode reservoirs, and cause the dynamic pH shifts. After about 24 hours the conditions are acidic enough near the anode to cause chromium precipitation as oxides and hydroxides. This rapidly lowers the ionic strength of the pore liquid, and near the anode the conductivity becomes very low. As a result the current drops off quickly to an eventual very low steady-state value.

Kaolinite clay reached a higher maximum current of about 90 mA, relative to nearly 78 mA for EPK kaolin, however the steady-state current reached in the EPK kaolin system was higher that for kaolinite. As mentioned previously, the NOM layer surrounding EPK kaolin adds significant buffering capacity to the soil, and therefore the system is not subjected to such dramatic pH shifts. The neutralization of some of the acid and base fronts generated at the electrodes also lowers the current within the electrokinetic cell. However the basic conditions at the cathode in the EPK kaolin system cause dissolution of NOM from the EPK kaolin surface into the pore water. This ultimately adds to the ionic strength and the result is a higher steady-state current.

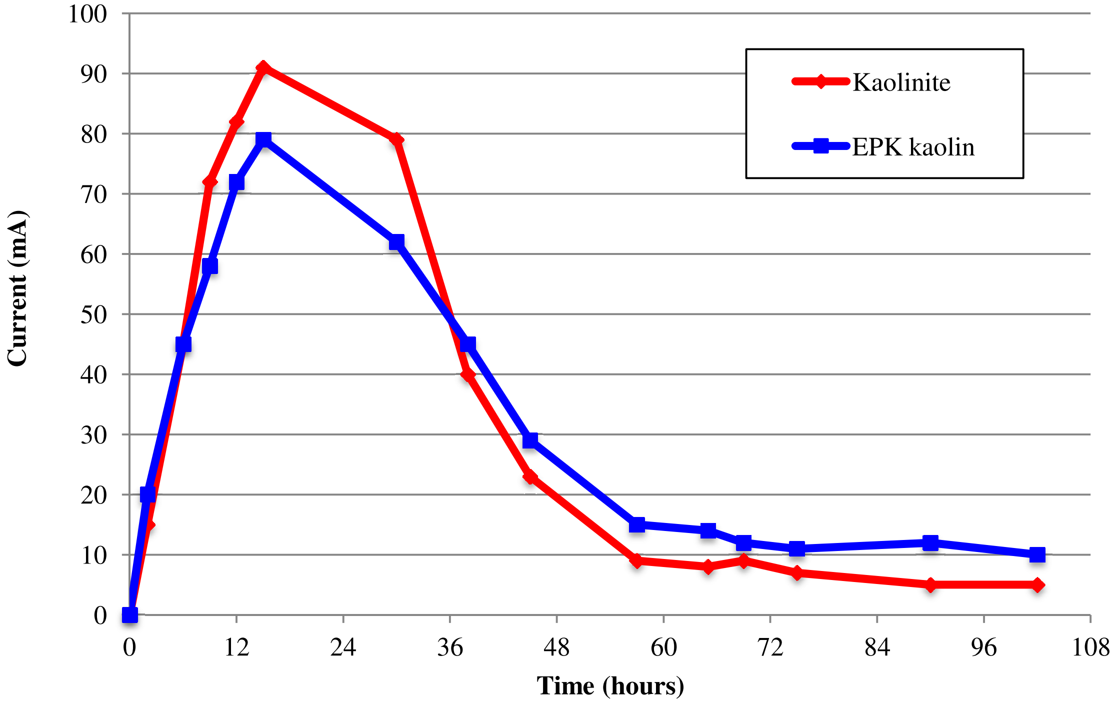

Figure 3.15 Current measured within electrokinetic cells for the kaolinite and EPK kaolin clay soils.

3.4 Conclusions

The two clays used in this study represent clay minerals typically found in subsurface formations. While clay soils can vary in their mineral structure and surface bound NOM, a general understanding of clay soils with contaminants may be applicable to future remediation efforts. In the adsorption isotherm studies, EPK kaolin was found to have a higher adsorption capacity than kaolinite. The Langmuir model parameters, Qo, representing the adsorption capacity were calculated to be 1.75 µg Cr^{VI} per gram and 1.25 µg Cr^{VI} per gram for EPK kaolin and kaolinite, respectively. As discussed, the mechanisms involved in Cr^{VI} removal from EPK kaolin included physical adsorption as well as chemical reduction from surface bound NOM, whereas the only significant removal mechanism in kaolinite clay was adsorption. These mechanisms were apparent in the results of the rate study, which indicated that the natural organic matter layer was capable of rapidly reducing Cr^{VI}. The addition of high concentrations of dissolved humic acid (>100 mg/L) increased the rate of Cr^{VI} reduction, however not with great significance. Analysis of the surface bound NOM responsible for giving EPK kaolin its Cr^{VI} reductive capacity verified it to have many similar functional groups to a typical humic acid.[29-30] This experiment demonstrated how effective surface bound NOM can be as a reductant. The experiments following this rate study evaluated Cr^{VI} reduction by dissolved humic acid, and verified that Cr^{VI} reduction by dissolved humic acid is a very slow process at neutral pH values.

Lastly, electrokinetic transport of chromium was observed through kaolinite and EPK kaolin soils, however transport was inhibited after 24 hours by reactions resulting from the formation of pH gradients at the anode and cathode. The experimental data indicated transport was not occurring through kaolinite clay columns after 24 hours, and the electrokinetic transport results for EPK kaolin were inconclusive. Reduction of Cr^{VI} was rapid in the presence of EPK kaolin due to the NOM surface coating, and thus it was difficult to determine if changes in Cr^{VI} concentration were a result of transport or chemical reduction. EPK kaolin is a unique clay soil due to the high content of natural organic matter. A better understanding of this clay and the mechanisms involved in its ability to reduce Cr^{VI} could lead to new strategies for the treatment of chromium contaminated groundwater. Furthermore, for effective electrokinetic remediation in clay soils with negligible amounts of NOM, enhancement techniques are necessary to minimize the formation of pH gradients and the numerous associated impacts.

3.5 Chapter 3 References

1. Bhattacharyya, K. G., & Sen Gupta, S. (2006). Adsorption of Chromium(VI) from Water by Clays. *Industrial & Engineering Chemistry Research*, *45*(21), 7232–7240.
2. Hizal, J., & Apak, R. (2006). Modeling of copper(II) and lead(II) adsorption on kaolinite-based clay minerals individually and in the presence of humic acid. *Journal of colloid and interface science*, *295*(1), 1–13.
3. Palmer, C. D., & Puis, R. W. (1994). EPA Ground Water Issue: Natural Attenuation of Hexavalent Chromium in Groundwater and Soils. *Environmental Research*.
4. Li, Y., Yue, Q.-Y., & Gao, B.-Y. (2010). Effect of humic acid on the Cr(VI) adsorption onto Kaolin. *Applied Clay Science*, *48*(3), 481–484.
5. Kyziol, J., Twardowska, I., & Schmitt-Kopplin, P. (2006). The role of humic substances in chromium sorption onto natural organic matter (peat). *Chemosphere*, *63*(11), 1974–82.
6. Schmitt, D., Taylor, H. E., Aiken, G. R., Roth, D. a, & Frimmel, F. H. (2002). Influence of natural organic matter on the adsorption of metal ions onto clay minerals. *Environmental science & technology*, *36*(13), 2932–8.
7. Jardine, P. M., Fendorf, S. E., Mayes, M. a., Larsen, I. L., Brooks, S. C., & Bailey, W. B. (1999). Fate and Transport of Hexavalent Chromium in Undisturbed Heterogeneous Soil. *Environmental Science & Technology*, *33*(17), 2939–2944.
8. Chen, J., Gu, B., Leboeuf, E. J., Pan, H., & Dai, S. (2008). Spectroscopic characterization of the structural and functional properties of natural organic matter fractions, *48*(2002), 59–68.
9. Ecology, T., & April, R. (2005). Sorption of Cu and Pb to kaolinite – fulvic acid colloids□: Assessment of sorbent interactions. *Geochimica*, *69*(7), 1675–1686.
10. Bartlett, R.J., and J.M. Kimble (1975) Behavior of Chromium in Soils: II. Hexavalent Forms, *Journal of Environmental Quality,* 5(4):383-386.
11. Fukushima, M. A., Nakayasu, K., Tanaka, S., & Nakamura, H. (1997). Speciation analysis of chromium after reduction of chromium (VI) by humic acid. *Toxicological & Environmental Chemistry*, *62*(1), 207–215.
12. Kim, S., Moon, S., & Kim, K. (2001). Removal of heavy metals from soils using enhanced electrokinetic soil processing. *Methods*, 259–272.
13. Reddy, K. (2003). Effects of initial form of chromium on electrokinetic remediation in clays. *Advances in Environmental Research*, *7*(2), 353–365.
14. Al-Hamdan, A. Z., & Reddy, K. R. (2006). Geochemical reconnaissance of heavy metals in kaolin after electrokinetic remediation. *Journal of environmental science and health. Part A, Toxic/hazardous substances & environmental engineering*, *41*(1), 17–33.
15. Al-Hamdan, A. Z., & Reddy, K. R. (2008). Transient behavior of heavy metals in soils during electrokinetic remediation. *Chemosphere*, *71*(5), 860–71.
16. Reddy, K. R., Xu, C. Y., & Chinthamreddy, S. (2001). Assessment of electrokinetic removal of heavy metals from soils by sequential extraction analysis. *Journal of hazardous materials*, *84*(2-3), 279–96.
17. Virkutyt, J., Sillanpää, M., & Latostenmaa, P. (2002). Electrokinetic soil remediation--critical overview. *The Science of the total environment*, *289*(1-3), 97–121. Retrieved from

18. Gent, D. B., Bricka, R. M., Alshawabkeh, A. N., Larson, S. L., Fabian, G., & Granade, S. (2004). Bench- and field-scale evaluation of chromium and cadmium extraction by electrokinetics. *Journal of hazardous materials*, *110*(1-3), 53–62.
19. Sawada, A., Mori, K., Tanaka, S., Fukushima, M., & Tatsumi, K. (2004). Removal of Cr(VI) from contaminated soil by electrokinetic remediation. *Waste management (New York, N.Y.)*, *24*(5), 483–90.
20. Kim, S.-O., Kim, K.-W., & Stüben, D. (2002). Evaluation of Electrokinetic Removal of Heavy Metals from Tailing Soils. *Journal of Environmental Engineering*, *128*(8), 705.
21. Reddy, K. R., & Chinthamreddy, S. (2003). Sequentially Enhanced Electrokinetic Remediation of Heavy Metals in Low Buffering Clayey Soils. *Journal of Geotechnical and Geoenvironmental Engineering*, *129*(3), 263.
22. Pamukcu, S., Weeks, A., & Wittle, J. K. (2004). Enhanced reduction of Cr(VI) by direct electric current in a contaminated clay. *Environmental science & technology*, *38*(4), 1236–41.
23. Page, M. M., & Page, C. L. (2002). Electroremediation of Contaminated Soils. *Journal of Environmental Engineering*, *128*(3), 208.
24. Kaya, A., & Yukselen, Y. (2005). Zeta potential of soils with surfactants and its relevance to electrokinetic remediation. *Journal of hazardous materials*, *120*(1-3), 119–26.
25. Deng, B., & Stone, A. T. (1996). Surface-Catalyzed Chromium(VI) Reduction: Reactivity Comparisons of Different Organic Reductants and Different Oxide Surfaces. *Environmental Science & Technology*, *30*(8), 2484–2494.
26. Reddy, K.R., and Cameselle, C., Electrochemical Remediation Technologies for Polluted Soils, Sediments and Groundwater, John Wiley & Sons, Inc., Hoboken, New Jersey, 2009.
27. Gu, B., & Chen, J. (2003). Enhanced microbial reduction of Cr(VI) and U(VI) by different natural organic matter fractions. *Geochimica et Cosmochimica Acta*, *67*(19), 3575–3582.
28. Lumsdon, D.G., and Fraser, A.R. (2005). Infrared Spectroscopic Evidence Supporting Heterogeneous Site Binding Models for Humic Substances. *Environmental Science and Technology,* **39** (17), 6624-663.
29. Xu, D., Zhu, S., Chen, H., and Li, F. (2006). Structural Characterization of Humic Acids Isolated from Typical Soils in China and their Adsorption Characteristics to Phenanthrene. *Colloids and Surfaces, Part A: Physicochemical and Engineering Aspects,* **276**, 1–7.
30. Chen, J., Gu, B., Leboeuf, E. J., Pan, H., & Dai, S. (2008). Spectroscopic characterization of the structural and functional properties of natural organic matter fractions, *48*(2002), 59–68.
31. Wittbrodt, P. R., & Palmer, C. D. (1995). Reduction of Cr(VI) in the Presence of Excess Soil Fulvic Acid. *Environmental science & technology*, *29*(1), 255–63.
32. Al-Hamdan, A.Z. (2002) Speciation, Distribution, and Mobility of Heavy Metals in Soils During Electrokinetic Remediation, *Ph.D. Thesis, 73-75.*
33. Paul A. Siracusa, P. Somasundaran, The role of mineral dissolution in the adsorption of dodecylbenzenesulfonate on kaolinite and alumina, Colloids and Surfaces, Volume 26, 1987, Pages 55-77.
34. Sposito G. (1989). *The Chemistry of Soils.* New York: Oxford University Press.

Chapter 4 : Integration of Electrokinetic and Zero-Valent Iron Technology for Treatment of Cr^{VI} in Sandy Soils and the Effects of Humic Acid

4.1 Introduction

Lab-scale research from many institutions has clearly illustrated the incredible reduction capacity of nZVI and highlighted the ability of nZVI to treat a gamut of contaminants through various mechanisms.[2-10,12,14] Many follow up investigations have also highlighted the shortcomings of this technology, namely the tendency to form large aggregates, its rapid oxidation in water, the difficulty to evenly distribute nZVI in the subsurface, and the influences of natural groundwater chemistry and constituents, namely divalent cations and natural organic matter.[15-20, 22-24]

Field scale-investigations have recently had some success in significantly reducing concentrations of both organic and inorganic pollutants alike, however complications related to injectability of nZVI, porosity of receiving soil or groundwater system, and oxidative subsurface environments continue to inhibit the function of nZVI.[1] The nZVI must come into close contact with the target contaminant while still in a highly reduced state to drive the desired reaction, and this can be difficult to achieve economically for wide spread contamination. In a full-scale application in the Czech Republic for example, 82 injection wells were bored for a targeted area of 120 x 60 m contaminated with PCE, TCE, and DCE. This represents nearly one injection well for every 9 x 9 m square. After a total injection of 300 kg of nZVI, concentrations had dropped from as high as 70 mg/L in some areas to 20-30 mg/L.[2]

Much attention from industry and academia is focused on nanoparticle technology, and attempts to improve the ability of the nanoparticle to reach the contaminant. The purpose of this chapter however is to demonstrate the benefits of taking the opposite approach, i.e. transporting the target contaminant to the nanoparticle. Leveraging the strong foundation already existing regarding transport of contaminants by electrokinetic phenomena, this study aims to evaluate the feasibility and potential benefits of using an applied electric potential to transport Cr^{VI} through the subsurface, and investigate its reduction in the presence of nZVI injected in the path of the Cr^{VI} plume. For a more detailed theoretical background on nZVI and groundwater remediation applications, please see Chapter 2.5.

4.2 Materials and Methods

Materials

Chemicals

All chromium stock solutions were prepared by dissolving 2.828 g of ACS reagent grade (≥99.0% purity) potassium dichromate in 1.0 L of distilled-deionized (DDI) water for a final Cr^{VI} concentration of 1000 mg Cr^{VI} /L. A 1.0 M stock bicarbonate buffer solution was prepared from ACS reagent grade (99.7-100.3% purity) $NaHCO_3$, and diluted as required for experiments. A calcium chloride stock solution of 1000 mg/L was made by dissolving 1.0 g of bioreagent grade (≥ 96%) $CaCl_2$ in 1.0 L of distilled deionized water. All solutions were refrigerated at 3°C until use.

The humic acid chosen for this study was technical grade humic acid from Sigma-Aldrich. This is a well-characterized humic acid and is commonly used to represent natural organic matter in water supplies. Dried humic acid was dissolved in DDI water at pH 12 for four hours under constant agitation for a concentration of 2.0 g/L, then filtered through a 0.45 μm pore size membrane to remove any insoluble fractions in solution.

The eluent solution required for Cr^{VI} determination by ion-exchange chromatography was prepared by dissolving 66.0 g of ammonium sulfate in 1 L of DDI water with the addition of 13.0 mL of 29% ammonium hydroxide. The solution was diluted to a final volume of 2.0 L with DDI water.

A pH adjustment buffer solution was added to samples to stabilize Cr^{VI} while in storage before analysis. The buffer solution was prepared by dissolving 3.3 g of ammonium sulfate in about 75 mL of DDI water with the addition of 6.5 mL of 29% ammonium hydroxide, then diluting to a volume of 100 mL.

A post-column reagent solution was used for colorimetric determination of Cr^{VI} by absorption spectrophotometry at 530 nm. A specified volume of sulfuric acid (98% purity) was added to about 500 mL of DDI water, then cooled to room temperature. While cooling, 0.5 g of 1,5-diphenylcarbazide was added to about 75 mL of HPLC-grade methanol, and the 1,5-diphenylcarbazide was dissolved by sonication. Once dissolved, methanol was added to reach a final volume of 100 mL. This solution was added to the cooled sulfuric acid solution and brought to a volume of 1.0 L with DDI water.

A 1000 mg/L inorganic carbon (IC) standard solution was prepared by dissolving appropriate amounts of reagent grade sodium bicarbonate and sodium carbonate in 1.0 L of DDI water. Similarly, a 1000 mg/L organic carbon (TOC) standard solution for TOC calibration was prepared by adding an appropriate amount of reagent grade potassium hydrogen phthalate to 1.0 L of DDI water.

All pH adjustments were carried out using dilute solutions of NaOH or HCl, and all chemicals were obtained from Sigma-Aldrich unless otherwise specified.

Silica Sand

The silica sand used in column studies was a 40-mesh silica sand (Carmeuse Industrial Sands, Orange County, CA), with effective particle diameters of 0.45-0.55 mm, and a uniformity coefficient of < 1.5.

Zero-Valent Iron Nanoparticles

The nZVI used in experiments is the Nanofer 25s product supplied by Nano Iron s.r.o. (Czech Republic). The Nanofer 25s product contains a slurry of nZVI dispersed in an organic stabilizer solution designed to increase negative surface charge on the nanoparticles and inhibit aggregation. The nZVI have a Fe^0 core and a thin layer of FeO coating the surface. The nZVI dispersion is 20% iron by weight, and roughly 85% of the total iron is in the zero-valent oxidation state. The dispersion density is 1210 kg/m^2, and therefore the nZVI suspension contains approximately 206 g Fe^0/L. The average particle size is reported by the supplier to be less than 50 nm.

Methods

Zeta Potential of nZVI in Water: Effects of Surface Oxidation of nZVI

In 50 mL centrifuge tubes, nZVI was added to bicarbonate buffered solution adjusted to pH 5, 7, 9, and 11 to achieve a final concentration of 500 mg nZVI/L. Samples were shaken continuously for three days and zeta potential was measured at times zero, 8 hours, 28 hours, and 72 hours.

Zeta Potential of nZVI in Water: Effects of Background Humic Acid

A 10^{-2} M bicarbonate buffered water was used to make five different humic acid solutions with concentration of 0, 10, 50, and 100 mg/L. Each humic acid solution was divided into four parts that were adjusted to pH 5, 7, 9, and 11. Lastly, nZVI were added to these humic acid solutions to achieve a final concentration of 500 mg nZVI/L. At the end of a 1-hour equilibration time, the zeta potential was measured.

Reduction of Cr^{VI} by nZVI under Oxic and Anoxic Conditions

For oxic conditions, dilution water for the chromium standard solutions was prepared by adding phosphate buffer to DDI water for a final concentration of 10 mM and adjusting the pH to 7.0±0.05. With this water, Cr^{VI} solutions of 5 mg/L, 10 mg/L, 20 mg/L, 30 mg/L, and 50 mg/L were prepared. Exactly 50 mL of each standard was transferred to a 50-mL centrifuge tube in duplicates. These were stored at 3°C until use.

For anoxic conditions, approximately 110 mL of each standard solution was transferred to 250 mL capacity Duran jars to begin preparation of the anoxic chromium standard solutions. The solutions were purged with N_2 for 60 minutes to expel dissolved oxygen, quickly sealed, and transferred to a nitrogen glove box. The de-oxygenated solutions were analyzed for dissolved oxygen content under the nitrogen atmosphere. In the glove box, 50 mL of each anoxic Cr^{VI} solution was added to anaerobic jars in duplicates. These were left exposed to the nitrogen atmosphere overnight. Once both sets of standards were prepared, the reaction vessels were prepared for the rate studies.

The injection of nZVI into the reaction vessels was carried out in a nitrogen glove box for both oxic and anoxic experiments to avoid exposing the nZVI dispersion to oxygen. Additionally, humic acid and $CaCl_2$ were added to the reaction vessels under the nitrogen atmosphere to achieve final concentrations for the specific experiment.

The nZVI addition was done by pouring approximately 20 mL of the nZVI dispersion into a 50-mL beaker. Exactly 1.0 mL of the nZVI solution was added to a pre-weighed 1.5 mL micro-centrifuge tube. This was removed from the glove box and reweighed. Using the weight, the amount of nZVI solution was added to each reaction vessel was calculated such that the final Fe^0 concentration was 0.025 g/L. Some agglomeration of nZVI in the slurry provided by the supplier was evident. In order to ensure reproducibility between individual experiments, a prior calculation was performed to adjust Fe^0 addition. The volume of nZVI required in each reaction vessel was calculated based on the difference between the theoretical density of the stock solution and the actual density, for a target amount of 0.025 g/L. The volume of nZVI determined from this basic calculation was added to each reactor. The nZVI stock solution was routinely mixed during this process to ensure a homogenous mixture. The reactors were capped and removed from the glove box, placed on a shake plate, and sampled at 0 h, 0.5 h, 1 h, 2 h, 4 h, 8 h, and 24 hours. Sampling consisted of removing 1.0 mL of the sample by micropipette, followed by immediate centrifugation at 12,000 rpm for 10 minutes, and then filtration through 0.22 μm syringe filters tips to remove all iron from solution before storage. After filtration, 7.0 μL of buffer was added to each filtered sample to stabilize Cr^{VI} in solution before storage at 3°C. Samples were analyzed for Cr^{VI} by ion-exchange chromatography.

Dynamic Electrokinetic Column Studies

The experimental apparatus used for the dynamic column studies is illustrated in Figure 4.1. In these studies the column size remained the same as the semi-batch tests, however typical aquifer silica sand was used in the soil column. The Cr^{VI} solution was pumped through the columns from the bottom up (up-flow feed), and flow rate could be carefully controlled.

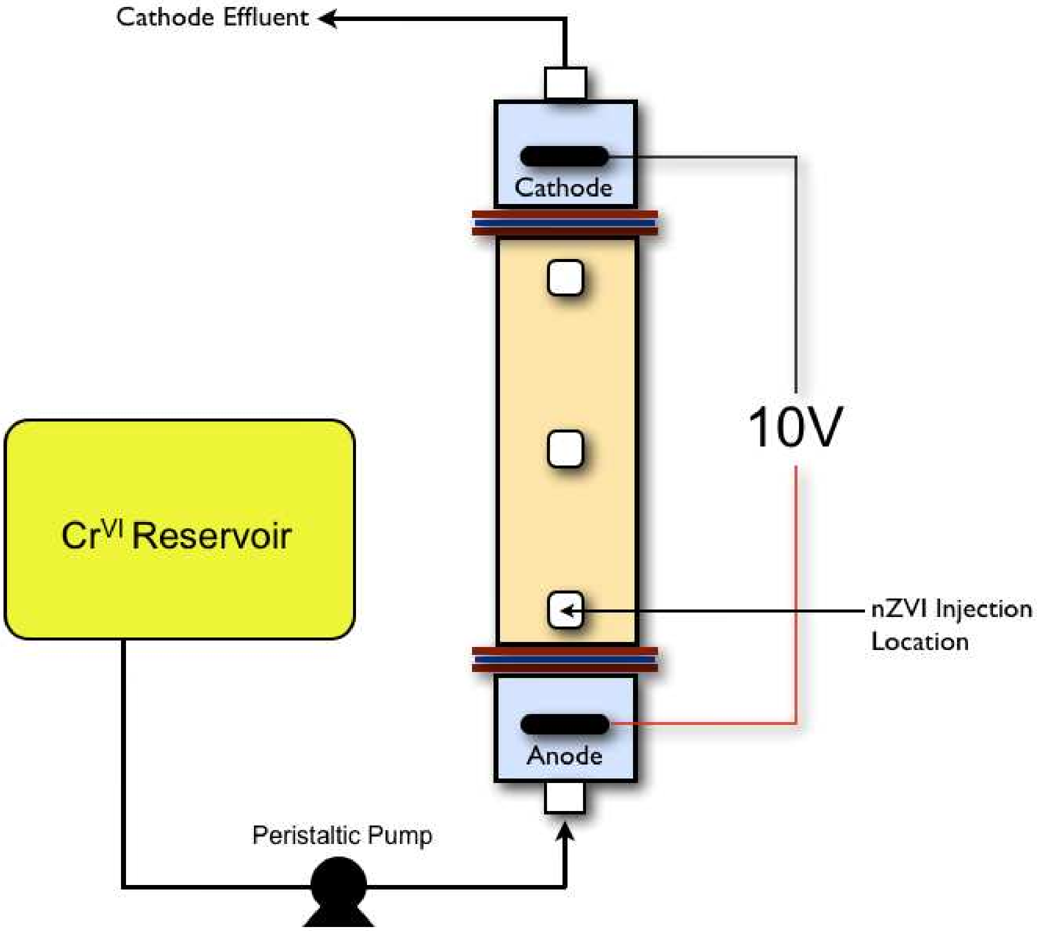

Figure 4.1 A schematic of the experimental apparatus used in dynamic electrokinetic studies.

Two columns were run in parallel during each experiment; one column contained the bare silica sand (column 1), and the other contained silica sand equilibrated with a dissolved humic acid solution (column 2). The humic acid equilibration was performed by mixing the silica sand with a 100 mg/L humic acid solution. This is anticipated to be enough humic acid to saturate the sand particles, and was verified by TOC analysis. Measurement of TOC of the humic acid solution before and after the 24-hour equilibration period was used as an indicator the amount of humic acid adsorbed to sand particle surfaces, and also indicated when equilibration was reached. The sand was then be loaded into the column, and saturated with a 3.0 mg/L Cr^{VI} and 10^{-2} M carbonate buffer solution.

The silica sand column, column 1, was prepared by thoroughly rinsing sand with DDI water to remove any undesirable particulate matter that may be weakly bound to the sand particles. The sand was then charged to the columns. The anode and cathode reservoirs, as well as the sand column were loaded with a 3.0 mg/L Cr^{VI} solution with a 10^{-2} M carbonate buffer. Once loaded with sand and filled with the chromium solution, the columns were allowed to reach equilibrium before electric potential was applied.

A 3.0 mg/L Cr^{VI} solution was continuously pumped into the anode reservoir with a peristaltic pump, and the flow rate was maintained at 12 mL hr^{-1}. This value was chosen because it represents a median value for typical groundwater flow in a sandy aquifer. Electric potential was changed between different sets of experiments from 0.5 V/cm, to 1.0 V/cm, to 1.5 V/cm. Sampling from the sand column as well as from the cathode reservoir effluent was performed routinely to measure Cr^{VI} transport through the column, and the development of any pH gradients was monitored.

The dynamic electrokinetic experiments were repeated with nZVI injection into the sand column near the anode reservoir (Figure 4.1). The nZVI dispersion was diluted in DDI water before injection to reduce self-aggregation within the sand column. In one set of experiments 25 μL of the nZVI stock dispersion was diluted to 2 mL and then injected into the column, which amounted to 5.15 mg of nZVI per injection. In a second set of experiments, 50 μL of the nZVI stock solution was diluted to 2 mL with DDI water for a total nZVI addition of 10.3 mg per injection.

Analytical Methods

Ion-Exchange Chromatography

Samples were analyzed for Cr^{VI} by ion-exchange chromatography (Dionex ICS-1000, Sunnyvale, CA). See Chapter 3.2 for a more detailed description.

Dissolved Organic Carbon

Dissolved organic carbon analysis was performed using a Shimadzu TOC-V CSH total organic carbon analyzer (Shimadzu Corp., Kyoto, Japan), in accordance with EPA method 415.1. Samples were filtered to remove particulates and any non-dissolved organic matter before analysis.

Zeta Potential

Zeta potential measurements were taken using a Zeta Meter 3.0+ (Zeta Meter Inc., New York) equipped with a microprocessor unit, allowing statistical calculations to be made immediately for each sample. nZVI was added to 10^{-2} M carbonate buffered DDI water for a final concentration of 100 mg of solids/L, and the pH was adjusted and stabilized prior to analysis using concentrated HCl and NaOH.

Dissolved Oxygen Determination

Dissolved oxygen was measured with a Hach HQ40d Dual Input Multi-Parameter portable meter and a LDO101 Luminescent Dissolved Oxygen probe (Hach Corp.; Loveland, Colorado).

4.4 Results and Discussion

Zeta Potential of nZVI in Water: Effects of Surface Oxidation of nZVI

For nZVI to be an effective sorbent in groundwater systems, it must remain suspended in water long enough to reach contamination plumes and interact with the target contaminants. Zeta potential measurements taken over a period of three days provided some indication as to how these particles will behave in an aquifer. The results indicate that nZVI are more stable in water with increasing pH. This is anticipated as deprotonation of surface iron-hydroxide, and deprotonation of functional groups on the organic dispersant increase with increasing pH, which results in a higher negative surface charge density. Time has a significant impact on nZVI stability in water as well, as seen by the significant drop in stability observed in each suspension after 28 hours. After this point a small increase in stability is observed (Figure 4.2).

Immediately upon injection of nZVI into simulated natural water solution, multiple reactions begin to occur simultaneously. The nZVI undergoes oxidative dissolution, where the zero-valent iron is oxidized to Fe^{2+} and can be released into the solution. Additionally, this mechanism releases the organic dispersant into solution. The particles are therefore losing a fraction of their stability from dissolution of the organic layer, as well as losing stability by the formation of iron oxides on the surface that carries a charge dependent on solution pH. The decrease in zeta-potential over the first 28 hours is a product of these destabilization mechanisms.

As shown in Figure 4.2, the apparent increase in nZVI stability between hour 28 and hour 72 is a product of changes in solution chemistry, and not representative of a specific change in nZVI surface characteristics. During zeta potential analysis that the iron transitioned from its initial black color to entirely orange as a result of oxidation. Additionally, the majority of the particles were associated with large aggregates that moved very slowly under the applied electric filed due to their size-induced hydrodynamic constraints. In an aquifer system these particles would likely be filtered out by size-exclusion or settle out by gravity. The particles that were measured at the 72-hour time-point were those that were not associated with large aggregates, however these particles were much less abundant in solution, and difficult to observe in the orange colored solution. It can be postulated that immediately upon the introduction of nZVI to water, the iron dispersion will become less stable due to a series of redox reactions at the nZVI surface.

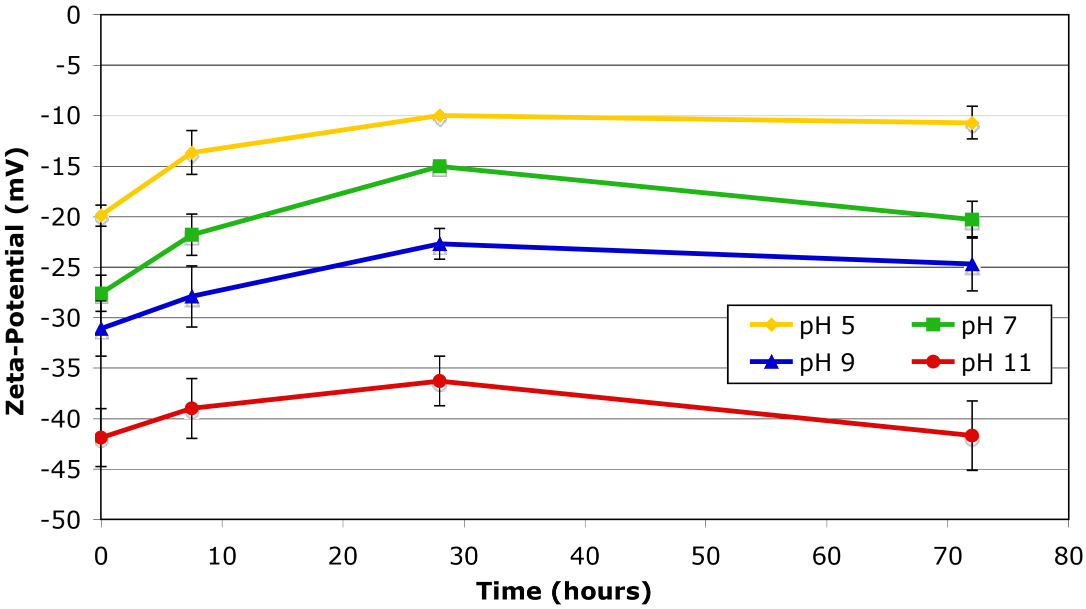

Figure 4.2 Zeta-potential of nZVI in DDI water with a 10^{-2} M carbonate buffer at different pH values.

Zeta Potential of nZVI in Water: Effects of Background Humic Acid

The effects of humic acid on the stability of nZVI in water were investigated over a range of pH 5 to pH 11 (Figure 4.3). Particle stability was shown to increase with humic acid concentration, and also with increasing pH. In the presence of 10 mg/L of humic acid, the zeta potential increased by an average of 4.2 mV across the entire pH range as compared to the sample with no humic acid present. An average increase of 3.5 mV was observed with a humic acid concentration of 50 mg/L relative to the solution with a 10 mg/L humic acid concentration. The solution containing 100 mg/L of humic acid however showed a decrease in particle stability as compared to the 50 mg/L humic acid solution.

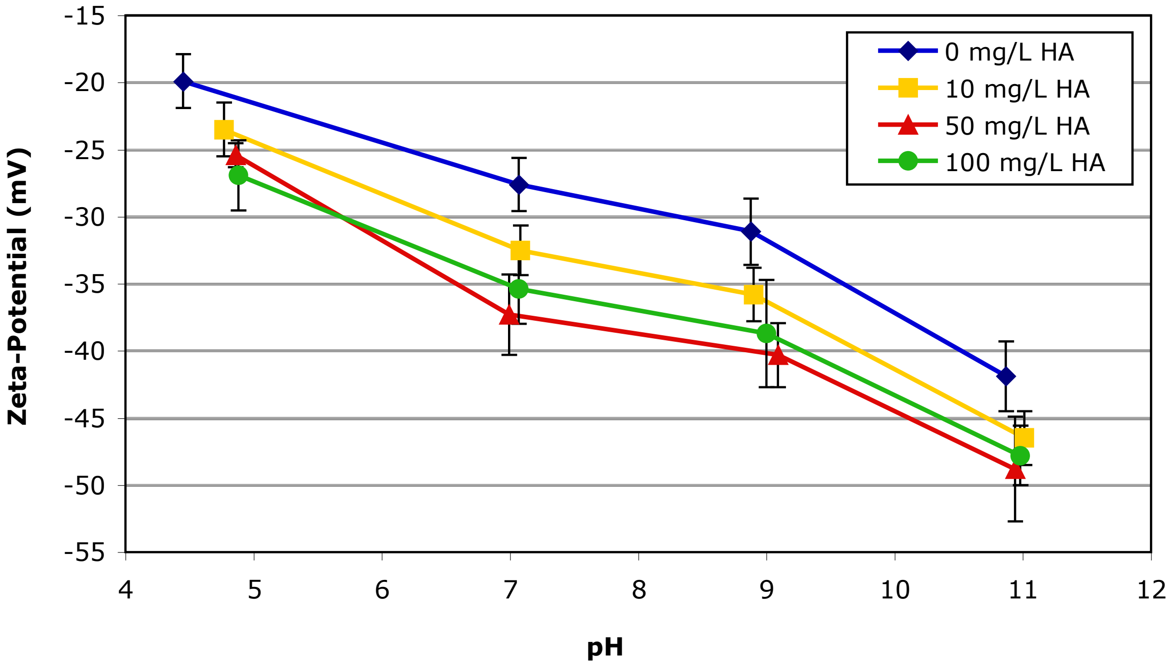

Figure 4.3 Zeta-potential of nZVI in 10^{-2} M carbonate buffered solutions with different humic acid concentrations.

The results of this investigation reveal the effects of the organic dispersant coating on the nZVI. This coating gives the particles enhanced stability across a wide pH range, as indicated by the absence of a point of zero charge. This is a significant improvement to bare nZVI, which typically have a point of zero charge near pH 6.[17] In the presence of 10 mg/L and 50 mg/L of humic acid, the negative surface charge density increased as a result of humic acids binding to either the nZVI particles themselves or to the organic dispersant that coats the nZVI. In the presence of 100 mg/L of humic acid, a decrease in particle stability was observed. The high concentration of humic acid was likely forming bridges between particles, increasing the amount of nZVI aggregation. As the aggregates increase in size, drag associated with electrophoretic movement through the water as well as gravity effects decrease horizontal velocity.

The pH had significant effects on the solution chemistry of the solutions containing 50 mg/L and 100 mg/L of humic acid. At pH 5 the solutions containing 50 and 100 mg/L humic acid were very cloudy and it appeared humic acid precipitates were forming, likely as a result of Fe^{2+}-humate complexation.[30] At pH 7 and pH 9 the solution only had a faint yellow-brown color from the humic acid, however aggregation was obvious by the presence of large, brown flocs. At pH 11 it was very difficult to discern nZVI particles that had not agglomerated. These results indicate that low concentrations of humic acid can enhance nZVI stability in water, however high concentrations (>50 mg/L) of humic acid cause increased agglomeration and have a destabilizing effect on nZVI.

Reduction of Cr^{VI} by nZVI under Oxic and Anoxic Conditions

Oxic Conditions

A series of CMBR rate experiments were conducted to investigate Cr^{VI} reduction by nZVI and the effects of humic acid and calcium under anoxic and oxic conditions. The first set of experiments were conducted under an oxic environment with the following conditions: i) Cr^{VI} in a 10^{-2} carbonate buffered solution, ii) Cr^{VI}, carbonate buffer, and 30 mg/L of humic acid, and iii) Cr^{VI}, carbonate buffer, 30 mg/L of humic acid, and 40 mg/L of Ca^{2+}. The concentration of Cr^{VI} was varied from 5 mg/L to 50 mg/L, and nZVI was added to each CMBR for a final concentration of 0.025 g/L. The dissolved oxygen concentration was measured between 8.7 - 8.8 mg/L in each CMBR before iron addition.

As can be seen in Figures 4.4 through 4.6, equilibrium was reached after approximately 6 hours. In the absence of calcium and humic acid, 96.7% percent of Cr^{VI} was reduced from an initial Cr^{VI} concentration of 5 mg/L. A summary of the percent removal from each study is presented in Table 4.3. The removal percentages for samples containing higher concentrations of Cr^{VI} are consistent with saturation of the finite number of reactive sites on nZVI. At the equilibrium stage, the Cr^{VI} reduction data were fit to the

Langmuir isotherm model, which described the adsorption data reasonably well (Figure 4.7). The adsorption capacity of nZVI for Cr^{VI} (Q^o) in the absence of humic acid and calcium was determined to be 229.1 mg Cr^{VI} per gram of nZVI. Q^o was calculated to be 205.6 mg Cr^{VI} per gram of nZVI in the presence of humic acid. The addition of a 40 mg/L calcium solution decreased Q^o further to 188.0 mg Cr^{VI} per gram of nZVI. The Langmuir isotherm parameters are listed in Table 4.4.

Reaction rate constants were determined for the pseudo-first order reduction of Cr^{VI} by nZVI that occurred within the first 1.5 hours of reaction (Table 4.1). It was anticipated that the rate constants would indicate that the rates of approach to equilibrium are highest in absence of humic acid and calcium. However in the absence of humic acid and calcium, the reaction rates were lower than those in the solution containing just humic acid. The rates decreased in the humic acid and calcium solution, however they remained higher than those in the solution absent of humic acid and calcium. These results are likely a result of experimental error, from using an old batch of nZVI that had undergone significant agglomeration.

The results show that the effectiveness of nZVI for groundwater remediation is reduced in the presence of humic acid, and even further inhibited by the combination of humic acid and calcium. The following explanation provides a mechanistic speculation for this phenomenon. Humic acid rapidly binds to the nZVI surface, which competitively occupies surface reactive sites. Additionally, humic acid can lead to increased nZVI aggregation, which causes nZVI to be less effective in remediation efforts due to a decrease in reactive surface area and intrinsic reactivity. The addition of calcium has a further inhibitory affect by its ability to complex humic acid leading to precipitation of a calcium-humate complex on the nZVI surface.[42]

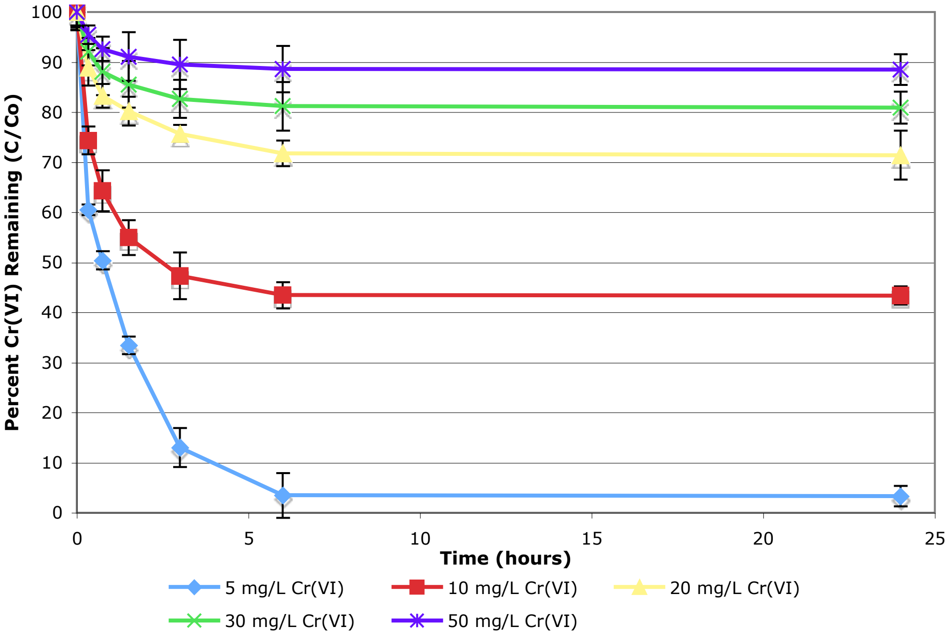

Figure 4.4 CMBR rate study for the reduction of Cr^{VI} by nZVI under oxic conditions.

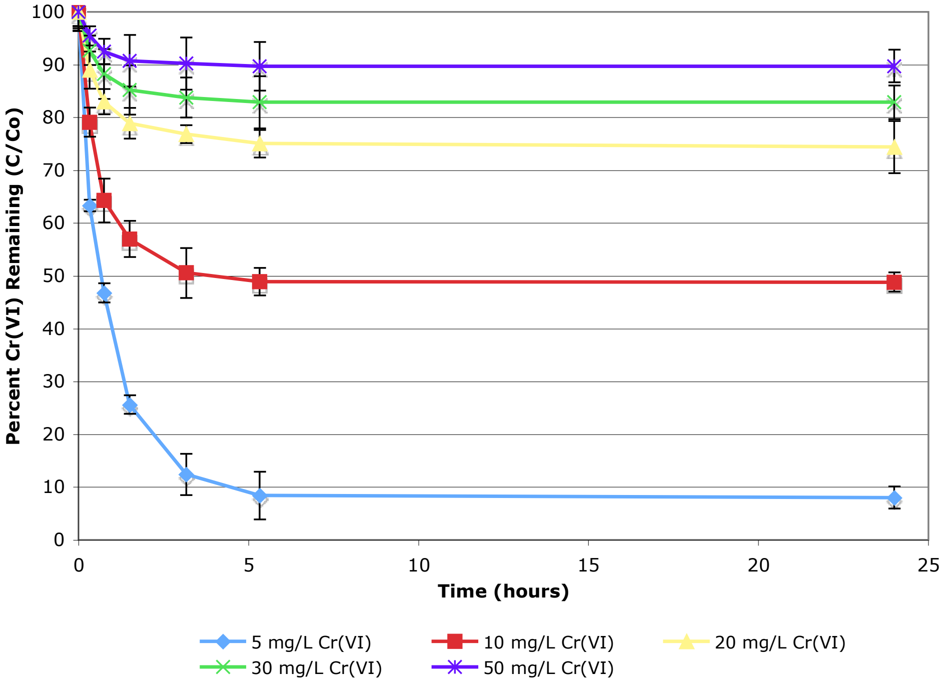

Figure 4.5 CMBR rate study for the reduction of Cr^{VI} by nZVI under oxic conditions in 30 mg/L humic acid.

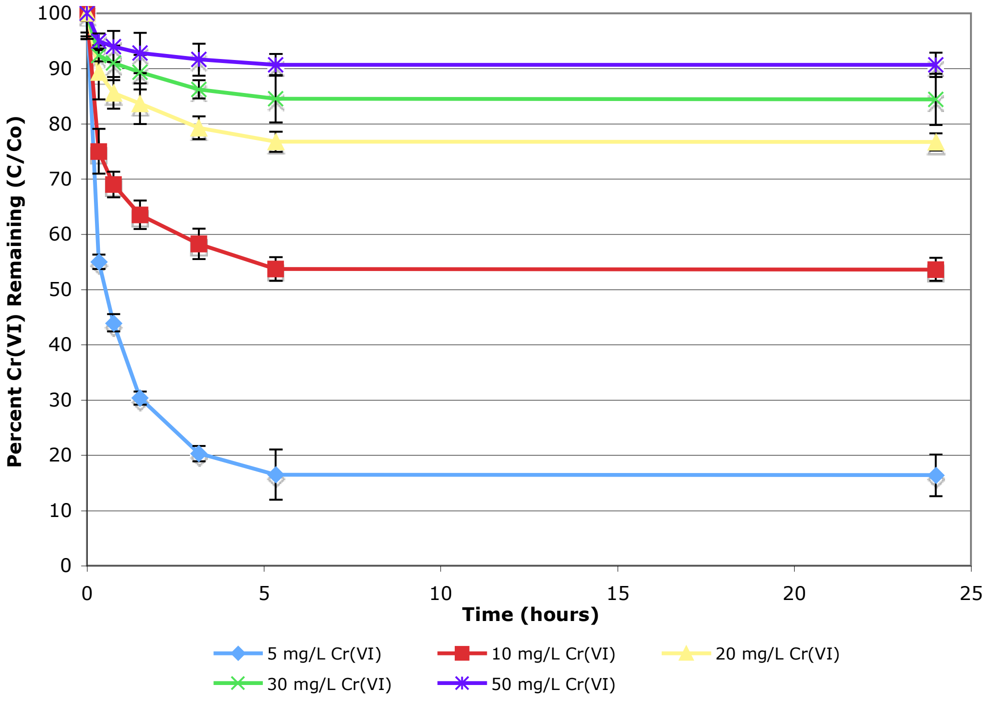

Figure 4.6 CMBR rate study for the reduction of Cr^{VI} by nZVI under oxic conditions in 30 mg/L humic acid and 40 mg/L Ca^{2+}.

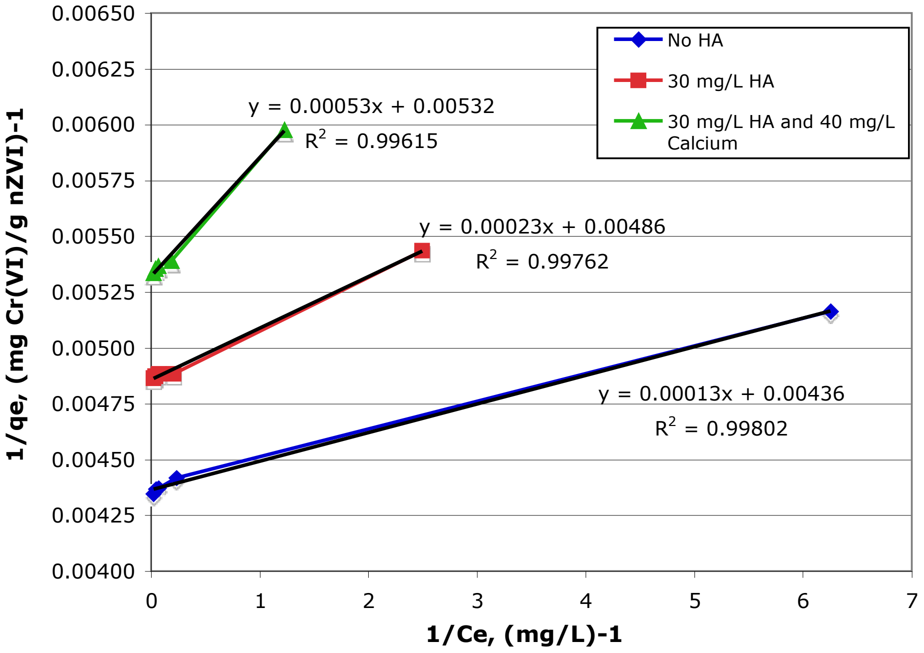

Figure 4.7 Langmuir isotherm model fit to the adsorption equilibria data for oxic conditions.

Table 4.1 Reaction rate constants for the pseudo first-order reduction of Cr^{VI} by nZVI under oxic conditions.

Oxic Studies	No HA or Calcium		30 mg/L HA		30 mg/L HA and 40 mg/L Calcium	
Initial Cr^{VI} Concentration	***k* (hr^{-1})**	**r^2**	***k* (hr^{-1})**	**r^2**	***k* (hr^{-1})**	**r^2**
5.00	0.678	0.930	0.877	0.985	0.731	0.895
10.00	0.369	0.884	0.361	0.894	0.268	0.771
20.00	0.136	0.826	0.147	0.865	0.107	0.755
30.00	0.096	0.836	0.101	0.877	0.065	0.710
50.00	0.058	0.849	0.0609	0.865	0.043	0.721

Anoxic Conditions

CMBR rate studies were conducted under anoxic conditions in a similar fashion as described earlier for the oxic conditions. The dissolved oxygen levels were measured at 1.3-1.5 mg/L at the commencement of each experiment. The anoxic environment provided conditions much more favorable for Cr^{VI} reduction by nZVI than that of oxic conditions. For an initial Cr^{VI} concentration of 5 mg/L in the absence of humic acid and calcium, no Cr^{VI} was present in solution after two hours of reaction time (Figure 4.8). For a 10 mg/L Cr^{VI} solution, 85.4% of Cr^{VI} was removed after 6 hours of reaction time. Over 17% of Cr^{VI} was removed from the solution containing an initial Cr^{VI} concentration of 50 mg/L. As can be seen in comparison of Figures 4.8 through 4.10, the reduction percentages in the presence of humic acid and calcium decreased significantly. Additionally, the reaction rates (*k*-values) decreased similarly to the oxic studies with humic acid and calcium present. The observed reaction kinetics were pseudo-first-order in the first 1.5 hours of reaction, and the observed *k*-values decreased with the addition of humic acid, and decreased further the presence of humic acid and calcium (Table 4.2). The reaction rate constants were considerably higher than those determined in the oxic studies, as a result of a higher intrinsic reactivity in the absence of dissolved oxygen. The solution with an initial Cr^{VI} concentration of 5 mg/L was reduced to below detectable levels within minutes of reaction time so this data was not used in determining adsorption isotherm parameters. In the absence of humic acid and calcium, the highest observed pseudo first-order reaction rate was 1.04 hr^{-1} for the 10 mg/L initial Cr^{VI} solution. This reaction rate was reduced by nearly 50% with the introduction of humic acid, and reduced further with the addition of humic acid and calcium.

From the rate data, an adsorption isotherm was developed once equilibrium had been established. The Langmuir adsorption isotherm model satisfactorily described equilibrium data for all three systems (Figure 4.11). The adsorption capacity (Q^o) for the system with Cr^{VI} alone was calculated to be 350 mg of Cr^{VI} per gram of nZVI. The introduction of humic acid lowered the adsorption capacity to 329 mg $gram^{-1}$, and addition of calcium lowered the adsorption capacity further to 325 mg $gram^{-1}$ of nZVI. A summary of the experimental Langmuir adsorption isotherm parameters is presented in Table 4.4. The trends in nZVI functionality observed in this study were attributed to the same factors highlighted in the oxic experiments.

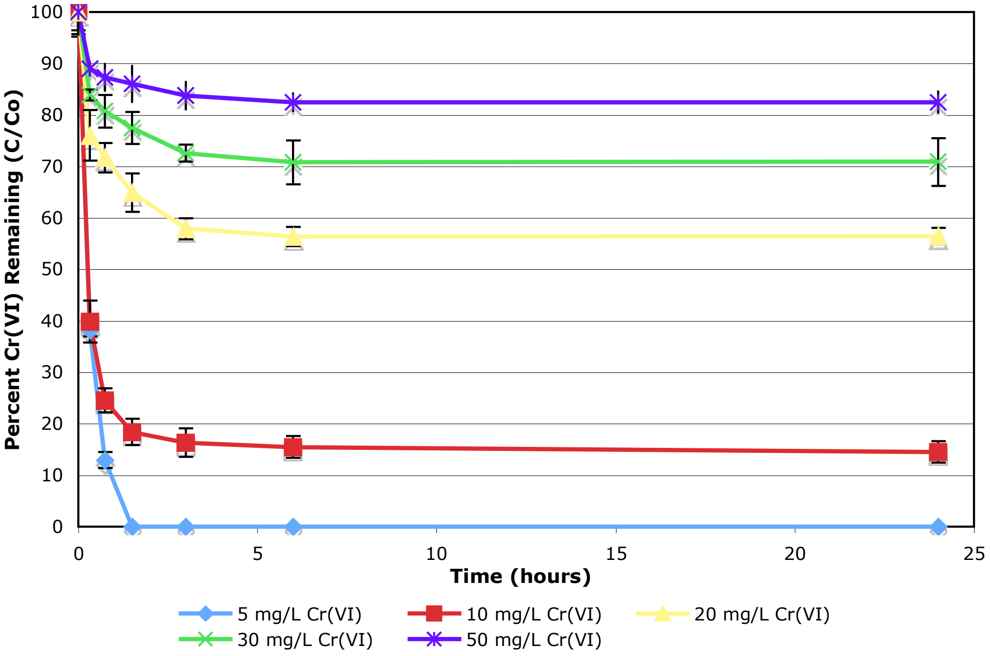

Figure 4.8 CMBR rate studies for the reduction of Cr^{VI} by nZVI under anoxic conditions.

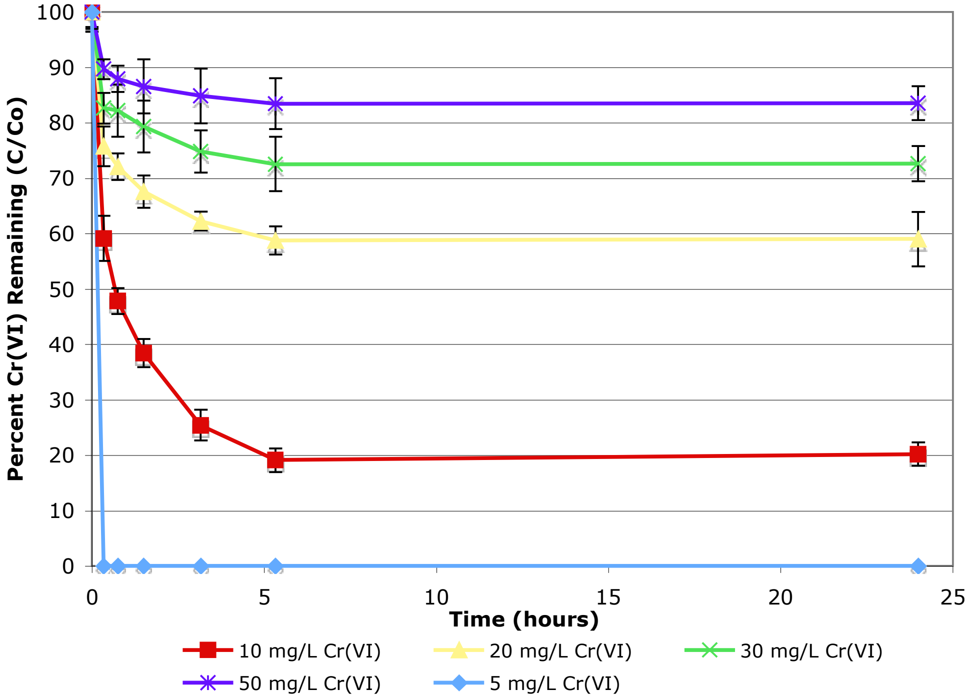

Figure 4.9 CMBR rate studies for the reduction of Cr^{VI} by nZVI under anoxic conditions in 30 mg/L humic acid.

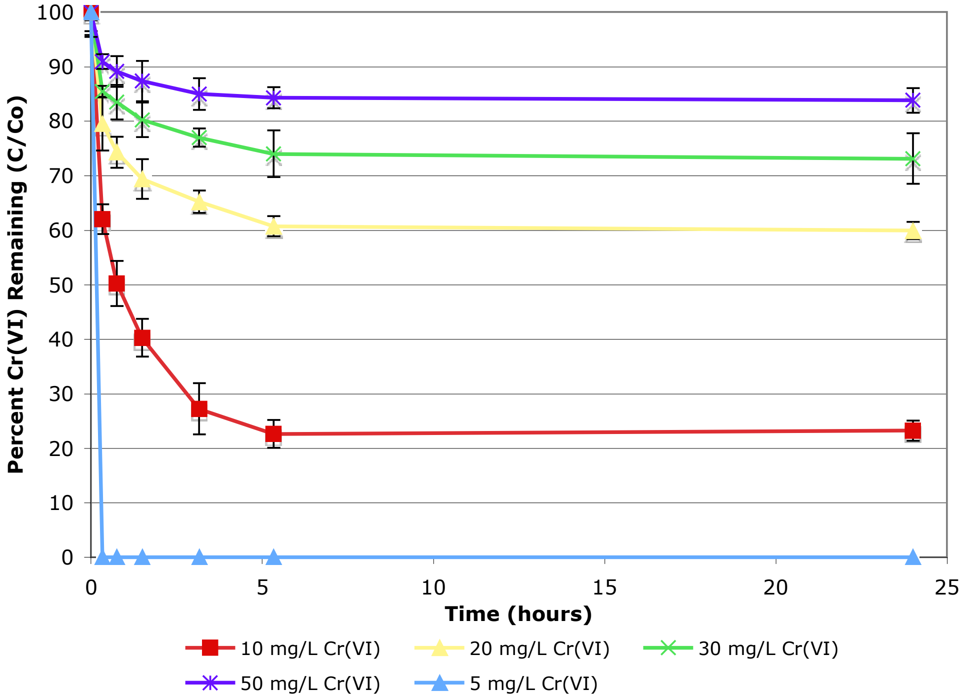

Figure 4.10 CMBR rate studies for the reduction of Cr^{VI} by nZVI under anoxic conditions in 30 mg/L humic acid and 40 mg/L Ca^{2+}.

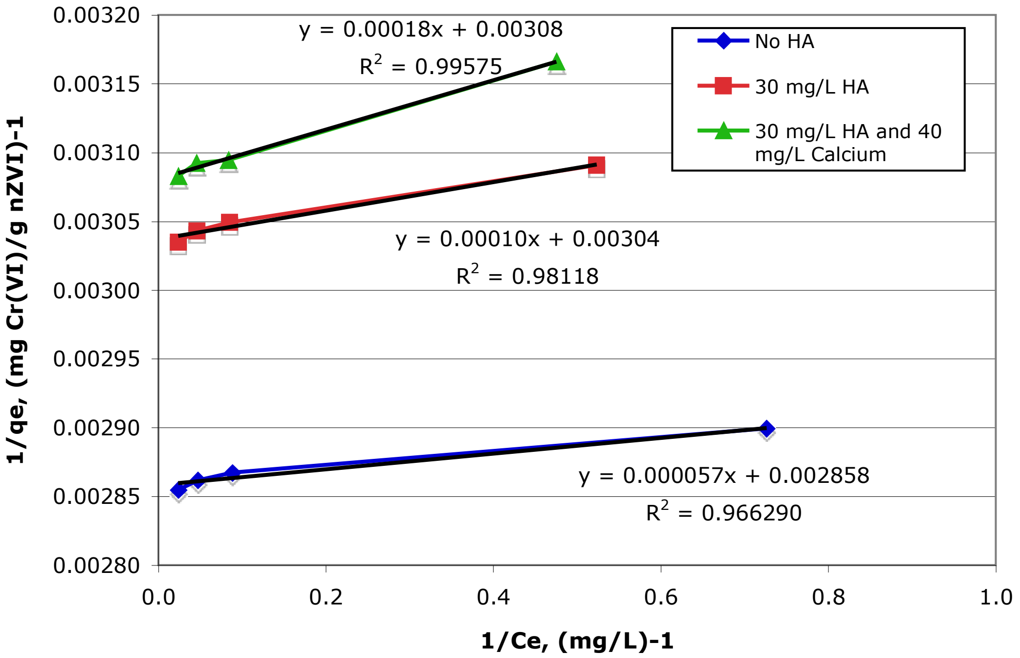

Figure 4.11 Langmuir isotherm model fit to the adsorption isotherm equilibria data from the anoxic studies.

Table 4.2 Reaction rate constants for the pseudo first-order reduction of Cr^{VI} by nZVI under anoxic conditions.

Anoxic Studies	**No HA or Calcium**		**30 mg/L HA**		**30 mg/L HA and 40 mg/L Calcium**	
Initial Cr^{VI} Concentration	***k* (hr^{-1})**	**r^2**	***k* (hr^{-1})**	**r^2**	***k* (hr^{-1})**	**r^2**
5.00	NA	NA	NA	NA	NA	NA
10.00	1.039	0.822	0.582	0.842	0.558	0.862
20.00	0.254	0.786	0.225	0.709	0.217	0.780
30.00	0.148	0.725	0.127	0.611	0.126	0.708
50.00	0.085	0.65	0.0819	0.655	0.078	0.704

Table 4.3 lists the percent removal of Cr^{VI} for each of the various rate studies. This summarizes the equilibrium data from Figures 4.4 through 4.6 and Figures 4.8 through 4.10. As previously discussed, removal percentages are much higher in the anoxic studies, and percent removal is seen to decrease with the presence of humic acid and calcium.

Table 4.3 Percent removal of Cr^{VI} from solution by nZVI in the presence and absence of humic acid and calcium.

	Percent removal with no HA or Calcium		**Percent removal with 30 mg/L HA**		**Percent removal with 30 mg/L HA and 40 mg/L Calcium**	
Initial Cr^{VI} Concentration	**Oxic**	**Anoxic**	**Oxic**	**Anoxic**	**Oxic**	**Anoxic**
5.00	96.70	100	91.9	100	83.7	100
10.00	56.60	85.44	51.2	79.84	46.4	76.8
20.00	28.60	43.5	25.6	41	23.3	40.1
30.00	19.08	29.12	17.1	27.4	15.6	26.88
50.00	11.50	17.51	10.3	16.5	9.4	16.22

A primary finding in the comparison of oxic and anoxic experiments is that there exists a significant increase in nZVI adsorption capacity for Cr^{VI} under anoxic conditions. A chart displaying the calculated adsorption capacities for the oxic and anoxic studies is shown in Figure 4.12. Through a side-by-side comparison, the difference in magnitude is very apparent. The reaction rates were also observed to be greater in the absence of dissolved oxygen, and humic acid and calcium. It is postulated that nZVI readily reacts with any oxidized species in water, and it is well documented that nZVI will corrode rapidly in the presence of dissolved oxygen. The dissolution products include soluble Fe^{II} species, and some Fe^0 reactive sites will remain as well in the nZVI surface, although in a much lower abundance than in the anoxic studies. The reaction rates are much faster in the oxic studies, because the kinetics Cr^{VI} reduction by nZVI are significantly faster than the reduction of Cr^{VI} by Fe^{II} species. Additionally in the anoxic studies, a larger number of reactive surface sites exist on the nanoparticles, resulting in a much larger adsorption capacity. Other chemical constituents in water compete for reaction with nZVI as well, which rapidly exhausts nZVI reactivity and results in a slower reduction of the target contaminant, and a lower removal percentage.

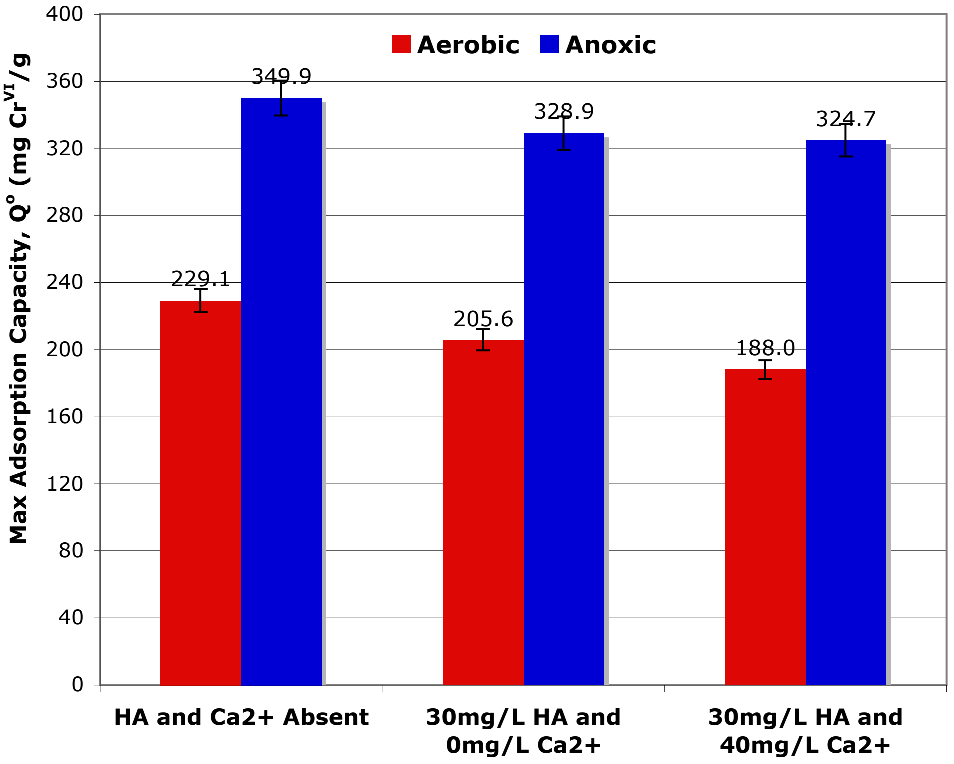

Figure 4.12 Comparison of the maximum adsorption capacities as determined by the Langmuir adsorption isotherm model.

Table 4.4 Adsorption parameters determined from the Langmuir adsorption isotherm model.

Experimental Conditions	***Q°*** (mg Cr^{VI}/g nZVI)	***b*** (function of enthalpy of adsorption)
Oxic – HA and Ca^{2+} Absent	229.1	33.58
Oxic – 30mg/L HA	205.6	21.15
Oxic – 30mg/L HA and 40mg/L Ca^{2+}	188.0	10.04
Anoxic – HA and Ca^{2+} Absent	349.9	50.14
Anoxic – 30mg/L HA	328.9	30.40
Anoxic – 30mg/L HA and 40mg/L Ca^{2+}	324.7	17.11

Dynamic Electrokinetic Studies

Cr^{VI} Transport

Dynamic electrokinetic experiments were conducted to: i) investigate the effects of electrokinetic phenomena in flowing water, and ii) evaluate the use of nZVI in a simulated aquifer environment. To provide a baseline, the primary electrokinetic experiment was conducted using a typical aquifer sand in batch mode with no nZVI addition. After applying 1.0 V/cm electric potential for 24 hours, Cr^{VI} concentrations in the anode reservoir reached 4124 μg/L, and also experienced a pH change from 7.7 to 3.3. In the cathode reservoir, Cr^{VI} concentrations decreased from 2895 μg/L to 96 μg/L within 24 hours, and underwent a pH change from 7.7 to 10.1. Additionally, the Cr^{VI} concentration in the center of the sand column increased lightly from 2895 μg/L to 2986 μg/L within the first 24 hours, and the pH rose from 7.7 to 8.8. The concentration of Cr^{VI} throughout the column decreased significantly after the 24-hour time point. In the cathode reservoir and the sand column the concentration of Cr^{VI} dropped to below the detection limit after 32 hours, and in the anode reservoir the Cr^{VI} concentrations dropped to non-detectable levels μg/L after 46 hours of electric potential application. This information is shown in Figure 4.13.

These results are similar to those of the electrokinetic experiments using kaolinite clay, and likely the same mechanisms are responsible for the initial rapid transport of Cr^{VI} toward the anode, as indicated by the decline in Cr^{VI} concentrations after 24 hours. After 53 hours of electric potential application, the pH values of solution in the anode reservoir, cathode reservoir, and sand column were 2.0, 12.4, and 11.3, respectively.

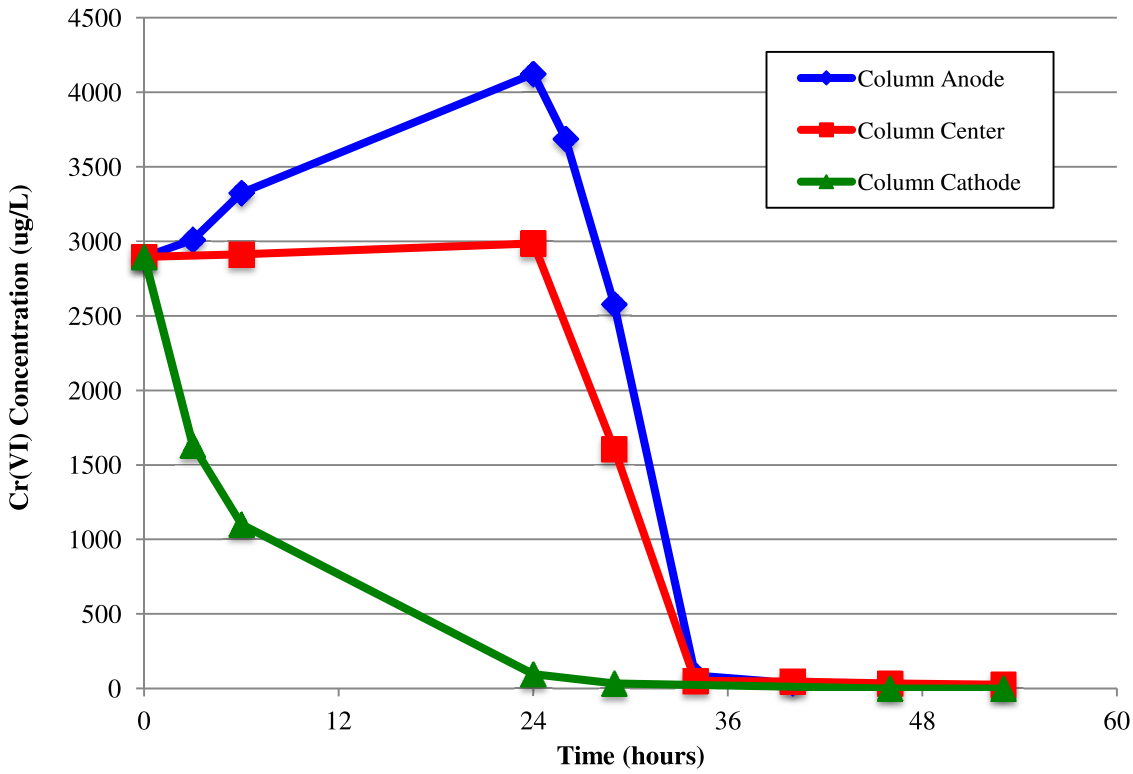

Figure 4.13 Concentrations of Cr^{VI} in the anode reservoir, sand column, and cathode reservoir of a batch electrokinetic cell under an electric potential of 1.0 V/cm.

Transport of ions in electrokinetic systems is influenced heavily by pH, which changes consistently throughout electrokinetic experiments. As the anode becomes very acidic and the cathode becomes highly basic, oxidation-reduction reactions, and dissolution-precipitation phenomena dominate local environments within the electrokinetic cell. In the system presented here, precipitation reactions near the anode involving Cr^{III} species reduce the overall ionic strength of the pore water, and as a result the current passing through the column is reduced. This slows the transport of remaining Cr^{VI} species, ultimately to a point where no more transport is occurring. This has been verified through measuring the current during electrokinetic experiments identical to the system described here. These results are discussed in detail in Chapter 5. It is important to note the effects of pH gradients on the electrokinetic system, as it also provides more depth into the trends observed in Figure 4.13.

A more detailed look into the transport of Cr^{VI} through the electrokinetic column is presented in Figure 4.14. An experiment similar to that previously presented was run, and more sample ports were used to get a better idea of where Cr^{VI} is within the column with time. Each color represents a different concentration range, with red being the highest concentration and purple being the lowest. It is interesting to note that Cr^{VI} exists in significant concentrations (1.0 – 1.5 mg/L) adjacent to the anode reservoir even after 48 hours, when Cr^{VI} no longer exists elsewhere in the column. At this location, the pH is likely high enough for Cr^{VI} to remain stable, however the current is so low at this time that transport is no longer occurring.

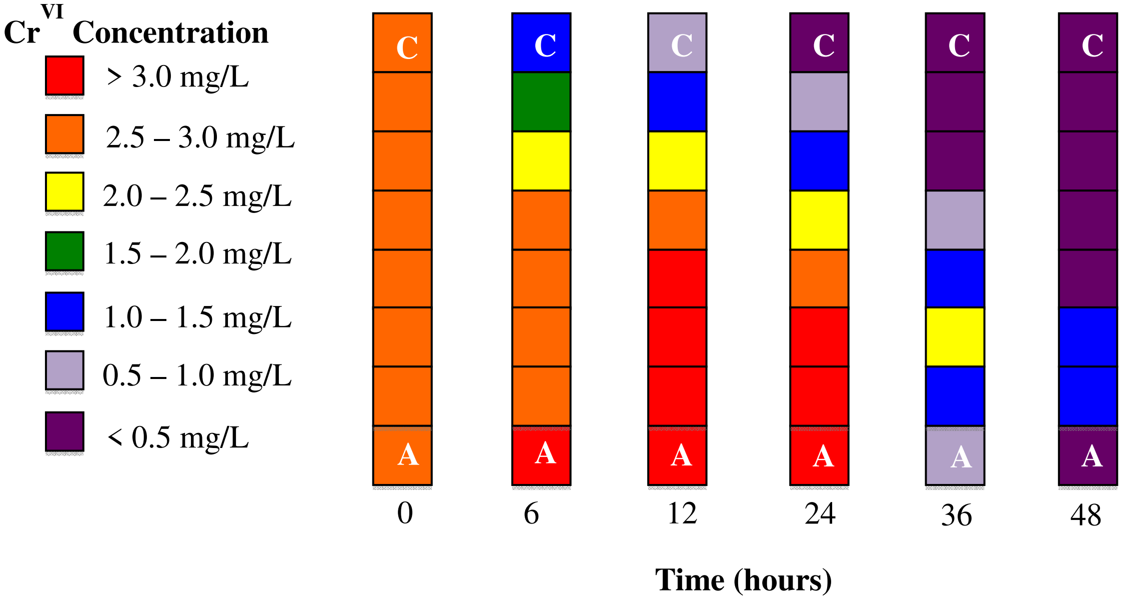

Figure 4.14 Cr^{VI} concentration profiles during electrokinetic experiments in a sandy soil over 48 hours.

Cr^{VI} Reduction by nZVI Injection

The dynamic electrokinetic studies were performed with a simulated groundwater solution spiked with Cr^{VI} pumped through the column at a constant rate of 1.0 L per day. In each of the experiments, electric potential was applied for 48 hours to allow for equilibrium to be reached between transport by electrokinetic phenomena and the advective transport from the flow of the feed solution. After sampling at the 48-hour time point, nZVI was injected into to the sand column 2 cm above the anode reservoir. Injections were performed on 24-hour intervals for the duration of the experiment.

The primary experiment was conducted with a 1.0 V/cm electric potential and 5 mg nZVI injections. The simulated groundwater solution contained 3000 μg/L Cr^{VI}, and a 10^{-2} M bicarbonate buffer. Equilibrium between the advective flow and electrokinetic transport was reached within 24 hours of electric potential application. After 24 hours, the anode reservoir Cr^{VI} concentration reached 3400 μg/L, in the sand column the Cr^{VI} concentration increased to about 3200 μg/L, and in the cathode reservoir concentrations dropped to around 2850 μg/L (Figure 4.15). After nZVI addition, concentrations of Cr^{VI} dropped throughout the electrokinetic cell. The daily nZVI injections reduced Cr^{VI} concentrations to 3235 μg/L in the anode reservoir, 3034 μg/L in the sand column, and 2425 in the cathode reservoir effluent. The overall Cr^{VI} removal percentage was 20.9%.

In the following experiment the electric potential was increased to 1.5 V/cm, and the iron addition remained consistent with the previous experiment. At the point of equilibration between the advective transport and the electrokinetic transport of Cr^{VI} the concentrations in the anode reservoir, sand column, and cathode reservoir were 3750 μg/L, 3300 μg/L, and 2540 μg/L, respectively (Figure 4.16). Upon addition of nZVI to the sand column the Cr^{VI} concentrations decreased in the anode reservoir, sand column, and cathode reservoir to 3110 μg/L, 2632 μg/L, and 2140 μg/L, respectively, for an overall Cr^{VI} removal percentage of 30.2%.

The third electrokinetic study was conducted with an electric potential application of 1.5 V/cm, and 20 mg injections of nZVI. Similar to the previous study, an increase in Cr^{VI} concentration was observed in the anode reservoir from 3066 μg/L to about 3730 μg/L, and in the sand column from 3066 μg/L to about 3320 μg/L. A decrease in concentration in the cathode reservoir from 3066 μg/L to 2530μg/L was observed as well (Figure 4.17). These results indicate the increase in iron addition improved overall Cr^{VI} removal to 58.7%.

The results from each experiment had the same characteristic trends; an initial increase in concentration attributed to the electrokinetic transport of Cr^{VI} towards the anode, followed by a decrease in concentration upon the addition of nZVI, and a new equilibrium concentration maintained by sequential nZVI addition.

The injection of iron lowered Cr^{VI} concentrations, however the maximum removal achieved was on 58.7%. Information gathered from the CMBR studies evaluating Cr^{VI} removal by nZVI indicated that under oxic conditions 1.0 g of nZVI is capable of reducing well over 200 mg of Cr^{VI}. However in the sand column, a 5.0 mg injection of nZVI was only capable of reducing about 900 μg/L over 24 hours. The difference in reduction capacity appears to be multiple orders of magnitude, however the batch studies were mixed continuously and contained no soil. There was no mixing in the sand column, and the presence of sand introduced a new mechanism for nZVI inactivation. A large percentage of nZVI likely exhausted reactivity by interaction with sand particles, and nZVI were only exposed to Cr^{VI} species in the vicinity of the injection location. When the quantity of nZVI added per injection was increased from 5 mg to 20 mg, a 51% increase in Cr^{VI} reduction was observed. For Cr^{VI} concentrations in the cathode reservoir effluent to comply with the California EPA standards, at least 40 mg of nZVI would need to be injected daily to the column.

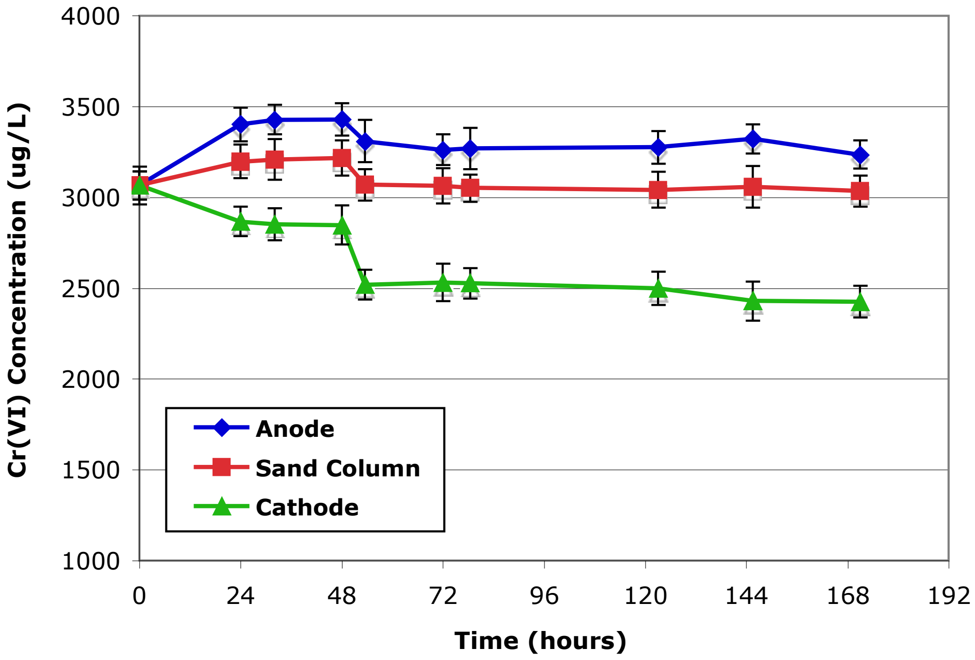

Figure 4.15 Concentrations of Cr^{VI} in the anode reservoir, sand column, and cathode reservoir of a dynamic electrokinetic cell under an electric potential of 1.0 V/cm with daily injections of 5 mg nZVI.

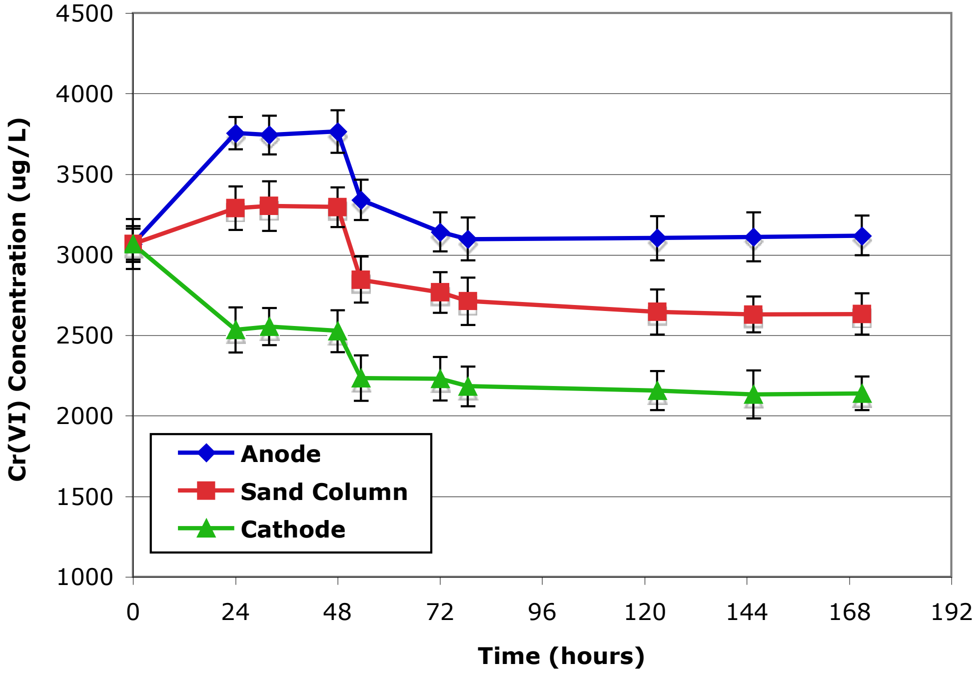

Figure 4.16 Concentrations of Cr^{VI} in the anode reservoir, sand column, and cathode reservoir of a dynamic electrokinetic cell under an electric potential of 1.5 V/cm with daily injections of 5 mg nZVI.

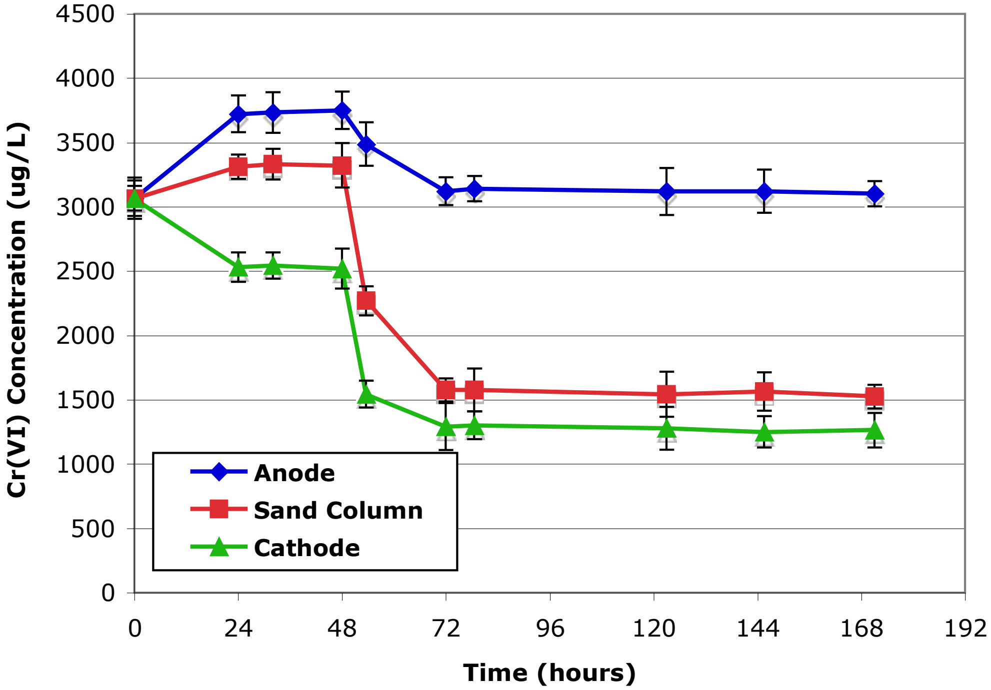

Figure 4.17 Concentrations of Cr^{VI} in the anode reservoir, sand column, and cathode reservoir of a dynamic electrokinetic cell under an electric potential of 1.5 V/cm with daily injections of 20 mg nZVI.

Cr^{VI} Reduction by nZVI and the Effects of Background Humic Acid

An identical series of electrokinetic experiments were run with a 30 mg/L humic acid concentration in the feed solution. The trends in Cr^{VI} concentrations shown in Figures 4.18 - 4.20 illustrate the same characteristics observed in experiments without humic acid, however with a decrease in overall Cr^{VI} reduction. The addition of humic acid decreased Cr^{VI} removal by 7.8% with an electric potential application of 1.0 V/cm and 5 g nZVI injections. A removal decrease of 9.5% was observed in each of the additional experiments with an electric potential application of 1.5 V/cm and nZVI injections of 5 g and 20 g. Humic acid was likely accumulating near the anode reservoir in the same general zone as Cr^{VI}, at the location of nZVI injection. Therefore upon injection, nZVI was introduced to a solution containing high humic acid content, leading to a decrease in capacity for Cr^{VI} removal. The decrease in removal percentage was slightly higher than that observed in the batch nZVI reduction studies, likely due to the higher concentration of humic acid at the area of injection relative to that in the batch studies. Lastly, the pH in the area of nZVI injection remained near 7 for the entire experiment, so it can be assumed that Cr^{VI} removal by complexation with humic acid was negligible.

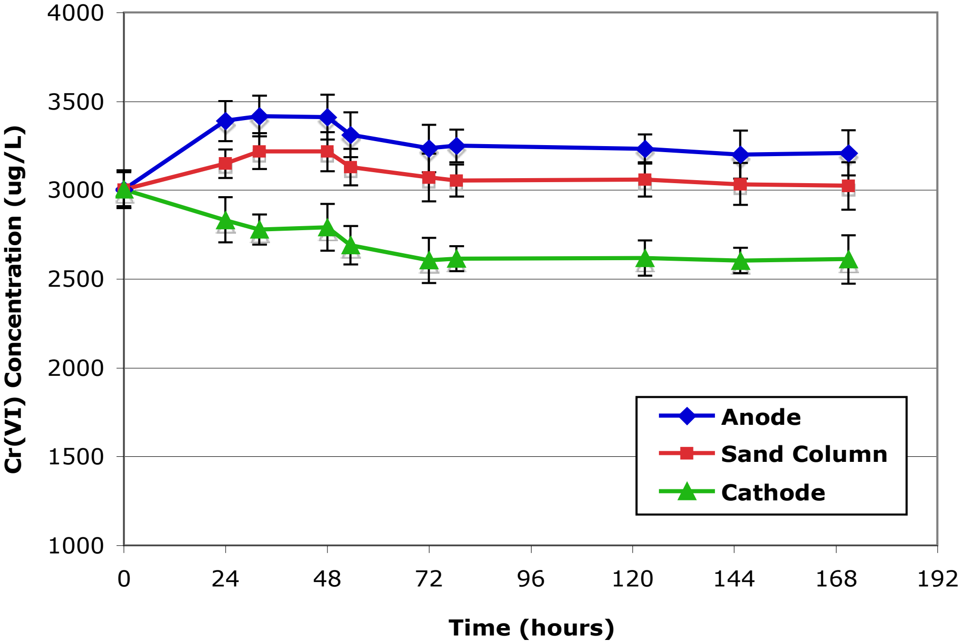

Figure 4.18 Concentrations of Cr^{VI} in the anode reservoir, sand column, and cathode reservoir of a dynamic electrokinetic cell under an electric potential of 1.0 V/cm with daily injections of 5 mg nZVI, and 30 mg/L of humic acid in the simulated groundwater feed.

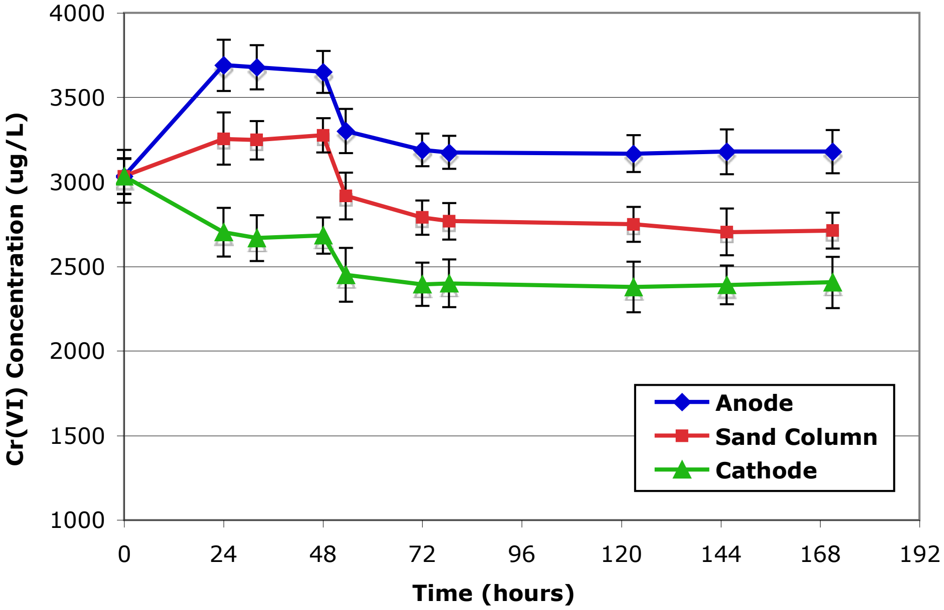

Figure 4.19 Concentrations of Cr^{VI} in the anode reservoir, sand column, and cathode reservoir of a dynamic electrokinetic cell under an electric potential of 1.5 V/cm with daily injections of 5 mg nZVI, and 30 mg/L of humic acid in the simulated groundwater feed.

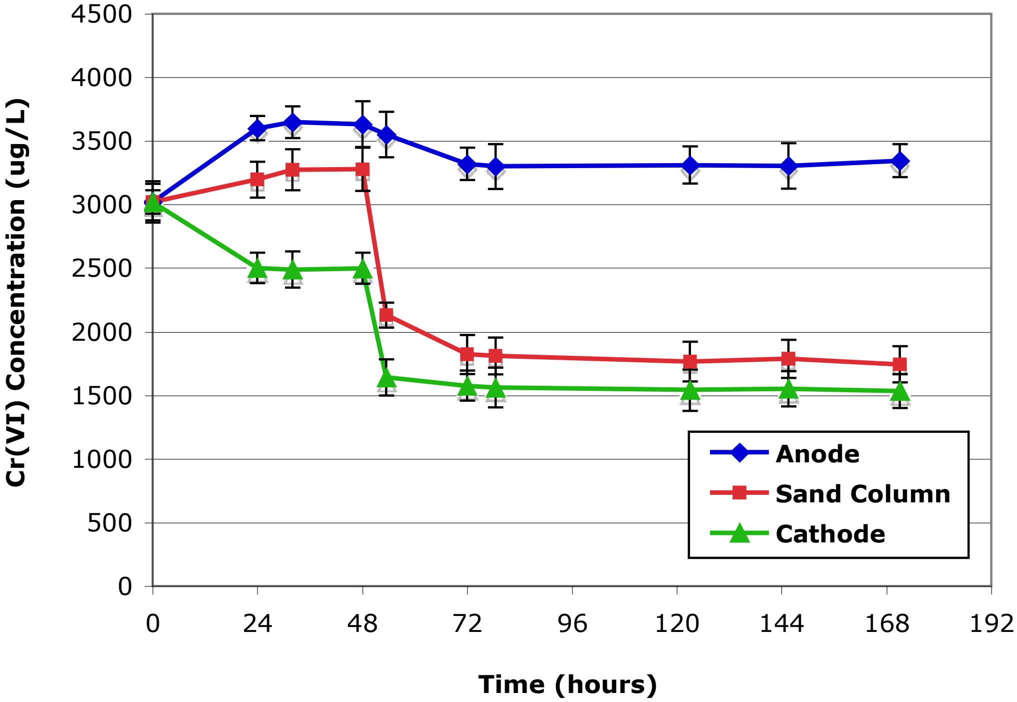

Figure 4.20 Concentrations of Cr^{VI} in the anode reservoir, sand column, and cathode reservoir of a dynamic electrokinetic cell under an electric potential of 1.5 V/cm with daily injections of 20 mg nZVI, and 30 mg/L of humic acid in the simulated groundwater feed.

Integration of electrokinetic technology with nZVI injection enhanced the removal of Cr^{VI} in the sand columns. By maintaining higher Cr^{VI} concentrations near the anode reservoir than the concentration in the feed solution, the amount of Cr^{VI} transported to the cathode reservoir by with the advective water flow was minimized. The concentration of Cr^{VI} was highest adjacent to the anode reservoir in each experiment, which was chosen as the optimal location for nZVI injection. Sequential nZVI injections reduced Cr^{VI} in the liquid phase, however the reductive percentages achieved were orders of magnitude lower than indicated by the nZVI reduction studies. The presence of humic acid in the feed solution decreased Cr^{VI} removal most notably under an applied electric potential of 1.5 V/cm, due to enhanced transport of humic acids towards the anode reservoir, near the point of nZVI injection. Table 4.5 summarizes the removal capacities observed in each of the six experiments.

Table 4.5 Summary of Cr^{VI} removal in dynamic electrokinetic experiments with and without humic acid.

Electric Potential (V/cm)	nZVI Addition (mg/injection)	Removal Percentage (%) without HA	Removal Percentage (%) with 30 mg/L HA
1.0	5	20.9	13.1
1.5	5	30.2	20.7
1.5	20	58.7	49.2

4.5 Conclusions

The CMBR rate studies illustrated the high reduction capacity of nZVI for CrVI. In anoxic systems, the capacity was much higher than the oxic systems. The presence of humic acid and calcium additionally inhibited reduction.

The electrokinetic studies showed that nZVI and electrokinetic transport integration is a feasible and beneficial combination. Electrokinetic transport of Cr^{VI} to the anode reservoir allowed for specific targeting of the contaminants with nZVI injection. With this approach, nearly 60% of the influent concentration of Cr^{VI} was removed in the process. Removal percentages were slightly lower for systems containing humic acid, consistent with the results observed in the CMBR rate studies between systems with and without humic acid. Overall however, the reactivity of nZVI was greatly reduced in the sand column in comparison to the CMBR studies. Interactions with the soil media, particle aggregation, and a lack of thorough mixing were hypothesized to the primary contributors to the excess nZVI required to achieve significant Cr^{VI} removal.

The method of nZVI application resulted in the formation of a permeable reactive barrier after many injections, which supports the theory that particle aggregation was a significant factor. No nZVI was noted in the column effluent, and near the point of injection iron was clearly visible as an orange and black cloud. The observations suggested that the daily injections of fresh nZVI to the column were effective, however more frequent injections would likely provide better Cr^{VI} removal. The nZVI plume was nearly a uniform orange color after each 24-hours period. The results suggest that nZVI can rapidly reduce Cr^{VI}, however in an environmental settings new approaches to nZVI application will be required to utilize the reductive capacity of the nZVI effectively.

Humic acid had noticeable effect on removal percentages, and lowered the removal percentage by almost 10%. This was due to humic acid complexation with nZVI corrosion products, as well as reactive with nZVI reactive surface sites. Humic acid carries a predominant negative charge in waters of neutral pH, and will migrate by electrokinetic phenomena towards the anode reservoir just as Cr^{VI} does. Therefore nZVI is not only being injected to a concentrated plume of Cr^{VI}, but also humic acids, and any other anionic species present in the receiving waters.

The most essential finding of this study was that the continuous flow system did not undergo large pH variations. For the duration of the experiment the pH remained neutral throughout the electrokinetic cell. This eliminated the detrimental effects caused by pH gradient formation observed in batch studies. While many research groups have been focused on the use of electrokinetic transport in soils of low hydraulic conductivity, this study shows electrokinetic transport of contaminants can be effective in a flowing system, in a typical aquifer soil. Sandy soils are about an order of magnitude less conductive than clay soils, so the current flowing for a given applied voltage will be much lower than that of clay soils, however the need for enhancement techniques to mitigate pH change is eliminated. The applications of electrokinetic transport can be extended to many different scenarios.

4.6 Chapter 4 References

1. Mueller, N.C., J. Braun, J. Bruns, M. Cernik, P. Rissing, D. Rickerby, B. Nowak (2012) Application of nanoscale zero valent iron (NZVI) for groundwater remediation in Europe, *Environ Sci Pollut Res,* 19:550-558.

2. Cernik, M. (2010) Chemically supported in situ remedial technologies. *Vydavatelství VŠCHT Praha.*

3. Gheju, M., & Balcu, I. (2010). "Hexavaelnt chromium reduction with scrap iron in continuous-flow system. Part 2: Effect of scrap iron shape and size." *Journal of Hazardous Materials,* 182, 484-493.

4. Ponder, S. M., Darab, J. G., Bucher, J., Caulder, D., Craig, I., Davis, L., Edelstein, N., et al. (2001). Surface Chemistry and Electrochemistry of Supported Zerovalent Iron Nanoparticles in the Remediation of Aqueous Metal Contaminants. *Electroanalytical Chemistry*, (250), 479–486.

5. C. Noubactep, A. Schöner, Metallic iron for environmental remediation: Learning from electrocoagulation, Journal of Hazardous Materials, Volume 175, Issues 1–3, 15 March 2010, Pages 1075-1080

6. Ponder, S. M., Darab, J. G., & Mallouk, T. E. (2000). Remediation of Cr (VI) and Pb (II) aqueous solutions using supported, nanoscale zero-valent iron. *Environmental Science & Technology*, *34*(12), 2564–2569.

7. Reardon, E. (1995) Anaerobic corrosion of granular iron: Measurement and interpretation of hydrogen evolution rates, *Environ. Sci. and Technol.,* 29:2936-2945.

8. Furukawa, Y., J.-W. Kim, J. Watkins, R.T. Wilkin (2002) Formation of Ferrihydrite and Associated Iron Corrosion Products in Permeable Reactive Barriers of Zero-Valent Iron, *Environ. Sci. Technol.,* 36:5469-5475.

9. Zhang, W. (2003). Nanoscale iron particles for environmental remediation: An overview. *Journal of nanoparticle Research*, *5*(3), 323–332.

10. Puls, R.W., and R.M. Powell (1997). Permeable Reactive Subsurface Barriers for the Interception and Remediation of Chlorinated Hydrocarbon and Chromium (VI) Plumes in Ground Water, 1–4. *U.S. EPA Remedial Technology Fact Sheet.*

11. Li, X., Elliott, D. W., & Zhang, W. (2006). Zero-Valent Iron Nanoparticles for Abatement of Environmental Pollutants□: Materials and Engineering Aspects, 111–122.

12. Phillips, D. H., B. Gu, D. B. Watson, Y. Roh, L. Liang, and S. Y. Lee. 2000. Performance evaluation of a zerovalent iron reactive barrier: Mineralogical characteristics. *Environmental Science & Technology* 34, (19): 4169-76.

13. Kamolpornwijit, W., L. Liang, OR West, GR Moline, and AB Sullivan. 2003. Preferential flow path development and its influence on long-term PRB performance: Column study. *Journal of Contaminant Hydrology* 66, (3-4): 161-78.

14. Keane, E. (2010). *Fate, Transport and Toxicity of Nanoscale Zero-Valent Iron (nZVI) Used During Superfund Remediation*. Duke University.

15. He, F., Zhao, D., 2005. Preparation and characterization of a new class of starch-stabilized bimetallic nanoparticles for degradation of chlorinated hydrocarbons in water. *Environ. Sci. Technol.* 39, 3314–3320.

16. Xu, Y.H., Zhao, D.Y., 2007. Reductive immobilization of chromate in water and soil using stabilized iron nanoparticles. Water Res. 41, 2101–2108.

17. Giasuddin, A. B. M., Kanel, S. R., & Choi, H. (2007). Adsorption of humic acid onto nanoscale zerovalent iron and its effect on arsenic removal. *Environmental science & technology*, *41*(6), 2022–7.

18. Yang, G. C. C., Tu, H., & Hung, C. (2007). Stability of nanoiron slurries and their transport in the subsurface environment. *Test*, *58*, 166–172.

19. Phenrat, T., & Saleh, N. (2007). Aggregation and Sedimentation of Aqueous Nanoscale Zerovalent Iron Dispersions. *Environmental Science & Technology*, *41*(1), 284–290.

20. Christian, P., Von der Kammer, F., Baalousha, M., & Hofmann, T. (2008). Nanoparticles: structure, properties, preparation and behaviour in environmental media. *Ecotoxicology (London, England)*, *17*(5), 326–43.

21. Chen, J., Z. Xiu, G.V. Lowry, and P.J.J. Alvarez (2010) Effect of natural organic matter on toxicity and reactivity of nanoscale zero-valent iron, *Water Research*m 45:1995-2001.

22. Wang, Q., Qian, H., Yang, Y., Zhang, Z., Naman, C., & Xu, X. (2010). Reduction of hexavalent chromium by carboxymethyl cellulose-stabilized zero-valent iron nanoparticles. *Journal of Contaminant Hydrology*, *114*(1-4), 35–42.

23. Lo, I.M.C., C.S.C. Lam, K.C.K. Lai (2005) Competitive effects of trichloroethylene on Cr(VI) removal by zero-valent iron, *Journal of Environmental Engineering,* 131:1598-1606.

24. Lo, I.M.C., C.S.C. Lam, K.C.K. Lai (2006) Hardness and carbonate effects on the reactivity of zero-valent iron for Cr(VI) removal, *Water Resources,* 40:595-605.

25. Wang, C.-B., and W.X. Zhang (1997) Nanoscale metal particles for dechlorination of PCE and PCBs. *Environ. Sci and Technol.* 31(7), 2154-2156.

26. Gu, B., Schmitt, J., Chen, Z., Liang, L., & MaCarthy, J. F. (1994). Adsorption and desorption of natural organic matter on iron oxide mechanisms and models. Environ- mental Science & Technology, 28, 38–46.

27. Quinn, J., Geiger, C., Clausen, C., Brooks, K., Coon, C., O'Hara, S., Krug, T., et al. (2005). Field Demonstration of DNAPL Dehalogenation Using Emulsified Zero-Valent Iron. *Environmental Science & Technology*, *39*(5), 1309–1318.

28. Jones, E. H., Reynolds, D. A., Wood, A. L., & Thomas, D. G. (2009). Use of Electrophoresis for Transporting Nano-Iron in Porous Media. *Ground Water*, 1–12.

29. Chowdhury, A.I.A., D.M. O'Carroll, Y. Xu, and B.E. Sleep (2012) Electrophoresis enhanced transport of nano-sclae valent iron, *Advances in Water Resources*, 40:71-82.

30. Tipping, E. *Cation Binding by Humic Substances;* Cambridge University Press: Cambridge, 2002.

31. Powell, R.M., Puls, R.W., Hightower, S.K., Sabatini, D.A. (1995). Coupled iron corrosion and chromate reduction: mechanisms for subsurface remediation. *Environ. Sci. Technol.* 29, 1913-1922.

32. Blowes, D.W., W. Ptacek, C.J., and Jambor, L.J. (1997). In site remediation of Cr(VI)-contaminated groundwater using permeable reactive walls: Laboratory Studies. *Environ. Sci. and Technol.,* 31(12), 3348-3357.

33. Alowitz, M.J., Scherer, M.M. (2002). Kinetics of nitrate, nitrite, and Cr(VI) reduction by iron metal. *Environ. Sci. Technol.* 36, 299-306.

34. Wilkin, R.T., Su, C., Ford, R.G. and Paul, C.J. (2005). Chromium-removal processes during groundwater remediation by a zero-valent iron permeable reactive barrier. *Environ. Sci. Technol.,* 39(12), 4599-4605.

35. A.R. Bowers, C.A. Ortiz and R.J. Cardozo (1986). Iron processes for treatment of Cr(VI) wastewater, *Metal Finishing*, 84, 37-41.

36. A.H. El-Shazly, A.A. Mubarak, A.H. Konsowa, Hexavalent chromium reduction using a fixed bed of scrap bearing iron spheres, *Desalination*, Volume 185, Issues 1–3, 1 November 2005, Pages 307-316.

37. Tony R. Lee, Richard T. Wilkin, Iron hydroxy carbonate formation in zerovalent iron permeable reactive barriers: Characterization and evaluation of phase stability, *Journal of Contaminant Hydrology*, Volume 116, Issues 1–4, 30 July 2010, Pages 47-57.

38. Vega, A., Fiuza, A., & Guimarães, F. (2010). Insight into the Phenomenology of the Cr(VI) Reduction by Metallic Iron Using an Electron Probe Microanalyzer. *Langmuir*, *26*(14), 11980–11986.

39. António Fiúza, Aurora Silva, Goreti Carvalho, António V. de la Fuente, Cristina Delerue-Matos, Heterogeneous kinetics of the reduction of chromium (VI) by elemental iron, Journal of Hazardous Materials, Volume 175, Issues 1–3, 15 March 2010, Pages 1042-1047.

40. Jan Dries, Leen Bastiaens, Dirk Springael, Stefaan Kuypers, Spiros N. Agathos, Ludo Diels, Effect of humic acids on heavy metal removal by zero-valent iron in batch and continuous flow column systems, Water Research, Volume 39, Issue 15, September 2005, Pages 3531-3540.

41. Mark S.H. Mak, Irene M.C. Lo, Influences of redox transformation, metal complexation and aggregation of fulvic acid and humic acid on Cr(VI) and As(V) removal by zero-valent iron, Chemosphere, Volume 84, Issue 2, June 2011, Pages 234-240.

42. Liu, T., & Lo, I. M. C. (2010). Influences of Humic Acid on Cr(VI) Removal by Zero-Valent Iron From Groundwater with Various Constituents: Implication for Long-Term PRB Performance. *Water, Air, & Soil Pollution*, *216*(1-4), 473–483.

43. Wang, Q., Cissoko, N., Zhou, M., & Xu, X. (2011). Effects and mechanism of humic acid on chromium (VI) removal by zero-valent iron (Fe 0) nanoparticles. *Physics and Chemistry of the Earth, Parts A/B/C*, *36*(9), 442–446.

44. Cantrell, K.J., Kaplan, D.I., Wietsma, T.W. (1995). Zero-valent iron for the in-situ remediation of selected metals in groundwater. *J. Hazard. Mat.* 42, 201-212.

Chapter 5 : The Effects of Humic Acid on Microbial Fuel Cell Performance for Chromium Remediation in Groundwater and Integration with Electrokinetic Technology

5.1 Introduction

Cr^{VI} species, usually found as chromate or dichromate, can be treated in water by reduction to Cr^{III} species, which generally are sparingly soluble at neutral pH values and have negligible toxicity.[1] One method to achieve this result is with chemical reducing agents. Reduction can occur naturally in groundwater and soils under reducing conditions by reactions with readily oxidizable natural organic matter or metal ions such as Fe^{II}, or S^{2-}.[2,3] Reduction can also occur biologically as the end result of a complex electron transport chain that is a product of metabolic activity in exoelectrogenic bacteria. Reduction of Cr^{VI} by *Pseudomonas* was first reported in 1977 by Romanenko and Koren'kov.[3] Since this discovery, many different species of bacteria have been identified as capable of performing extracellular electron transfer, most notable being *Shewanella* and *Geobacter*. *Shewanella* sp. are facultative anaerobes proven to be proficient at respiring a wide array of substrates including toxic metals and electrodes.[4]

Microbial Cr^{VI} reduction is carried out by electron transfer from bacterial cells to Cr^{VI} in solution, via nanowires and/or redox mediators.[5] Nanowires are conductive filaments comprised of oligomeric pilin protiens, a material thought to be an electric insulator. Recently however, these nanowires have been shown to be electrically conductive and act similar to metals in terms of the ability to transport electrons over relatively long distances. The conductivity of *Geobacter sulfurreducens* biofilms were on the same scale as synthetic organic metals over distances of greater than 1 cm.[6]

Shewanella sp. form very thin biofilms relative to *Geobacter*, however offer the advantage of being a facultative anaerobe. The thickness and conductive nature of *Geobacter* biofilms is largely due to the network of conductive nanowires that form complex webs throughout the consortium. *Shewanella* have the capacity to form nanowires under anaerobic conditions[7], however the thin films they produce rely on additional means of extracellular electron transport. Brutinel and Gralnick discuss the significance of soluble electron shuttles in the electron transport chain of *Shewanella*, in support of this concept which has been described by various groups over the last decade.[5,8-10] Redox-active flavin compounds have been isolated and identified as electron shuttles produced by *Shewanella* that assist in transferring electrons from the cell surface to terminal electron acceptors (TEAs).[11-12] Substances found naturally in groundwater can also serve as redox mediators, such as humic substances. The presence of humic substances have been documented to enhance electron transport to terminal electron acceptors.[9,13] Additionally, soil humic acids (HAs) may enhance the persistence of Cr^{VI} species in groundwater through the formation of stable Cr^{VI}-HA micelles via supermolecular chemical processes.[14]

Humic acid also impacts the redox balance in a microbial fuel cell (MFC) system. Reduction potential is generally reported as E_h, which is the potential between a platinum electrode and a standard hydrogen electrode for a given solution.[15] This can be difficult to measure in natural soil-water systems due to the lack of response of platinum electrodes to many reactions involving solids phases, as well as some soluble-phase redox couples commonly found in groundwater such as O_2-H_2O, SO_4^{2-}-H_2S, CO_2-CH_4, and NO_3-N_2. To accurately measure redox potential in systems containing more than one redox couple, the reactions must all be in thermodynamic equilibrium.[21] The dynamic electrochemical effects of electrokinetic transport (see Chapter 2: Theoretical Background) maintains a transient environment in the area between electrodes, adding to the difficulty in estimating these parameters in a lab-scale or full-scale remediation study. Some investigations have attempted estimating reduction potential in bench-scale experimental work involving electrokinetic transport. Pamukcu *et al.* in 2004 investigated Cr^{VI} reduction in an electrokinetic system amended with ferrous iron.[20] The reduction potential at different points within the electrokinetic cell between the anode and cathode was determined (Figure 2.3). Near the anode, E_h averaged approximately +0.7 V, and at the cathode the reduction potential was approximately +0.3 V. This study highlighted that the redox conditions within the electrokinetic cell near the anode favor the stability of Cr^{III} species.

In an MFC the electrochemical processes occurring can be exploited for power production and reduction of heavy metals in groundwater remediation applications. The

MFC system is comprised of an anode, where bacteria metabolize organic matter, and a cathode, where bacteria facilitate the migration of electrons to a terminal electron acceptor. The redox potential in the anode is maintained at a value lower than that of the cathode to promote the transfer of electrons from anode towards the cathode, creating a steady flow of electrons through a circuit. Many heavy metals including Cr^{VI} and U^{VI} can be added to the cathode side to serve as a TEA and be reduced to insoluble species that can be removed.[16] MFCs offer the potential of being a green remediation technology, as they can degrade organic matter in the anode compartment and treat water for heavy metal contamination at the cathode. The only by-product of this process is a small amount of CO_2 and power production from the current flowing from the anode to the cathode.

Production of power from an MFC is dependent primarily on kinetics of the reduction taking place at the cathode, and thus cathodic limitations inhibit MFC systems from reaching maximum efficiency. These losses, referred to as activation losses, increase as more current is taken from an MFC and result in a lower cell potential.[18] Oxidants with a higher redox potential can reduce the cathodic activation losses, however for remediation applications the target TEA is the target contaminant. In the case of Cr^{VI} (as $HCrO_4^-$), the redox potential is fixed 0.382 V, relatively low in comparison to NO_3^- (+0.74 V), Fe^{3+} (+0.771 V), or O_2 (+0.815 V). When Cr^{VI} is introduced in low concentrations such as those typically found in groundwater of contaminated sites, power production is extremely low due to the small reduction potential gradient between anode and cathode resulting from activation losses.

Pre-concentrating Cr^{VI} before introduction to the MFC can help with cathode limitation, and this can be done *in situ* by electrokinetic transport. The idea of heavy metal transport through soils has been around for decades, spurring from an accidental discovery of this phenomenon during an electrokinetic dewatering process on dredged sediment.[19] Since then, electrokinetic transport has been comprehensively investigated by numerous research groups from around the world. Electrokinetic remediation is a technique that can be used for transporting ionic contaminants, including Cr^{VI} (as $HCrO_4^-$), by the application of an electric potential across a contaminated aquifer. The integration of an electrokinetic transport system with MFC technology has potential to benefit a remediation effort by a) producing more power by introducing a higher concentration of the target TEA into the cathode, and b) speeding up treatment time by transporting the target contaminants to a desirable location.

Electrokinetic remediation is often limited by pH change due to electrolysis reactions. These reactions create OH^- at the cathode and H^+ at the anode, which migrate towards the opposite electrodes by electrokinetic phenomena. At the point of intersection of these fronts a significant drop in electrical conductivity occurs, causing transport to slow or stop completely. Additionally, the dynamic pH change affects precipitation and dissolution reactions, which govern the solution chemistry and availability of the contaminant for transport. Many enhancement techniques have been investigated to mitigate this problem, however they can add significant economic and environmental cost.

This study investigates the potential to enhance electrokinetic transport of Cr^{VI} in groundwater while also promoting its reduction to Cr^{III} by integrating an electrokinetic system with microbial fuel cell (MFC) technology. *Shewanella putrefaciens* MR-1 bacteria have been documented to be effective biocatalysts for this application, and different carbon sources including lactate, acetate, formate, and pyruvate have demonstrated to be effective electron donors in the anode compartment.

In the setting of an integrated MFC-electrokinetic system, it is important to consider the production of $O_{2(g)}$ at the anode of the electrokinetic system. This will oxygenate the waters near the anode, which is also the point of Cr^{VI} accumulation, and the extraction point for transfer to the MFC cathode. The O_2/H_2O redox couple has a reduction potential of +0.815, and will preferentially accept electrons over the $HCrO_4^-/Cr^{3+}$ couple (+0.382). Sparging the cathode of the MFC with N_2 will displace the dissolved O_2 over time, however the steady flow of oxidized water into the MFC will raise the reduction potential. This will affect the MFC system in two ways: a) provide dissolved oxygen, serving as a competing electron acceptor, and b) raise the reduction potential difference between MFC chambers, increasing power production.

5.2 Scope and Objectives

In this study, four separate sets of experiments were performed to evaluate the ability of *Shewanella oneidensis* MR-1 to reduce Cr^{VI} and produce power in a microbial fuel cell, as well as investigate the effects of humic acid on the biotransformation of hexavalent chromium.

I) Rate studies were performed to evaluate Cr^{VI} reduction by MR-1 in the presence and absence of humic acid. The Monod model described the experimental data well and allowed the extraction of biokinetic parameters, namely the half saturation constant, and the maximum specific growth rate. A more detailed explanation of these parameters is given in Chapter 6. A comparison of these parameters in parallel studies with and without humic acid provided insight into the advantages posed by microbial reduction of heavy metals in soils and groundwater rich in organic matter.

II) Following the rate studies, MFCs were employed for Cr^{VI} reduction. Batch MFC experiments were run with sequential injections of Cr^{VI} to the cathode compartment and an excess of lactate in the anode compartment. Power production and Cr^{VI} reduction were evaluated in the presence and absence of humic acid.

III) Next, integration of the MFC with a soil column charged with silica sand and spiked with a Cr^{VI} solution under an applied electric potential was investigated. The goal of this integrated system was to quantify the benefits of Cr^{VI} transport to the anode of the soil column before treatment in the MFC in terms of overall treatment time, as well as study any improvements in power production. Identical column studies were conducted in the presence of humic acid.

IV) The final experiment took the integrated system one step further by introducing continuous flow of a simulated groundwater solution containing Cr^{VI} and evaluated the sustainability of such a treatment approach. The experimental set-up was the same as study III, however the simulated groundwater solution spiked with Cr^{VI} was pumped through the column continuously.

5.3 Materials and Methods

Materials

Shewanella oneidensis MR-1 used in these studies were prepared from cultures obtained from Pacific Northwest Laboratory (PNL). The cultures were stored at -80°C before use. All chemicals used in preparation of growth media were reagent grade unless otherwise noted. The MR-1 minimal media solution used for growth was prepared with the components of Table 1. Cultures of MR-1 were diluted to the appropriate cell density using 50 mM molecular biological grade PIPES buffer. Humic acid was obtained from was prepared according to methods described in Chapter 3. All chromium solutions were diluted from a stock Cr^{VI} solution prepared by dissolving ACS reagent grade potassium dichromate in DDI water. Adjustments to pH were performed using dilute HCl and NaOH solutions.

Microbial fuel cells were constructed out of acrylic, and have a capacity of approximately 300 mL in each electrode compartment. Carbon sponge electrodes were cut from vitreous carbon sheets (80ppi; ERG Aerospace; Oakland, CA) into the size of 3" x 4" x ½". An SEM image of a clean electrode is presented in Figure 5.1, illustrating the porous structure. A conductive carbon epoxy was used to fix titanium leads to the electrodes. The electrodes were soaked in DDI water for 24 hours prior to use to saturate the pore space. The proton exchange membranes (model CMI-7000) were obtained from Membranes International, Inc., Glen Rock, NJ. The membranes were stored in DDI water until use. The acrylic fuel cell (Figure 5.2) was assembled with the cation exchange membrane separating the anode and cathode compartments. Leak tests were performed by filling one of the chambers with DDI water and kept undisturbed overnight to ensure no liquid passed to the other chamber. Upon verification that no leakage occurred, the other chamber was loaded with DDI water to keep the membrane saturated. The voltage monitoring equipment (Model 2700; Keithly Instruments, Inc.; Cleveland, OH) and the operating computer were set-up concurrently with the MFC. A 10-ohm resistor was integrated into the circuit for each fuel cell.

The soil columns were loaded with a 40-mesh silica sand under an applied electric potential as described in detail in Chapter 4.

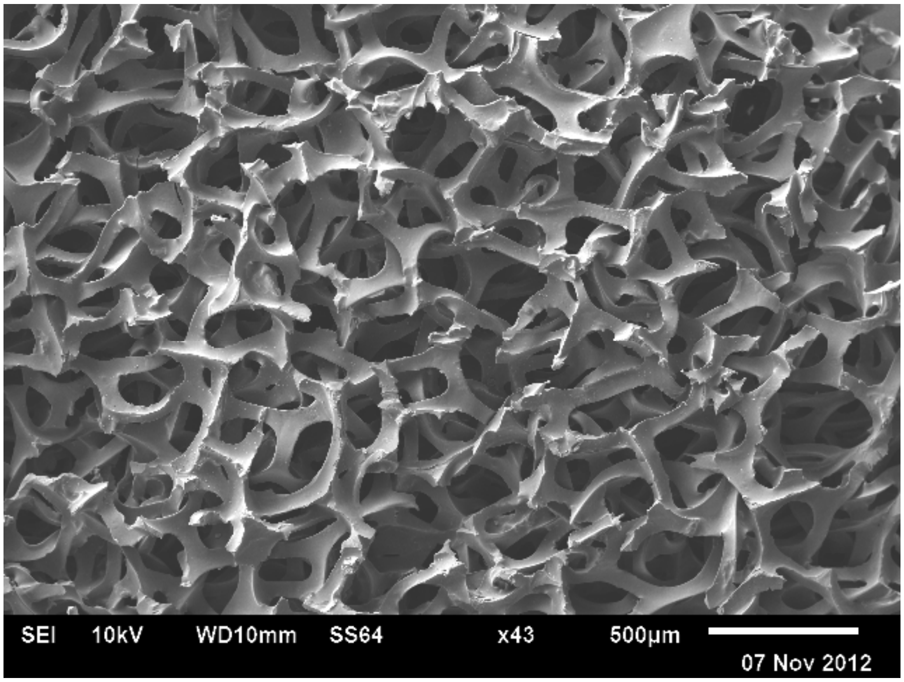

Figure 5.1 SEM image of the carbon sponge electrode illustrating the highly porous nature and high surface area.

Methods

Cr^{VI} Reduction Rate Studies with Shewanella oneidensis MR-1

A microbial culture of *Shewanella oneidensis* MR-1 was used in all of the experimental work in this study. MR-1 were chosen for use as they typically serve as a model *Shewanella* species and have been proven to be effective in heavy metal reduction and power production within an MFC.[29] Three days prior to MFC start-up, Luria-Broth was inoculated with *Shewanella oneidensis* MR-1, and incubated at 30°C for 16-24 hours on a shaker at 100-130 rpm. A minimal media solution was prepared during this period consisting of the components listed in Table 5.1. 0.250 mL of the Luria-Broth culture were added to a 250 mL minimal media solution in a 500 mL Erlenmeyer flask. The mixture was incubated for 1-2 days at 30°C on a shaker at 100-130 rpm. The inoculated minimal media was diluted with 50 mM PIPES buffer to an optical density at 600 nm (OD_{600}) of 0.5 ± 0.05, which approximately corresponds to a cell density of 10^9 CFU mL^{-1}.

Figure 5.2 Composition of minimal media used for growing cultures of *Shewanella* species

Chemical	Conc (mM)
PIPES buffer	5.00 x 10
Sodium Hydroxide	1.25 x 10^{2}
Ammonium Chloride	2.80 x 10
Potassium chloride	1.00
Sodium phosphate, monobasic	4.00
Sodium Lactate	variable on application
Nitrilotriacetic Acid	7.85 x 10^{-2}
Magnesium Sulfate Heptahydrate	1.22 x 10^{-1}
Manganese Sulfate Monohydrate	2.96 x 10^{-2}
Sodium Chloride	1.71 x 10^{-1}
Ferrous Sulfate Heptahydrate	3.60 x 10^{-3}
Calcium Chloride Dihydrate	6.80 x 10^{-3}
Cobalt Chloride Hexahydrate	4.20 x 10^{-3}
Zinc Chloride	9.54 x 10^{-3}
Cupric Sulfate Pentahydrate	4.01 x 10^{-4}
Aluminum Potassium Disulfate Dodecahydrate	2.11 x 10^{-4}
Boric Acid	1.62 x 10^{-4}
Sodium Molybdate Dihydrate	1.03 x 10^{-4}
Nickel Chloride Hexahydrate	1.01 x 10^{-3}
SodiumTungstate	7.58 x 10^{-4}
Biotin	8.19 x 10^{-5}
Folic Acid	4.53 x 10^{-5}
Pyridoxine HCl	4.86 x 10^{-4}
Riboflavin	1.33 x 10^{-4}
Thiamine HCl monohydrate	1.41 x 10^{-4}
Nicotinic Acid	4.06 x 10^{-4}
d-Pantothenic Acid, Hemicalcium Salt	2.10 x 10^{-4}
Vitamin B12	7.38 x 10^{-7}
p-Aminobenzoic Acid	3.65 x 10^{-4}
Thioctic Acid	2.42 x 10^{-4}
L-Glutamic Acid	1.36 x 10^{-1}
L-Arginine	1.15 x 10^{-1}
DL-serine	1.90 x 10^{-1}

The Cr^{VI} reduction rate experiments were performed in an anaerobic chamber (Coy Labs, Inc; Grass Lake, MI) with an atmosphere of 5% H_2 and 95% N_2. Cr^{VI} as potassium dichromate ($K_2Cr_2O_7$) was added to 250 mL of each diluted species culture for a final concentration of 5.0 mg L^{-1} in a 500 mL glass reactor inside the anaerobic chamber. In parallel experiments, humic was added for a final concentration of 30 mg L^{-1}. Mixing was performed continuously for the 3-hour experimental period by magnetic stir plate operating at approximately 100 rpm.

MFC Batch Studies

For this study, a microbial culture of *Shewanella oneidensis* MR-1 was diluted with PIPES buffer to an optical density at 600 nm (OD_{600}) of 0.2 ± 0.1, corresponding to a cell density of approximately 10^7 CFU mL^{-1}. The MFCs were connected to the voltage monitoring equipment and upon stabilization of a baseline signal the anode chamber of the MFC was injected with a concentrated lactate solution for a final concentration of 4 mM (a stoichiometric excess of 2 mM).[16] The MFC was left to equilibrate for two hours and once the baseline voltage had again stabilized, Cr^{VI} was charged to the cathode compartment for a final concentration of 5 mg L^{-1}. Samples were taken periodically and analyzed for Cr^{VI}.

The system was left undisturbed for three days except for periodic sampling, at which point the voltage had decreased to the initial baseline levels. Another injection of Cr^{VI} for a final concentration of 5 mg L^{-1} was carried out, and this process was repeated once more for a total of three exposures. This experiment was repeated identically with the addition of concentrated humic acid for a final concentration of 30 mg L^{-1}.

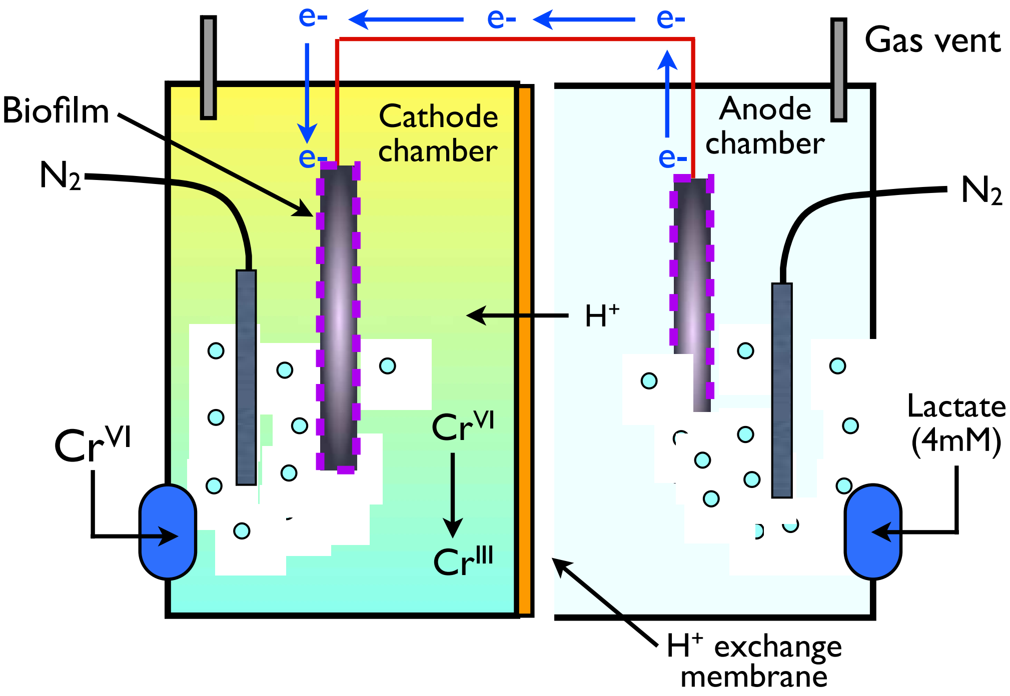

Figure 5.3 Schematic of the microbial fuel cell used in experimental work.

Electrokinetic-Microbial Fuel Cell (EK-MFC) Semi-Batch System

The MFC-EK semi-batch system was designed to evaluate the integration of the MFC and electrokinetic systems. A schematic of the experimental arrangement is presented in Figure 5.4. The soil column was charged with silica sand that had been sieved to remove smaller particle fractions. The sand was rinsed in 0.05 M HNO_3 prior to use to remove any organic matter fractions bound to the particles. The sand was excluded from the reservoirs by use of 0.1 mm fiberglass mesh. The sandy porous media was chosen as a representative of materials common in aquifers used as drinking water sources.[22] Approximately 340 g of sand was charged to the column center, and the entire column including electrode reservoirs was charged with a 3.0 mg L^{-1} Cr^{VI} solution. The porosity was determined experimentally to be 0.36, and the empty bed volume of the entire column was 360 mL. A 30 V electric potential was applied across the column continuously for the duration of the experiment, representing approximately 1.5 V per centimeter length of column. This was the most effective voltage application for transport determined from previous work (see Chapter 4).

The electrokinetic system was run for 24 hours prior to integration with the MFC. At the 24-hour point, the solution in the anode reservoir of the column was pumped at a rate of 12 mL hr^{-1} into the cathode chamber of the MFC, corresponding to a 20-hour residence time in the column. This value was chosen also as it represents a typical aquifer flow rate, and has been used in previous electrokinetic studies (see Chapter 4). To maintain a constant liquid volume in the MFC and the column, an effluent stream from the MFC was circulated back to the sand column and pumped into the cathode reservoir at the same flow rate. Voltage was monitored constantly and samples were taken from the column influent, effluent, and MFC cathode compartment. Multiple experiments were run with this experimental orientation, and the time required to lower Cr^{VI} to undetectable levels was used as the primary metric to compare effectiveness of one experiment to the next.

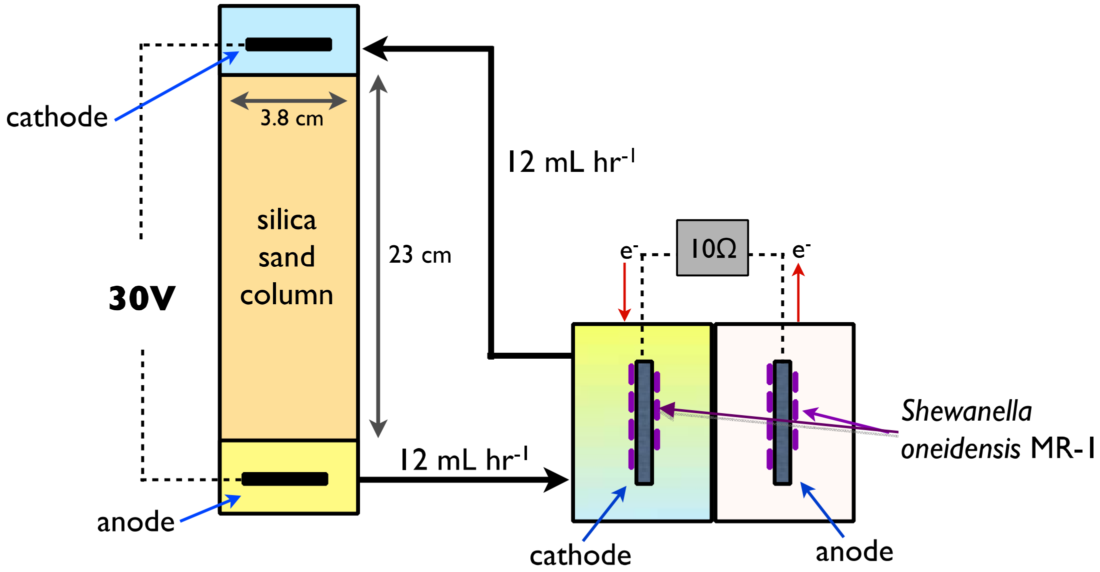

Figure 5.4 Experimental set-up for the semi-batch EK-MFC system.

Continuous Flow Electrokinetic-Microbial Fuel Cell (EK-MFC) System

An integrated electrokinetic and microbial fuel cell treatment system was developed to investigate the efficiency of the dynamic system. The schematic in Figure 5.5 illustrates the continuous flow MFC-EK system. A simulated groundwater containing a carbonate buffered solution with 3.0 mg L^{-1} Cr^{VI} was pumped into the anode reservoir of the electrokinetic cell at 12.0 mL hr^{-1}. Electrokinetic transport transported Cr^{VI} (as $HCrO_4^-$) towards the anode reservoir of the soil column-EK system, the point of accumulation. The anode solution of the electrokinetic cell was pumped continuously at 12 mL hr^{-1} to the top of the MFC cathode to serve as the primary electron acceptor in the MFC system. The same pump pulled solution from the bottom of the MFC at 12 mL hr^{-1} and pumped it back into the electrokinetic cell adjacent to the anode reservoir. This maintained a constant volume of liquid in the MFC such that the cathode remained submerged, and the location of effluent and influent streams ensured Cr^{VI} introduced to the MFC would remain in the chamber for the allotted residence time.

The reason for this particular experimental arrangement was due to the fact that the effectiveness of electrokinetic transport could be better quantified when transporting ions in the opposite direction of the pore liquid flow. Previous work with electrokinetic transport in a flowing system during the experimental work presented in Chapter 4 lead to this discovery, as co-current flow of contaminants from pumping and electrokinetic transport provided inconclusive evidence of transport.

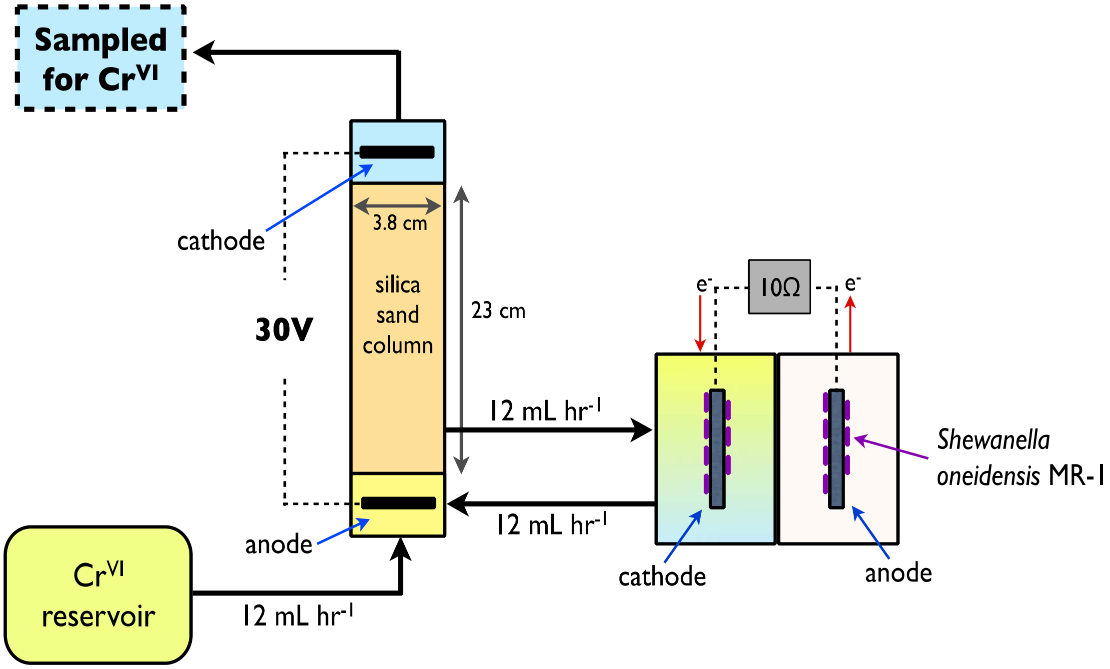

Figure 5.5 Schematic of the experimental set-up for the continuous flow EK-MFC system.

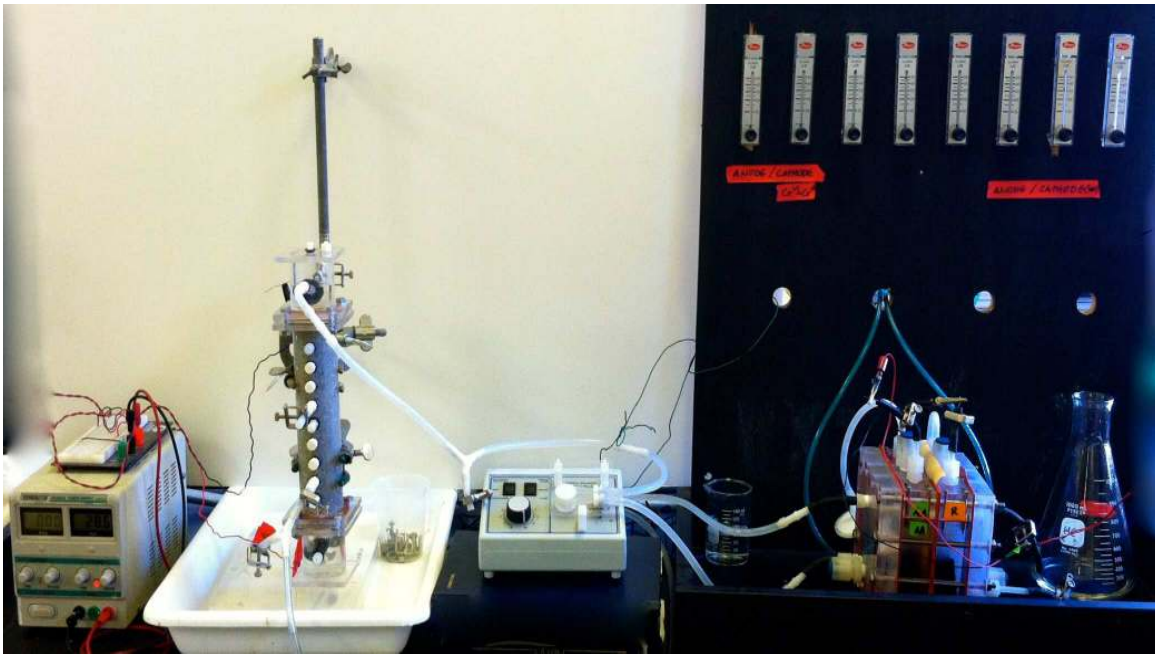

Figure 5.6 Photograph of the continuous flow EK-MFC system arrangement in the lab.

Scanning Electron Microscopy (SEM)

Scanning electron microscopy was used to observe the morphology of biomass attached to the MFC electrode surfaces. Following the completion of experiments, small sections of electrode were prepared and fixed in a 2.5% gluteraldehyde solution. The fixation step was followed by sequential ethanol dehydration (0%, 25%, 50%, 75%, 95%, 100%) and critical point drying. The samples were set on double sided conductive tape atop aluminum studs and gold coated. Electron microscopy was carried out using a scanning electron microscope (JSM-6610LV; JEOL USA Inc.; Peabody, MA) operated with a 10 kV acceleration voltage.[16]

Cr^{VI} Analysis

Samples were analyzed for Cr^{VI} by ion-exchange chromatography (Dionex ICS-1000, Sunnyvale, CA) in accordance with EPA method 218.6. To enhance sensitivity a high-capacity IonPac® AS7 anion exchange column is employed to separate Cr^{III} from Cr^{VI} (Dionex Technical Note 26). The product of the postcolumn reaction between Cr^{VI} and diphenylcarbazide is detected by absorbance at 530 nm using a spectrophotometer, which yields a detection limit of 0.4 μg L^{-1}.

Monod Model Development

The Monod Model is the most basic representation of microbial growth based on Michaelis-Menton biochemical kinetics, and can be written as:

$$\mu_i = \frac{\mu_{max,i} S_i}{K_{S,i} + S_i} \qquad (1)$$

In equation 1, μ_i represents the specific growth rate of microorganisms or biomass (h^{-1}), μ_{max} is the maximum specific substrate utilization rate (h^{-1}), $K_{s,i}$ is the half-saturation constant, and S_i is the substrate concentration. The maximum specific substrate utilization rate is commonly referred to as the maximum specific growth rate, and is a theoretical value representative of ideal maximum growth. The half saturation constant is also termed the half-velocity constant as it represents the substrate concentration when μ_i is half of μ_{max}. This value is indicative of the efficiency of which a microbe utilizes a substrate for growth. These two parameters can be estimated by fitting the model to each set of experimental data.

MATLAB (v.R2011b) was used to fit the Monod Model to the experimental data. The ODE solver *ODE15s* was employed to solve the differential form of the Monod equation:

$$\frac{dS_i}{dt} = \frac{-\mu_{max}*S_i}{K_{s,i}+S_i} \qquad (2)$$

The function *nlinfit* was used to estimate coefficients for the nonlinear regression response to *ODE15s*. The estimation of coefficients follows an iterative least squares method based on specified initial values.

5.4 Results and Discussion

Cr^{VI} Reduction Rate Studies in Batch Systems

As shown in Figure 5.7, *Shewanella oneidensis* MR-1 are capable of rapidly reducing Cr^{VI} to below detection limits. In the absence of humic acid, Cr^{VI} was reduced by MR-1 to negligible levels after 100 minutes of reaction time, and in the presence of humic acid it took only 45 minutes to reach this level. The Monod Model was fit to the experimental data to determine biokinetic parameters K_s, the half saturation constant, and μ_{max}, the maximum specific growth rate. As mentioned earlier, these parameters are useful in evaluating the efficiency by which bacteria can utilize a substrate for growth.

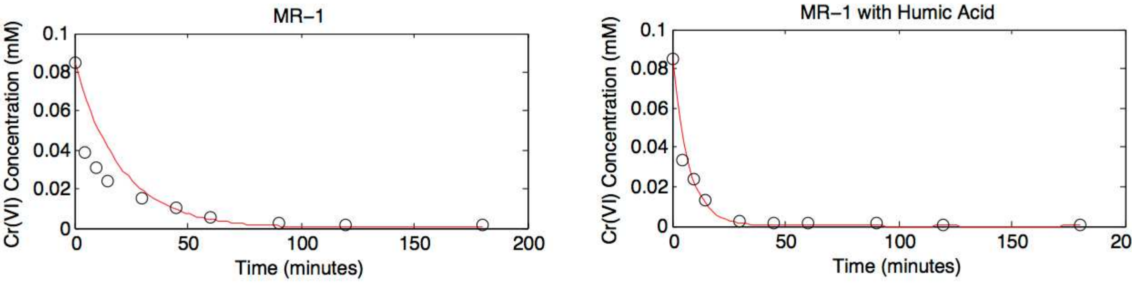

Figure 5.7 Cr^{VI} reduction by *Shewanella oneidensis* MR-1 results in the absence (a) and presence (b) of humic acid.

The Monod Model curve fitting results yielded the maximum specific growth rate and the half-saturation constant for MR-1 in the presence and absence of humic acid, as presented in Table 5.2.

Table 5.1 Biokinetic parameters from the Monod Model fit to reduction rate study data.

Parameter	MR-1 in the absence of HA	MR-1 in 30 mg L^{-1} HA
K_s (mg L^{-1})	1.48	1.39
μ_{max} (hr^{-1})	7.96	12.7

A greater maximum specific growth rate, μ_{max}, for the system with humic acid (12.7 hr^{-1}) as compared to the system without humic acid (8.0 hr^{-1}) indicates that humic acid enhances to the growth rate of MR-1 because of its ability to shuttle electrons from the cell surface to TEAs in solution. Furthermore, the complexation reaction between humic acid and soluble Cr^{III} species limits the bioavailability and exposure of Cr^{III} species to MR-1. A research study of chromium reduction kinetics by a type strain *Shewanella alga* in different growth media determined μ_{max} to be nearly 1.5 orders of magnitude lower than the values experimentally determined here.[23] The enhanced kinetics presented in this study using MR-1 can be attributed to using a *Shewanella* species and carbon source combination proven to be effective in Cr^{VI} reduction.

The half saturation constant, K_s, for the systems with and without humic acid are very similar, however the system with humic acid has a slightly lower value. The experimentally determined half saturation constants are similar to previously reported values determined for a *Shewanella alga* stain.[23] Although the values are too close to make a definitive deduction, the smaller K_s value could be caused by interactions between lactate and humic acid. This type of complexation could render the lactate non-bioavailable, decreasing the concentration of available substrate for MR-1.

Batch MFC Studies

Chromium Reduction

These experiments were conducted to determine the extent of Cr^{VI} treatment in an MFC system, and to investigate the magnitude of power generation. The voltage generated across the MFC was monitored continuously, and samples were taken from the cathode reservoir regularly to determine the extent of Cr^{VI} reduction. Lactate was charged to the anode compartment in excess in accordance with previous work.[16] The concentration of Cr^{VI} measured in the MFC cathode compartment at different time intervals is shown in Figure 5.8.

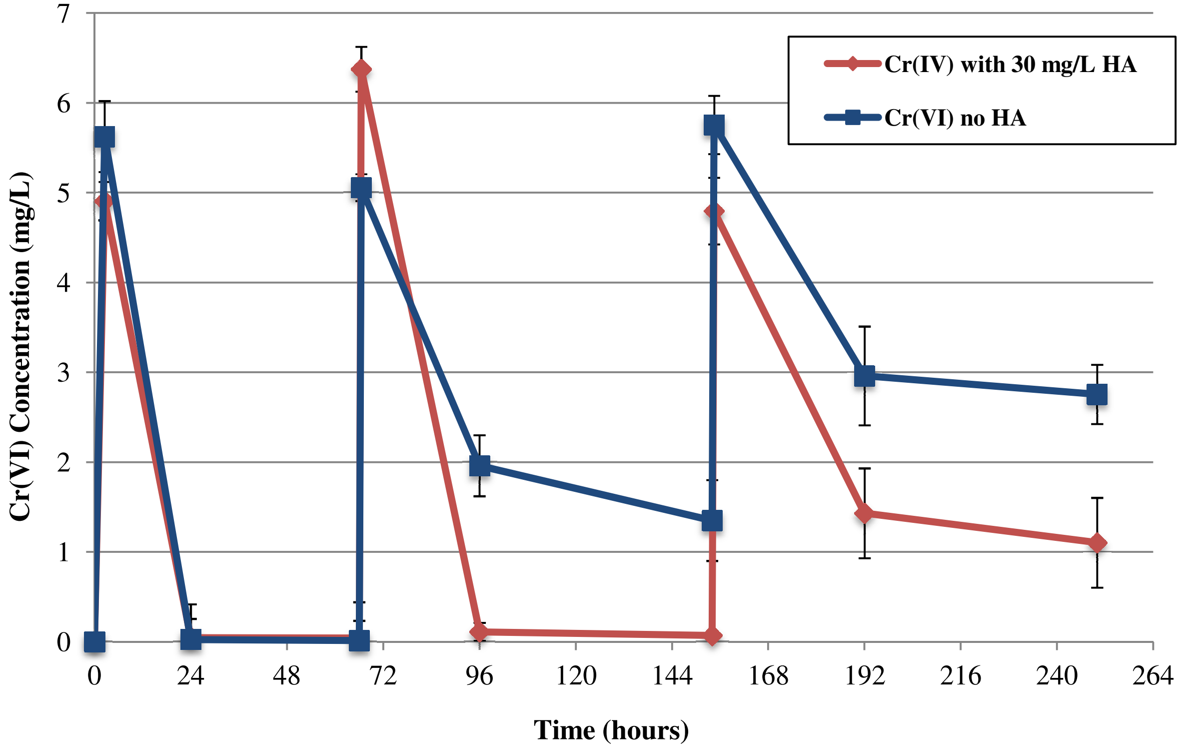

Figure 5.8 **Cr^{VI} reduction profiles for three individual Cr^{VI} exposures in MFC batch studies.**

The initial target Cr^{VI} concentration was 5 mg L^{-1}, however some variability was experienced due to difficulty in mixing the concentrated Cr^{VI} solution upon its injection by syringe with the solution in the cathode compartment. After the first exposure, Cr^{VI} was removed entirely from each system. The second exposure saw nearly complete removal of Cr^{VI} from the system containing humic acid, and 73% removal was observed in the non-humic acid system. The third and final exposure was the least effective, with 77% removal from the system with humic acid and 52% removal by the system without. A summary of the experimental conditions and batch study results is presented in Tables

5.3 and 5.4. The percent chromium removal represents the amount of Cr^{VI} reduced after each exposure, and the DC peak voltage is the voltage peak (DCV) immediately after the MFC cathode compartment was charged with Cr^{VI}.

Table 5.2 Summary of batch MFC results in the system absent of humic acid.

Exposure	Cr^{VI} initial (mg/L)	Cr^{VI} residual (mg/L)	% Cr^{VI} Removal	DCV Peak (mV)
1	4.91	0.04	99.2	7.12
2	6.38	0.07	98.9	3.96
3	4.80	1.102	77.0	2.35

Table 5.3 Summary of batch MFC results in the presence of 30 mg L^{-1} of humic acid.

Exposure	Cr^{VI} initial (mg/L)	Cr^{VI} residual (mg/L)	% Cr Removal	DCV Peak (mV)
1	5.63	0.013	99.8	6.47
2	5.06	1.35	73.3	4.53
3	5.76	2.755	52.1	2.71

The enhanced performance of the MFC containing humic acid can be explained from different perspectives. It is known that humic acids can serve as electron shuttles, allowing for more efficient electron shuttling from the cathode surface to TEAs, in this case Cr^{VI}, in solution.[7] Another explanation for this phenomenon may be related to toxicity of soluble Cr^{III} species formed in the reduction of Cr^{VI}. Various Cr^{III} species such as Cr^{3+}, or as a hydroxyl complex such as $Cr(OH)^{2+}$ or $Cr(OH)_2^+$ can bind non-specifically to DNA and other cellular components in the cytoplasm, ultimately interfering with transcription and DNA replication processes.[23] Humic acids are known to complex with Cr^{III} species[25] and due to this complexation the Cr^{III} species are sparingly bioavailable as bacteria have no means of transporting bulky humic acids across cell membranes. As a result, the destruction caused by Cr^{III} within cells can be slowed, prolonging Cr^{VI} reduction potential when humic acid is present.

Voltage and Power Production

Slight differences in voltage produced across the MFC were observed between the systems with and without humic acid. A voltage reading was taken every five minutes in these batch studies, however due to high background noise in the readings only specific points were plotted to illustrate the trends in voltage as shown in Figure 5.9. The peaks correspond to Cr^{VI} exposures at the time of injection, and the valleys are a result of low residual Cr^{VI} concentrations. With each exposure, the resulting peak is much smaller than the preceding peak, which is a direct reflection on the toxicity of Cr^{VI} in biological systems. The capacity for MR-1 to further reduce Cr^{VI} decreases with each exposure, as there exists a finite amount of Cr^{VI} each bacterium is capable of reducing. The Cr^{VI} reduction inhibition is a product of an interrupted electron transport chain, and the system becomes increasingly cathode limited as the reduction overpotential at the cathode increases.[25]

Overall, the system with humic acid produced a higher baseline voltage, and after each consecutive exposure the baseline voltage settled at a higher value relative to the system without humic acid. This could be attributed to the following reasons: a) humic acid serves as an electron shuttle, increasing the reaction kinetics in the cathode compartment, and b) the presence of humic acid raises the redox potential slightly, widening the redox potential difference between the anode and cathode compartments.[26]

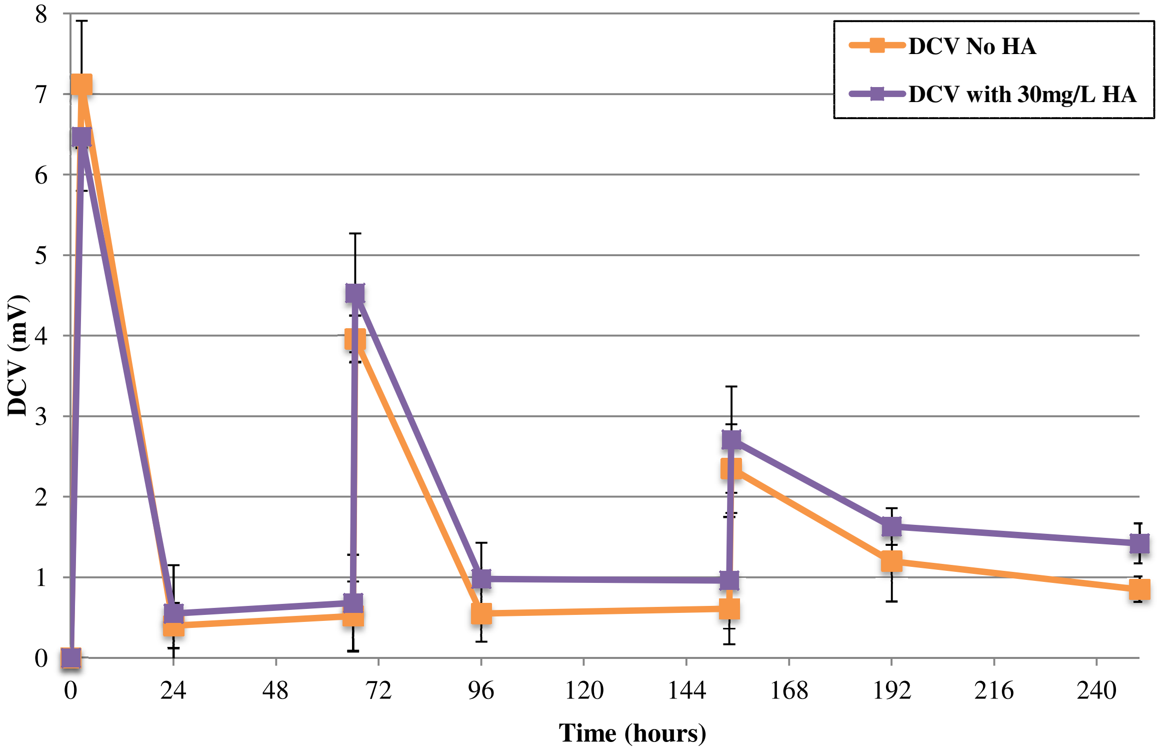

Figure 5.9 Voltage produced during MFC operation for three exposures to Cr^{VI}.

The Cr^{VI} reduction data and the voltage data are presented in Figure 5.10. The peak data points are plotted for each exposure, to illustrate the observed trends. The voltage peaks and Cr^{VI} removal percentage decline at a proportional rate, as these parameters are dependent on each other. It is anticipated that with a more concentrated injection of Cr^{VI} to the cathode compartment of the MFC, a larger voltage peak would be observed. However, if a more concentrated dose of Cr^{VI} were added to the MFC, the removal of Cr^{VI} per exposure would drop off more markedly.

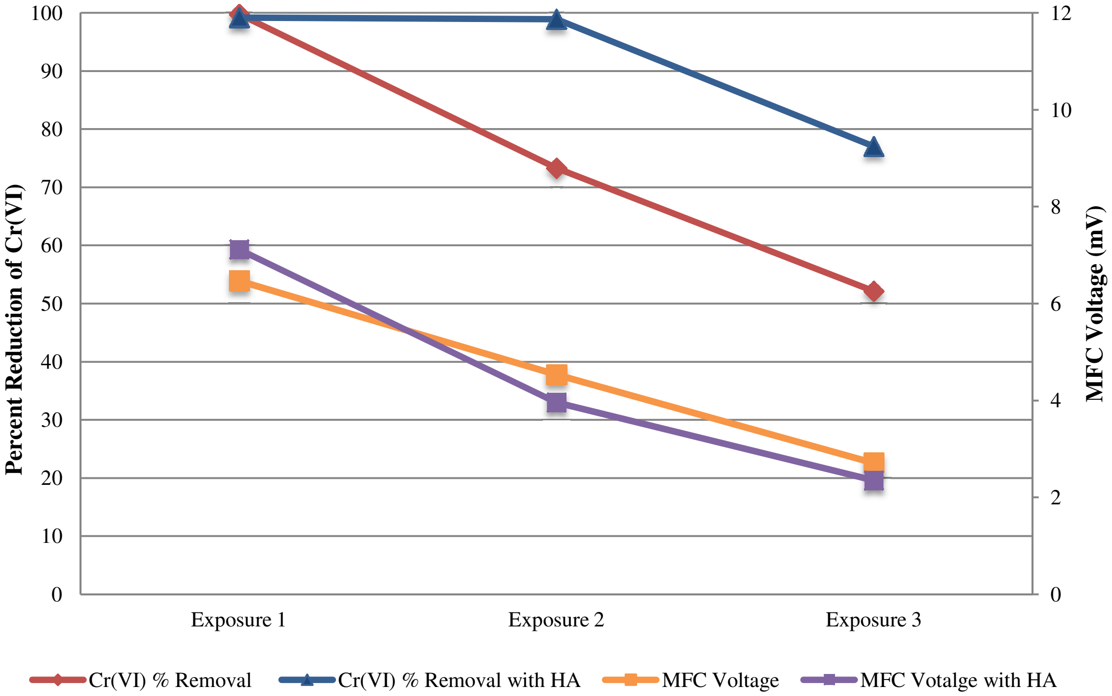

Figure 5.10 Comparison of peak voltage data and Cr^{VI} concentration data for three exposures.

An estimation of power density produced during peak voltage moments was calculated as

——— (3)

Where P is the power density, E_{MFC} is the voltage across the MFC, A_{an} is the surface area of the anode, and R_{ext} is the external resistance applied to the circuit. The results of the power calculation are presented in Table 5.4. The power density is directly proportional to the voltage produced (E_{MFC}), and therefore follows the same trends observed in Figure

9. The first exposure to Cr^{VI} produced the largest power density, and the system without humic acid produced a 17% higher power density than the system with humic acid (0.0253 μW/cm^2 versus 0.0209 μW/cm^2). However the system with humic acid produced more power compared to the system without humic acid during the second and third exposures to Cr^{VI}. The power densities are very similar to those determined by Hsu *et al.* (28) from linear polarization sweeps.

Table 5.4 Peak power density produced during MFC operation.

Exposure	**Peak Power - no HA (μW/cm^2)**	**Peak Power - 30 mg L^{-1} HA (μW/cm^2)**
1	0.0253	0.0209
2	0.0078	0.0103
3	0.0028	0.0037

Scanning electron microscopy was used to observe the nature of the biofilm formed on the carbon electrodes after the completion of the experiment. SEM micrographs (Figure 5.11) showed a semi-uniform distribution of MR-1 across the electrode surface. The MR-1 coverage was typical of several representative samples investigated in this study. Nonetheless, this type of population density was anticipated since MR-1 are known to typically form thin biofilms on surfaces.

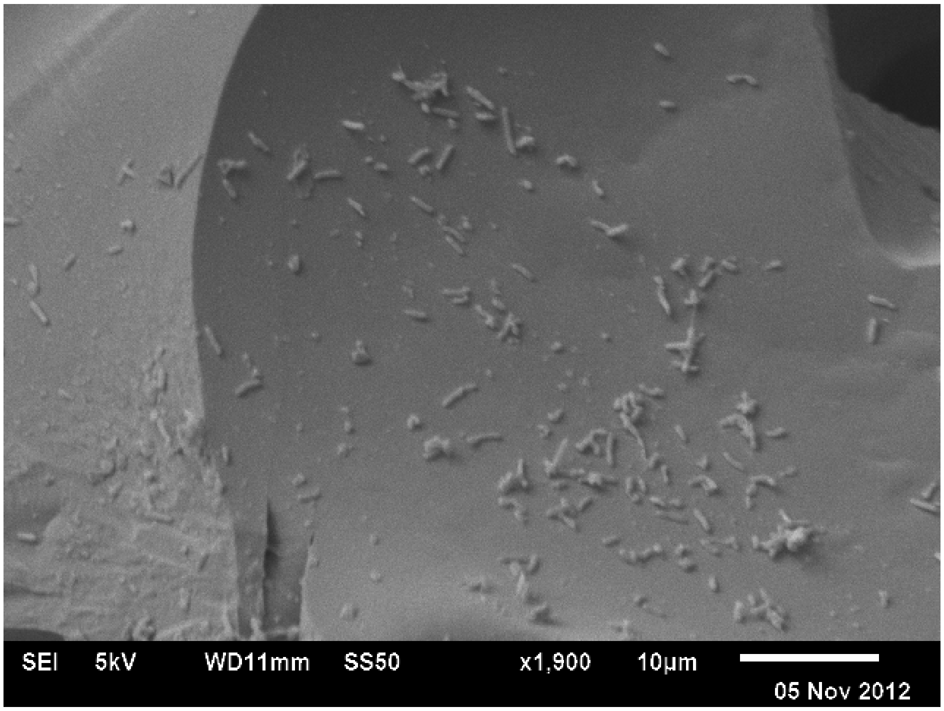

Figure 5.11 SEM image of *Shenwanella oneidensis* MR-1 biofilm on the MFC anode at 1,900x magnification.

Upon closer examination of the anode electrode, nanowires were evident. In Figure 5.12, a clumping of biomass including the rod-shaped MR-1 shows a small network of nanowires connecting bacteria to one another and to the electrode surface. As previously discussed, nanowires play an essential role in the transport of electrons in bioelectrochemical systems, and may also serve as means of communication between bacteria. At the anode in the MFC, these nanowires allow bacteria to transfer electrons directly to the electrode surface. This is an efficient means of electron transfer, as these conductive filaments are effective in electron transport over distances of many microns.[27]

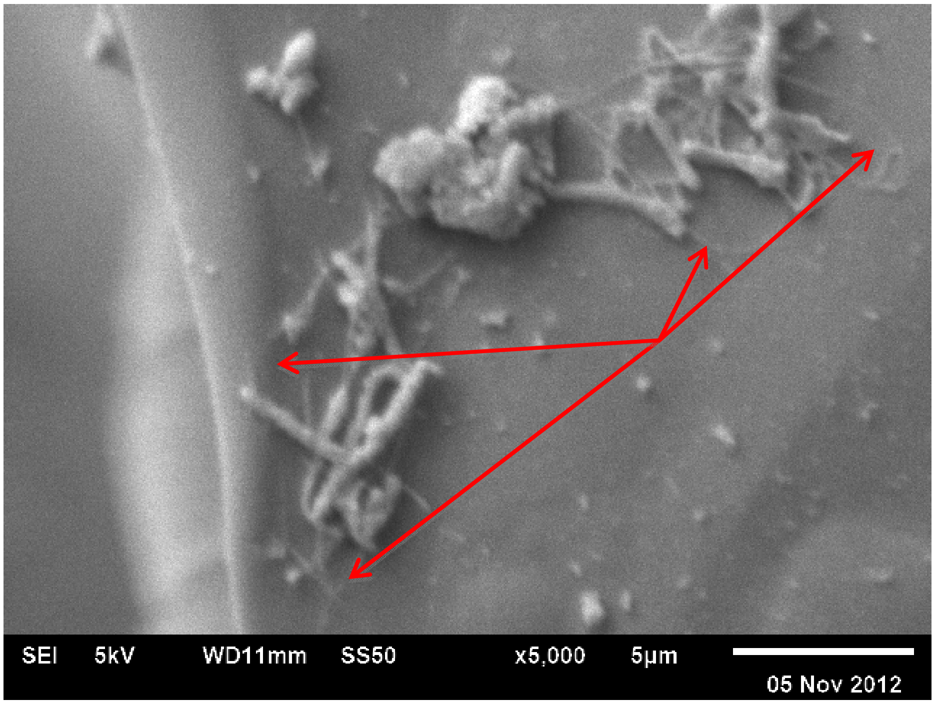

Figure 5.12 SEM image of biomass on the MFC anode at 5,000x magnification showing a network of nanowires (red arrows).

The dispersed state of the microbial population on the electrode surface are an additional limiting factor in this work. Optimizing the biofilm development on the electrode could be a means of increasing substrate utilization on the anode side of the MFC, creating a larger pool of electrons. At the cathode side, a more-developed biofilm may result in faster reduction kinetics, and reduce cathodic activation losses.

Electrokinetic-Microbial Fuel Cell (MFC-EK) Semi-Batch System

pH Gradient

Shifts in pH occur in electrokinetic systems as a result of electrolysis reactions at the anode and cathode reservoirs. It is important to monitor these shifts as they can cause significant inhibitive effects on electrokinetic transport phenomena. In the EK-MFC semi-batch studies, the pH in the anode dropped to 3.2 in the system without humic acid and to 3.8 for the system with humic acid after 24 hours. The pH in the cathode reached 11.8 in the system without humic acid, and reached 11.2 in the system with humic acid. The difference between the two systems at both the anode and cathode is simply explained by the improved buffering capacity from the presence of humic acid. The pH variation with time for each study is shown in Figure 5.13. These results are in good agreement with previous electrokinetic studies performed (see Chapter 4).

The concentrated Cr^{VI} solution in the anode reservoir of the electrokinetic cell was pumped into the cathode compartment of the MFC at the 24-hour mark, shown in Figure 5.13 as the black dashed line. The pH in the MFC was monitored closely in order to ensure that the acidic solution from the electrokinetic cell anode reservoir did not create adverse conditions for sustaining the bacteria population on the MFC cathode. As seen in Figure 13, the pH of the anode and cathode reservoirs returned to near neutral values within 10 hours of integrating the electrokinetic system with the MFC as a result of slowly flushing the electrokinetic cell with the well buffered fluid from the MFC cathode compartment. It is important to note that the pH in the cathode compartment of the MFC remained above 6.8 for the entire study.

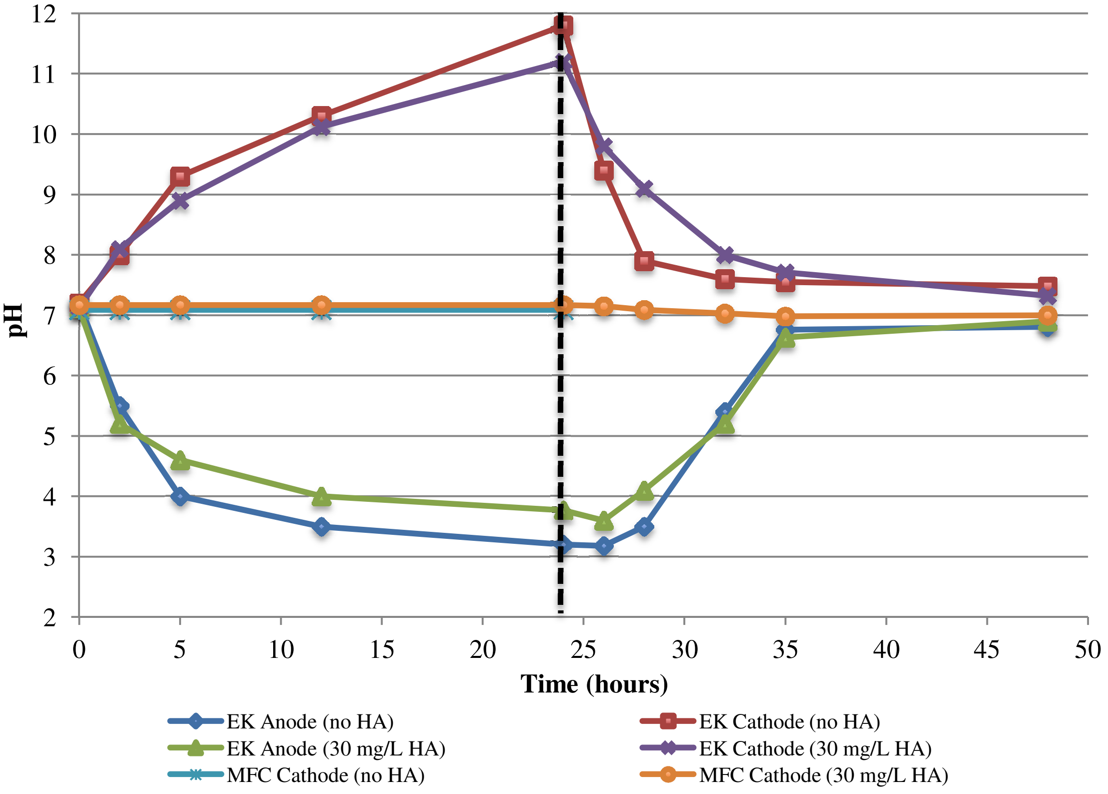

Figure 5.13 pH profiles recorded from the electrokinetic cell anode and cathode reservoirs and the MFC cathode during the integrated batch study.

It was observed in initial studies that the EK-MFC semi-batch system is highly sensitive to pH changes. Furthermore, studies show that *Shewanella oneidensis* MR-1 respond immediately to pH shifts, and can become inactive in moderately acidic solutions.[28] Similarly, acidic conditions will have a significant impact on Cr^{VI} speciation and transport in an electrokinetic system. The eventual moderation of pH throughout the EK-MFC integrated system signifies the importance of sustainability for this type of treatment system. In these studies, the well-buffered solution in the MFC effectively neutralized the influent acidic solution from the anode reservoir of the electrokinetic cell, promoting continuous transport of Cr^{VI} and favorable reactor conditions for microbial reduction of Cr^{VI} in the MFC.

Current in the Electrokinetic Cell

Electrokinetic transport is a product of current passing through the groundwater zone under the applied electric potential. Current is proportional to the concentration of ionic species in the pore fluid for a given applied voltage, and upon starting an electrokinetic treatment system the current will rise rapidly from zero as H^+ and OH^- are generated at the anode and cathode, respectively. However as the pH drifts too far from neutral in either direction, precipitation and/or dissolution reactions dominate the solution chemistry. Cr^{VI} species are capable of reacting with H^+ in acidic waters to form Cr^{III} species according to the reaction[29]:

$$HCrO_4^- + 7H^+ + 3e^- \rightarrow Cr^{3+} + 4H_2O \qquad +0.382\ V$$

Cr^{III} species rapidly precipitate out as chromium oxides and chromium hydroxide. In an electrokinetic cell, these reactions cause a substantial decline in the concentration of free ions in solution and subsequently the current will drop rapidly. Current is a parameter that can be used to describe the inhibitive effects of pH gradient formation in electrokinetic cells.

Humic acid can increase the electrical conductivity of groundwater, and as mentioned previously adds to the buffering capacity as well. However the low solubility of humic acid under acidic conditions ($pH < 2.0$) and the low pH conditions that form at the anode of the electrokinetic system can lead to humic acid precipitation. Cr^{III} and humic acid complexes can form rapidly near the anode where chromium concentrations are high and the pH reaches as low as 2. This phenomenon can result in a series of precipitation reactions involving humic acid, Cr^{III} species, and other ionic species present. The end result of these precipitation reactions is a zone of very low conductivity within the column, and thus, low current throughout the electrokinetic cell.

In the study presented here, it was hypothesized that integration of the MFC with the electrokinetic column would help maintain a higher steady-state current throughout the soil column, as compared to a static electrokinetic experiment. The current through the electrokinetic cell was measured during static electrokinetic experiments (without integration with MFCs) in the presence and absence of humic acid, and in EK-MFC semi-batch experiments without humic acid. In the EK-MFC semi-batch study, the system was static for the first 24-hours before changing to the continuous flow dynamic system.

Figure 5.14 shows the current measured in the electrokinetic studies. In these static electrokinetic experiments the current rose rapidly upon application of electric potential and reached a maximum within about 10 hours. The maximum was followed by a rapid drop, which is explained by precipitation reactions decreasing the conductivity of the system. The current measured in the static system without humic acid peaked at 10.1 mA after 10 hours, then declined to a steady-state value of 2.5 mA around the 72-hour point. The static system with humic acid rose to a maximum current of 13.6 mA after 13 hours, then dropped to a stead-state value of 2.0 mA after about 80 hours. The delay in response observed in the system with humic acid can be explained by a slower development of H^+ and OH^- fronts due to the enhanced buffering capacity. Humic acid mitigates the rapid development of pH changes, and delays the formation of precipitates that cause the decline of current. This allows the current to rise to a higher maximum peak than the system without humic acid. However humic acid was also the cause for the static system to reach the lowest steady-state current, as it was responsible for complexation and precipitation reactions when the conditions became acidic.

The current measured in the EK-MFC semi-batch studies followed a very similar upward trajectory to that of the static electrokinetic experiments, as shown in Figure 5.14.

Pumping to the MFC started at the 24-hour point, and the current in the system without humic acid fell to a steady-state value of 6.8 mA within 48 hours. The system with humic acid dropped to a steady-state value of 7.7 mA. In the static electrokinetic experiments the presence of humic acid resulted in a lower steady-state current than the system without humic acid. The opposite result was determined in the semi-batch studies, where the steady-state current for the system with humic acid was nearly 1 mA larger than the system without humic acid. The circulation of fluid between the column and the MFC was instrumental in maintaining a conductive system in the semi-batch systems by mitigating pH changes. This limited the amount precipitation reactions involving chromium and humic acid within the electrokinetic cell, which is a primary contributor to the decrease in current observed in the static experiments. This was reflected in the current reaching steady-state values over three times higher than the static electrokinetic experiments.

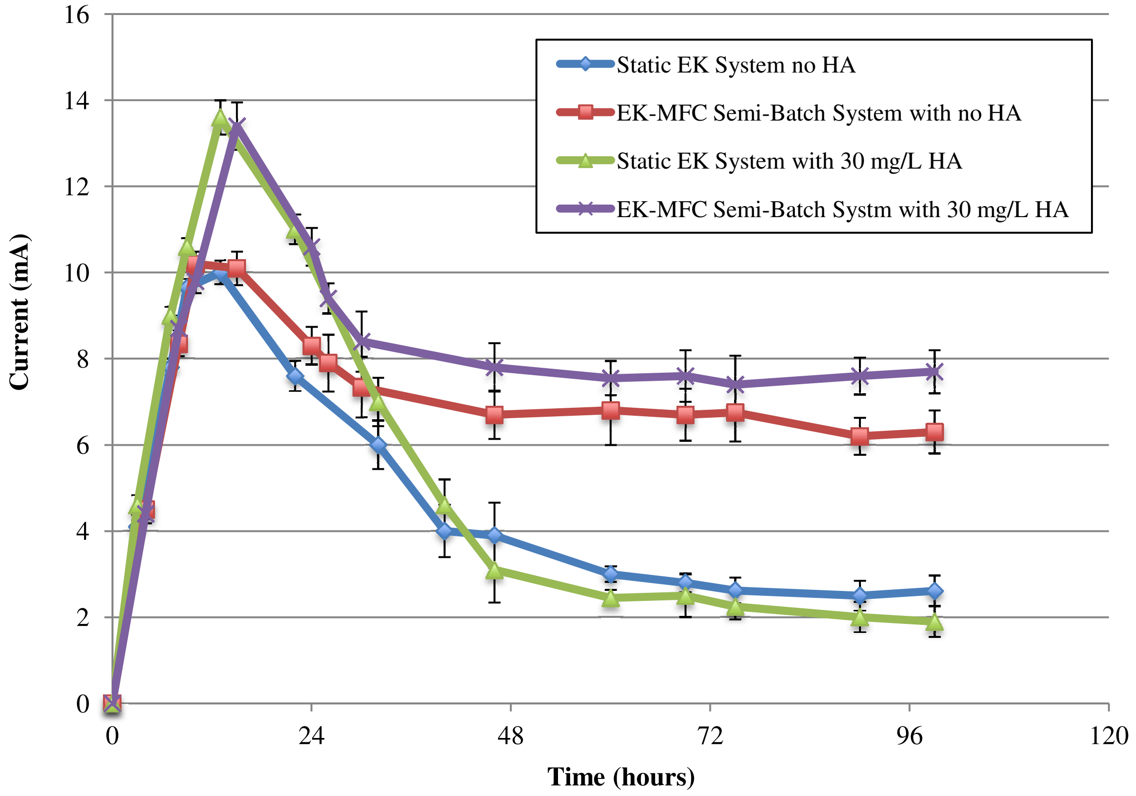

Figure 5.14 Current measured in sand columns under an applied electric potential of 1.5 V/cm.

Voltage Across the MFC

The voltage across the MFC increased with addition of humic acid to the cathode reservoir in the EK-MFC semi-batch studies. These results are in good agreement with the results from the MFC batch studies. Figure 5.15 shows the voltage measured across the MFCs with and without humic acid once they were integrated with the electrokinetic cells. Voltages peaked at 1.6 mV and 1.1 mV in the systems with humic acid and without humic acid, respectively. The system with humic acid produced a higher voltage than the system without over the duration of the study. After 12 hours the humic acid system was recording about 1 mV, and the non-humic acid system recorded about 0.25 mV. By hour 30, the non-humic acid system was reading zero voltage, and the humic acid system was recording about 0.6 V. Humic acid appeared to be aiding in electron shuttling to Cr^{VI} species, as indicated by the significantly higher voltage production. However after about 12 hours no Cr^{VI} was detected within the MFC cathode compartment of either system, and the voltage production from the system with humic acid was greater than the initial spike observed in the system without humic acid. These results suggest that humic acid served as a TEA towards the end of this study.

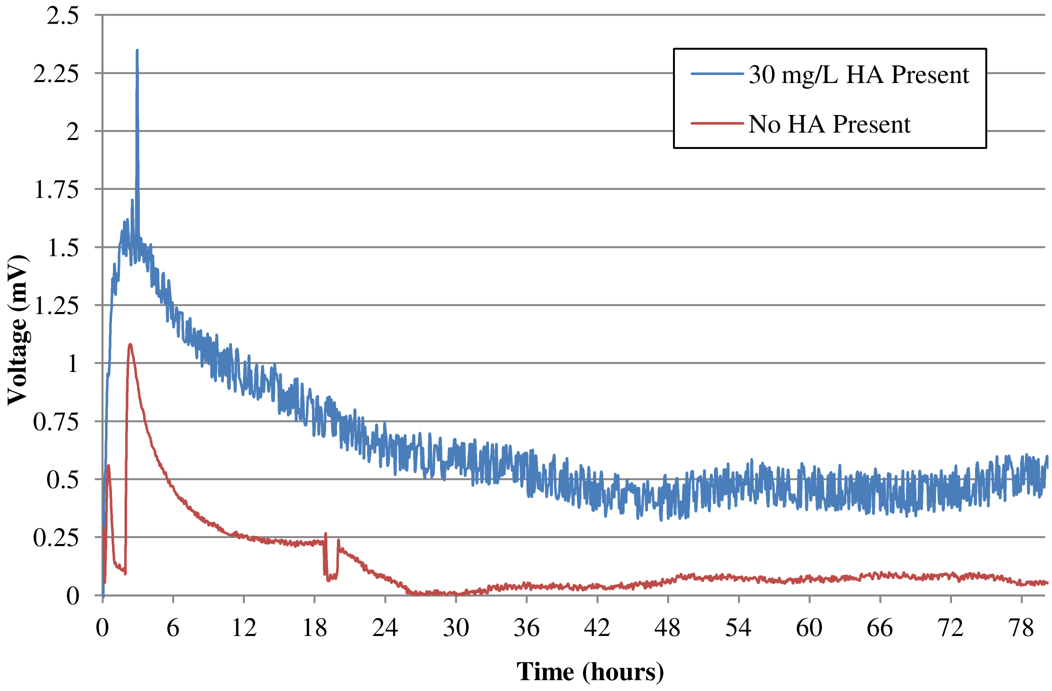

Figure 5.15 Voltage produced during the EK-MFC semi-batch experiments for systems with and without humic acid.

The peak voltage in this study was much lower than the batch systems, because the total Cr^{VI} concentration within the MFC was orders of magnitude less. The Cr^{VI} solution from the anode reservoir of the electrokinetic cell was at a maximum concentration of 4 mg L^{-1} when introduced to the MFC cathode compartment, and was serving as the primary electron acceptor. Nevertheless, the influent stream was substantially diluted within the MFC, lowering the availability of electron acceptors.

Chromium Profiles

The chromium concentrations measured in the electrokinetic cells with and without humic acid were very similar within the first 24-hours (Figure 5.16). The slight differences observed in this figure are primarily a result of different initial Cr^{VI} concentrations. The anode concentrations increased by nearly 50% in experiments with and without humic acid from electrokinetic transport, and the cathode concentrations declined to below 0.1 mg L^{-1} as Cr^{VI} moved towards the anode. The results from the initial transport are in good agreement with results presented in Chapter 4 regarding Cr^{VI} transport, and a more detailed discussion is presented there. At the 24-hour mark (indicated by the black dashed line), pore fluid was pumped from a port adjacent to the anode reservoir of the electrokinetic cell, at a location where Cr^{VI} concentration was the highest.

Cr^{VI} concentrations drop dramatically as a result of integration with the MFC, as Cr^{VI} in the anode reservoir is drained out and flushed with a low-Cr^{VI} concentration pore fluid from upstream in the column. The center of the electrokinetic cell (column center) undergoes a similar decline in Cr^{VI} concentration. The pore fluid upstream of the column center contains very low concentrations of Cr^{VI} as indicated by the undetectable concentrations at the cathode after 24 hours. Once pumping to the MFC began, the column center was flushed with pore fluid containing very little Cr^{VI}.

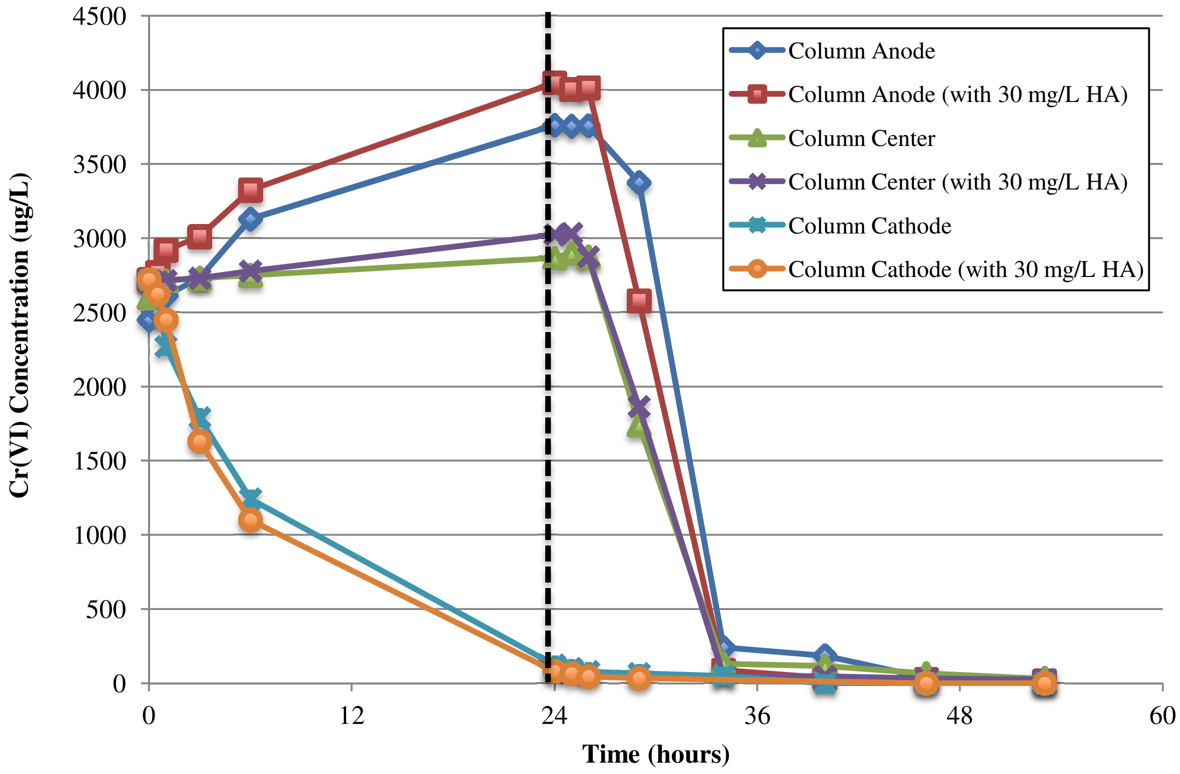

Figure 5.16 Cr^{VI} concentrations near the anode, the center of the sand column, and the cathode for the dynamic batch system. Results are shown for systems with and without humic acid.

The presence of humic acid had no significant influence on the EK-MFC semi-batch system. The low concentrations of Cr^{VI} introduced to the column throughout the experiment didn't limit the microbial reduction in the time frames observed. The total amount of Cr^{VI} passed through the MFC was less than the amount introduced in a single exposure during the batch studies. Additionally, Cr^{VI} was introduced slowly over a matter of hours as opposed to one concentrated injection. These conditions were favorable for sustaining the population of MR-1 in the MFC cathode compartment, and as a result complete reduction of Cr^{VI} was observed. To see the effects of humic acid in an EK-MFC system, a much higher Cr^{VI} concentration would be required, or a larger volume of contaminated water would need to be flushed through the MFC.

The experimental orientation of the EK-MFC integration allowed for a direct comparison of a treatment system with and without using electrokinetic transport. The residence time of Cr^{VI} in the column was calculated to be approximately 20 hours, and therefore it is expected that if the entire volume of pore liquid were pumped from the sand column to the MFC, it would take 20 hours of pumping to treat the column. The electrokinetic transport step and the pre-concentration of Cr^{VI} lowered the amount of time to remove all Cr^{VI} from the column to 12 hours. This translates to 40% less time required for pumping, which is generally the largest cost associated with a pump-and-treat system.[30]

Electrokinetic-Microbial Fuel Cell (MFC-EK) Continuous Flow System

The EK-MFC semi-batch system effectively treated a low concentration of Cr^{VI} within a short period time, but gave no indication of the sustainability of such an integrated treatment approach. The continuous flow EK-MFC system was designed to investigate parameters that were not evaluated by the semi-batch system, namely: a) determine the Cr^{VI} reduction capacity of the MFC, and b) quantify the benefits of the presence of humic acid in a groundwater system undergoing treatment in a microbial fuel cell.

The continuous flow EK-MFC system employed a large reservoir feeding the flow-through column under an applied electric potential integrated with an MFC for Cr^{VI} treatment, as shown in Figure 5.5. An identical system without electrokinetic transport was evaluated for comparison. The Cr^{VI} concentration profiles for various sampling points from the soil column and the MFC are shown in Figure 5.17. The electrokinetic transport and flow-through system were run for 24-hours before integration with the MFC, indicated by the black dashed line. This allowed the system to reach a state of equilibrium. A slight increase in Cr^{VI} concentration in the anode reservoir was observed after 24-hours from an initial value of 2.90 mg L^{-1} to 3.21 mg L^{-1}. A slight decrease in concentration was observed in the cathode over the same time frame from 2.90 mg L^{-1} to 2.72 mg L^{-1}. These results are is agreement with continuous-flow column experiments discussed in Chapter 4, where a more detailed discussion of electrokinetic transport is presented.

After the equilibration period, the concentrated Cr^{VI} solution from the anode reservoir of the electrokinetic cell was pumped to the cathode compartment of the MFC for microbial reduction. An initial spike in Cr^{VI} concentration in the cathode of the MFC was observed after 4 hours of treatment time. Concentrations of Cr^{VI} in the cathode compartment of the MFC were measured to be below 0.05 mg L^{-1} for the remainder of the experiment. The system containing humic acid had nearly identical Cr^{VI} concentrations in the MFC cathode compartment over the duration of the experiment. As seen in the semi-batch studies, the low influent Cr^{VI} concentrations and significant dilution factor upon introduction to the MFC allowed for effective reduction.

The most significant parameter analyzed in this study was the soil column effluent stream, as it was used to determine the extent of Cr^{VI} treatment in the integrated system. The concentration of Cr^{VI} in the column effluent (adjacent to the cathode reservoir) for the continuous flow system without humic acid underwent a slight initial drop as a result of electrokinetic transport of Cr^{VI} towards the anode, consistent with previous studies (see Chapter 4.3). Upon integration with the MFC the concentration dropped significantly from around 2.6 mg L^{-1} to 0.41 mg L^{-1} within 24 hours, and remained at that level for the duration of the experiment. The system containing humic acid resulted in very similar chromium profiles. The concentration of Cr^{VI} in electrokinetic anode reservoir increased from 2.95 mg L^{-1} to 3.14 mg L^{-1} over 24 hours, and the cathode concentration was nearly identical to that of the system without humic acid over the first 24 hours. The column effluent Cr^{VI} concentration in the humic acid system however dropped more rapidly relative to the system without humic acid, and to a lower final concentration of 0.30 mg L^{-1}.

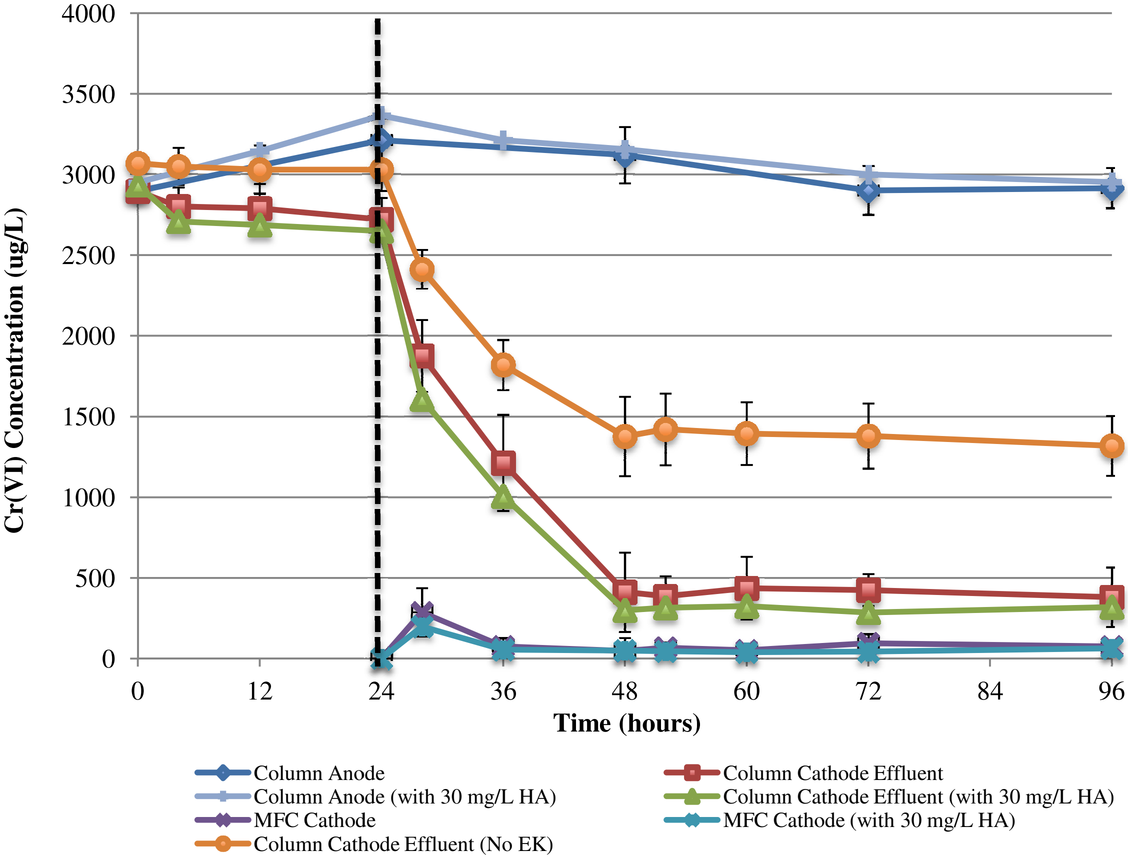

Figure 5.17 Cr^{VI} concentrations recorded at the soil column anode and cathode, as well as the MFC cathode for systems with and without humic acid.

The presence of humic acid was responsible for a slightly more effective removal of Cr^{VI} from the soil columns. The concentration of Cr^{VI} in the MFC effluent was negligible for the duration for this experiment, so the advantages posed to this system by humic acid were not involved in the electron transport process within the MFC. The results obtained from measuring the current in the EK-MFC semi-batch studies as shown previously in Figure 5.14 showed that humic acid increased the flow of current. The higher Cr^{VI} removal percentage seen in the continuous flow EK-MFC studies with humic acid is a result of a higher current passing through the system, and more effective Cr^{VI} transport to the anode reservoir of the electrokinetic cell.

Sustainability of Cr^{VI} Treatment in an MFC

A concern of the experimental set-up was that Cr^{VI} being introduced to the anode reservoir of the electrokinetic cell would be pumped directly into the MFC, as the influent port and the effluent to the MFC were within close proximity. An experiment was run with an identical orientation as Figure 5.5 without electrokinetic application to serve as a comparison. Cr^{VI} was transported by the advective flow to the cathode reservoir of the electrokinetic cell, and the effluent concentrations were measured at 1.4 mg L^{-1}. This indicated that about half of the Cr^{VI} introduced to the column was being successfully transported through the column, and provided a basis for comparison with the experiments involving electrokinetic transport. Integrating electrokinetic transport was effective in a) preventing or slowing transport of Cr^{VI} towards the cathode with the advective flow in the column, and likely to some extent b) transporting Cr^{VI} towards the anode against the advective current from the pressurized flow. The system with electrokinetic transport maintained effluent Cr^{VI} concentrations below 0.5 mg L^{-1}, nearly 1 mg L^{-1} lower than the system without electrokinetic transport.

The continuous flow EK-MFC system demonstrated effective Cr^{VI} reduction, and showed that integration of electrokinetic transport and microbial fuel cell technology is beneficial. As a means to investigate the sustainability of this treatment approach, the MFCs were run with a continuous influent stream of Cr^{VI} to the cathode compartment for over three weeks to determine a breakthrough curve for Cr^{VI} from the MFC cathode compartment effluent. The influent and effluent streams in the extended continuous flow experiment were fixed at a flow rate of 12 mL hr^{-1}, resulting in a residence time of about 24 hours. The breakthrough curve of Cr^{VI} from an abiotic MFC is shown on Figure 5.18 for reference. This curve represents simply the breakthrough of 3 mg L^{-1} Cr^{VI} being introduced to a compartment of an MFC initially containing only carbonate buffered water at pH 7. Note that the breakthrough time from the abiotic MFC was approximately 20 hours, however in Figure 5.18 the curve was shifted along the x-axis and superimposed for direct comparison to the other experimental curves.

The MFC system without humic acid in the feed solution reduced Cr^{VI} to below 0.05 mg L^{-1} for 10 days, at which point a degradation of reductive capacity ensued. The Cr^{VI} concentrations after day 12 increased steadily at a slow rate of about 0.3 mg L^{-1} day^{-1}

for about three days. The breakthrough curve slope between these days was nearly an order of magnitude less than the slope of the abiotic control, which was calculated to be approximately 2.8 mg L^{-1} day^{-1}. This indicated that Cr^{VI} reduction was still taking place within the MFC, but at a rate slower than Cr^{VI} introduction to the MFC. Between days 15 and 17, the Cr^{VI} concentrations rose rapidly to the influent concentration of 3.0 mg L^{-1}, at a rate of 0.92 mg L^{-1} day^{-1}. The slope of the breakthrough curve at this point was representative of very little Cr^{VI} reduction within the MFC.

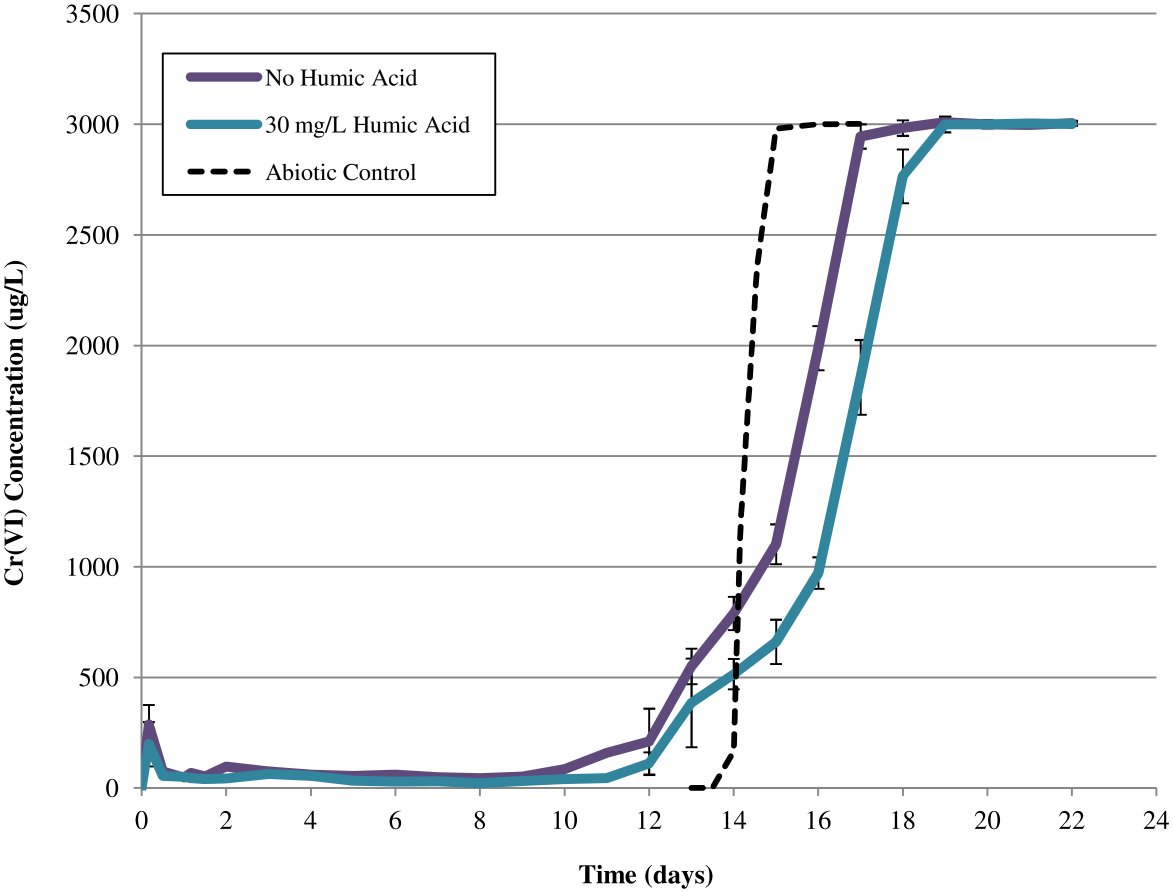

Figure 5.18 Cr^{VI} **concentrations within the MFC cathode with a continuous feed of 12 mL hr^{-1} of a 3.0 mg L^{-1} Cr^{VI} solution.**

A parallel experiment containing humic acid in the influent Cr^{VI} feed increased the capacity of the MFC to reduce Cr^{VI}, as can be seen by the delay in the breakthrough curve. The breakthrough curve trend was very similar to the system without humic acid, however between days 10 and 15 some differences were observed. MFC effluent concentrations did not begin to increase until day 11, one day later than the system without humic acid. From day 12 to day 16 the slope of the breakthrough curve was 0.22 mg L^{-1} day^{-1}, indicating a slower breakthrough relative to the system void of humic acid. After this point, the breakthrough curve followed trends nearly identical to the system without humic acid. Humic acid in this system extended the time to reach complete breakthrough of Cr^{VI} by nearly 2 days. These results corroborate evidence that humic acid aids in the reduction of Cr^{VI} by mediating electron transfer from the bacteria to Cr^{VI} resulting in its ultimate reduction to Cr^{III} species.

Over the duration of this experiment, the MFC system without humic acid was capable of reducing a total 8.6 mg of Cr^{VI} before any breakthrough was observed. The system with humic acid reduced a total of 9.5 mg of Cr^{VI} before breakthrough occurred.

5.5 Conclusions

This research highlighted the benefits of using a bioremediation approach for treating heavy metals in groundwater in the presence of natural organic matter. Humic acid was used a proxy for natural organic matter and was shown to enhance the capability of *Shewanella oneidensis* MR-1 to reduce Cr^{VI}, and to produce more power from a microbial fuel cell. Humic acid serves many functions within the integrated electrokinetic and MFC systems evaluated. Complexation of humic acids with soluble Cr^{III} species reduced the bioavailability of Cr^{III} and thereby reduced the toxic effects of soluble Cr^{III} species on the *Shewanella oneidensis* MR-1 population. This resulted in faster reduction of Cr^{VI}, and was observed in the Cr^{VI} reduction rate studies, the MFC batch studies, and the extended continuous flow study.

This study illustrated many important points regarding the feasibility of an integrated MFC-EK system for a chromium-contaminated groundwater. A primary advantage of the integrated system was mitigation of pH gradients in the electrokinetic cell. This maintained a steady-state current on the order of 8 mA for the duration of the experiment, and enhances Cr^{VI} transport to the electrokinetic anode reservoir. Another advantage of the integrated system was from the benefits of transport and pre-concentration of the contaminants before the treatment within the MFC. This dramatically reduced the overall volume of pore fluid that required treatment, and therefore reduced the amount of treatment time by nearly 40%. The pre-concentration also resulted in more power production, as the MFC cathode was flooded with a higher concentration of terminal electron acceptors. Cathode limitation is the primary factor limiting the power production from the MFC so maintaining a higher concentration of Cr^{VI} aids in reducing some of these loses.

Humic acid was shown to benefit the integrated system by increasing the current measured across the electrokinetic cell for a given applied voltage. The larger current produced relative to systems without humic acid led to more effective electrokinetic Cr^{VI} transport. This was seen in the continuous flow EK-MFC system as the system with humic acid was more effective in Cr^{VI} removal, as supported by the data presented in Figure 5.14.

A final benefit observed resulting from the presence of humic acid was more power production. This was experienced in all MFC studies, and supports existing theories that humic acid can shuttle electrons to TEAs. This reduces the need for microbes to produce chemical mediators for the specific purpose of shuttling electrons from the cell surface to TEAs in solution. In the EK-MFC semi-batch studies humic acid also served as the TEA once all available Cr^{VI} had been reduced, as was apparent by the significantly higher voltage reading relative to the system without humic acid.

Integration of electrokinetic and MFC technologies was shown to be feasible and relevant. In contaminated waters containing significant concentrations of humic acid the use of these technologies can be optimized. The pure cultures of *Shewanella oneidensis* MR-1 used as the biocatalysts for Cr^{VI} reduction will reduce a finite quantity of Cr^{VI}, and once they become inactivated the old cultures can easily be replaced with new cultures. Many questions still remain regarding a larger scale EK-MFC integrated system, however this study illustrates the potential for this to be an environmentally conscious and non-invasive groundwater treatment option.

5.6 Chapter 5 References

1. Rai, D., L.E. Eary, and J.M. Zachara, 1989. Environmental Chemistry of Chromium. *The Science of the Total Environment*, 86:15-23.
2. Stepniewska, Z., K. Bucior, and M. De Boodt, 2000. Chromium and its forms in soils in the proximity of the old tannery waste lagoon. *Int. Agrophysics*, 15:121-124.
3. Romanenko, V.I. and V.N. Koren'kov, 1977. A Pure Culture of Bacterial Utilizing Chromates and Bichromates as Hydrogen Acceptors in Growth Under Anaerobic Conditions. *Mikrobiologiya*, 46(3):414-417.
4. Nealson, K., and Scott J., 2006. *The prokaryotes*. Springer Science, New York.
5. Brutinel, E.D., and Jeffrey G.A., 2012. *Appl Microbiol Biotechnol,* 93:41-48.
6. Malvankar, N. S. *et al*. Tunable metallic-like conductivity in microbial nanowire networks. *Nature Nanotech.* 7 Aug 2011.
7. Gorby, Y. A., Yanina, S., McLean, J. S., Rosso, K. M., Moyles, D., Dohnalkova, A., Beveridge, T. J., Chang, I. S., Kim, B. H. & other authors (2006). Electrically conductive bacterial nanowires produced by Shewanella oneidensis strain MR-1 and other microorganisms. *Proc Natl Acad Sci U S A* 103, 11358–11363.
8. Straub, K.L., Schnik, B. (2004) Ferrihydrite-dependent growth of *Sulfurospirillum deleyianum* through electron transfer via sulfur cycling. Appl Environ Microbiol. 70:5744-5749.
9. Lovely, D.R., D.E. Holmes, K.P. Nevin (2004) Dissimilatory Fe(II) and Mn(IV) reduction. *Adv. Microb Physiol.* 49:219-286.
10. Stams, A.J., F.A. de Bok, C.M. Plugge, M.H. van Eekert, J. Dolfing, G. Schraa (2006) Exocellular electron transfer in anaerobic microbial communities. *Envrion Microbiol.* 8:371-382.
11. von Canstein, H., J. Ogawa, S. Shimizu, J.R. Lloyd (2008) Secretion of flavins by *Shewanella* species and their role in extracellular electron transfer. *Appl Environ Microbiol.* 74:615-623.
12. Marsili, E., D.B. Baron, I.D. Shikhare, D. Coursolle, J.A. Gralnick, D.R. Bond (2008) *Shewanella* secretes flavins that mediate extracellular electron transfer. *Proc Natl Adac Sci* USA, 105,3968-3973.
13. Lovely, D., J. Coates, E. Blunt-Harris, E. Phillips, J. Woodward (1996) Humic substances as electron acceptors for microbial respiration. *Nature* 382:445-448.
14. Leita, L., A. Margon, A. Pastrello, I. Arcon, M. Contin, D. Mosetti (2009) Soil humic acids may favor the persistence of hexavalent chromium in soil. *Environmental Pollution* 157,1862-1866.
15. Reddy, K.R., and Cameselle, C., Electrochemical Remediation Technologies for Polluted Soils, Sediments and Groundwater, John Wiley & Sons, Inc., Hoboken, New Jersey, 2009
16. Hsu, L., S. Masuda, K. Nealson, and M. Pirbazari (2012) Evaluation of microbial fuel cell *Shewanella* biocathodes for treatment of chromate contamination. *RSC Advances,* 2:5844-5855.
17. G.C. Gil, I.S. Chang, B.H. Kim, M. Kim, J.K. Jang, H.S. Park, H.J. Kim, Operational parameters affecting the performance of a mediator-less microbial fuel cell. *Biosens. Bioelectron*. 18 (2003) 327–334.

18. Hamid, R.Y., S.M. Carver, A.D. Christy, O.H. Tuovinen (2008) Cathodic limitations in microbial fuel cells: An overview. *Journal of Power Sources* 180:683-694.

19. Sengall, B.A., CE O'Bannon, JA Matthias (1980) Electro-osmosis chemistry and water quality. *Journal of Geotechnical Engineering Division* 106:1148-1152.

20. Pamukcu, S., A. Weeks, J.K. Whittle (2004). Enhanced Reduction of Cr(VI) by Direct Electric Current in a Contaminated Clay. *Environ. Sci. Technol.* 38:1236-1241.

21. D.L. Nealson and M.M. Cox, *Lehninger Principles of Biochemistry*, Worth Publishers, New York, NY, 2000.

22. Powers, S.E., L. Abriola, W.J. Weber Jr. (1994). An experimental investigation of non-aqueous phase dissolution in saturated subsurface systems: Transient mass transfer rates. *Water Resources Research*. 30(**2**):321-332.

23. Guha, H., K. Jayachandran, F. Maurrasse (2001) Kinetics of chromium (VI) reduction by a type strain *Shewanella alga* under different growth conditions, *Environmental Pollution*, 115:209-218.

24. Bencheikh-Latmani, R., A. Obraztsova, M. Mackey, M. Ellison, and B.M. Tebo (2007): Toxicity of Cr(III) to *Shewanella* sp. Strain MR-4 during Cr(VI) Reduction, *Environ. Sci. Technol.*, 41:214-220.

25. Comber, S., M. Gardner (2003), Chromium redox speciation in natural waters, *Journal of Environmental Monitoring*, 5(3):410-413.

26. Rismani-Yazdi, H., S.M. Carver, A.D. Christy, and O.H. Tuovinen (2008) Cathodic limitations in microbial fuel cells: An overview, *Journal of Power Sciences*, 180:683-694.

27. Sachs, S., G. Bernhard (2011) Humic acid model substances with pronounced redox functionality for the study of environmentally relevant interaction processes of metal ions in the presence of humic acid, *Geoderma,* 162(1-2):132-140.

28. M.Y. El-Naggar, Y.A. Gorby, W. Xia, and K.H. Nealson. The molecular density of states in bacterial nanowires, *Biophysical Journal*, 95 (1), L10-L12, 2008.

29. Hsu, L. (2011), Evaluation of Chromium Remediation in Groundwater: Investigations Using Microbial Fuel Cells and Electrokinetic Systems, *Dissertation Document*, Chapter 3, pp. 48-50.

30. Kotaś, J., & Stasicka, Z. (2000). Chromium occurrence in the environment and methods of its speciation. *Environmental pollution (Barking, Essex□: 1987)*, *107*(3), 263–83.

31. US EPA, *Cost Analysis for Selected Groundwater Cleanup Projects: Pump and Treat Systems and Permeable Reactive Barriers,* Solid Waste and Emergency Response, EPA 542-R-00-013.

32. World Health Organization, *Guidelines for drinking-water quality, 3rd edition incorporating 1st and 2nd addenda,* 2006.

Chapter 6 : Performance Predictive Modeling of Chromate in Soil Columns in the Presence and Absence of Humic Acid Using: I) Biofilm Coated Sand, and II) Iron Oxide Coated Sand

6.1 Introduction

The removal of toxic metals such as Cr^{VI} from potential drinking water sources is a concern of many public and private institutions alike, as water supplies become increasingly scarce. Biological Cr^{VI} removal through its reduction to sparingly soluble Cr^{III} species *in situ* can be an economic and non-invasive method of treatment. Several investigations have been reported on the aerobic and anaerobic biotransformation of Cr^{VI} to Cr^{III} under different environmental conditions. The aerobic activity associated with Cr^{VI} reduction is generally associated with a soluble protein fraction utilizing NADH as electron donor either by necessity or for maximizing the microbial activity. Several researchers have also investigated the effects of the following aspects on the Cr^{VI} transformation: biomass density, chromium (Cr^{VI}) concentration, carbon source (electron donors), pH, temperature, dissolved oxygen, oxidation-reduction potential (ORP), and presence of other oxyanions as well as other metal ions.[1-6]

The reduction of Cr^{VI} to Cr^{III} by microorganisms including metal reducing bacteria (MRB) such as iron-reducing bacteria, and sulfate reducing bacteria (SRB), in the presence of different electron donors has been well established in literature. Aerobic as well as facultative anaerobic bacteria are capable of reducing Cr^{VI} to the Cr^{III} oxidation state through Cr^{VI} reductase activity. These microorganisms include *Escherichia coli, Pseudomonas putida, Paracocus denitrificans, Bacillus subtilis* and several strains of SRB. Bioreduction of chromium by iron-reducing bacteria can also occur in both aerobic and anaerobic environments. Various microorganisms can reduce iron by coupling its reduction to the oxidation of hydrogen or organic carbon. The reduction of Fe^{III} to Fe^{II} can be accomplished by stimulation of indigenous dissimilatory metal-reducing bacterial strains. Microbially produced Fe^{II} can chemically react with Cr^{VI} to form insoluble Cr^{III}. In one study, the *Shewanella alga* strain *BrY* was found effective in transforming Cr^{VI} to

Cr^{III} through the microbial reduction of Fe^{III} to Fe^{II}.[5] It is also well documented that sulfide produced by SRB during anaerobic processes can easily combine with heavy metals to form insoluble metal sulfides. A study by Tebo and Obrastzova (7) reported that SRB may also directly reduce Cr^{VI} to Cr^{III}.

Biochemical studies of enzymatic Cr^{VI} reduction reveal that Cr^{VI}-reducing mechanisms are likely associated with bacterial electron transport systems and, as such, are not identical across the spectrum of Cr^{VI} reducing bacterial genera.[8] Consequently, several researchers have proposed that Cr^{VI} reduction is mediated by enzymes that are not substrate-specific for Cr^{VI} and that "chromate reductases" may be serendipitous contributors to Cr^{VI} reduction while engaged in other primary physiological functions.

Myers et al. (8) studied the biochemistry of Cr^{VI} reduction in MR-1 and showed that Cr^{VI} reduction activity is associated, at least in part, with the cytoplasmic membrane. They hypothesized that the reduction process is mediated by a multicomponent electron transport mechanism that could possibly include cytochromes, quinones, flavoproteins, and other proteins with iron-sulfur centers. In previous studies, it was shown that Cr^{VI} reduction by MR-1 is accomplished by more than one Cr^{VI} -reducing mechanism and that processes involved in Cr^{VI} reduction are inducible during anaerobic respiration.[1,4,5,9]

Different models have been proposed of how the terminal metallic electron acceptor is finally reduced. MtrC and OmcA have been shown to directly reduce iron minerals in vitro.[1] The transferrates to ferric iron are rather low and cannot explain entirely the fast rates of iron reduction by whole cells. It has therefore been proposed that endogenous flavin redox shuttles are involved in this electron transfer process. However, reduction of the flavin shuttle molecules depends on the whole electron transfer chain, since they apparently cannot pass the outer membrane and therefore also have to be reduced by outer-membrane cytochromes.[3]

In the aquatic sediments from which *Shewanella oneidensis* MR-1 was originally isolated, humic acids are frequently present, and they represent exogenous electron shuttles. Consequently, it was shown by some researchers that Fe^{III} reduction by the microbial strain was stimulated by humic substances at concentrations as low as 5–10 mg carbon per liter. Humic substances can occur in dissolved or solid-phase form, and both have been studied extensively with respect to their effect on microbial Fe^{III} reduction due to electron shuttling. Under the circumstances, humic substances may also increase the reduction of Cr^{VI} to Cr^{III} by serving as electron shuttles. This may not be observed in the case of complex formations of Cr^{VI} with complexing agents such as EDTA.

The first part of this study investigated the use of *Shewanella* bacteria for the reduction of Cr^{VI}. Furthermore, the effects of humic acid on Cr^{VI} reduction are evaluated. Reduction rate studies of Cr^{VI} by seven different strains of *Shewanella* were used to determine biokinetic parameters derived from the Monod model. Additionally, the dual-enzyme model as proposed by Viamajala et al. (10) is tested to investigate its reliability in describing the reduction rate data.

Following the rate studies, *Shewanella oneidensis* MR-1 were grown in a silica-sand media loaded into a column to simulate an aquifer environment. A simulated groundwater solution containing lactate as an electron source and Cr^{VI} as an electron acceptor was pumped through the column and samples from the effluent were taken to develop an experimental Cr^{VI} breakthrough curve. Identical experiments were run containing humic acid to determine its effects on the system. A predictive model previously developed by the Pirbazari group at University of Southern California was modified and tested to describe the experimental data.[11-15]

Further, a potential method for Cr^{VI} removal by iron oxide coated sand (IOCS) as a permeable reactive barrier (PRB) was tested. IOCS has been applied for treatment of heavy metals in water treatment applications.[16] Ferrihydrite is most commonly used in heavy metal treatment processes, because it promotes the coagulation of precipitated metal oxides or hydroxides. However an often-overlooked benefit of the precipitation-coagulation practice is the adsorption of the target metals onto ferrihydrite. Adsorption processes are typically made more effective by increasing the concentration of the adsorbent, however in the case of ferrihydrite this also means a corresponding increase in sludge production. Optimization of the use of ferrihydrites involves minimizing their use as opposed to increasing dosages. This can be done through coating sand with iron oxide, and creating a more versatile adsorbent.

For a well-designed system, adsorption-based processes can remove metals to lower levels and over a wider pH range as opposed to precipitation.[17] Also, metal-bound organic or inorganic complexes that are typically not removed in traditional treatment processes can be removed by adsorption.[18] In the second part of this study, the capability of adsorption processes to remove oxyanionic metals such as chromate ($HCrO_4^-$) was of particular interest. An abiotic treatment process using iron oxide coated sand was employed to reduce Cr^{VI} in small-scale experiments to simulate the use of IOCS as a PRB. A predictive mathematical model was used to describe Cr^{VI} breakthrough profiles in the IOCS column, and verified to be accurate. The IOCS column was operated at flow rates significantly greater than those observed for groundwater for the sake of model verification, then used to simulate of Cr^{VI} breakthrough curves for flow rates equivalent to those used in the bioactive column studies. The results reflect the effectiveness of IOCS for Cr^{VI} adsorption and as an *in situ* remediation option.

6.2 Background

Shewanella strains

The genus *Shewanella* consists of gram-negative proteo-bacteria typically rod-shaped, 2-3 µm in length and 0.4-0.7 µm diameter, that are facultative anaerobes found in marine environments.[19] Modern characterization techniques have been employed since 1988 exemplified by DNA-DNA hybridization and 16S rRNA sequencing, and more than 40 distinct species of *Shewanella* have been identified. The significant features that characterize the genus include good psychro-tolerance, mild halophilicity, and more importantly, an excellent capacity for reduction of an unparalleled array of inorganic and organic compounds for respiration.[20] The ability of Shewanella to respire on various metals and to produce endogenous hydrocarbons has created scientific and technological interest in the extensive characterization and potential application of these microorganisms. *Shewanella* was originally identified as one of the multiple species of bacteria growing in putrid butter.[20] It was at first classified as a genus of *Achromobacter*, but was subsequently reclassified several times based on the following factors emerging from research activities: its polar flagella for locomotion and attachment, its non-fermentative characteristic as a marine bacteria, and its guanine-cysteine protein fraction of DNA.[20] However, after the advent of 5S rRNA sequencing techniques, the new name “Shewanella” was used for the genus as a tribute to the contributions of the microbiologist James M. Shewan.[21]

The utility of *Shewanella* in microbial processes can be attributed to their ability to respire on insoluble substances, form stable or robust biofilms on smooth solid surfaces such as glass, and to biosynthesize pilus effective for biofilm adhesion and surface coverage. These unique characteristics enable *Shewanella* to maintain good surface interactions even at low nutrient levels. A specific highlight is the ability of the *Shewanella* strains to utilize nutrients at high levels by aerobic catabolism in the presence of oxygen rather than investing energy for biofilm formation without energy conservation. In anaerobic environments, they are capable of forming biofilms and subsisting on types and concentrations of nutrients that other microbial species cannot utilize.

Several studies have indicated that *Shewanella* have developed three known ways for transferring electrons to insoluble species. The first involves cytochromes and associated proteins on the outer membrane that directly contact the exterior of metals for electron transfer. The second involves soluble riboflavin to facilitate electron transport to cellular acceptors, serving virtually as an electron shuttle. Lastly, the *Shewanella* strains such as *oneidensis* MR-1 have been shown to transport electrons across distances of over 50 μm using conductive nanowires developed around the microorganism even under electron-acceptor limiting conditions.

Metal Reduction

Microbial metal reduction is a commonly part of the respiratory process in anaerobic environments, and a large number of bacterial species have been identified with this capability. These species include strict anaerobes such as *Geobacter sulfurreducens*, and facultative anaerobes such as *Shewanella putrefaciens*, *Aeromaonas hydrophilia*, and *Pantooea agglomerans*.[22] *Shewanella putrefaciens* belongs to the gamma-group of the Proteobacteria and has been isolated from a number of freshwater and marine environments, oil fields, spoilt fish and other sources.[23] The species is capable of using a large number of terminal electron acceptors including oxygen, nitrate, nitrite and fumarate, besides insoluble metal oxides such as those of Mn^{IV} and Fe^{III}. When grown anaerobically in the presence of these metal oxides, *Shewanella putrefaciens* cells are exclusively found on the surface of the metal oxide particles. Bacterial contact is essential for metal reduction to occur, and this contact is mediated by proteins on the outer surface of the cells.[2] An investigation by Beliaev and Saffarini[22] designated and described an outer cell membrane protein, MtrB, containing a putative metal-binding site (CXXC) required for Fe^{III} and Mn^{IV} reduction. These researchers thought that the MtrB protein played a major role in metal binding during the reduction. Cell fractionation studies by Myers and Myers[24] had suggested the majority of the terminal Fe^{III} reductase activity of the *Shewanella putrefaciens* MR-1 was located on the outer cell membranes. A later investigation showed that the Fe^{III} reductase activity of the strict anaerobic species *Geobacter sulfureducens* was associated with the outer cell membrane.[25] At the time, these results were surprising because terminal reductases of Gram-negative bacteria were generally believed to be located in the cytoplasmic membrane (inner membrane). The o-type cytochromes, usually found in the cell membrane or in the periplasmic space of Gram-negative bacteria had also localized to the outer membrane of *Shewanella putrefaciens* MR-1.[26-27] The location of reductases on the outer membrane is believed or predicted to be an innate and inherent advantage enjoyed by metal-binding bacteria, and may therefore constitute a major mechanism of dealing with insoluble electron acceptors.

The mechanism of electron transfer leading to metal reduction is important and requires a detailed understanding. A cytochrome C3 designated as Cct that was isolated from *Shewanella frigid marina* was identified by Gordon et al. to be significantly involved in metal reduction.[28] Subsequently, Beliaev et al. described two types of c-type cytochromes, namely MtrA and MtrC, and stated that they were involved in the reduction of Fe^{III} and Mn^{IV}.[2] Additionally, these researchers noted through Western blot analysis and cell fraction studies that MtrC was located on the outer membrane of *Shewanella putrefaciens* MR-1, wherein MrtA appeared only in the periplasm. They further observed that the loss of MtrC led to decreased activity levels of Fe^{III} reductase in vitro, suggesting that the cytochrome would be required for terminal Fe^{III} reductase activity, or might be one of the essential components of the enzyme itself. They also presented a model for describing Fe^{III} reductase activity by *Shewanella putrefaciens* MR-1.

The *Shewanella putrefaciens* MR-1 species, later renamed *Shewanella oneidensis* MR-1, are the most commonly used species in metal reduction studies. As a result, a plethora of information is available regarding genome, their capacity to reduce many toxic metals, and most importantly the mechanisms involved in the complex electron transport chain required to reduce extracellular electron acceptors.

Iron oxide Coated Sand for Cr^{VI} Reduction

The removal of chromate with IOCS has been proven to be an effective technique with rapid reaction kinetics. Bailey, Bennett, and Benjamin of the University of Washington have researched two different types of iron for coating silica sand: ferric nitrate and ferric chloride. Ferric chloride was found to be a slightly better adsorbent than ferric nitrate, and ferric chloride exhibited effectiveness over a much longer time frame. The ferric chloride IOCS treated 235 bed volumes of a simulated wastewater solution containing 20 mg L^{-1} Cr^{VI} at 50% breakthrough, and the ferric nitrite IOCS treated 185 bed volumes at 50% breakthrough.[29]

Much of the focus for heavy metal treatment in potable water sources has shifted recently to zero-valent iron (ZVI), and nanoscale zero-valent iron (nZVI) due to its high intrinsic reactivity and benefits from its size. Zero-valent iron can treat Cr^{VI} through a reduction reaction where Cr^{VI} oxidizes the ZVI or nZVI surface, resulting in mixed Cr^{III}-Fe^{III} (oxy)hydroxide solids.[30] A more detailed description of ZVI and nZVI can be found in Chapter 4.

Zero-valent iron has been successful on the bench-scale, however full scale demonstrations are limited due to the difficulties of maintaining iron in the zero-valent state. Any exposure to oxygen results in rapid oxidation, and an immediate loss of the advantages offered from the zero-valent state. The primary application of ZVI and nZVI alike is to environmental remediation, either in the form of a permeable reactive barrier (ZVI) or through injection directly to a contaminated area (nZVI).[31,32] Alternatively, the use of IOCS has been proposed for use in water treatment systems, either integrated into a water treatment plant, or for use in personal filtration systems in developing countries.[33] While treatment by nZVI, ZVI, or IOCS may sound similar the removal mechanisms are much different. For example, arsenic is removed through forming inner sphere complexes with IOCS.[34] Arsenic is typically found in the anionic form of arsenite ($H_2AsO_3^-$) and arsenate ($H_2AsO_4^-$, $HAsO_4^{2-}$) in the natural environment, and many attempts to removal these toxic compounds from water have been successful with IOCS.[35,36]

The mechanisms of Cr(VI) removal are believed to be similar to those of arsenite and arsenate. IOCS have been reported to have a point of zero charge in the pH range of 7.0 – 8.6, indicating the IOCS surface will carry a neutral to net positive charge in the pH range of natural waters.[34,37] The negatively charged chromate ion will have an electrostatic attraction to the IOCS surface, promoting rapid adsorption. Figure 6.1 illustrates the three primary steps involved in the adsorption process. The first step occurs at the IOCS surface, and chromate adsorbs through surface complexation with hydroxyl sites governed by the following reaction:[38]

$$SOH + H^+ + CrO_4^{2-} \Leftrightarrow SOH_2^+ - CrO_4^{2-} \qquad (1)$$

Once bound at the IOCS surface, the second mechanism involves chromate undergoing reactions with ferrous iron to form Cr^{III} species according to:

$$HCrO_4^-{}_{(aq)} + 3Fe^{2+}{}_{(s)} + 7H^+{}_{(aq)} \rightarrow 3Fe^{3+}{}_{(aq)} + Cr^{3+}{}_{(aq)} + 4H_2O_{(l)} \qquad (2)$$

Following this reaction, the coprecipitation of Cr^{III} species and Fe^{III} species can occur, the third mechanism in the adsorption process, which can be written as:[39]

$$(1-x)Fe^{3+} + (x)Cr^{3+} + 2H_2O \rightarrow Fe_{(1-x)}Cr_xOOH_{(s)} + 3H^+ \qquad (3)$$

The final product of this series of reactions is a $Fe_{(1-x)}Cr_xOOH$ solid on the surface of the IOCS. Reported work has substantiated this by determining no soluble Cr^{III} species exist in the equilibrium solution after interaction with IOCS. Further, regeneration processes have recovered greater than 90% of adsorbed chromium.[29]

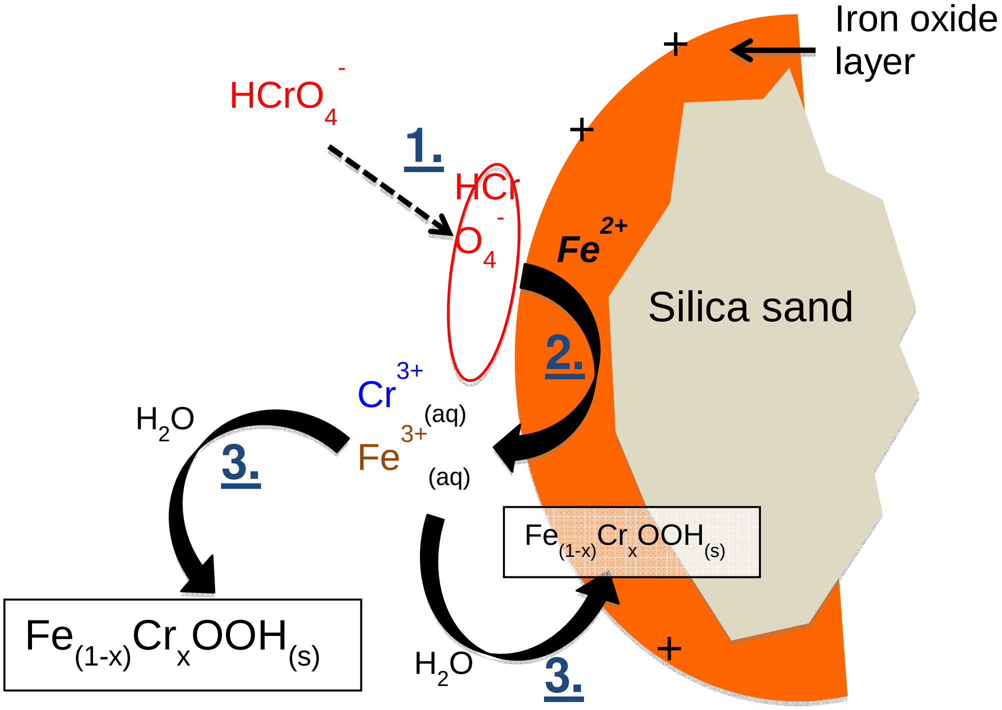

Figure 6.1 **Schematic of the adsorption-reduction mechanism occurring in the reduction of Cr^{VI} by IOCS. The process results in Cr^{III}-Fe^{III} (oxy)hydroxide precipitates on the IOCS surface or free in solution.**

Biokinetic Models for Metal Reduction

Several models are currently available that can describe batch biochemical reactions and biomass growth due to single or multiple substrates. In these models the microbial growth and substrate depletion can be described as follows:

$$\frac{dX}{dt} = \mu X \qquad (1) \qquad\qquad \frac{dS_i}{dt} = \frac{\mu_i X}{Y} \qquad (2)$$

The above relations are generally valid when maintenance requirements are negligible, a typical assumption for rapidly growing microbial cells whose metabolism is associated with growth. The specific growth rate for a substrate "i" can be described by any of the biochemical kinetic models. The simplest model is the Monod Model based on Michaelis-Menten or Briggs-Haldane type of biochemical kinetics as shown in Eq. 3.

$$\mu_{\mathrm{i}} = \frac{\mu_{\mathrm{max,i}} \mathrm{S_i}}{\mathrm{K_{S,i}} + \mathrm{S_i}} \tag{3}$$

Single substrate biokinetic experiments may be performed and the data used to estimate the parameters μ_{max} and K_S for the substrates. The estimation process employs a fit of the Monod model to the experimental data represented in terms of the specific growth rate as a function of substrate concentration.

Owing to the toxic nature of chromium, substrate inhibition model might appear more suitable than the pure Monod model, and can be written as follows:

$$dS = \frac{\mu_{\mathrm{max,i}} \mathrm{S_i}}{\mathrm{K_{S,i}} + \mathrm{S_i} + \mathrm{S_i^2}/\mathrm{K_I}} \tag{4}$$

The term K_I refers to the inhibition coefficient in this model, and therefore, the three kinetic parameters μ_{max}, K_S, and K_I must be estimated from the experimental data pertaining to the variation of specific growth rate as a function of substrate concentration. These kinetic parameters determined from single component biochemical processes can be retained and employed in specific growth and rate models where more than one growth-limiting substrate is encountered. However, it must be realized that the degree of complexity is increased in modeling multiple-substrate biochemical reactions due to various substrate interactions. In analogy to enzyme kinetics, different models can be employed to describe biochemical kinetics relevant to specific growth rates and substrate disappearance. The analogy between enzyme and cellular kinetics is possible because the reaction is enzyme catalyzed, so that inhibition of enzyme activity also results in inhibition of microbial activity along the same or similar pattern. If several metal ions are present, there may be competitive interactions so that electron donors or electron acceptors compete for binding sites in order to undergo bacterial metabolization. The competitive substrate inhibition model (Eq. 4) can be rewritten in the following form:

$$\frac{dS}{dt} = \frac{\mu_{max,i} S_i}{K_{s,i}\left[1+\frac{S_i}{K_I}\right]+S_i} \qquad (5)$$

A second type of inhibitive interactions may arise due to non-competitive inhibition wherein a non-reactive complex is formed when both substrates are bound to one enzyme so that the relationship takes the form

$$\mu_i = \frac{\mu_{max,i} S_i}{[K_{S,i} + S_i][S_I / K_{S_I}]} \qquad (6)$$

Uncompetitive inhibition is another interaction that can occur in the case of multiple substrates, when each substrate is expected to bind to one enzyme, and the kinetic relationship can be written as

$$\mu_i = \frac{\mu_{max,i} S_i}{[K_{S,i} + S_i][1 + S_I / K_{S_I}]} \qquad (7)$$

The model that can account for substrate interactions without directly specifying the type of interaction can be described by the relation

$$\mu_i = \frac{\mu_{max,i} S_i}{K_{S,i} + S_i + I_{2i}\, S_I]} \qquad (8)$$

This model is referred to as the summation kinetics with interaction parameters (SKIP) equation, wherein the contribution of each substrate to biomass growth is incorporated as

$$\mu = \mu_1 + \mu_2 + \ldots + \mu_i + \ldots + \mu_n = \frac{\mu_{max,1} S_1}{K_{S,1} + S_1} +. \frac{\mu_{max,2} S2}{K_{S,2} + S_2} + \ldots + \frac{\mu_{max,i}\, S_i}{K_{S,i} + S_i} + \ldots + \frac{\mu_{max,n} S_n}{K_{S,n} + S_n} \qquad (9)$$

The summation kinetics model is applicable to situations wherein there are no substrate interactions and simple Monod kinetics is considered. The limitation of the model is that it does not take into consideration the biomass concentration capable of metabolizing or transforming each particular substrate, when it is incorporated into the basic equations presented above (Eqs. 1 and 2). However, summation kinetic equations have been used to describe biomass growth for pure microbial strains degrading or transforming mixtures of substrates, wherein the fraction of the pure culture transforming each substrate is not considered. The measured biomass concentration is multiplied by each term accounting for the biomass growth due to one substrate in the kinetic equation; and this implies that the entire biomass population will metabolize or transform each substrate. Littlejohns and Daugulis used the summation kinetics approach to predict the growth of a bacterial consortium with minimal knowledge of its composition.[40]

In essence, the purpose of the above models is to provide the most accurate fit of the experimental data for a certain pair of substrates, affording due considerations to substrate interactions as well as to determination of the nature of such interactions. Once the nature of the interactions is determined, a specific growth rate equation can be determined for mixed substrates with more than two components, taking into account the interactions of each compound present. An example of the SKIP model for four interacting components can be written as follows:[40]

$$\mu_i = \frac{\mu_{max,i} S_i}{K_{S,i} + S_i + I_{2i}\, S_2 + I_{3i}\, S_3 + I_{4i}\, S_4} \tag{10}$$

Models considering interactions between more than two substrates can be employed in summation kinetics format for describing biomass growth. In the case of co-metabolization, the specific growth rate due to metabolization of a component is assumed zero as the substrate is not metabolized for energy purposes. Nonetheless, a relationship is required to describe the change in concentration of a co-metabolized species. The change in the concentration of a non-growth substrate during the co-metabolization process can be represented by the following relationship:[41]

$$\frac{dS_N}{dt} = -\left[T_G^C\left(\frac{dS_N}{dt}\right)\left(\frac{1}{X}\right)\right]\left[\frac{S_N}{K_{S,N}+S_N}\right]X \quad (11)$$

Dual Substrate Model

Previously, with other microorganisms, kinetic models for Cr^{VI} reduction have been developed using a Michaelis-Menten approach based on the assumption of a single Cr^{VI}-reducing enzyme. However, Viamajala and coworkers suggested that since Cr^{VI} reduction in MR-1 did not appear to be the function of a single enzyme, such kinetic models should not be used.[10] These investigations take into account the existence of multiple Cr^{VI} reduction mechanisms in MR-1, they developed and tested a dual-enzyme kinetic model to describe Cr^{VI} reduction in stationary phase MR-1 cultures. In the study described herein, the kinetic parameters of Cr^{VI} reduction by MR-1 are compared to those reported in literature for other microorganisms.

Based on the fundamental hypothesis that Cr^{VI} reduction in *Shewanella oneidensis* MR-1 is mediated by more than one enzyme, a dual-enzyme kinetic model to describe Cr^{VI} reduction by stationary-phase cultures of MR-1 was developed and tested.[10] They observed that their results indicated the presence of a rapid enzymatic mechanism that is deactivated during Cr^{VI} reduction, and a slower enzymatic mechanism that remains active during Cr^{VI} reduction. They further stated that the rapid Cr^{VI} reduction mechanism might be different for nitrate- and fumarate-grown MR-1 cultures.

The parallel reactions leading to chromium reduction (Cr^{VI} reduction) can be written as follows:

$$Cr^{VI} + E_d \rightarrow E_d^* + Cr^{III*} \quad (1)$$

$$Cr^{VI} + E_s \rightarrow E_s + Cr^{III*} \quad (2)$$

In the above reactions, E_d represents the deactivating enzyme that reacts rapidly with the substrate (hexavalent chromium), but is converted to an activated form E_d^* during the reaction; E_s represents the stable enzyme that is not deactivated by the Cr^{VI} reduction; and $Cr^{III}*$ is the reduced chromium species (Cr^{III}) produced during the enzymatic reactions.

The overall reduction rate of Cr^{VI} is effectively the sum of the reaction rates denoted by reactions (1) and (2). Hence the net reaction rate can be written as follows:

$$-r_S = \frac{dS}{dt} = \left[\frac{dS}{dt}\right]_d + \left[\frac{dS}{dt}\right]_s \tag{3}$$

Each of the two reactions denoted by (1) and (2) can be formulated in terms of Michaelis-Menten kinetics as follows:

$$r_S = -\frac{dS}{dt} = \frac{\mu_{max} S}{K_S + S} E^* \tag{4}$$

In the aforementioned relationships, r_S is the rate of Cr^{VI} reduction (mM h^{-1}), S is the concentration of Cr^{VI} at any time t, μ_{max} is the maximum specific reduction rate, K_S is the Michaelis or Monod coefficient (mM) and E* is the enzyme concentration (mg-enzyme L^{-1}).

One of the principal assumptions of the dual substrate model is that the enzymes responsible for metal reduction (chromium reduction) are saturated so that $K_S << S$ and that the overall reaction can be written as follows:

$$r_S = -\frac{dS}{dt} = k_1 E_d X + k_2 E_s X \tag{5}$$

In the above equations, the relevant terms are defined as follows:

k_1, k_2 = rate coefficients for reactions (1) and (2), respectively, both zero order, mM h^{-1},
E_d = specific deactivating enzyme concentration, (mg-enzyme) (mg-cell protein) $^{-1}$,
E_s= specific stable enzyme concentration, (mg-enzyme) (mg-cell protein) $^{-1}$,
X = total cell protein concentration, (mg-cell protein). L^{-1}.

The total enzyme concentrations during the reactions for the deactivating and stable enzymes shall be denoted by E_d X and E_s X, respectively. According to the dual-enzyme model, the amount of enzyme deactivated is stoichiometrically proportional to the Cr^{VI} concentration, and so

$$-\mathrm{d}[\mathrm{E_d\ X}] = -\mathrm{k_d}\ S_\mathrm{d} \qquad (6)$$

In the above relation, k_d is analogous to a stoichiometric coefficient for Eq. 1 expressed as (mg-enzyme/L)/(mM-S). Under stationary phase operation of the reactor system (operated as a batch reactor), there is no biomass growth and X is assumed constant. Hence the above differential equation (6) can be written as

$$\mathrm{E_{d0}\,X - E_d\,X = k_d\,[S_0 - S_d]} \qquad (7)$$

where E_{d0} and S_0 are the respective initial concentrations at $t = 0$. The rate of chromium reduction due to the deactivating enzyme is therefore

$$-\frac{\mathrm{dS_d}}{\mathrm{dt}} = \mathrm{k_1\ E_d\,X} \qquad (8)$$

Combining the results of equations (7) and (8), we can write the chromium reduction relationship due to the deactivating enzyme as

$$-\frac{\mathrm{dS_d}}{\mathrm{dt}} = \mathrm{k_1\ E_{d0}\,X - \ k_1 k_d\,[S_0 - S_d]} \qquad (9)$$

or

$$-\frac{\mathrm{dS_d}}{\mathrm{dt}} = \mathrm{r_{d0}\ - k_d^{'}\,[S_0 - S_d]} \qquad (10)$$

In the above relation, $r_{d0} = k_1$ E_{d0} X, the initial reduction rate due to the deactivating enzyme, and $k_d^{'} = k_1\ k_d$, a lumped kinetic coefficient of first order (h^{-1}).

The solution to the above relationship, assuming an initial condition of $S = S_0$ at $t = 0$, can be written as follows:

$$S_0 - S_d = \frac{r_{d0}}{k_d^{'}}[1 - \exp(-k_d^{'}t)] \qquad (11)$$

The above relation provides the amount of Cr^{VI} transformed to Cr^{III} at any time *t*, attributed to the deactivating enzyme E_d. An analogous relationship can be written for the chromium reduction due to the stable enzyme as shown below:

$$-\frac{dS_s}{dt} = k_2\, E_s\, X \qquad (12)$$

The assumption of the dual-substrate model is that the stable enzyme concentration remains constant and leads to the relation

$$-\frac{dS_s}{dt} = k_2\, E_{s0}\, X = r_{s0} \qquad (13)$$

The following definitions are important with reference to the above relationship: $E_{s0}X$ is the stable enzyme concentration at $t = 0$, and r_{s0} is the initial reaction rate due to the stable enzyme E_s. The solution to equation (13) is

$$S_0 - S_s = r_{s0}\, t \qquad (14)$$

The above equation represents the Cr^{VI} consumption at any time *t* during the reduction reaction attributed to the stable enzyme E_s. The overall mass balance of chromium reduction due to the deactivating enzyme as well as the stable enzyme can be written as

$$\Delta S = \Delta S_d + \Delta S_s \qquad (15)$$

or

$$S_0 - S = (S_0 - S_d) + (S_0 - S_s) \tag{16}$$

Using the results of equations (11) and (14) in equation (16), the overall Cr^{VI} concentration S in the batch reactor can be written as

$$S = S_0 - \left\{ r_{s0}\, t + \frac{r_{d0}}{k_d^{'}}[1 - \exp(-k_d^{'} t)] \right\} \tag{17}$$

In this study, the kinetics of chromium reduction are represented by a three-parameter model with r_{d0}, r_{s0}, and $k_d^{'}$ as the parameters to be estimated. Parameter estimation was carried out using MATLAB (v. R2011b).

6.3 Predictive Modeling for Removal of Cr^{VI} in Soil Columns

In order to assess the risk of groundwater contamination and to predict the success of remediation alternatives in the subsurface environment, it is indeed necessary to accurately model the transport and fate of contaminants in groundwater. During migration through porous media, the composition of groundwaters with reference to contaminants may be altered due to interactions with the various mineral phases present in the naturally heterogeneous solid matrices. It is indeed important to consider the role of subsurface bacteria in degradation, mineralization, and metabolization of organic or inorganic species in solution. Therefore, a contaminant transport model must be able to simulate these important biochemical and physiochemical processes.

Bioremediation processes in porous media are mainly influenced by microbial mediated redox reactions. Microbiologically mediated processes affect the chemical composition of contaminated water. The patterns of changes in water chemistry depend upon the relative abundance of electron donors and electron acceptors. In many cases heterotrophic bacteria metabolism is limited by the availability of electron donors (organic matter). The abundance and availability of organic substrates (electron donors) and inorganic substrates (terminal electron acceptors) are the primary factors influencing the distribution and activity of heterotrophic bacteria populations in the porous media.

Heterotrophic bacteria activity in the porous media is mainly driven by the net decomposition of available organic carbon, which provides the microorganisms with the energy, nutrients, and electrons they need to synthesize biomass and sustain life functions. However, carbon source feeding is required to maintain biological activity within the porous media. Progress in modeling of bioremediation in porous media is essential to improving our understanding of how physical, chemical, and biological processes are coupled in flow and their effect on bioremediation and the reactive transport of contaminants and bacteria. Numerical flow and reactive transport models can be a helpful tool in the designing and monitoring of *in situ* bioremediation measures and in predicting long-term effects of intrinsic bioremediation on contaminants transport. They can also be used for the quantitative interpretation of column studies of solute transport and bioremediation as well as in water treatment applications.

An important component of this work is the application of a mathematical model for performance prediction and forecasting of the bioremediation process and/or the treatment process for the removal of Cr^{VI}, the contaminant of interest. The model presented is tailored for the specific configurations using media such as sand, and iron oxide coated sand (IOCS). The present model employs the important features of previous models that were developed by Pirbazari and coworkers, and takes into consideration various process scenarios specific to certain applications.[11-15]

A modified verison has been developed for the removal of chromium from contaminated waters, wherein the equations and boundary conditions are appropriately tailored to address removals of component(s) by suppressing adsorption effects, or microbial biodegradation effect, as the case may be. In the case of aquifer remediation or engienered treatment systems where relatively non-adsorbing media such as sand surrounded by an active microbial biofilm, the biodegradation and metabolization effects are considered dominant and adsorption effects are suppressed. This will be the first scenario where the chromium species Cr^{VI} is poorly or insignificantly sorbed on sand, but shall undergo microbial reduction to trivalent chromium species. The second scenario will represent the use of a strongly adsorbing medium emloying IOCS, where microbial degradation and/or metabolization are insignficant removal mechansims as compared to sorption mechanisms.

Model I: Biodegradation alone

The general model featuring microbial degradation and adsorption is characterized by a set of several governing phenomena:

1. Advection-dispersion for contaminant transport through the media
2. Microbial degradation and/or metabolization of contaminants(s)
3. Growth and decay of microbial biofilms within the media

Model Assumptions

The assumptions of the model employed in these studies may be briefly summarized as follows:

(i) The sand column is considered as a plug flow reactor with dispersion under unsteady state conditions,

(ii) The media particles are homogenous in size and spherical in shape. The biofilm formed on the media particle, when microbial degradation mechanisms are operative, is assumed homogenous with reference to density, composition, and thickness.

(iii) The microbial degradation and/or metabolization of electron donor (lactate) and electron acceptor (Cr^{VI}) are assumed to occur in the biofilm phase, and the associated biochemical reactions are described by Monod kinetics, so that the carbon source (lactate) not a limiting nutrient.

(iv) The biofilm thickness increases with time, before eventually reaching a maximum level, when shear loss balances the growth rate, and excess biomass is transferred from the media particles to the suspension phase. The biofilm growth represents a "moving boundary" problem from a modeling standpoint.

Model Equations

The material balance on the substrate C, the electron acceptor Cr^{VI} species, along any differential segment of the reactor can be written as shown below:

$$\frac{\partial C(x,t)}{\partial t} = D_x \frac{\partial^2 C(x,t)}{\partial x^2} - v_x \frac{\partial C(x,t)}{\partial x} - \frac{3k_{fc}(r+L_f)^2}{r^3}\frac{(1-\varepsilon)}{\varepsilon}\left[C(x,t) - C_{fs}(x,t)\right] - \frac{\mu_{\max} C(x,t)}{Y_a\left[K_s + C(x,t)\right]} X(x,t) \qquad (1)$$

In the above equation, *C(x,t)* is the contaminant or substrate concentration in the bulk liquid phase as a function of axial position x and time t, C_{fs} is the contaminant concentration at the surface of the medium particle, X is the biomass concentration within the reactor as a function of position and time, D_x is the axial dispersion of the contaminant within the reactor, v_x is the axial velocity of the liquid phase through the reactor, k_{fc} is the reactor column film transfer coefficient of the contaminant through the liquid film surrounding the media particle, r is the radial coordinate on the media particle, r is the radius of the media particle (sand particles), L_f is the varying thickness of the biofilm surrounding the media particles as a function of time, ε is the porosity of the reactor bed. In the above relationship, μ_{max} and K_s represent the Monod maximum substrate utilization rate coefficient and the Monod half saturation coefficient, respectively, while Y_a denotes the Monod microbial yield coefficient (based on biomass production per unit mass of chromium reduced); and all of these parameters are defined with reference to the electron acceptor.

The initial and boundary conditions for equation (1) are stated as follows:

$$\mathrm{C}\,(\mathrm{x}, \mathrm{t} = 0) \;=\; \mathrm{C}_0 \qquad (2)$$

$$\frac{\partial C(x,t)}{\partial x}\Big|_{x=L} = 0 \qquad (3)$$

In the above conditions, C_0 represents the influent contaminant concentration to the reactor, and L represents the effective reactor length. The diffusion and biochemical reaction within the biofilm is described by the following equation:

$$\frac{\partial C_f(x,r,t)}{\partial t} = D_f \frac{\partial^2 C_f(x,r,t)}{\partial r^2} - \frac{\mu_{\max} C_f(x,r,t)}{Y_a\left[K_s + C_f(x,r_f,t)\right]} X \qquad (4)$$

The above relationship assumes that the substrate or contaminant concentration within the biofilm layer changes only in the direction normal to the surface of the biofilm represented by the radial coordinate *r*. Here, C_f represents the liquid phase contaminant concentration in the vicinity of the biofilm, D_f denotes the biofilm diffusion coefficient of the contaminant. The initial and boundary conditions are as follows:

$$C_f(x,r\ ,t=0) = C_{f0} \qquad (5)$$

$$k_{fc}\left[C(x,t) - C_{f0}(x,t)\right] = D_f \left.\frac{\partial C_f(x,r,t)}{\partial r}\right|_{r=L_f} \qquad (6)$$

$$\frac{\partial C_f(x,r=0,t)}{\partial r} = 0 \qquad (7)$$

In these conditions, C_{f0} represents the average initial contaminant concentration in the aqueous phase within the biofilm. Equation 6 represents the flux boundary condition, where the mass transfer of contaminant through the liquid film is balanced by the contaminant diffusion into the biofilm. This situation represents a moving boundary problem, wherein the radial coordinate *r* advances with the growth of the biofilm to a variable thickness L_f. The net growth of biofilm on the media particles can be written as shown below, where the biofilm thickness is described as a function of time on the basis of Monod kinetics:

$$\frac{\partial L_f}{\partial t} = \int_0^{L_f} \left(\frac{\mu_{\max} C_f(x,r,t)}{K_s + C_f(x,r,t)} - k_d \right) dr \qquad (8)$$

In the previous relationship, k_d represents the Monod microbial decay coefficient defined with respect to the electron acceptor. The initial condition for equation (9) shall be

$$L_f(x, t = 0) = L_{f0} \tag{9}$$

where L_{fo} denotes the initial biofilm thickness during the start-up of the reactor. It must be noted that the biomass lost from biofilm due to shear to liquid phase, a portion of which will leave the reactor with the effluent. The biomass lost to the bulk liquid phase due to biofilm shearing is represented by the relation

$$X_l(x, t \geq t_{\max}) = \frac{3(1-\varepsilon)}{\varepsilon} \frac{(L_f(x,t) - L_{f\max})(r + L_{f\max})^2}{r^3} X \tag{10}$$

where

$$L_f(x, t \geq t_{\max}) = L_{f\max} \tag{11}$$

Equations (10) and (11) imply that the biofilm will grow up to a maximum thickness L_{fmax} with time corresponding to a value $t_{\max}$, and any further growth will be gradually transferred to the liquid phase, creating a liquid phase biomass concentration of X_l. Due to the low flowrates employed in this study, it is assumed that biofilm shearing is negligible.

A summary of correlations used for the estimation of model parameters is presented in Table 6.1. These correlations are employed to estimate the free liquid diffusivity and the liquid film mass transfer for Cr^{VI}. The experimental techniques used for the estimation of adsorption equilibrium and rate parameters as well as biokinetic parameters are listed in Table 6.2.

Numerical Techniques

The system of differential equations along with initial and boundary conditions should be non-dimensionalized before being solved numerically. The non-dimentionalization technique by Kim and Pirbazari is discussed herein.[11] A computationally efficient hybrid numerical technique combining finite difference and orthogonal collocation methods was used for solving the model. This hybrid technique method proved successful in solving the model for bioactive fixed-bed and fluidized-bed adsorbers. This technique was found numerically stable, consistent, efficient, and rapidly convergent in comparison to pure finite difference schemes. Pirbazari and coworkers[11,42,43] observed that this technique required less computational time than the pure orthogonal collocation technique for solving problems involving surface diffusion, film transfer, biofilm diffusion, and biofilm degradation of the contaminants. This technique involved the transformation of partial differential equations into ordinary differential equations which could be easily numerically integrated using the GEAR software, the theoretical aspects of which are discussed elsewhere.[55-57] The orthogonal collocation grid points were used for the reactor liquid-phase transport equations. The choice of grid points in the axial and radial directions were based on the roots of shifted asymmetric Legendre polynomials. The theoretical aspects regarding the application of Legendre polynomials as trial functions with orthogonality properties are discussed elsewhere.[11, 44-47] The cylindrical shells in radial direction are denoted by curvilinear and parallel cylindrical planes, while the axial grids are represented by parallel planes, orthogonal to the axial direction. The Crank-Nicholson grid was used for obtaining finite difference approximations to the advection-diffusion equation. The rationale for this hybridization scheme was that surface diffusion or pore diffusion were relatively slow processes as compared to advection and axial dispersion or microbial reactions. Finite difference approximation schemes seemed appropriate, because the concentrations along the reactor were expected to vary sharply, especially in the transition from the saturated zone to the mass-transfer zone where the sorption occurs. This aspect shall play an important role when adsorption mechanisms are operative as in the forthcoming model employed for predicting the performance of reactor using IOCS adsorbent medium. In comparison, the concentration profiles in the media pore volumes and the media surface are comparatively smooth, and could very well be approximated by larger grid intervals using a relatively sparse collocation mesh, lowering the computation time and improving the computational accuracy.

Table 6.1 Correlations employed for parameter estimation.

Correlation	Description of relationship
$D_l = \dfrac{RT}{F^2 Z_1}\left(\dfrac{\nu_1+\nu_2}{\nu_1\nu_2}\right)\left(\dfrac{\lambda_1\lambda_2}{\lambda_1+\lambda_2}\right)$	Wilke-Chang correlation (1968) and also based on Green and Perry (2008) for estimating the free liquid diffusivity D_l of Cr^{VI} in aqueous solution
$Sh = 2 + 0.44Re^{0.63} Sc^{1/3}$ $(12 < Re < 190, 250 < Sc < 2300)$	Sherwood correlation for determining liquid film transfer coefficient k_f using the Reynolds, Schmidt and Sherwood numbers, respectively
$Sh = k_f d_p / D_l$, $Re = \dfrac{\varepsilon^{1/3} d_p^{4/3}}{v}$, and $Sc = \dfrac{v}{D_l}$	Dimensionless numbers for terms used in Sherwood correlation

Table 6.2 Summary of parameter estimation procedures.

Parameter type	Parameter and description	Determination procedure	References
Adsorption equilibrium parameters	K_F: Freundlich capacity constant n: Freundlich intensity constant	Adsorption isotherm studies in completely mixed batch reactors	Pirbazari et al., 1996; Badriyha et al., 2003
Adsorption kinetic parameters	D_s : surface diffusivity k : film transfer coefficient	Adsorption rate studies in completely mixed batch reactors	Badriyha et al., 2003; Tsai et al. 2004
Biokinetic parameters	$\mu_{m,a}$: Monod maximum utilization rate $K_{s,a}$: Monod half-saturation coefficient k_d : endogenous decay coefficient Y_a : microbial yield coefficient	Batch reactor biokinetic studies	Pirbazari et al., 1996.

Model II: Adsorption only

The sorption of metal ions (in this case the Cr^{VI} species in ionic form) on iron oxide coated sand (IOCS) essentially consists of the following steps as shown in the Figure 6.1.

1. transport of metal ions from the bulk solution to the IOCs surface through the liquid film surrounding the particle;
2. diffusion through IOCS pore structure;
3. sorption of metal ions and subsequent reduction with the iron oxide layer immobilized on the sand particle surface.

The first step involves the mass transfer of the metal ions from the bulk fluid to the liquid film surrounding the adsorbent IOCS particle. This phenomenon is dependent on the free liquid diffusivity of the metal ions, and the fluid dynamic regime in the vicinity of the particle. The second step involves the penetration of the metal ions through the iron oxide coating seeking sites for attachment, most likely the functional groups on the iron oxide that can result in the formation of a ligand or complex between the iron oxide entity and the metal ion. Some important interactions might occur including the reduction of the metal ion on the iron oxide surface. The sorption and immobilization of the iron oxide on the sand particle surface may be dependent on the pH and the surface functional groups on the silicate surface that forms the bond with the iron oxide species.

The intraparticle diffusion of the metal ions could be a combination of the pore diffusion and surface diffusion mechanisms as observed by several earlier researchers.[44] It is quite possible that the metal ions diffuse through the pores or diffuse along the surface of the pores of the IOCS particle. In the case of a layer of porous surface such as iron oxide film as compared to adsorbent such as activated carbon, surface diffusion is the most dominant intraparticle transport mechanism. It is hypothesized at this stage that as the free metal ions enter the IOCS pores, they are attracted iron oxide species to form a metallic-complex that causes simultaneous chromium reduction and iron oxidation. This is the third step in the entire process, and the chromium-metal oxide (metal-iron oxide) complex formation and redox reactions are rapid processes. This process will continue until all the sites of the IOCS are exhausted. It must be noted that the second and third steps often occur simultaneously as the chromium species is sorbed and reduced on the

IOCS adsorbent surface. It is important to note that sorption of metal ions on IOCS adsorbent must be regarded merely as the sorption of the charged metal ion on a charged adsorbent surface, but conceptually viewed as the formation of a complex of the metal ions with the functional groups of the iron oxide entities followed by oxidation-reduction reactions. Thus, the movement of metal ions into the adsorbent surface prior to complex formation and redox reactions is essentially a mass-transfer process.

The model formulation is based on the concept that the combination of sorption and reduction process is attributed to the reactions of the metal ions (chromium ions) on IOCS. Therefore, the formation of the metal ion-IOCS sorption is important with regard to the overall uptake of the metal ions and their subsequent reduction. A fundamental assumption is that the metal-IOCS sorption complex is stable enough to achieve the metal reduction and iron oxidation. The metal uptake and reduction involves mass transfer of the metal ions from the liquid phase into the IOCS adsorbent phase through the liquid film surrounding the particle, followed by diffusion of the metal ions through the pore fluid and the IOCS surface, and sorption and redox reactions of the metal ions with the iron oxide entities immobilized on the sand particles, as previously discussed. Thus, it might be stated that in this dual resistance, model pore diffusion and surface diffusion phenomena may generally be operative. Pore diffusion is dominated by the free liquid diffusivity of the species as it occurs due to the movement of the molecules or ions through the pore liquid of the adsorbent. Surface diffusion, on the other hand, is controlled by the availability of surface area within the pores of the adsorbent. It is a general notion that surface diffusion occurs by the hopping of molecules or ionic species, as in this case, between adsorption sites.

In the sorption of metal ions on a surface-modified adsorbent such as IOCS where the sand particle is not highly porous, but exhibit low levels of porosity, it would be appropriate to assume that surface diffusion shall be the main mechanisms due to the charge effects. It is also quite possible that either film diffusion transport or adsorbent particle diffusion transport of the metal ions will be the rate-limiting step, as complex formation and redox reactions between the metal ions and the iron oxide entities of the IOCS adsorbent are expected to generally exhibit relatively fast kinetics.

Model Assumptions

The model for the sorption of metal ions on IOCS is conceptualized based on the following assumptions:

- The IOCS packed-bed reactor is assumed as a plug flow system with axial dispersion.
- The uptake of the metal ions by the IOCS adsorbent is controlled by a two-step mass-transport mechanism: external liquid-film mass transfer from the bulk liquid phase to the adsorbent surface, and intraparticle solid-phase diffusion.
- The intraparticle solid-phase diffusion essentially involves surface diffusion and pore diffusion, although pore diffusion may be neglected in this case.
- The IOCS particles are homogeneous and uniform with respect to shape (spherical), porosity, composition, and density,
- The sorption of metallic ions such as Cr^{VI} on IOCS is irreversible.

Model Equations

The material balance for metal ions in a fixed-bed reactor system is represented by the advection-diffusion phenomena coupled with adsorption can be written in general form as follows:

$$\frac{\partial C}{\partial t} = \nabla.(\mathrm{D}.\nabla C) - v.\nabla C - \chi_{\mathrm{ad}} \tag{1}$$

In the above equation written in the tensor form, *D* is the diffusion tensor for the metal ion through the reactor bed, *v* is the velocity vector representing the average linear fluid velocity, *C* represents the metal ion concentration in the reactor at any given position and time, and χ_{ad} represents the rate of metal ion removal from the liquid phase by sorption on IOCS particle. It would be appropriate to assume a cylindrical coordinate system with the axial direction denoted by the *x* coordinate, and the radius of the reactor represented by radial coordinates. The Laplacian and gradient operators denote the generalized three-dimensional case, wherein the first and second terms on the right hand side represent the diffusion and advection terms, while the third term χ_{ad} denotes the adsorption term. The above equation can be appropriately modified for the one-dimensional case, wherein the flow is in the axial direction. Neglecting the diffusivity of the metal ions in the radial direction, the above tensor equation can be written as follows:

$$\frac{\partial C}{\partial t} = D_x \frac{\partial^2 C}{\partial x^2} - v_x \frac{\partial C}{\partial z} - \frac{3k_{fc}(1-\varepsilon)}{R\varepsilon}\left(C - C_S\right) \qquad (2)$$

where D_x is the axial dispersion coefficient of the metal ion within the reactor, v_z is the bulk fluid (liquid) velocity in the axial direction. The adsorption term represents the rate of metal ions uptake by IOCS, and is controlled by the film transfer coefficient k_{fc} for the metal ions, the medium porosity ε, and the particle radius R, besides the concentration gradient between the bulk liquid and the adsorbent surface. Here, the term C_s represents the metal ion concentration at the adsorbent-liquid film interface.

The initial and boundary conditions are based on the assumptions that at time t_{s0} there is no metal ion in the liquid phase within the adsorber reactor, and that the concentration gradient is zero at the adsorber entrance. Therefore, the initial and boundary conditions can be represented as follows:

$$C(x, \mathrm{t} = 0) \; = \; 0$$

$$C(x = 0^+, t) \; = \; C_0 + \left(\frac{D_x}{v_x}\right)\left(\frac{\partial C(x = 0^+, t)}{\partial x}\right) \qquad \text{and}$$

$$\frac{\partial C(x = L^-, t)}{\partial t} \; = \; 0 \qquad (3)$$

where C_0 is the influent concentration of metal ions. The general partial differential equation representing the pore and surface diffusion model can be written as follows:

$$\frac{\partial q}{\partial t} = \frac{1}{r^2} \frac{\partial}{\partial r}\left(r^2 D_s \frac{\partial q}{\partial r}\right) \qquad (4)$$

In the above equation, *q* denotes the solid-phase concentration of the metal ion on IOCS, D_s represents the surface diffusion coefficient of the metal ions into the iron oxide coating of the adsorbent particle, and r represents the radial coordinate within the adsorbent particle.

The initial condition for the above partial differential equation is the following:

$$\text{At}\quad t = 0,\ \text{for}\ 0 \le r \le R,\ \text{and}\ \ 0 \le x \le L,\ \ q\ =\ 0 \tag{5}$$

The boundary conditions for reactor adsorbent particles can be written as

$$\text{At}\quad r = 0,\ \text{for}\ a\text{ll}\ \ t,\ \text{and}\ \ 0 \le x \le L,\ \ q\ =\ 0 \tag{6}$$

In the above initial and boundary conditions, L denotes the effective reactor length, and R represents the radius of the media particle. The boundary condition for the adsorbent particle balancing the temporal variation of the metal ions within the adsorbent and pore liquid with the metal ion flux through the liquid film surrounding the adsorbent is the following:

$$\frac{\partial}{\partial t}\int_0^R q\, r^2\, dr\ =\ \frac{k_{fc}\ R^2(1-\varepsilon)}{\rho_a}\left(C - C_S\right) \tag{7}$$

In the above partial differential equation, as well as in the initial and boundary conditions, ε is the intra-particle volume fraction for the adsorbent phase, *r* is the radial position within the spherical and ρ_a is the solid bulk density of the adsorbent particle. It is assumed that equilibrium exists between the adsorbent and the liquid phases with respect to the sorption of metal ions on IOCS. Adsorption of metal ions on IOCS can be assumed irreversible during the operation of the reactor system, although the spent adsorbent can be processed under low pH conditions for regeneration. The adsorption equilibrium is described by the Freundlich equation as follows:

$$q = K_F C_S^n \tag{8}$$

Here K_F and n are denoted the Freundlich capacity and intensity constants, respectively. Mass balance must be established as the rate of accumulation of the metal ions within the IOCS sorbent particle is balanced by the rate of substrate transport of metal ions from the bulk liquid phase through the liquid film. This relationship can be represented by the partial integro-differential equation as shown below:

$$\frac{\partial}{\partial t} \int_0^R 4\pi r^2 \, \mathrm{q} \; dr = \frac{k_{fc} \; \mathrm{A_p} \; \mathrm{R}^3(1-\varepsilon)}{3 \; v_x \rho_a} \left(C - C_S\right) \tag{9}$$

In the above relationship, $\mathrm{A_p}$ denotes the total surface area available for mass transfer on the medium particle.

The free liquid diffusivity of the metal ions can be estimated using the correlation shown in Table 6.2.[49] The surface diffusion coefficient D_s and the batch reactor film transfer coefficient k_{fb} are estimated from the adsorption rate data obtained from completely mixed batch reactor studies. These adsorption rate data are fitted with the batch reactor model simulation results to estimate these mass-transfer parameters using the homogenous surface diffusion model (HSDM).[11] It must be noted that the batch reactor film-transfer coefficient will provide only an estimate of the reactor column film-transfer coefficient k_{fc}, which is referred to as k_f in the above adsorber equations. However, the least-square curve-fitting techniques on the batch reactor data can provide accurate determinations for the surface diffusion coefficient. The adsorber column film-transfer coefficient for the metal ions k_{fc} is estimated from different correlations relating the Sherwood number *Sh,* to a function of the Reynolds number *Re,* and the Schmidt number *Sc*. In these studies, the correlation of Williamson et al. was found appropriate for evaluating the reactor column film transfer coefficient.[50] These correlations are shown in Table 6.2. The model equations are non-dimensionalized and solved using the hybrid numerical techniques previously described for the biodegradation model.

6.4 Materials and Methods

Preliminary biokinetic studies

For this study, seven *Shewanella* species including *S. baltica OS155*, *S. frigidimarina NCIMB 400*, *S. putrefaciens* 200, *S. putrefaciens* CN-32, *S. lohica* PV-4, *S. oneidensis* MR-1, and *S. amazonensis* SB2B, were obtained from Pacific Northwest National Laboratory (PNNL) an stored at -80°C (Table 6.3).

Table 6.3 Shewanella species used in these studies.

Species	Location of isolation
S. baltica OS155	Deep anoxic water basin (Baltic Sea)
S. frigidimarina NCIMB 400	Coastal seawater (North Sea)
S. putrefaciens 200	Crude-oil pipeline (Alberta, Canada)
S. putrefaciens CN-32	Anaerobic sandstone (New Mexico, USA)
S. lohica PV-4	Hydrothermal sea vent (Hawaii, USA)
S. oneidensis MR-1	Freshwater lake sediment (Lake Oneida, New York, USA)
S. amazonensis SB2B	Shallow marine sediment (Amazon River delta)

Cultures of the various species of *Shewanella* were prepared as described in Chapter 5: Materials and Methods.

Dynamic Column Studies

A schematic of the sand column system is shown in Figure 6.2. The columns were constructed from 0.25-inch acrylic of 1.5-inch internal diameter and 12-inch length. An acrylic flow distributor was placed at the column entrance to minimize channeling. A variable speed ultra low-flow peristaltic pump (Control Company; Friendswood, TX) was used to pump solution effluent from the column. The influent feed solution was withdrawn from a reservoir to the column entrance by siphon. The reservoir was loaded with a sterile simulated groundwater solution containing lactate to serve as the electron donor and oxygen as the terminal electron acceptor for bacterial growth. The column was packed with uniform silica sand with an average particle size of 500 μm. Details of the column and packing material properties are summarized in Table 6.4.

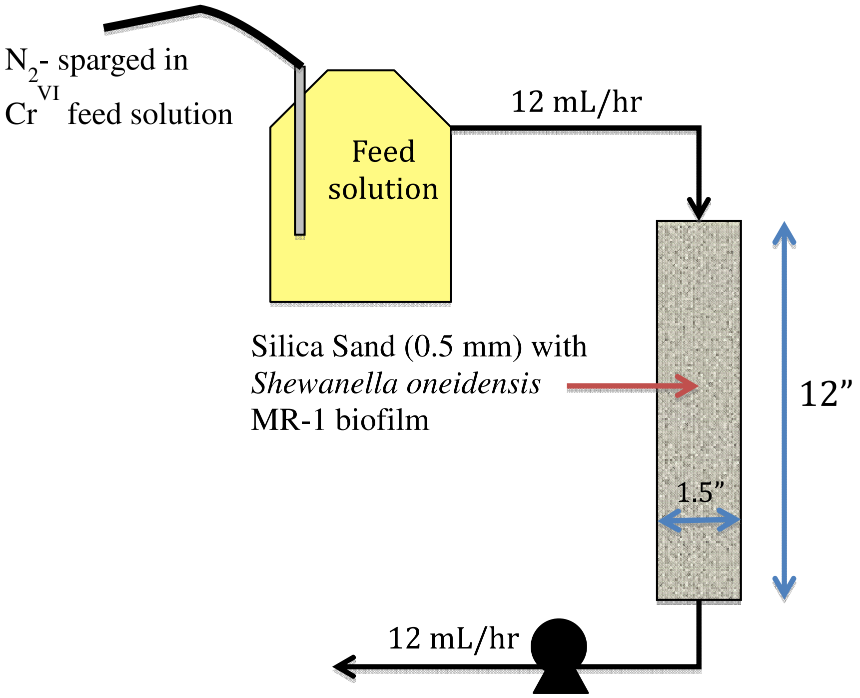

Figure 6.2 Experimental set-up for bioactive column studies.

Table 6.4 Sand column parameters.

Column Parameter	Value
Length	12 inches
Inner diameter	1.5 inches
Empty bed volume	360 mL
Sand mass	480 g
Pore volume (loaded)	128 mL
Porosity	0.36

Column Startup

The silica sand was washed with 5% HNO_3 to remove any residual metals and autoclaved at 120°C for 20 minutes to sterilize. The empty column and tubing were sterilized by multiple washes with a 70% ethanol solution, followed by multiple rinses with boiling water. The columns were charged with a slurry of sand and MR-1, prepared by mixing approximately 300 g of pretreated sterile sand with 250 mL of MR-1 culture in a 500 mL sterile Erlenmeyer flask. The slurry was left on a shake plate (DS-500, VWR; Radnor, PA) at 80 rpm for 4 hours before being charged to the column to allow for attachment of bacteria to the soil media. The column was flushed with two pore volumes of the minimal media solution (see Chapter 5: Materials and Methods) containing no lactate to remove unattached biomass from inter-particle pore spaces, as this would be flushed out with the first addition of feed solution containing chromium. The minimal media solution containing 3 mM lactate as the electron donor and oxygen as the electron acceptor was then fed to the column at a flow rate of 12 mL min^{-1} corresponding to a residence time of approximately 12 hours. The feed solution was pumped through the column for 7 days to allow for biomass development within the soil media. No Cr^{VI} was applied to the column during this period due to the observed toxicity leading to growth inhibition even at low concentrations (0.015 mM Cr^{VI}).[10] Cr^{VI} at concentration of 3 mg/L was introduced to the column on day 7 in a carbonate buffered solution containing 3 mM lactate. For column experiments with humic acid, a concentrated humic acid solution was added to the feed solution for a final concentration of 30 mg L^{-1}. A sterile column without MR-1 served as an abiotic control.

Sampling

Column effluent samples were collected at regular time intervals and immediately centrifuged (5415D, Eppendorf; Hauppauge, NY) at 14000 rpm for 5 minutes. The samples were immediately filtered with 0.2 µm cellulose acetate syringe filters (Membrane Solutions; Planor, TX) to remove any remaining suspended cells or precipitates. The column influent and the filtered effluent samples were refrigerated at 4°C for subsequent Cr^{VI} analysis.

Biomass Quantification

Biomass was quantified primarily by measuring absorbance of suspended cultures at 600 nm using a UV-Visible spectrophotometer (Model DU530; Beckman Coulter, Inc.; Brea, CA). Relation of absorbance to both volatile suspended solids and colony forming units was determined by EPA method 1684 and the dilution-to-extinction method. □

Iron Oxide Coated Sand Preparation

Iron oxide coated sand was prepared as described by Baily et al. (29). 40-mesh silica sand (Carmeuse Industrial Sands, Orange County, CA) was acid washed for 24 hours in a 50% sulfuric acid solution, rinsed multiple times with DDI water, then dried at 106°C. Approximately 1600 mL of sand was weighed into Pyrex glass baking dishes, and 640 mL of a 0.25 M $FeCl_3$ and 3.70 mL of a 4.0 M NaOH solution were added. Concentrations were diluted by a factor of 10 from the referenced recipe to limit the amount of rinsing required to remove excess $FeCl_3$. The sand-iron solutions were placed in an oven at 110°C and stirred hourly for 6 hours, at which point the sand was dry. The sand was then transferred to a furnace set to 550°C and ignited for 3 hours. Next, the sand was divided into four 400 mL aliquots and each was mixed with 160 mL of a 0.25 M $FeCl_3$ solution. These were heated overnight at 110°C. The sand was placed in a hood to cool, and allowed to sit overnight during which period the sand became damp due to its hygroscopic properties. It was dried at 110°C again for 3 hours and left to sit overnight again in the hood. This process was repeated 5 times, after which the sand no longer absorbed noticeable amounts of moisture from the air. At this point the sand was ready for use.

Simulated Contaminated Water

The simulated contaminated water solution was prepared with reagent grade chemicals from Sigma-Aldrich (St. Louis, MO). A concentrated Cr^{VI} stock solution was prepared from potassium dichromate ($K_2Cr_2O_7$), which was diluted as required for the appropritae Cr^{VI} concentration. Bicarbonate was added as a buffer for a final concentration of 10 mM, and the solution pH was adjusted to 7.0 ± 0.1 with dilute HCl.

All dilutions were prepared with distilled, deionized water (Mega-Pure Still, Thermo Scientific USA).

Rate Studies

A simulated contaminated water containing 10 mg L^{-1} Cr^{VI} at pH 7.1 was mixed with IOCS in 50 mL polypropylene centrifuge tubes (VWR, USA). 40 mL of the contaminated water was added to each tube, and the mass of IOCS added in each tube was as follows: 0.5 g, 1.0 g, 1.5 g, and 2.5 g. Mixing was performed continuously on a roller mixer at approximately 70 rpm, and samples were taken routinely. Each IOCS-Cr^{VI} mixture was run in duplicate.

Adsorption Isotherm Studies

The equilibrium concentrations determined from the rate studies were used to describe the adsorption equilibrium process. The equilibrium concentrations were plotted against the concentration of Cr^{VI} adsorbed to the surface of the IOCS, and evaluated to determine if the adsorption was best described by the Langmuir or Freundlich adsorption isotherm model.

Column studies

A schematic of the IOCS column experimental system is shown in Figure 6.3, and a photograph is shown in Figure 6.4. The columns were constructed from 0.25-inch acrylic of 1.5-inch internal diameter and 12-inch length. The columns were packed with 480 g of IOSCs, and the porosity was determined experimentally to be 0.36. An acrylic flow distributor was placed at the entrance or the influent stream to minimize channeling. Approximately 5 pore volumes of DDI water were flushed through the column prior to Cr^{VI} introduction to rinse any excess, unbound $FeCl_3$ from the sand particles. After the 5 rinses, the column effluent was clear to the eye. A variable speed peristaltic pump (Control Company; Friendswood, TX) was used to pump a feed solution from a feed reservoir into the column (Figure 6.3). The reservoir was filled with a simulated contaminated water solution containing 3.0 mg/L Cr^{VI} as chromate, a 10 mM carbonate buffer, and adjusted to pH 7.0 ± 0.05. The simulated contaminated solution was pumped through the column at a flow rates or 6, and 10 mL min^{-1} corresponding to 24-minute, and 11-minute residence times, respectively. Samples were taken on regular intervals and analyzed for Cr^{VI}.

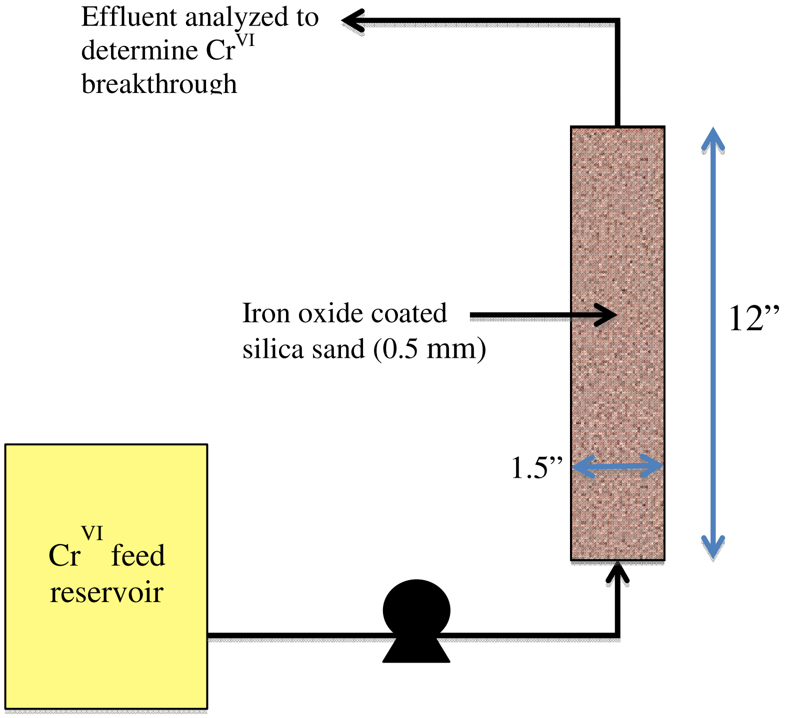

Figure 6.3 Schematic of the experimental arrangement for IOCS column studies.

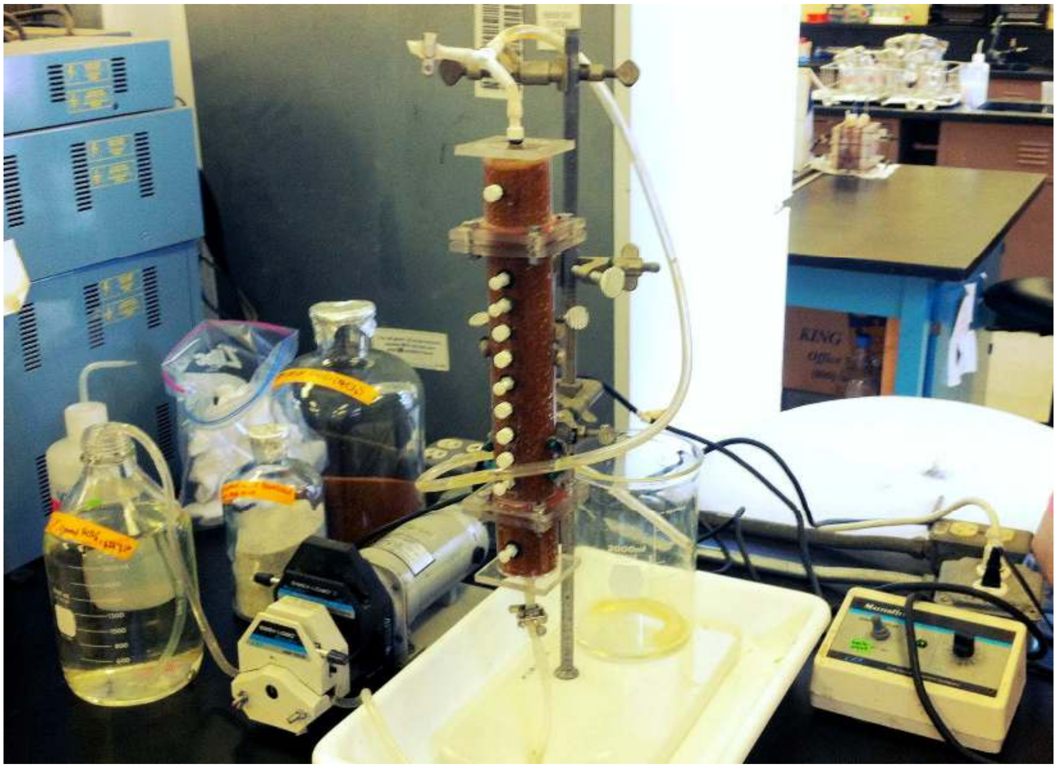

Figure 6.4 Photograph of the experimental apparatus for IOCS column experiments.

Cr^{VI} measurement

Samples from the anaerobic reactors were immediately placed on ice after collection to prevent further bioreduction of Cr^{VI} in the sample. After samples were collected from all reactors for a given time point, biomass was removed by centrifugation at 17,000g for 5 minutes. Supernatant was immediately collected and evaluated for Cr^{VI} with an ion chromatography method (see Chapter 3.2).

6.5 Results and Discussion

Cr^{VI} Reduction by *Shewanella oneidensis* MR-1

Rate Studies: Dual Enzyme Model Results

Previous studies on biological Cr^{VI} reduction indicate that this enzymatic reaction is finite for a given culture of bacteria, however the mechanisms behind this limitation are not well understood.[51] The ability of *Shewanella* to reduce Cr^{VI} becomes inhibited with time and exposure, likely due to two primary factors: 1) the deactivation of enzymes involved in the Cr^{VI} reduction process after one or multiple interactions with Cr^{VI}, and/or 2) Cr^{III} precipitates forming around and inside the cell as a result of Cr^{VI} reduction, which inhibits the release of enzymes and interferes with electron transfer. Accordingly, the dual-enzyme model[10] may offer a logical model to describe these phenomena.

When Cr^{VI} is present in low concentrations, the maximum rate of reduction as defined by the Michaelis-Menton equation due to the deactivating and stable enzymes can be equated to r_{do} and r_{so} respectively. This assumption can be made because the half saturation constants, K_m, for the enzymes are much smaller than the concentration of Cr^{VI} Additionally, these values can be used to quantify the initial reduction rates by dividing by the cell concentration. The slope of the initial rapid reduction of Cr^{VI} is proportional to the r_{do} value, which is apparent in comparing the curves of *Shewanella sp.* with the most rapid and slowest reduction. Observed values for r_{do} range from 1.58 mM- Cr^{VI} hr^{-1} (Baltica), to 0.087 mM-Cr^{VI} hr^{-1} (CN-32). These values are obtained from the Cr^{VI} curves (Figure 6.5), as Baltica underwent the most rapid decline in Cr^{VI} concentration, and CN-32 had the most gentle reduction curve.

In some cases, the species with slower reaction kinetics were able to reduce more Cr^{VI} overall in the 3-hour time period than those with rapid reaction kinetics. Residual Cr^{VI} concentrations were highest in the Baltica sample at 0.122 mg L^{-1}, while the CN-32 sample had a residual of 0.056 mg L^{-1}. PV-4 was able to reduce Cr^{VI} concentrations to the greatest extent, leaving a residual concentration of 0.004 mg L^{-1} and also had a rapid initial rate of reaction with an r_{do} value of 0.0367 mM-Cr^{VI} hr^{-1}. Reaction kinetics can be significant in designing reactor systems, however it is also essential that the species of *Shewanella* used be capable of reducing Cr^{VI} to below the target value.

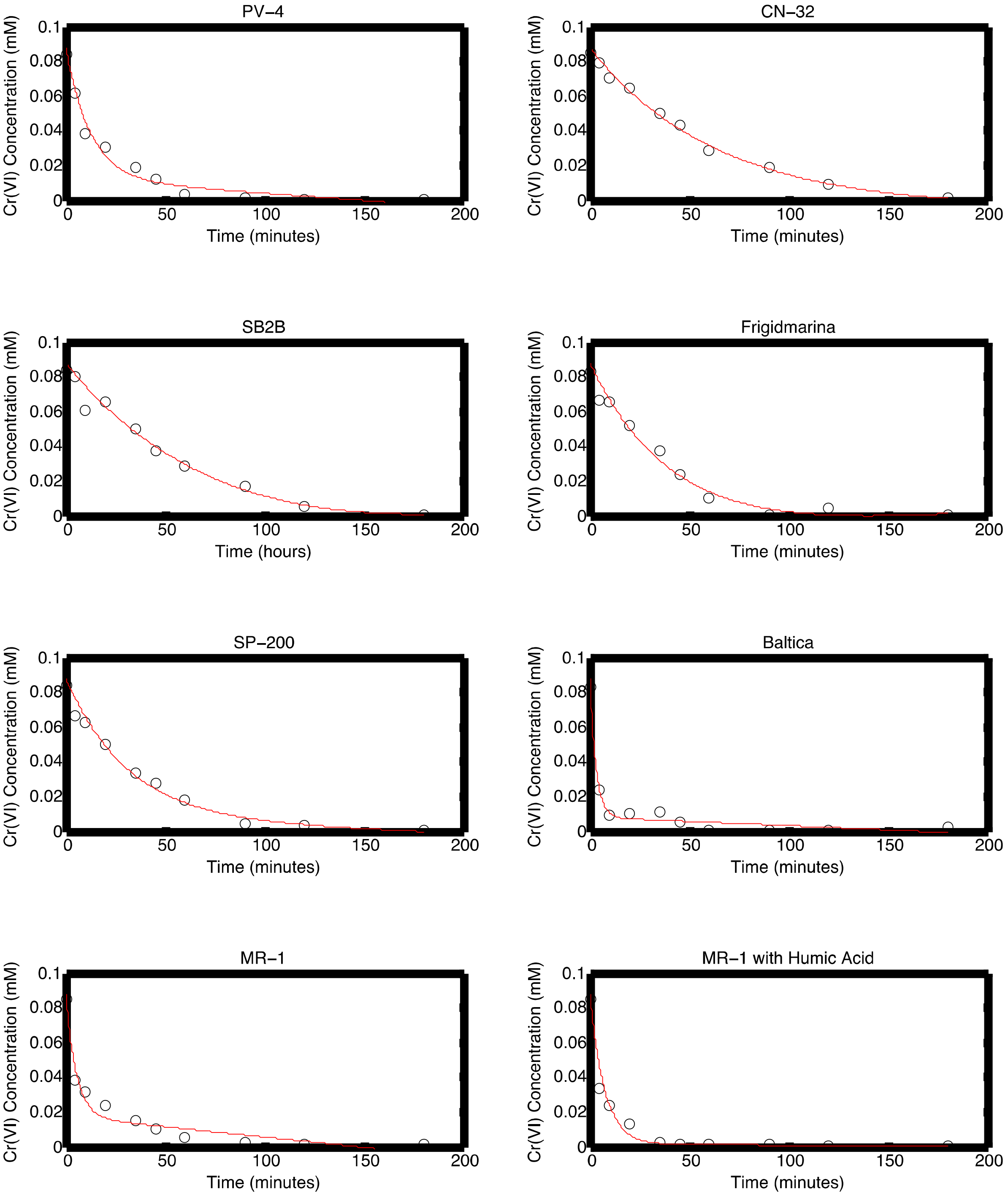
PV−4

CN−32

SB2B

Frigidmarina

SP−200

Baltica

MR−1

MR−1 with Humic Acid

Figure 6.5 Results of dual enzyme model fit to experimental data.

Table 6.5 Parameters r_{so}, r_{do}, and k_d determined from the dual-enzyme model.

Species	r_{so} (mM-Cr(VI) hr^{-1})	r_{do} (mM-Cr(VI) hr^{-1})	k_d (hr^{-1})
PV-4	4.98E-03	0.367	4.855
SB2B	1.42E-06	0.099	0.653
MR-1	7.12E-03	0.812	11.508
Baltica	2.94E-03	1.575	19.715
CN-32	3.79E-06	0.087	0.924
Frigidmarina	5.19E-06	0.149	1.437
SP200	2.52E-03	0.154	1.905
MR-1 with HA	2.09E-04	0.705	8.133

Rate Studies: Monod Model Results

The Monod growth model with an inhibition term to account for Cr^{VI} toxicity was fit to the data to determine the biokinetic parameters required in the model development for breakthrough curve prediction in the column studies. It was discovered however that the inhibition term is irrelevant because of the low concentrations (5.2 mg L^{-1}) being used in experimental work. This is consistent with findings by Guha (4), who determined that an inhibition term was only relevant for Cr^{VI} concentrations well above 37 mg L^{-1}. This was also made apparent by the orders of magnitude variation in the inhibition term estimation, and a sensitivity analysis that illustrated only a zero value for K_I would cause an obvious change in the curve. Therefore the inhibition term is eliminated and the simplest form of the Monod model is used to determine the maximum growth rate (μ_{max}) and the half-saturation constant (K_s). The results are shown in Figure 6.6.

The maximum specific growth rate describes the microbe's ability to utilize Cr^{VI} as an electron acceptor in the growth process. The MR-1 species in the presence of humic acid had the highest value of μ_{max} of 0.2116 hr^{-1}, and the lowest observed μ_{max} was 0.0155 hr^{-1} from SB2B. The study of MR-1 without humic acid and the Baltica study also yielded relatively high μ_{max} values of 0.1326 hr^{-1} and 0.1402 hr^{-1}, respectively. The estimated half saturation constant was indicative of the efficiency of substrate utilization. *Shewanella* species Baltica and SB2B had the lowest half-saturation constants of 0.56 mg L^{-1} and 0.77 mg L^{-1}, respectively, illustrating their capacity to utilize substrate effectively. Conversely, MR-1 and CN-32 had the largest K_s values of 1.48 mg L^{-1} and 1.73 mg L^{-1}, respectively, demonstrating an inefficient use of substrate.

The curves fit the experimental data with a confidence level greater than 95% with the exclusion of the inhibition parameter.

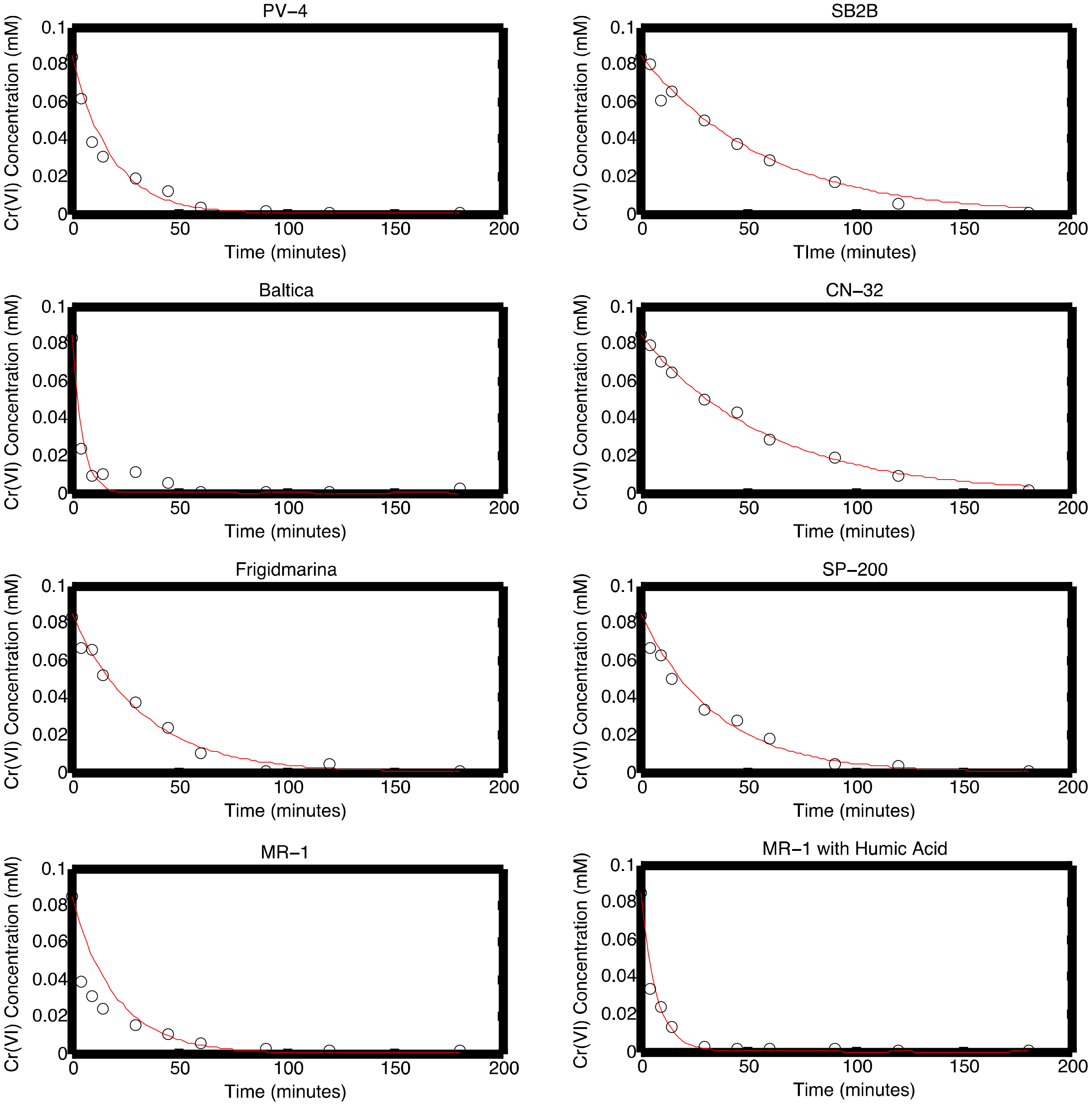

Figure 6.6 Results of the Monod model with inhibition fit to the experimental data.

In summary, the Monod model was used to determine biokinetic parameters used for dynamic breakthrough curve prediction, and the dual-enzyme model was used in hypothesizing a possible mechanism for Cr^{VI} reduction. Understanding these fundamental concepts of enzymatic reduction and determining biokinetic parameters were the first steps in this study to aid in analyzing experimental observations as well as in breakthrough curve prediction.

Table 6.6 Biological parameters μ_{max} and K_s determined from the Monod model fit to the experimental data.

Species	μ_{max} **(hr^{-1})**	K_s **(mg L^{-1})**
PV-4	3.51	1.036
SB2B	0.93	0.769
MR-1	7.96	1.479
Baltica	8.41	0.558
CN-32	1.77	1.729
Frigid Marina	2.46	1.399
SP200	1.76	1.031
MR-1 with HA	12.70	1.387

The reduction data for all species followed pseudo-first order reduction kinetics when truncated to the 60-minute point (Table 6.7). The species with the highest maximum specific growth rate including Baltica, PV-4, and MR-1 had more rapid reaction kinetics. Nonetheless, the rate constants ranged from the slowest reduction rate for SB2B and CN-32 at 0.0172 min^{-1} to the fastest kinetics of 0.0566 min^{-1} for OS155.

Table 6.7 First-order rate constants from the Monod model truncated at 60 minutes.

Strain	**k' (min^{-1})**	**r^2**
S. loihica PV-4	0.0463	0.969
S. amazonensis SB2B	0.0172	0.951
S. oneidensis MR-1	0.0399	0.937
S. baltica OS155	0.0566	0.799
S. putrefaciens CN-32	0.0172	0.977
S. frigidmarina NCIMB 400	0.0329	0.948
S. putrefaciens 200	0.0245	0.996
S. oneidensis MR-1 (in humic acid)	0.0649	0.896

Use of Shewanella oneidensis MR-1 for Bioremediation Studies

One of the best-studied model organisms from the standpoint of biotechnology applications is *Shewanella oneidensis* MR-1. It is classified as a c-proteobacterium with 41 “putative” c-type cytochromes encoded in its genome. Several of these c-type cytochromes have been shown to form a respiratory network extending the respiratory chain from the cytoplasmic membrane through the periplasm to the outer membrane. This is indeed an important aspect in metal reduction applications of the microorganism. In *Shewanella oneidensis*, the reduction of most extracellular electron acceptors is based on a protein complex formed by MtrA, MtrB and MtrC (Mtr standing for ‘metal reducing’). This complex is most probably the extracellular terminal reductase.

Shewanella oneidensis MR-1 was a mid-range performer in terms of reaction kinetics, however was also capable of reducing Cr^{VI} to below detectable levels. Despite their performance in comparison to other species, MR-1 are often chosen in experimental work because they are the best understood of the over 40 *Shewanella sp.* Their genome has been thoroughly mapped,[52] which has accommodated unique studies into their physiology and behavioral attributes. A study by Gorby *et al.* determined the primary proteins responsible for the production of conductive nanowires that can extend microns from the cell surface.[53] The production of these nanowires requires the Mtr pathway, which was illustrated when mutants of proteins OmcA and MtrC produced non-conductive filaments.

Shewanella however do not require nanowires to reduce extracellular electron acceptors, as they generate soluble electron shuttles that contribute to electron transfer to both minerals and anodes.[54,55] While these electron shuttles, or redox-mediators can be difficult to isolate and classify, they have been identified for *S. oneidensis* MR-1 as riboflavin and riboflavin mononucleotide.[9] These are likely the MR-1 enzymatic activity products released during the metabolism of substrate. Inhibition of this process form exposure to Cr^{VI}, or from an encapsulation process by the precipitation of Cr^{III} on the cell membrane causes the decline in Cr^{VI} transformation capacity. Several potential mechanisms of electron transfer for *Shewanella sp.* have been offered, however a recent investigation supports an undeniable significance of soluble electron shuttles.[3] Extensive information is available regarding MR-1, as it has served as a model *Shewanella* species in countless studies from investigating methods of imaging to mapping genomes.

Dynamic Cr^{VI} Transport Prediction in Bioactive Columns

Model prediction and simulation studies are important in determining the reactor dynamics for Cr^{VI} removal under a variety of operating and process conditions, and for optimal design, operation, and upscaling or downscaling the appropriate processes. Model verification and validation using experimental data from reactor dynamics studies were conducted for use in bioactive column and then separately IOCS columns. The parameters employed in the bioactive column studies included the mass transfer coefficient, diffusion coefficients, biokinetic coefficients and other reactors characteristics such as media particle size and density, initial and maximum biofilm thickness, influent contaminant concentration, and reactor flow rates as depicted in Table 6.8.

Table 6.8 Operational model parameters for bioactive sand columns during chromium reduction.

Model parameter	Unit	Value	References
Media characteristics			
Sand column reactor diameter, *d*	cm	3.81 cm	This study
Sand column reactor length, *L*	cm	25.4 cm	This study
Particle size (average radius), *R*	cm	0.025	This study
Particle density of medium (sand), ρ	g/cm^3	2.65	This study
Column bed porosity	none	0.36	This study
Amount of medium, *W*	g	480	This study
Influent characteristics			
Influent chromium concentration, C_0	mg/L	3	This study
Influent flow rate, *Q*	mL/min	0.2 to 0.4	This study
Recycle flow rate, Q_r (no recyle scenario)	L/h	0	This study
Biological parameters: lactate without humic acid			
Monod specific growth rate, $\mu_{max,a}$	h^{-1}	0.1326	This study
Monod half saturation constant, $K_{s,a}$	mg/L	1.4791	This study
Microbial yield coefficient, Y_a	mg/mg	0.30	This study
Decay coefficient, $k_{d,a}$	h^{-1}	0.005	This study
Biological parameters: lactate with humic acid			
Monod specific growth rate, $\mu_{max,a}$	h^{-1}	0.2116	This study
Monod half saturation constant, $K_{s,a}$	mg/L	1.387	This study
Microbial yield coefficient, Y_a	mg/mg	0.30	This study
Decay coefficient, $k_{d,a}$	h^{-1}	0.004	
Biofilm characteristics			
Initial biofilm thickness L_{f0}	µm	5	Estimated from microscopy
Maximum biofilm thickness, L_{fmax}	µm	30	Estimated from microscopy
Mass transfer parameters			
Free liquid diffusion coefficient for chromium species, D_l	cm^2/s	1.21×10^{-5}	Green and Perry (2004)
Biofilm diffusion coefficient for chromium species, D_f	cm^2/s	0.977×10^{-5}	Rittman and McCarthy (1978)
Substrate film transfer coefficient, k_{fc}	cm/s	4.0×10^{-3}	Williamson et al. (1963), Pirbazari et al. (1993)
Axial dispersion coefficient, D_x	cm^2/s	0.0020	Wakao and Funazkri (1963), Kim and Pirbazari (1987)
Non-dimensional groups			
Reynolds number, *Re*	none	0.00043-0.00086	This study
Schmidt number, *Sc*	none	991736	This study
Sherwood number, *Sh*	none	13223	This study

The experimental data for effluent Cr^{VI} concentration were obtained for each set of the reactor operating conditions. The reactor column dynamics have been evaluated at two flow rates of 12 and 24 mL hr^{-1} (0.2 and 0.4 mL min^{-1}) and different background solutions, one without humic acid and one containing 30 mg L^{-1} humic acid, each at an influent chromium Cr^{VI} concentration 3 mg L^{-1}. These data were compared with the predicted and simulated model profiles, and the results are presented in Figures 6.7 through 6.9. A summary of the reactor conditions is displayed in Table 6.9. A good agreement between the experimental data and theoretical predictions is evident with errors within 0-5 percent, establishing the predictive capability and utility of the model. In most cases, the predictions are reasonably accurate, although some minor deviations are observed in some cases. Analyses of the process dynamics indicate that the model over-predicts or under-predicts the effluent Cr^{VI} concentrations and therefore exhibit minor deviations in predicting the overall process efficiency.

Table 6.9 Operating conditions for the various bioactive column experiments.

Column #	Cr^{VI} conc. (mg L^{-1})	Humic acid conc. (mg L^{-1})	Flow rate (mL hr^{-1})	Figure
1	3	0	12	6.7
2	3	30	12	6.7
3	3	0	24	6.8
4	3	30	24	6.8

The reactor dynamics and the column breakthrough profiles manifest differences in the presence of humic acid in the influent solution. The electron donor sustaining the growth and development of a thin biofilm of *Shewanella oneidensis* MR-1 on the sand particles and in the liquid phase is lactate (besides the humic acid). It must be noted that humic acid serves as an additional electron donor, and the effect is well reflected by the overall degradation kinetics based on the comparison of the Monod parameters presented in Table 6.7. It can be observed that the Monod specific growth rate is slightly higher at 0.21 h^{-1} for the combination of lactate and humic acid as electron donors, while it is lower at 0.13 h^{-1} when lactate alone is used; the corresponding values of the Monod half-saturation coefficients for the two cases, respectively, are 1.48 and 1.39 mg L^{-1} (evaluated with respect to the chromium ions). The higher level of biochemical activity in the case of dual electron donors (lactate and humic acid) is also qualitatively reflected in the experimental observed and predicted column dynamics, although the differences are less significant than indicated by the Monod parameters. It can be easily seen in Figure 6.8 that at a high reactor flow rate of 24 mL hr^{-1}, the column breakthrough occurs after 11 hours and 12 hours for the two columns, the longer duration for breakthrough being observed for the column containing humic acid in the feed. A larger difference in column breakthrough time is observed when the reactor flow rate is reduced to 12 mL hr^{-1}, so that the reactor detention time is doubled; and the breakthrough durations are approximately 36 and 40 hours, respectively (Figure 6.7). The results clearly indicate that the microbial transformation of Cr^{VI} to Cr^{III} is more efficient in the presence of 30 mg L^{-1} of humic acid.

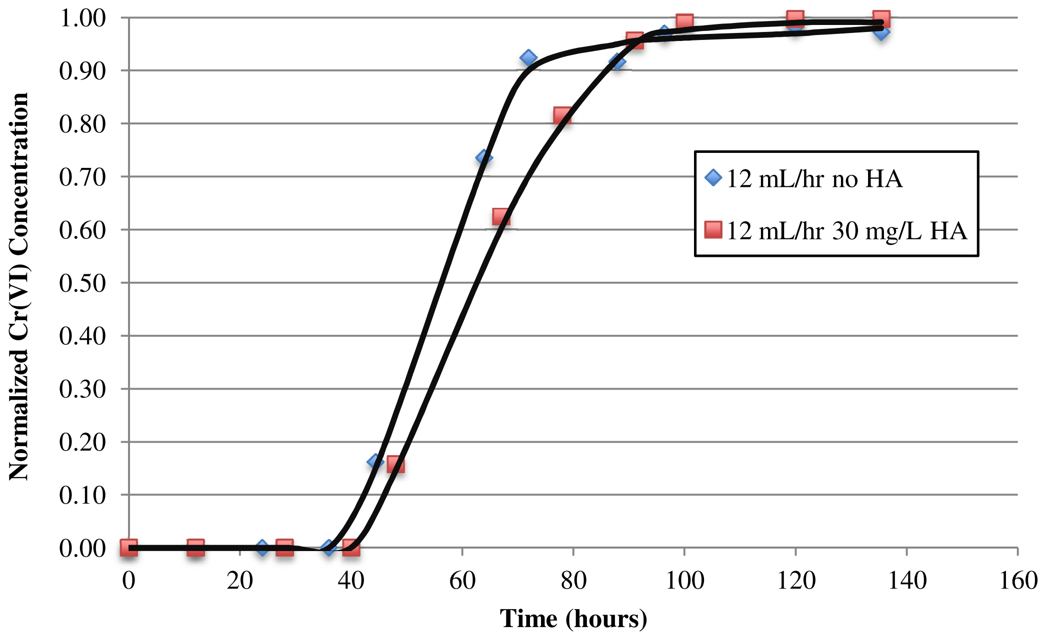

Figure 6.7 Experimental data and model predictions for the bioactive sand columns employed in the removal of Cr^{VI} with and without humic acid for a flow rate of 12 mL hr^{-1}.

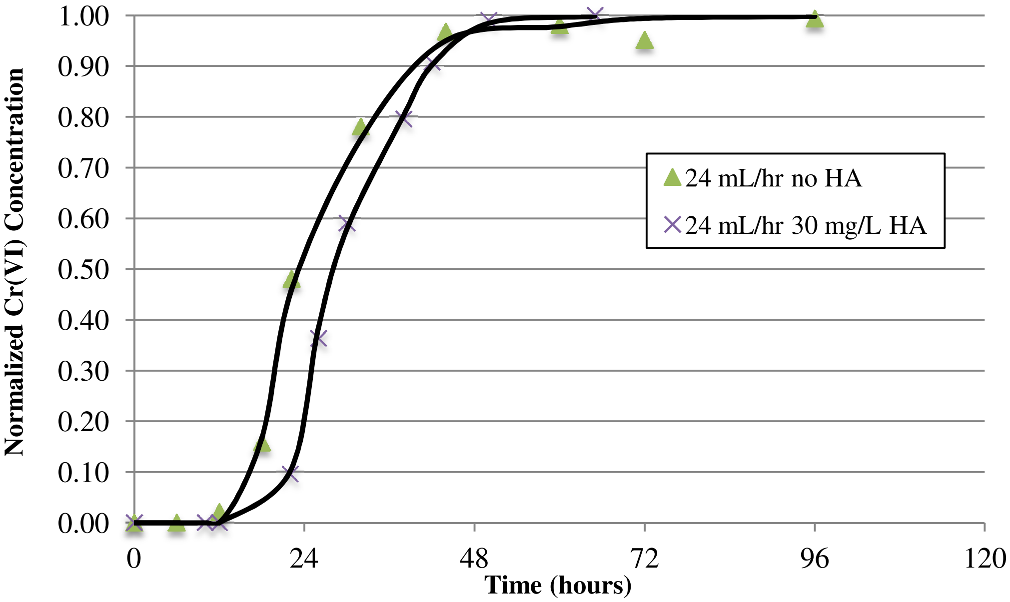

Figure 6.8 **Experimental data and model predictions for the bioactive sand columns employed in the removal of Cr^{VI} with and without humic acid for a flow rate of 24 mL hr^{-1}.**

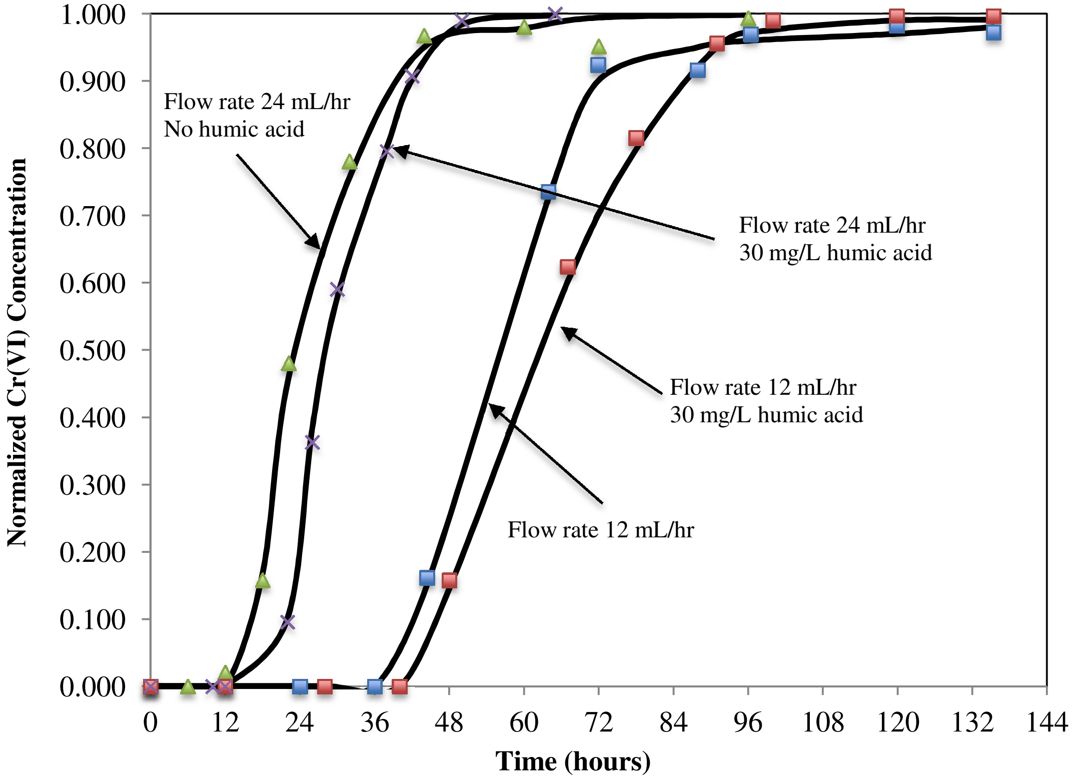

Figure 6.9 **Experimental data and model predictions for the sand columns employed in the removal of hexavalent chromium Cr^{VI} for all flow rates with and without the presence of humic acid.**

Cr^{VI} Reduction by IOCS

Rate Studies

The adsorption of Cr^{VI} by IOCS was shown to be a rapid process as illustrated in Figure 6.15. In each sample, a variable mass of IOCS (from 0.25 g to 2.6 g) was added to a 10 mg L^{-1} Cr^{VI} solution and mixed thoroughly. For all samples, reduction was complete within ten minutes, although the adsorption process was over 95% complete by the first sample time point at 5 minutes. This is consistent with findings that the adsorption process is immediate.[16,17]

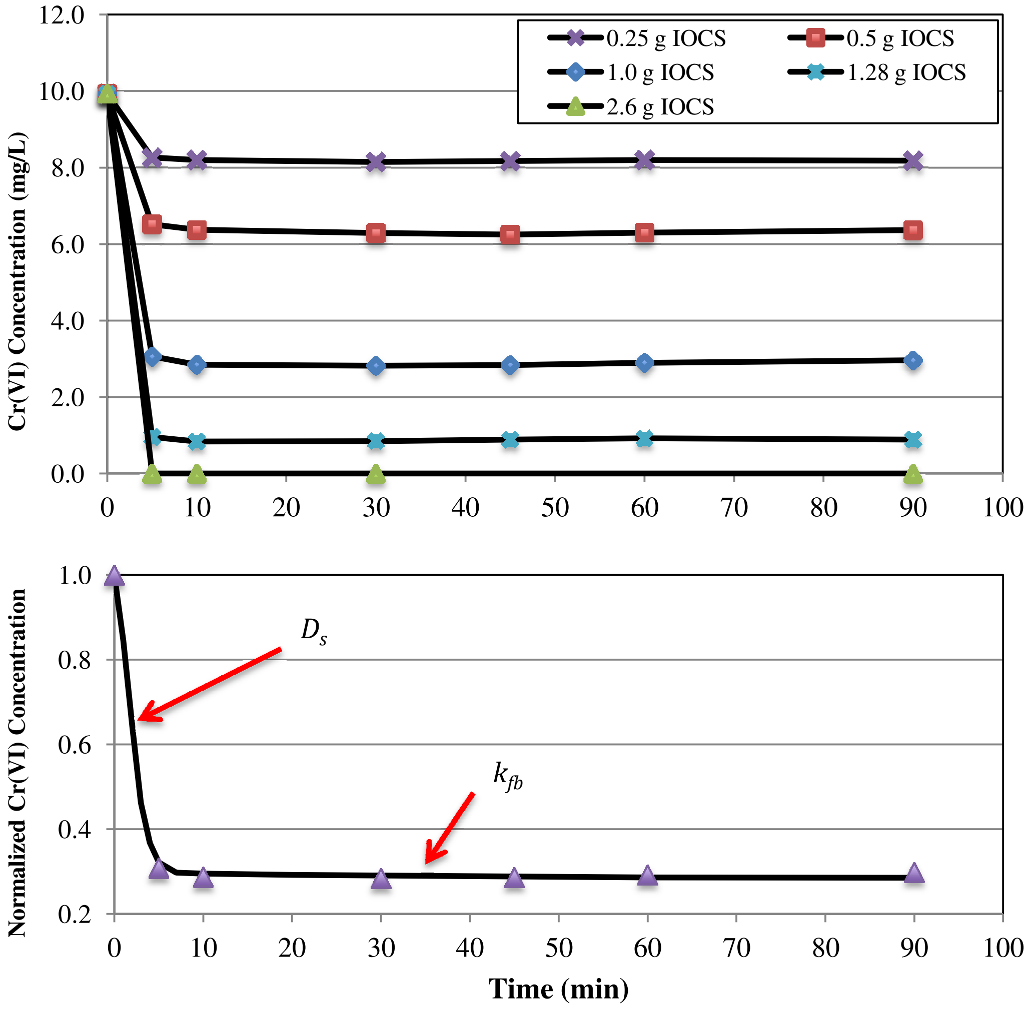

Figure 6.10 **top) Reduction rate studies with IOCS for a 10 mg/L influent Cr^{VI} concentration, and bottom) experimental adsorption rate data for IOCS used in chromium Cr^{VI} reduction.**

The purpose of the adsorption rate studies was to determine the mass transfer parameters for the homogeneous surface diffusion model (HSDM), namely, the surface diffusion coefficient D_s, and the film transfer coefficient k_{fb}. The rate data were employed to determine these mass transfer parameters using the HSDM (for batch reactor configuration) using a two-parameter search regression procedure described by Pirbazari and coworkers.[61] Typical experimental data for adsorption kinetic study, and the model predictions obtained from the batch reactor HSDM corresponding to the adsorption of chromium ions on IOCS are shown in Figure 6.10b. A two-parameter search algorithm was employed for estimating the two mass transfer parameters D_s and k_{fb}, wherein the normalized least square fit between the experimental value and the theoretically predicted value was minimized. In this regard, it is important to note that the k_{fb} values are generally higher than the k_{fc} values estimated from correlation techniques. This is so because in batch reactor systems a higher film transfer coefficient k_{fb} is encountered due to the formation of a thinner liquid film around the adsorbent particle under relatively more turbulent conditions that offers lower mass transfer resistance. In comparison, a lower film transfer coefficient k_{fc} is experienced in column operations owing to more laminar flow conditions.

Adsorption Isotherm Studies

Equilibrium data from the rate studies was used in developing an adsorption isotherm, and determining adsorption parameters relevant for the predictive model. The Freundlich adsorption isotherm model fit the data well as shown in Figure 6.16. The data were also well described by the Langmuir isotherm model, however the Langmuir model assumes a monolayer adsorption phenomenon, which is not believed to be the case with IOCS. It is assumed that the iron oxide layer has a defined thickness that allows for diffusion of the adsorbent, as described earlier. The Freundlich adsorption capacity, K_F, was determined to be 0.281 mg Cr^{VI} per g IOCS, and the Freundlich intensity coefficient, $1/n$, was found to be 0.0152. These terms are further explained and utilized in the predictive model.

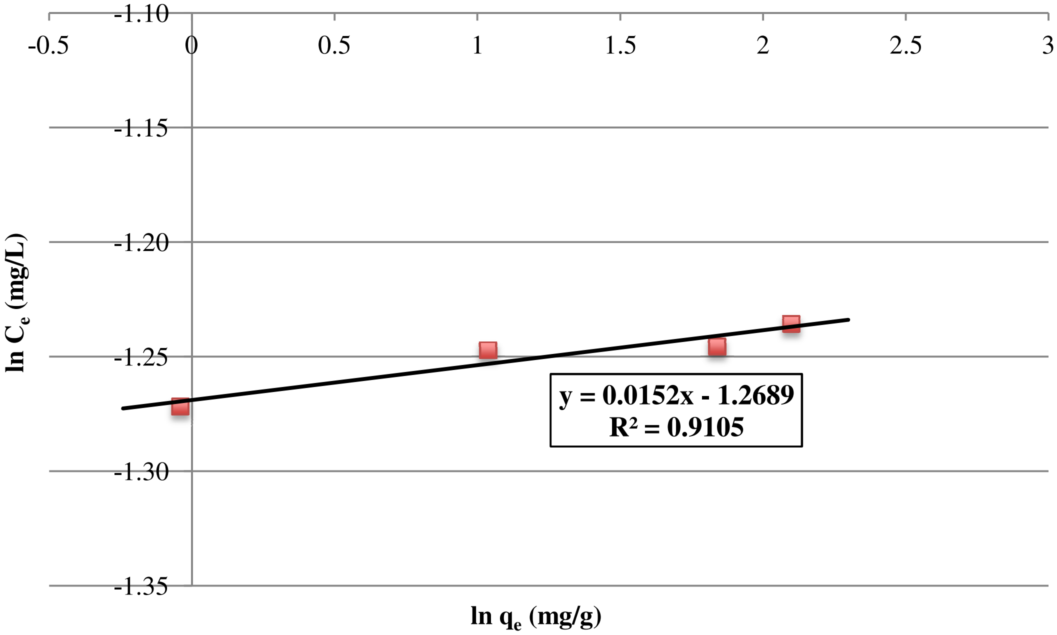

Figure 6.11 Freundlich adsorption isotherm model describing the adsorption of Cr^{VI} to IOCS.

IOCS Column Breakthrough Curve Model Prediction Results

The experimental data for effluent Cr^{VI} concentration were obtained for each set of the IOCS reactor operating conditions. These data were compared with the predicted and simulated model profiles, and the results are presented in Figure 6.12. A good agreement between the experimental data and theoretical predictions is evident with errors within 0-10 percent, establishing the predictive capability and utility of the adsorption model. In general, the predictions are satisfactory with some minor deviations as observed in the case of predictions for the biofilm model.

The reactor dynamics have been evaluated for the adsorptive IOCS column at two flow rates of 6 and 10 mL min^{-1}, more than an order of magnitude higher than those employed for the sand columns (0.2 and 0.4 mL min^{-1}). The rationale underlying the use of larger flow rates is based on the fact that microbial degradation in groundwater is a slower process than adsorption on IOCS particles of comparable dimensions. Breakthrough in the IOCS columns operated at 10 mL min^{-1} and 6 mL min^{-1} are 40 hours and 78 hours, respectively. The IOCs column dynamics indicate that the breakthrough times are approximately inversely proportional to the influent flow rate, suggesting a certain degree adsorbent capacity utilization for simultaneous sorption and reduction prior to breakthrough. This is also reflected by the approximate number of bed volumes of influent treated by the two reactors.

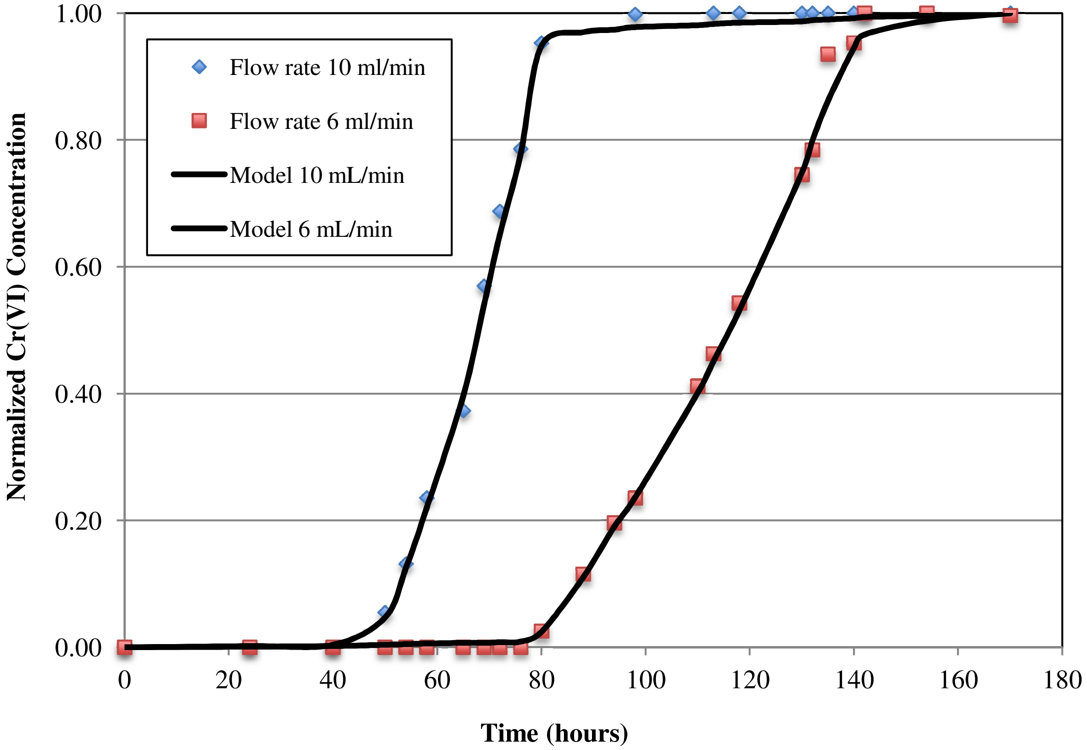

Figure 6.12 Cr^{VI} breakthrough curves for IOCS column studies with superimposed model predictions.

The main factors influencing the process dynamics and efficiencies are flow rate, influent concentration adsorption equilibria, adsorption kinetics, and overall mass transfer. In this regard, the adsorption equilibrium parameters K_F and n defined by the Freundlich relationship generally have a strong influence on the overall dynamics. In particular, the Freundlich capacity coefficient K_F has a profound significance in so far denoting the adsorbent capacity for the specific contaminant (Cr^{VI}), while the intensity coefficient is an indirect measure of the adsorption energy. Equally important are the mass transfer parameters that have a direct influence on the kinetics of the adsorption process, and these include the surface diffusion coefficient D_s of the chromium ions into the sorbing iron oxide layer over the sand particle (IOCS system), and the reactor column film transfer coefficient k_{fc} for Cr^{VI} transport through the aqueous liquid film surrounding the IOCS particle. These parameters are summarized in Table 6.10.

Table 6.10 Operational model parameters for IOCS columns during chromium reduction

Model parameter	Unit	Value	References
Media characteristics			
Sand column reactor diameter, d	cm	3.81 cm	This study
Sand column reactor length, L	cm	25.4 cm	This study
Particle size (average radius), R	cm	0.25 cm	This study
Particle density of medium (sand), ρ	g/cm^3	2.65	This study
Column bed porosity, ε	none	0.36	This study
Amount of medium, W	g	480	This study
Influent characteristics			
Influent chromium concentration, C_0	mg/L	5	This study
Influent flow rate, Q	mL/min	0.2 to 0.4	This study
Recycle flow rate, Q_r (no recycle scenario)	L/h	0	This study
Adsorption equilibrium parameters			
Freundlich capacity constant, K_F	$(mg/g)^{n-1}$ $(mg/L)^{-1}$	0.281	This study
Freundlich intensity constant, $1/n$	none	0.0152	This study
Mass transfer parameters			
Free liquid diffusion coefficient for chromium ion, D_l	cm^2/s	1.21×10^{-5}	Perry and Green (2004)
Surface diffusion coefficient for chromium ion, D_s	cm^2/s	5.5×10^{-7}	HSDM Model, Pirbazari et al. (1993)
Substrate film transfer coefficient, k_{fb} (for the batch reactor system)	cm/s	6.0×10^{-3}	HSDM Model, Pirbazari et al. (1993)
Substrate film transfer coefficient, k_{fc} (for the column reactor system)	cm/s	4.0×10^{-3}	Williamson et al. (1963), Pirbazari et al. (1993)
Axial dispersion coefficient, D_x	cm^2/s	0.0020	Wakao and Funazkri (1963), Kim and Pirbazari (1987)
Non-dimensional groups			
Reynolds number, Re	none	0.00043-0.00086	This study
Schmidt number, Sc	none	991736	This study
Sherwood number, Sh	none	13223	This study

Although beyond the experimental scope of this study, it is important to consider the effects of humic acid on Cr^{VI} removal in an IOCS treatment process. IOCS has been applied to removal of organic matter from water, and results show IOCS preferentially adsorbs acidic fractions enriched in aromatic and carboxylic carbon.[63,64] This process has even been considered as a pretreatment for membrane processes to reduce biofouling. When co-present in systems containing heavy metals targeted for removal, humic acid has been found to have discrete significance. For removal of metals such as copper and lead, the presence of humic acid was found to increase removal capacity.[65] As humic acid typically carries a significant negative charge, complexation with cationic contaminants can occur rapidly, effectively removing them from water. However a study by Mak et al. found humic acid to interfere with the removal of anionic contaminants such as arsenate and chromate.[66] Further, electrostatic repulsion between humic acid and anions discourages complexation reactions, and in the presence of IOCS these species will compete for the limited number of adsorption sites. The reduction in removal of these contaminants can be attributed to the deposition of humic acid on the IOCS surface.[66]

IOCS as a Permeable Reactive Barrier

As previously discussed, the IOCS predictive model was based on the assumptions that, i) the packed-bed reactor is a plug flow system with axial dispersion, ii) the uptake of metal ions by IOCS is a two-step mass transport mechanism limited by external liquid-film mass transfer from the bulk liquid to the adsorbant surface, iii) intra-particle solid-phase diffusion involves solely surface diffusion, iv) the IOCS particles are uniform and homogeneous, and v) the sorption process is irreversible. These principles are still applicable to an applied situation in which IOCS is placed in the ground as a permeable reactive barrier. The predictive model results, shown to accurately describe the IOCS column data, were used to simulate Cr^{VI} breakthrough at the flow rates typical to aquifer flow in the environment. The results are shown in Figure 6.13, and the *x*-axis is scaled logarithmically. Breakthrough of Cr^{VI} was observed after 85 days for the system operating at a flow rate of 24 mL hr^{-1}, and over 240 days for the system operated at 12 mL hr^{-1}. Garnering this data experimentally would have been a very difficult proposition given the immense amount of time required for attainment of breakthrough; so much so, the predictive model serves a very functional purpose of process simulation. Indeed, the results demonstrate the utility of the model, highlighting the importance of performance forecasting under different operational scenarios. The orders of magnitude difference in time scales elucidates the rapidity of treatment technologies as compared to engineered bioremediation systems.

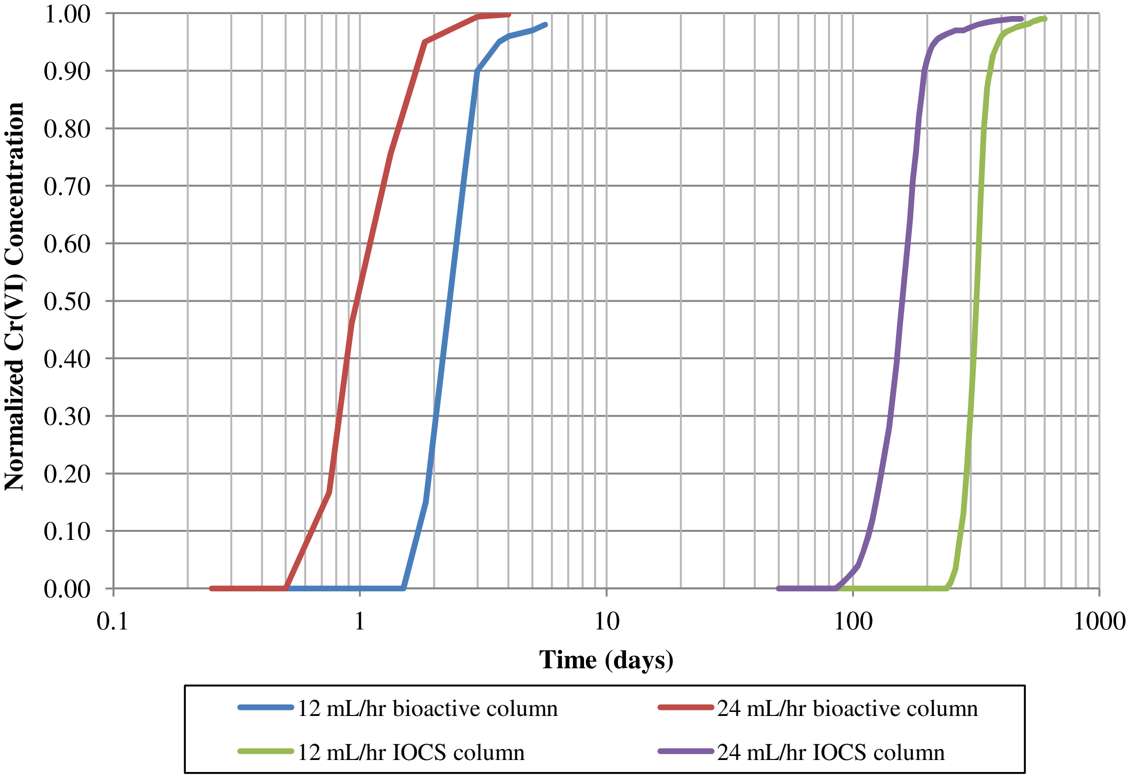

Figure 6.13 Cr^{VI} **transport through a bioactive soil and simulated** Cr^{VI} **transport through IOCS simulating a permeable reactive barrier.**

Model Sensitivity Studies of Process Dynamics

Sensitivity analyses in mathematical modeling presents certain advantages to process desgin and upscaling, that can be briefly summarized as follows: (i) It provides insight into the process dynamics, and quantifies changes in observed variables expected in response to variations in certain parameters and/or dependent variables. Thus, it provides relevant information on process conditions that can be altered by modifying certain parameters to enhance process efficiency. (ii) It offers a method for possible model expansion, reduction, or refinement, taking into consideration the relative importance of various model components. (iii) It enables improvement in methodologies for parameter estimation with reference to uncertainities of observable variables, also indicating certain conditions or features not suitable for such estimations.

There are two basic methods of sensitvity analyses, namely, the global method and the local method. Global methods establish the domains of parameteric importance over entire regions in parameter space, and the sensitivity information represents an ensemble or temporal average. Local methods, on the other hand, seek to find variations in observable variables at fixed points in parameter space. Local methods have more applicability in process modeling than global methods because they are amenable to more straightforward interpretations. Although sensitivity investigations were conducted for several model parameters, only selected parameters that profoundly influenced process dynamics are discussed.

Model prediction and simulation studies are important in determining the process dynamics of the bioactive sand reactors and the IOCS adsorption reactors under a variety of conditions and for optimal process design, operation, and upscaling or downscaling. Model simulation and sensitivity studies with reference to biological, adsorption, transport, and flow parameters provide a balanced evaluation of factors influencing the process dynamics under different scenarios. Their utilities in significantly improving process efficiencies are discussed here from several interrelated perspectives. Model sensitivity analyses were performed for each parameter by varying its value by ± 50 percent (0.5 and 1.5 times the normal values).

Sensitivity Analysis of the Bioactive Sand Reactor System

The results of sensitivity studies for the bioactive sand reactor system are presented in Figures 6.14 to 6.21. It can be easily seen that the process dynamics and the column breakthrough characteristics are strongly influenced by the process flow rate (*Q*) and the influent contaminant concentration. It can be observed that the influences of these two parameters are qualitatively similar. The process dynamics are largely sensitive to changes in the Monod rate parameters μ_{max} and K_s as well as in the yield coefficient Y_a and the biomass density X. These results depicted in Figures 6.16 through 6.19 show that the choice of the microorganism and the electron donor are important in engineering the process dynamics. This justifies the choice of the appropriate microbial species (*Shewanella oneidensis* MR-1) and the electron donor lactate as the carbon source. The choice of a dual carbon source such as lactate and humic acid (30 mg L^{-1}) increases the overall efficiency to some extent as reflected by an increase in μ_{max} and a decrease in $K_{s,}$ while the yield coefficient with respect to Cr^{VI} is approximately the same at 0.3 mg biomass mg^{-1} Cr^{VI}. Among the biological parameters, the Monod microbial decay coefficient k_d had negligible effect on the overall dynamics, and is hence not reported. The initial and maximum biofilm thicknesses L_{f0} and L_{fmax}, respectively, affected the reactor dynamics to a smaller extent than the other biological parameters, as reflected by the results presented in Figures 6.20 and 6.21. The biofilm thickness has a direct bearing on the biomass and enzyme activity, but simultaneously has a slight negative effect on the biofilm diffusion and redox-reaction rates. Therefore, the initial and maximum biofilm thicknesses of magnitudes 5 μm and K_s and 30 μm, respectively have a lesser influence on process dynamics than the Monod parameters, biofilm density and the yield coefficient

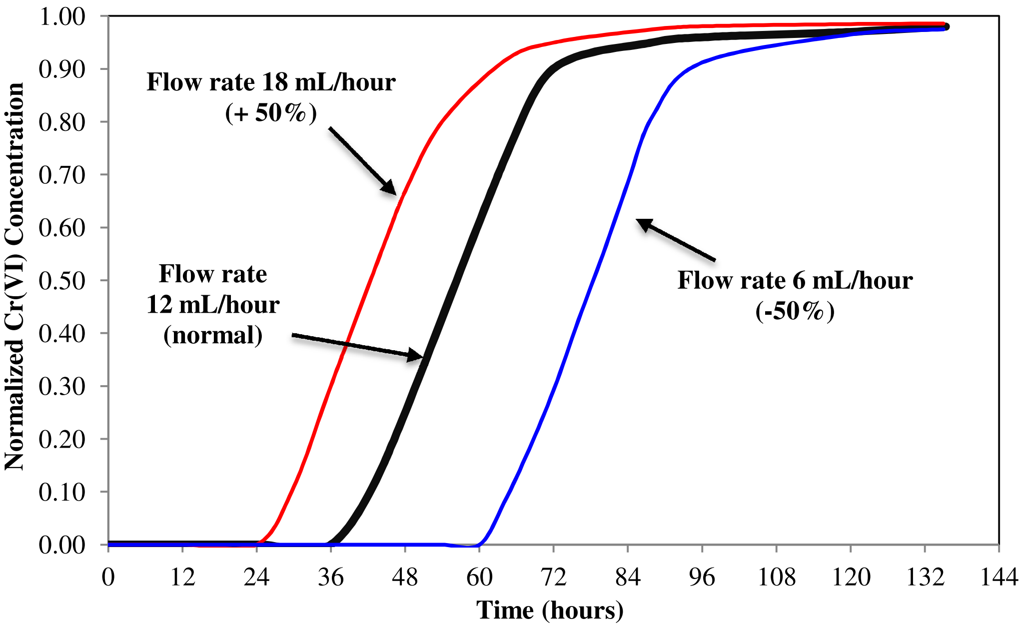

Figure 6.14 Model sensitivity to flow rate for the bioactive sand column.

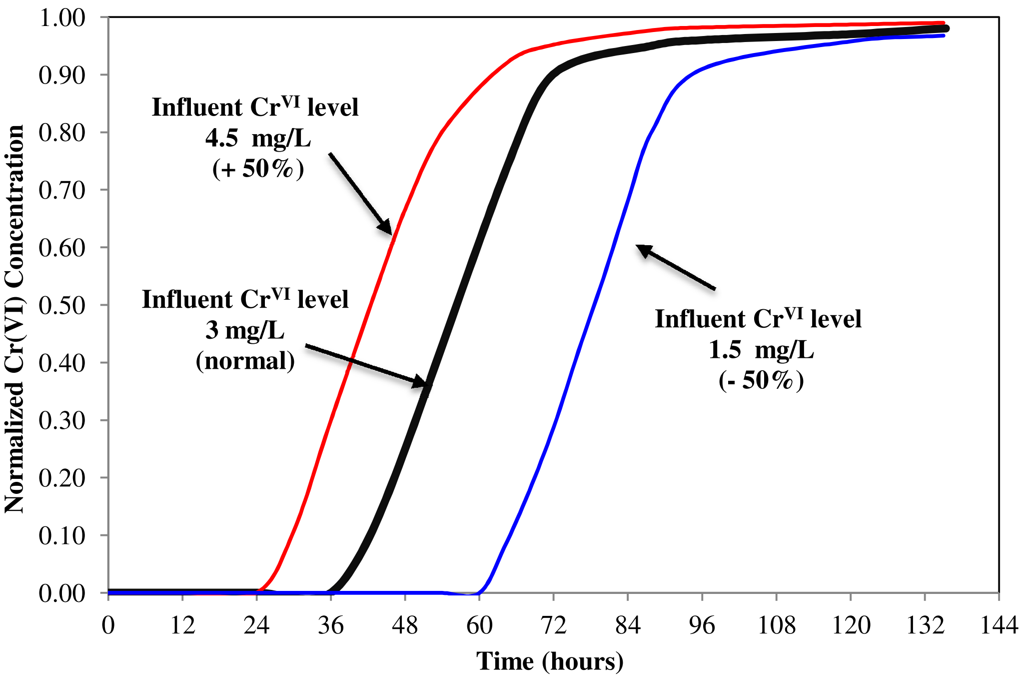

Figure 6.15 Model sensitivity to influent Cr^{VI} concentration to the bioactive sand column.

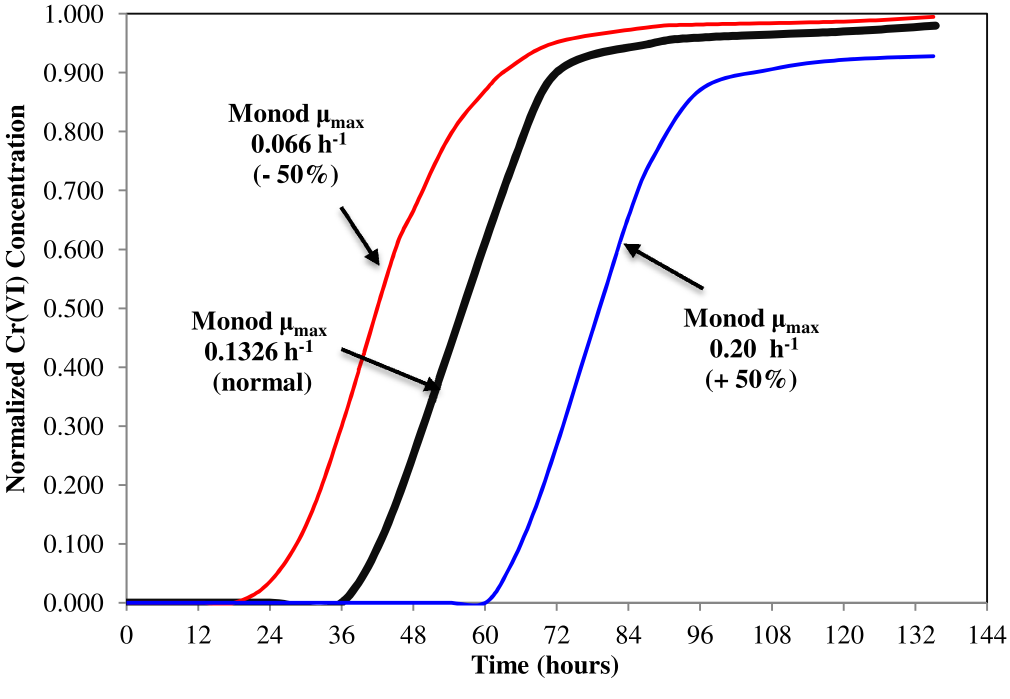

Figure 6.16 Model sensitivity to Monod maximum substrate utilization rate coefficient for the bioactive sand column.

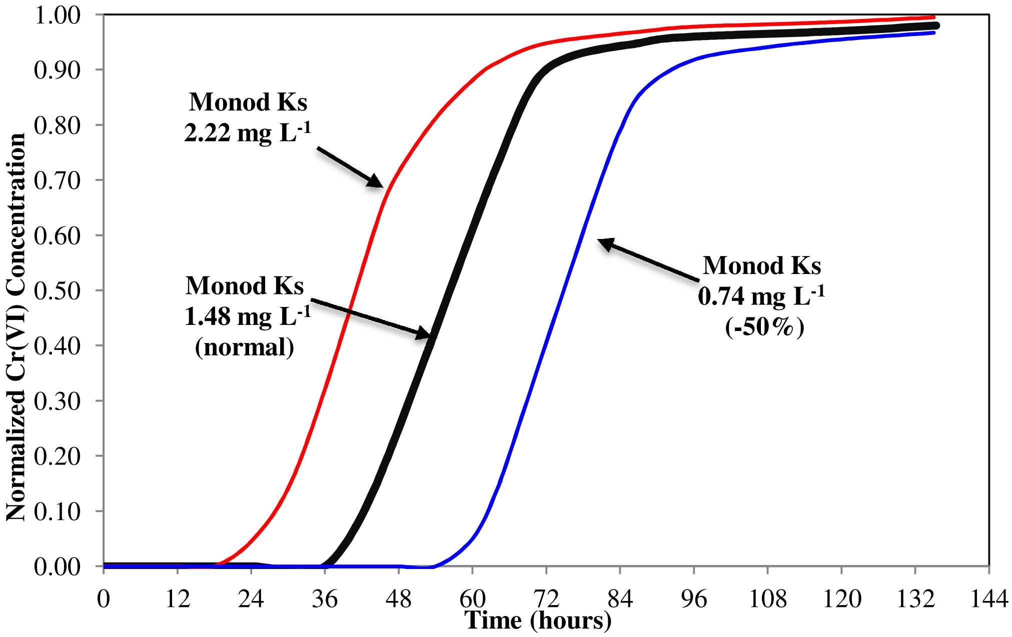

Figure 6.17 Model sensitivity to Monod half saturation coefficient for the bioactive sand column.

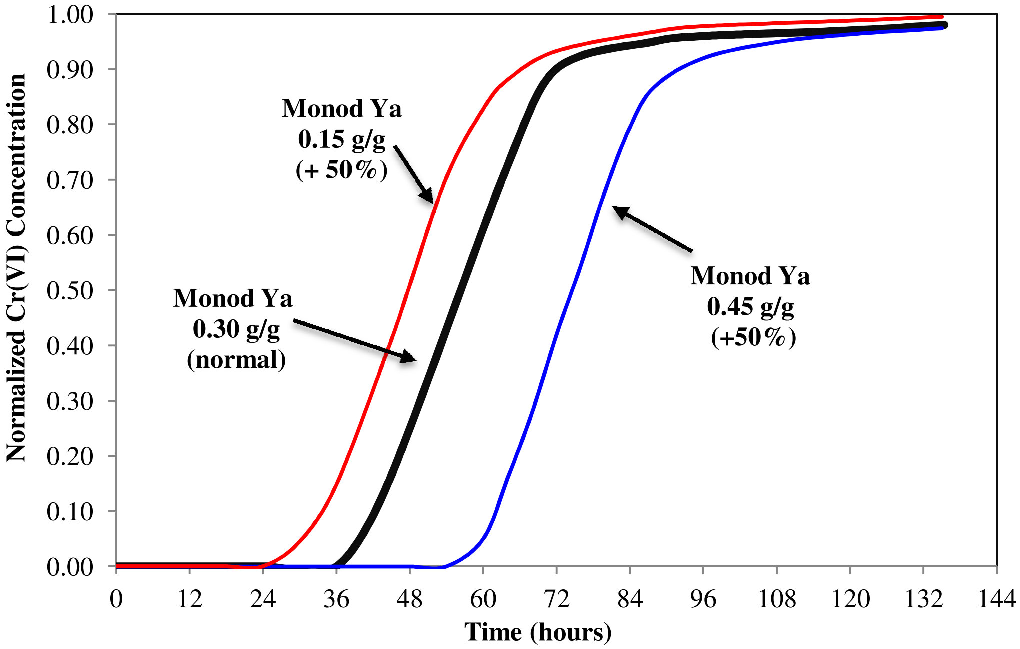

Figure 6.18 Model sensitivity to the Monod microbial yield coefficient for the bioactive sand column.

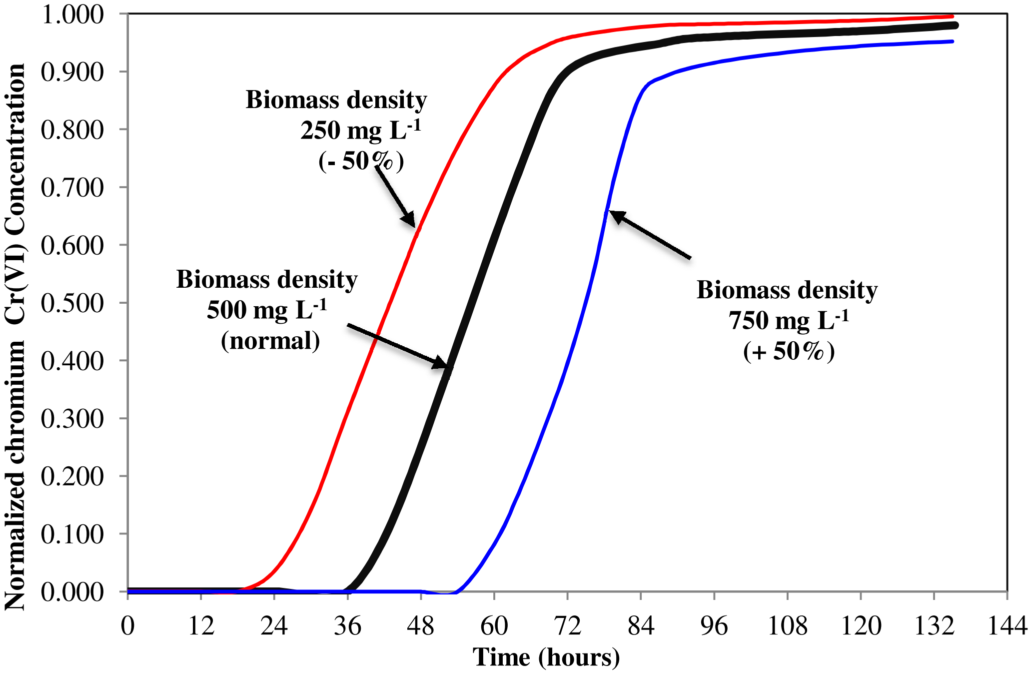

Figure 6.19 Model sensitivity to the biomass density *X* for the bioactive sand column.

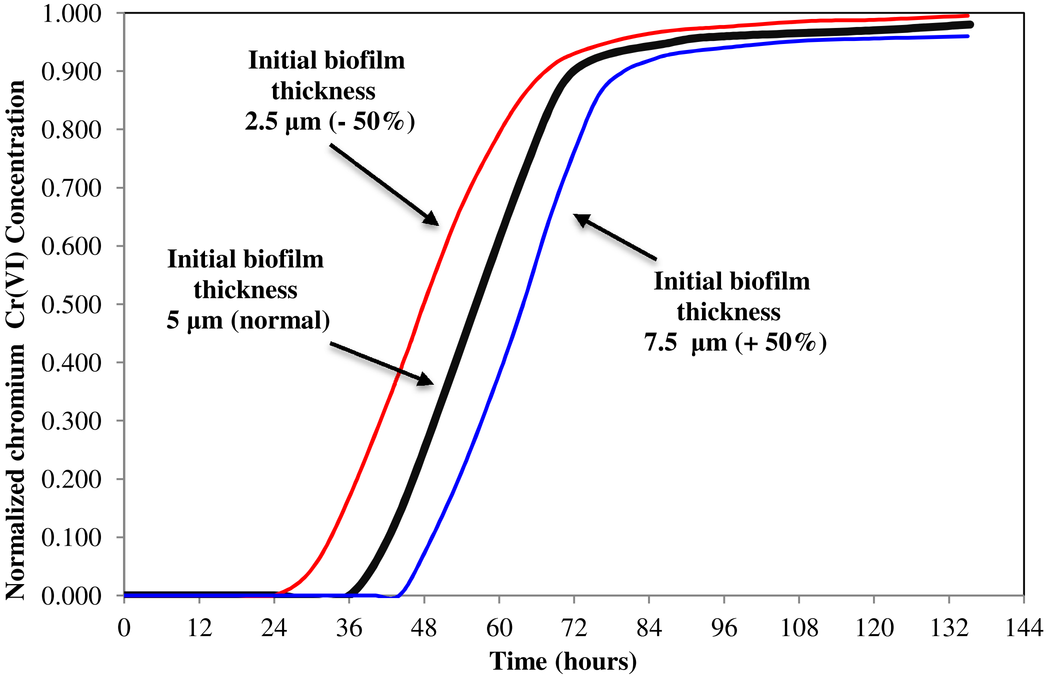

Figure 6.20 Model sensitivity to the initial biofilm thickness L_{f0} for the bioactive sand column.

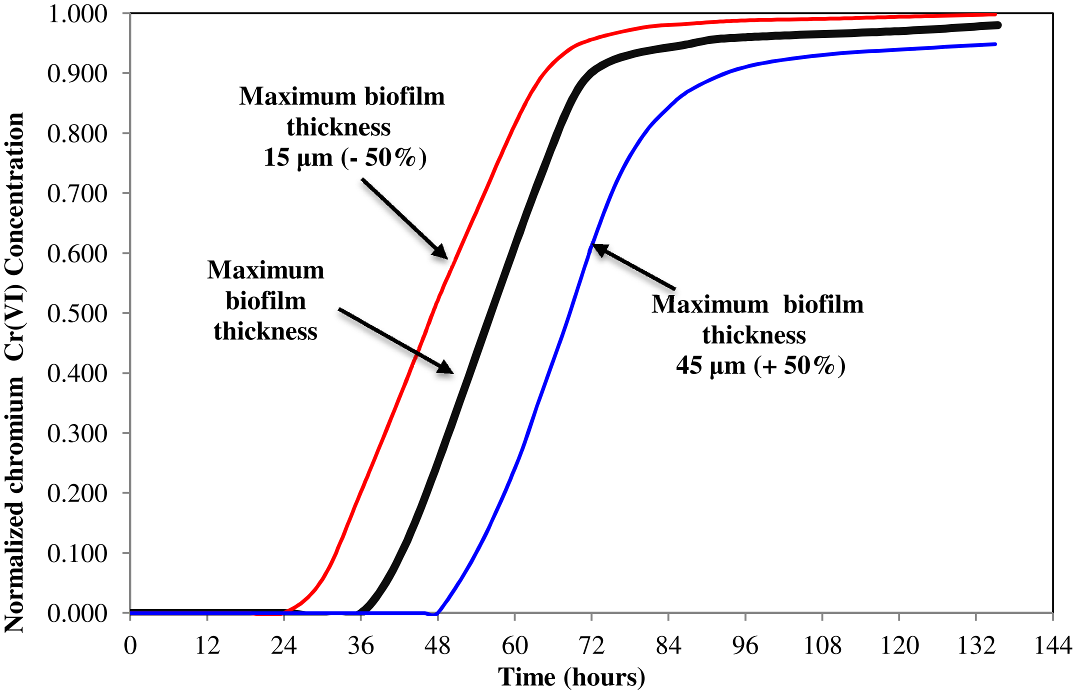

Figure 6.21 Model sensitivity to the maximum biofilm thickness L_{fmax} for the bioactive sand column.

Sensitivity Studies for the IOCS Reactor System Dynamics

The results of sensitivity studies for the adsorptive IOCS reactor system are presented in Figures 6.22 to 6.26. The results clearly demonstrate that the reactor flow rates and the influent contaminant concentrations have strong influences on the column dynamics. Similarly, the adsorbent capacity reflected by the Freundlich parameter K_F has a marked effect on the overall dynamics. The adsorbent diffusivity coefficient D_s and the film transfer coefficient k_f (in principle the column parameter k_{fc} vis-à-vis the batch reactor parameter k_{fb}) for the contaminant have an equally strong influence on the overall dynamics. These results indicate that both the adsorbent capacity and the adsorption rate equally affect the process efficiency towards contaminant removal. This is indeed indicative of the fact that the adsorbent must have favorable sorption stoichiometry or capacity besides desirable outward pore structure for rapid diffusive transport. In this regard, the IOCS appears an excellent adsorbent for the removal of Cr^{VI} even at trace concentration levels with favorable adsorption capacity and rate characteristics.

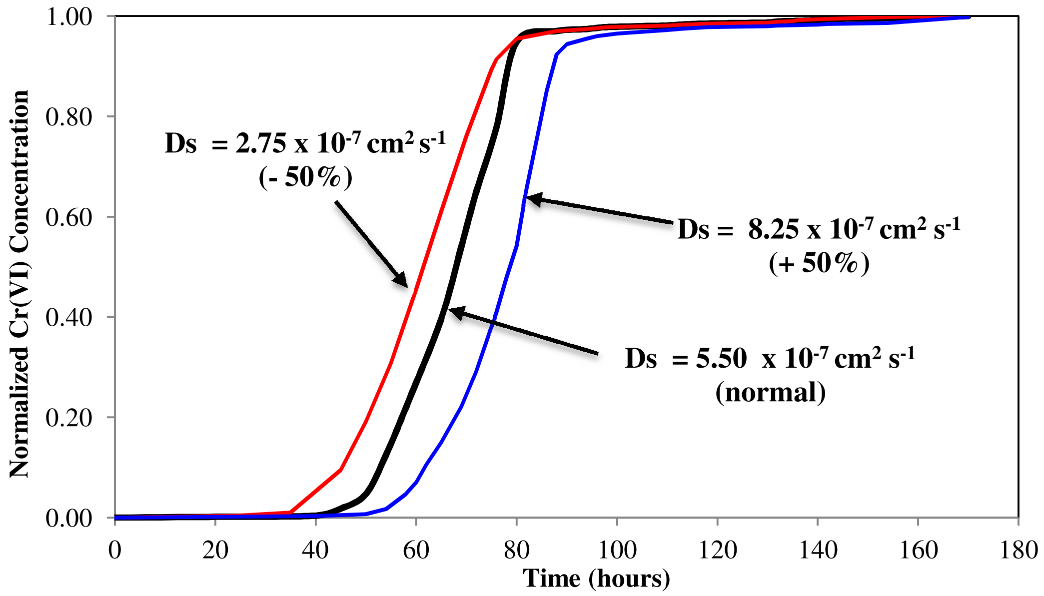

Figure 6.22 Model sensitivity to the surface diffusive coefficient for adsorptive IOCS column

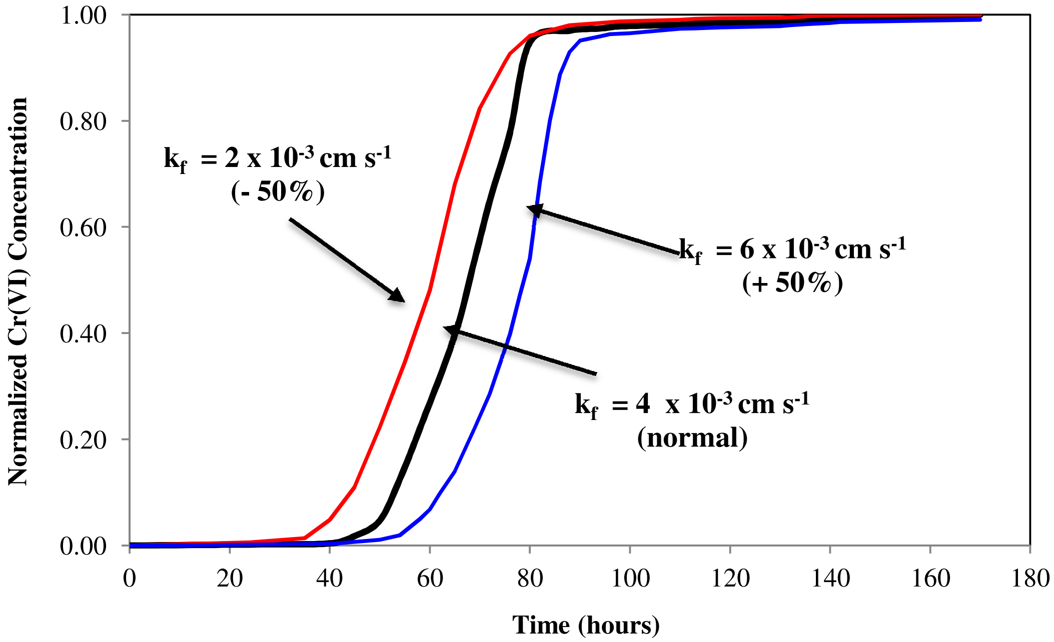

Figure 6.23 Model sensitivity to the film transfer coefficient for adsorptive IOCS column.

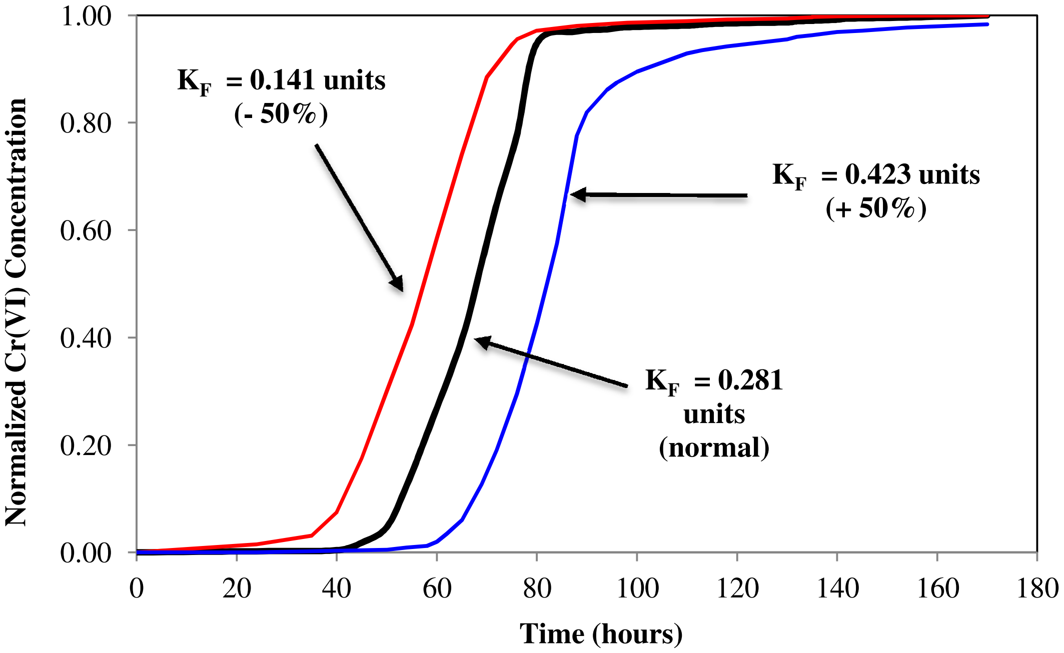

Figure 6.24 Model sensitivity to the Freundlich capacity constant K_F for adsorptive IOCS column.

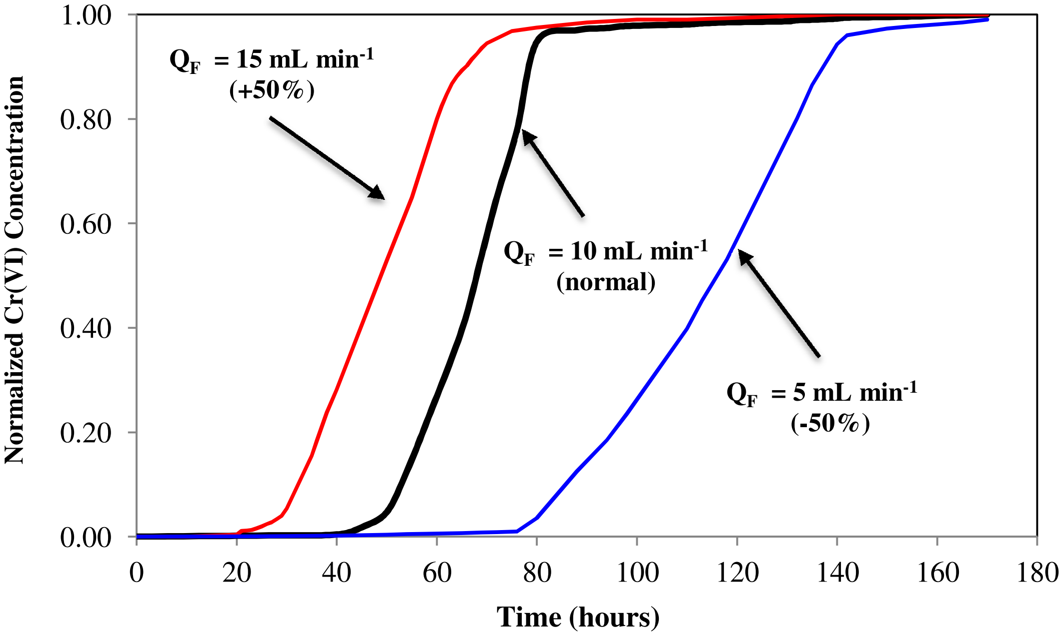

Figure 6.25 Model sensitivity to the flow rate Q for adsorptive IOCS column.

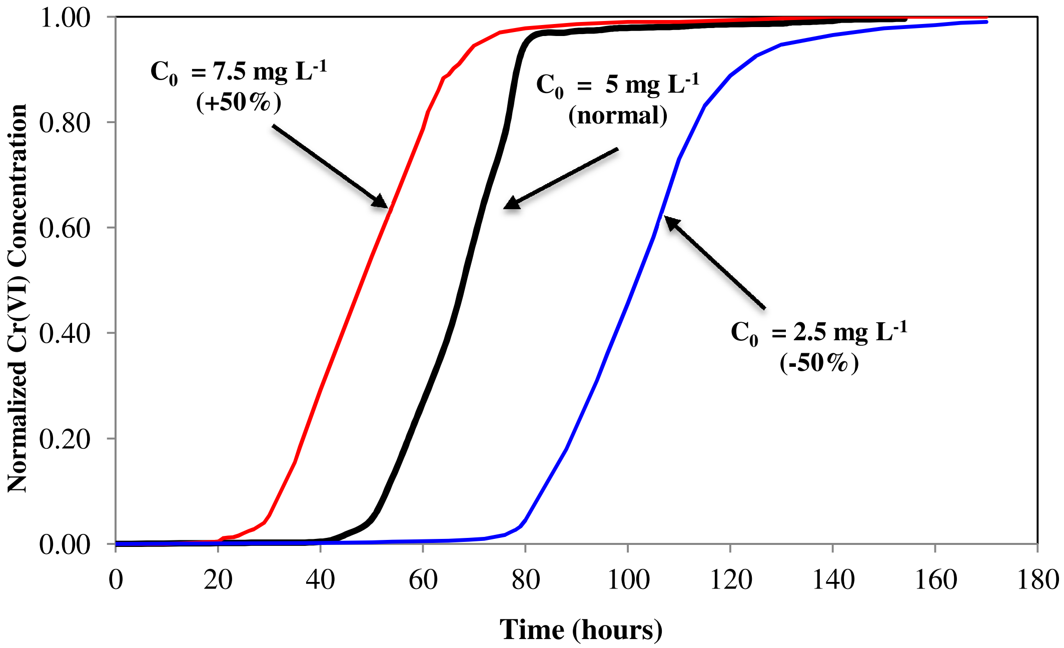

Figure 6.26 Model sensitivity to the influent Cr^{VI} concentration C_0 for adsorptive IOCS column.

6.6 Conclusions

The model sensitivity studies for the bioactive sand reactor system demonstrated that parameters pertaining to biokinetic coefficients and biofilm properties most significantly influenced the steady-state performance bioactive sand reactors. The breakthrough times of 11 and 36 hours for the sand columns operated at 24 and 12 mL h^{-1} (0.4 and 0.2 mL h^{-1}), respectively, are not exactly inversely related to their flow rates. In fact the column operating at half the flow rate is capable of treating more than three times the bed volumes treated by the other column prior to breakthrough. This is understandable because the amount of chromium reduced in the bioactive sand column is not directly related to the capacity of the adsorbent, but is dependent on the kinetics of microbial reduction and contaminant transport into the biofilm.

It must the noted that a high value of the Monod maximum substrate utilization rate coefficient (μ_{max}) indicates rapid substrate degradation due to high enzyme activity, while on the other hand, a high Monod half saturation coefficient K_S indicates resistance of substrate to degradation or metabolization owing to enzyme inhibition or high bond-dissociation energies. Combined activities of enzymes can greatly enhance the biodegradation of substrates or redox reaction energies, resulting in increased or reduced values of these coefficients. Improvements in these parameters could be achieved by a combination of the following factors: strain improvement, biofilm maintenance, and enhanced enzyme activity. Strain improvement through non-recombinant and/or recombinant methods had demonstrated enhancement in kinetics of rate-limiting steps within primary metabolic pathways, and consequent acceleration in metabolic or degradation rates of especially recalcitrant compounds, often reflected by an increase in μ_{max} or decrease in K_S values. The yield coefficient Y_a represents the stoichiometric ratio between the product formed (biomass) and the amount of substrate(s) consumed (Cr^{VI} metabolized or reduced) for that particular process, and is therefore characteristic of the specific microbial population and the substrate(s) utilized (pertaining to both electron donor and the electron acceptor in this case). It is a measure of the ability of the carbon source (lactate) and the electron acceptor (Cr^{VI}) to yield a certain amount of biomass corresponding to a microbial population (*Shewanella oneidensis* MR-1 for instance as in the present situation). A high yield will represent easy metabolization of the substrate(s) to yield the biomass of the desired microbial population. If a combination of substrates is used as a potential carbon source, the yield coefficient is indeed a compounded sum of various intrinsic yield coefficients for various substrates. This is exemplified by the use of lactate and humic acid as dual carbon source substrates in the bioactive sand reactors. The decay coefficient k_d is a measure of the microbial die-off rate and is important in determining the bacterial life span and sustainability. A detailed review on these aspects is presented by Vinci and Byng.[59]

Additionally, biofilm density, biofilm thickness, and biomass concentrations are critical parameters controlling the process dynamics. In general, for a given type and concentration of a limiting substrate, an "optimal balance" between biofilm density and thickness is required to maximize both substrate utilization and mass-transfer rates. Environmental factors such as limiting substrate types (electron donor and acceptor systems), nutrient limitations, ionic strength, and substrate compositions significantly influence biofilm and biomass characteristics.[58] Other than these parameters, the flow rate and the influent concentration may influence the reactor dynamics based on the overall mass throughput of the contaminant and the mass-transfer characteristics modified by the flow properties.

IOCS was shown to be very effective for Cr^{VI} removal. The IOCS column dynamics indicated that the breakthrough times are approximately inversely proportional to influent flow rate and also largely dependent on influent Cr^{VI} concentration. The Freundlich parameters were determined to be significant in process dynamics as well, as adsorption is considered the only Cr^{VI} removal mechanism. Model predictions extrapolated back to groundwater-like flow rates indicated IOCS could be successfully implemented as a permeable reactive barrier. In these simulations, the IOCS column was shown to have Cr^{VI} breakthrough after 85 days for a system flowing at 12 mL hr^{-1}, and 240 days for a system with flow rate of 12 mL hr^{-1}. In this work, the predictive model was verified by accurately depicting experimental data, and then used to simulate Cr^{VI} removal by IOCS as a permeable reactive barrier under typical groundwater flow conditions. The advantages of numerical flow and reactive transport models were shown here in the successful assessment of an IOCS permeable reactive barrier for groundwater remediation.

Notations

K_S	half saturation coefficient (mg/L)
K_I	inhibition coefficient (mg/L)
S	substrate concentration
μ	specific growth rate of microorganisms or biomass (h^{-1})
μ_{max}	maximum specific substrate utilization rate (h^{-1})
X	biomass concentration (dry weight) (mg/L)
Y	biomass yield coefficient (mg/mg)

Subscripts

1	first species present among mixed substrates
2	second species present among mixed substrates
3	third species present among mixed substrates
4	fourth species present among mixed substrates
G	growth substrate
i	species i, one of the components in the mixture of substrates
I	interacting species among mixed substrates
n	number of substrates present
N	non-growth substrate

Nomenclature

a_p = Total surface area available for mass transfer on the medium particle (L^2 , cm^2)
$C_{f,o}$ = Initial biofilm concentration (M/L^3, mg/L)
$C_{f,o}$ = Initial biofilm thickness (µm, L)
C = Bulk substrate concentration at any time t in the reactor (M/L^3, mg/L)
C_o = Influent substrate concentration (M/L^3, mg/L)
C_f = Substrate concentration within biofilm (M/L^3, mg/L)
$C_{f,s}$ = Substrate concentration at biofilm-hydrodynamic layer interface (M/L^3, mg/L)
d_p = Diameter of the medium particle (L, cm)
D_f = Biofilm substrate diffusion coefficient (L^2/T, cm^2/s)
D_l = Free liquid diffusivity (L^2/T , cm^2/s)
D_x = Axial substrate dispersion coefficient (L^2/T, cm^2/s)
Ga = Galileo number (dimensionless)
g = Gravitational acceleration (L/s^2, cm/s^2)
$k_{d,a}$ = Endogenous decay coefficient (1/T)
k_f = Substrate mass transfer coefficient (L/T)
$K_{s,a}$ = Half saturation constant (M/L^3, mg/L)
L = Length of the fluidized bed reactor (L, cm)
L_f = Biofilm thickness at any time t (L, µm)
L_{f0} = Initial biofilm thickness (at time zero) (L, µm)
$L_{f,max}$ = Maximum biofilm thickness (L, µm)

P_n = Number of media particles used for biofilm and biomass measurements (dimensionless)
Q = Fluid flow rate (L^3/T)
Q_r = Recycled fluid flow rate (L^3/T)
r = radial coordinate (L, cm)
r_f = Radial direction normal to the surface of the biofilm (L, cm)
R = Radius of the medium particle (L, cm)
R = the gas constant,
Re = Reynolds number (dimensionless)
Re_{mdf} = Modified Reynolds number (dimensionless)
Sc = Schmidt number (dimensionless)
Sh = Sherwood number (dimensionless)
t = Reaction time (T, h)
t_{max} = Time at which the biofilm thickness reaches its maximum value (T, h)
T = absolute temperature (K).
x = Axial coordinate (L)
X_f = Biomass density within the biofilm (M/L^3, mg/L)
X_l = Biomass concentration in liquid bulk phase (M/L^3, mg/L)
$X_{l,o}$ = Initial bulk liquid phase biomass concentration at time zero (M/L^3, mg/L)
X_o = Influent biomass concentration (M/L^3, mg/L)
$X_{l,f}$ = Biomass concentration that is lost from biofilm to liquid bulk phase (M/L^3, mg/L)
Y_a = Yield coefficient (M/M, mg biomass/mg of Cr(VI) reduced)

Greek symbols
ΔV = Volume of bed expansion due to growth of biomass (L^3, cm^3)
ε = Bed porosity (dimensionless)
λ_1, λ_2 = Limiting equivalent conductances of the metal ions and the corresponding anions, respectively in a salt molecule (mho/equivalent)
μ = Fluid viscosity (M/L.T, g/cm.s or poise)
$\mu_{m,a}$ = Maximum specific growth rate (1/T, s^{-1} or h^{-1})
v_1, v_2 = Numbers of the metal ions and the corresponding anions, respectively in a salt molecule
(mho/equivalent)
v_s = Superficial fluid velocity (L/T, cm/sec)
v_x = Interstitial fluid velocity (L/T, cm/sec)
ρ_a = Apparent density of medium particle (M/L^3, g/cm^3)
ρ_l = Fluid density (M/L^3, g/cm^3)
ρ_s = Actual density of medium particle when covered with biofilm (M/L^3, g/cm^3)

6.7 Chapter 6 References

1. Belchik, S.M., Kennedy, D.W,, Dohnalkova, A.C., Wang, Y., Sevinc, P.C., Wu, H., Lin, Y., Lu, H.P., Fredrickson, J.K., and Shi, L. (2011). Extracellular reduction of hexavalent chromium by cytochromes MtrC and OmcA of Shewanella oneidensis MR-1. Applied and Environmental Microbiology, 77 (12), 4035-404 (June issue, 2001).

2. Beliaev, A.S., Saffarini, D.A., McLaughlin, J.L., and Hunnicut, D. (2001). MtrC, an outer membrane decahaem c cytochrome required for metal reduction in Shewanella putrefaciens MR-1. Molecular Mirobiology, 39 (3), 722-730.

3. Brutinel, E., J. Gralnick (2012), Shuttling Happens: soluble flavin mediators of extracellular electron transfer in Shewanella. *Appl Microbiol Biotechnol. 93: 41-48.*

4. Guha, H., Jayachandran, K., and Maurrasse, F. (2001). Kinetics of chromium (VI) reduction by a type strain Shewanella alga under different growth conditions. Environmental Pollution, 115(2), 209-218.

5. Guha, H., Jayachandran, K., and Maurrasse, F. (2003). Microbiological reduction of chromium(VI) in presence of pyrolusite-coated sand by Shewanella alga simidu ATCC 55627 in laboratory column experiments. Chemosphere, 52, 175-183.

6. Han, R., Geller, J.T., Yang, L., Brodie, E.L., Chakraborty, R., Larsen, J.T., and Beller, H.R. (2010). Physiological and transcriptional studies of Cr(VI) reduction under aerobic and denitrifying conditions by an aquifer-derived pseudomonad. Environmental Science and Technology, 44 (19), 7491-7497.

7. Tebo, B.M, and Obraztsova, A.Y. (1998). Sulfate-reducing bacterium grows with Cr(VI), U(VI), Mn(IV), and Fe(III) as electron acceptors. FEMS Microbiology Letters, 162 (1), 193-198. (Federation of European Microbiological Societies).

8. Myers, J.M., and Myers, C.R. (2001). Role for outer membrane cytochromes OmcA and OmcB of Shewanella putrefaciens MR-1 in reduction of manganese dioxide. Applied and Environmental Microbiology, 67(1), 260-269.

9. von Canstein H, Ogawa J, Shimizu S, Lloyd JR, (2008) Flavin Electron Shuttles Dominate Extracellular Electron Transfer by *Shewanella oneidensis, Appl. Environ. Microbiol.*, 74:615-623.

10. Viamajala, S., Peyton, B. M., & Petersen, J. N. (2003). Modeling chromate reduction in Shewanella oneidensis MR-1: development of a novel dual-enzyme kinetic model. *Biotechnology and bioengineering*, *83*(7), 790–7.

11. Kim, S.H. and Pirbazari, M. (1989) Bioactive adsorber model for industrial wastewater treatment. Journal of Environmental Engineering, 115 (6), 1235–1256

12. Badriyha, B.N., Ravindran, V., and Pirbazari, M. (2003) Bioadsorber efficiency, design, and performance forecasting for alachlor removal. *Water Research,* 37, 4051-4072.

13. Tsai, H.H., Ravindran, V., Williams, M.D., Pirbazari, M., 2004. Forecasting the performance of membrane bioreactor process for groundwater denitrification. Journal of Environmental Engineering Science 3 (6), 507-521.

14. Tsai, H.H, Ravindran, V., and Pirbazari, M. (2005) Model for predicting the performance of membrane bioadsorber reactor process in water treatment applications. Chemical Engineering Science, 60, 5620–5636

15. Williams, M., V. Ravindran, Pirbazari, M. (2012) Modeling and process evaluation of membrane bioreactor for removal of biodegradable organic matter from water, *Chemical Engineering Science*, 84, 494-511.

16. Bailey, R.P., T. Bennet, and M.M. Benjamin (1992), Sorption onto and Recovery of Cr(VI) using Iron oxide-Coated Sand, *Wat. Sci. Tech.,* 26(5-6):1239-1244.

17. Benjamin, M.M., R.S. Sletton, R.P. Bailey, T. Bennet (1996), Sorption and filtration of metals using iron oxide-coated sand, *Water Resources*, 30(11)2609-2620.

18. Davis, J.A. and Leckie J.O. (1978) Effect of adsorbed complexing ligands on trace metal uptake by hydrous oxides. *Environ. Sci. and Technol.* 12, 1309-1315.

19. Venkateswaran, K., Moser, D.P., Dollhopf, M.E., Lies D.P., Saffarini, D.A., MacGregor, B.J., Ringelberg, D.B., White, D.C., Nishijima, M., Sano, H., Burghart, J., Stackebrandt, E., and Nealson, K.H. (1999). Polyphasic taxonomy of the genus Shewanella and description of *Shewanella oneidensis sp. nov*. *International Journal of Systemic Bacteriology*, 49(2), 705–24.

20. Hau, H.H., and Gralnick, J.A. (2007). Ecology and biotechnology of the genus *Shewanella*. Annual Review of Microbiology, 6, 237-258. [Review, October 2007].

21. MacDonell M.T., and Colwell, R.R. (1985). Phylogeny of the *Vibrionaceae*, and recommendation for two new genera, *Listonella and Shewanella*. Systematic and Applied Microbiology, 6 (2), 171–82.

22. Beliaev, A., and Saffarini, D. (1998). Shewanella putrefaciens mtrB encodes an outer membrane protein required for Fe(III) and Mn(IV) reduction. Journal of Bacteriology, 180 (23), 6292-6297.

23. Nealson, K., and Saffarini, D. (1994). Iron and manganese in anaerobic respiration: environmental significance, physiology, and regulation. Annual Review of Microbiology, 48, 311-343.

24. Myers, C.R., and Myers, J.M. (1997). Outer membrane cytochromes of Shewanella putrefaciens MR-1: spectral analysis, and purification of the 83-kDa c-type cytochrome. Biochimica et Biophysica Acta, 1326 (2), 307-318.

25. Gaspard, S., Vasquez, F., and Holliger, C. (1998). Localization and solubilization of the iron (III) reductase of Geobacter sulfurreducens. Applied and Environmental Microbiology, 64 (9), 3188-3194.

26. Myers, J.M., and Myers, C.R. (2000). Role of the tetraheme cytochrome CymA in anaerobic electron transport in cells of Shewanella putrefaciens MR-1 with normal levels of menaquinone. Journal of Bacteriology, 182 (1), 67-75.

27. Myers, C.R., and Myers, J.M. (1992). Localization of cytochromes to the outer membrane of anaerobically grown Shewanella putrefaciens MR-1. Journal of Bacteriology, 174 (11), 3429-3438

28. Gordon, E., Pike, A., Hill, A., Cuthbertson, P., Chapman, S., and Reid, G. (2000). Identification and characterization of a novel cytochrome c3 from Shewanella frigidimarina that is involved in Fe(III) respiration. Biochemical Journal, 349 (2), 153-158.

30. Dries, J., L. Bastiaens, D. Springael, S. Kuypers, S.N. Agathos, and L. Diels (2005) Effect of humic acids on heavy metal removal by zero-valent iron in batch and continuous flow column systems, *Water Research,* 39:3531-3540.

31. Shariatmadari, N., Weng, C., Daryaee, H., Engineering, C., & Iust, T. (2009). Enhancement of Hexavalent Chromium [Cr(VI)] Remediation from Clayey Soils by Electrokinetics Coupled with a Nano-Sized Zero-Valent Iron Barrier. *Environmental Engineering Science*, *26*(6).

32. Li, X., Elliott, D. W., & Zhang, W. (2006). Zero-Valent Iron Nanoparticles for Abatement of Environmental Pollutants□: Materials and Engineering Aspects, 111–122.

33. Ahammed, M.M., and V. Meera (2010) Metal oxide/hydroxide-coated dual media filter for simultaneous removal of bacteria and heavy metals from natural waters. *Journal of Hazardous Materials,* 181:788-793.

34. Mak, M.S.H., P. Rao, and I.M.C. Lo (2010), Zero-valent iron and iron oxide coated sand as a combination for removal of co-present chromate and arsenate from groundwater with humic acid, *Environmental Pollution*, 159:377-382.

35. Joshi, A., and M. Chaudhuri (1996) Removal of Arsenic from Ground Water by Iron Oxide-Coated Sand, *Journal of Environmental Engineering*, 122(8):769-771.

36. Hsu, J.-C., C.-J. Lin, C.-H. Liao, and S.-T. Chen (2008) Removal of As(V) and As(III0 by reclaimed iron oxide coated sands. *Journal of Hazardous Materials*, 153:817-826.

37. Benjamin M.M. and Bloom N.S. (1981) Effects of strong binding of anionic adsorbates on adsorption of trace metals on amorphous iron oxyhydroxide. In *Adsorption from aqueous solution* (Edited by Tewari P.), pp 41-60. Plenum Press, New York.

38. Rai, D., Eary, L. E., & Zachara, J. M. (1989). Environmental chemistry of chromium. *Science of The Total Environment*, *86*(1-2), 15–23.

39. Lee, T., Lim H., Lee, Y., Park, J. (2003) Use of waste iron metal for removal of Cr(VI) from water. *Chemosphere* 53, 479-485.

40. Littlejohns, J.V., and Daugulis, A.J. (2008). Kinetics and interactions of BTEX compounds durign degradation by a bacterial consortium. Process Biochemistrym 43 (1), 1068-1076.

41. Chang, M.K., Voice, T.C., and Criddle, C.S. (1993). Kinetics of competitive inhibition and cometabolism in the biodegradation of benzene, toluene, and p-xylene by two Pseudomonas isolates. Biotechnology and Bioengineering, 41 (11), 1057-1065 [May 1993 issue].

42. Ravindran, V., Pirbazari, M., Kim, S.H., Badriyha, B.N., 1996. Modeling of bioactive carbon adsorbers: a hybrid weighted residual-finite difference numerical technique. Ap.plied Mathematics and Computation, 76, 99-128.

43. Ravindran, V., Kim, S.H., Badriyha, B.N., Pirbazari, M., 1997. Predictive modeling for bioactive fluidized bed and stationary bed reactors: application to dairy wastewater. Environmental technology, 18, 861-884.

44. Villadsen, J.V., Stewart, W.E., 1967. Solution of boundary-value problems by orthogonal collocation. Chemical Engineering Science 22(11), 1483-150245. Finlayson, B.A., 1972. The Method of weighted residuals and variational principles. Academic Press, New York.

46. Finlayson, B. A., 1980. Nonlinear Analysis in Chemical Engineering. Mc-Graw-Hill, New York.

47. Jain, M.K., 1985. Numerical solution of differential equations. John Wiley and Sons, New York.

48. Chung, S.F., Wen, C.Y., 1968. Longitudinal dispersion of liquid flowing through fixed and fluidized beds. AIChE Journal 14(6), 857-866.

49. Green, D.W., Perry, R.H., eds., 2008. Perry's Chemical Engineer's Handbook, Eighth edition, McGraw-Hill, New York.

50. Williamson, J. E., Bazaire, K. E., Geankoplis, C. J., 1963. Liquid-phase mass transfer at low Reynolds numbers. Industrial and Engineering Chemistry Fundamentals, 2, 126

51. Hsu, L., S. Masuda, K.H. Nealson, and M. Pirbazari (2012) Evaluation of microbial fuel cell *Shewanella* biocathodes for treatment of chromate contamination, *RSC Advances*, 2, 5844-5855

52. Heidelberg JF, Paulsen IT, Nelson KE, Gaidos EJ, Nelson WC *(2002)* Genome sequence of the dissimilatory metal ion-reducing bacterium Shewanella oneidensis, *Nat Biotechnol.,* 20:1118-23.

53. Gorby, Y.A., S. Yanina, J.S. McLean, K.M. Rosso, D. Moyles, A. Dohnalkova, T.J. Beveridge, I.S. Chang, B.H. Kim, K.S. Kim, D.E. Culley, S.B. Reed, M.F. Romine, D.A. Saffarini, E.A. Hill, L. Shi, D.A. Elias, D.W. Kennedy, G. Pinchuk, K. Watanabe, S.i. Ishii, B. Logan, K.H. Nealson, J.K. Fredrickson, Electrically conductive bacterial nanowires produced by Shewanella oneidensis strain MR-1 and other microorganisms, *Proc. Natl. Acad. Sci. U. S. A.* 103 (2006) 11358–11363.

54. Marsili E., D.B. Baron, I.D. Shikhare, D. Coursolle, J.A. Gralnick, and D.R. Bond (2008) *Shewanella* secretes flavins that mediate extracellular electron transfer*Proc. Natl. Acad. Sci. U. S. A.,*105, 3968-3973.

55. Gear, C.W., 1971a. The automatic integration of ordinary differential equations. Communications of the Association of Computing Machinery 14, 176-179

56. Gear, C.W., 1971b. DIFSUB for solution of ordinary differential equations. Communications of the Association of Computing Machinery 14, 185-190.

57. Gear, C.W., 1976. Numerical initial value problems in ordinary differential equations. , Prentice-Hall, Engelwood Cliffs, New Jersey

58. Sutherland I.W., 1994. Structure-function relationships in microbial exopolysaccharides. *Biotechnology Advances* 12 (2), 393-448.

59. Vinci V.A., Byng G., 1999. Strain improvement by nonrecombinant methods, in : Demain A.L., Davies J.E., Atlas, R.M. (Eds.), Manual of Industrial Microbiology and Biotechnology, second ed., American Society for Microbiology (ASM) Press, Washington DC., Chap. 8, pp. 103-113.

60. Wakao, N., Funazkri, T., 1978. Effects of fluid dispersion coefficients on particle-to-fluid mass transfer coefficients in packed beds. *Chemical Engineering science*, 33(10), 1375-1384.

61. Pirbazari, M., Ravindran, V., Badriyha, B.N., Craig, S.L., McGuire, M.J., 1993. GAC adsorber design protocol for the removal of off-favors. *Water research*, 27, 1153.

62. Pirbazari, M., Ravindran, V., Badriyha, B.N., Kim, S.H., 1996. Hybrid membrane filtration process for leachate treatment. *Water Research* 30 (11), 2691-2706.

63. G.V. Korshin, M.M. Benjamin, R.S. Sletten, Adsorption of natural organic matter (NOM) on iron oxide: effects on NOM composition and formation of organo-halide compounds during chlorination Water Res., 31 (1997)

64. Gu, B., Schmitt, J., Chen, Z., Liang, L., & McCarthy, J. F. (1994). Adsorption and desorption of natural organic matter on iron oxide: mechanisms and models. *Environmental Science & Technology*, *28*(1), 38–46.

65. Lai, C. H., & Chen, C. Y. (2001). Removal of metal ions and humic acid from water by iron-coated filter media. *Chemosphere*, *44*(5), 1177–84.

66. Mak, M. S. H., Lo, I. M. C., & Liu, T. (2011). Synergistic effect of coupling zero-valent iron with iron oxide-coated sand in columns for chromate and arsenate removal from groundwater: Influences of humic acid and the reactive media configuration. *Water research*, *45*(19), 6575–84

Chapter 7 : Summary, Conclusions, and Recommendations

The objective of this research was to investigate the integration of electrokinetic contaminant transport with two emerging technologies for the remediation of Cr^{VI} in groundwater: zero-valent iron nanoparticles, and microbial fuel cell technology. Furthermore, this study aimed to evaluate of the effects of natural organic matter on these treatment technologies, as natural organic matter is ubiquitous in the environment and can be a significant factor in most remediation efforts. The following summaries and conclusion can be made upon the results and discussion presented herein.

7.1 Summary

The examination of surface bound and dissolved natural organic matter and their effects on the redox chemistry of Cr^{VI} were evaluated in two distinct clay soils, EPK kaolin and kaolinite. An organic layer naturally coating the EPK kaolin was found to play an important role in adsorption and reduction rate studies, whereas kaolinite exhibited predictable adsorption behavior. The Langmuir adsorption isotherm model was found to accurately describe adsorption behavior for both clay soils. After a 24-hour equilibration period, the adsorption capacities were determined to be 1.75 and 1.25 μg Cr^{VI} per g clay for EPK kaolin and kaolinite, respectively. Reduction rate studies showed that over a period of days EPK kaolin could reduce significantly more Cr^{VI} than the 24-hour isotherm data indicated. It was shown that reduction rate was enhanced in the presence of high concentrations of dissolved humic acid amended to reaction vessels. An FTIR examination of the surface bound natural organic matter on the EPK kaolin indicated that it predominantly contained carboxylic/carbohydrate groups, peptide moieties, and a strong presence of lignin. These groups are all considered to be active in the complexation and reduction of Cr^{VI}. It was concluded from these studies that surface bound natural organic matter resulted in much faster chromium reduction as compared to dissolved natural organic matter.

In the electrokinetic transport experiments using the clay soils, Cr^{VI} transport was found to be effective in the kaolinite clay soil only within the first 24 hours of electric potential application. The transport of Cr^{VI} through EPK kaolin was inconclusive due to a rapid reduction of Cr^{VI} by the NOM bound on the EPK kaolin surface. Further, the electrokinetic experiments involving both soils highlighted the adverse effects of pH gradient formation resulting from electrolysis reactions at the anode and cathode that has been well documented in literature.

It was found that the ability to transport contaminants by electrokinetic phenomena has the potential to be beneficial when integrated with different treatment technologies, such as nZVI. Many research groups are working to address the problems associated with nZVI transport through groundwater to reach contaminants, however this study shows that electrokinetic transport of contaminants to the point of nZVI injection may offer a realistic solution. In this approach, nZVI can be injected to a target location containing a high concentration of contaminants, transported electrokinetically. The results observed in the clay-soil electrokinetic studies and the multiple unsuccessful attempts to evenly disperse nZVI in the clay soils prompted an impetus to use more hydraulically-conductive soils. The silica sand that was chosen to substitute for the clay soils was representative of a typical subsurface material encountered in groundwater extraction operations. Further, it was used in the continuous-flow experiments that were carried out to simulate groundwater flow.

Before any electrokinetic column experiments were conducted to investigate the application of nZVI in a sandy soil, an investigation into the reduction-adsorption capacity of nZVI was carried out. Conditions varied in oxygen concentration (to simulate actual groundwaters of varying depth), humic acid concentration (to serve as a proxy for NOM), and divalent ion concentration (to represent hardness). The highest adsorption-reduction capacity was 350 mg Cr^{VI} per g nZVI for the system void of oxygen, humic acid, and divalent ions. Aerated water was found to most significantly reduce the adsorption-reduction capacity of nZVI for Cr^{VI}, and the presence of humic acid was found to further inhibit Cr^{VI} reduction. Humic acid was found to rapidly bind to nZVI, exhausting the reactivity of the nZVI, occupying reactive surface sites, and complexing nZVI corrosion byproducts that have the capacity to reduce Cr^{VI}.

Further, electrokinetic experiments were performed in sandy soil under flow-through conditions with frequent nZVI injection near the anode, the point of Cr^{VI}

accumulation. Results indicated that transporting Cr^{VI} towards the point of injection was highly advantageous. Humic acid introduced to the column feed solution was shown to reduce the amount of Cr^{VI} reduction, however not by more than about 10 percent. Additionally, it was discovered that in a continuous flow system with flow rates comparable to that of groundwater in a sandy soil, pH gradient formation didn't occur and thus electrokinetic transport was effective for the duration of each experiment. Lastly, it was determined that a large stoichiometric excess of nZVI was required for adequate Cr^{VI} removal from the sand column, due to rapid nanoparticle oxidation, aggregation, and interactions with sand particles.

Following the investigations of electrokinetic transport integrated with nZVI injection, focus shifted towards the integration of electrokinetic transport with biological treatment. This integrated treatment approach simulated a pump and treat system, with treatment occurring in the cathode of a microbial fuel cell (MFC) charged with a *Shewanella oneidensis* MR-1 culture. Cr^{VI} was transported through the sandy soil from an applied electric potential and pumped to the cathode of the MFC as, a) a semi-batch study, and b) as a continuous-flow system. The presence and absence of humic acid was evaluated in each set of experiments. Results of this study suggested that Cr^{VI} transport by electrokinetic phenomena enhanced the MFC power production by supplying the cathode compartment with a higher concentration of electron acceptors. In the semi-batch experiments, pre-concentrating Cr^{VI} at the anode reservoir of the electrokinetic cell by electrokinetic transport led to a 40% faster treatment time relative to systems without electrokinetic transport. In the continuous-flow experiments, Cr^{VI} was successfully transported against the simulated groundwater flow being pumped counter-current to electrokinetic transport, and influent Cr^{VI} concentrations were reduced by 50 percent due to reaction with nZVI within the soil. Furthermore, the presence of humic acid was found to be advantageous in these studies, improving Cr^{VI} reduction in the MFC system. This was a result of two phenomena: I) humic acid served as an extracellular redox mediator, shuttling electrons from the cell surface to terminal electron acceptors in solution, namely Cr^{VI} species and O_2, and II) complexation reactions between humic acid and soluble Cr^{III} species reduced the bioavailabilty of Cr^{III}, which has been shown to be toxic in high concentrations to *Shewanella spp.*

The integration of electrokinetic transport with nZVI again prevented the formation of destructive pH gradients. In the semi-batch experiments, fluid circulation between the MFC and electrokinetic maintained a near neutral pH for the duration of the study. In the continuous-flow system, the simulated groundwater solution pumped through the column had the same effect in preventing pH changes as the nZVI-electrokinetic dynamic experiments.

The final study presented in Chapter 6 evaluated Cr^{VI} reduction in simulated aquifer systems using a) bioactive columns with MR-1 biofilm growth in sand media simulating groundwater transport, and b) iron oxide-coated sand simulating a reactive barrier. Cr^{VI} reduction was achieved by a *Shewanella oneidensis* MR-1 biofilm in the sand media, and in the second study Cr^{VI} adsorption to IOCS was the primary removal mechanism. Model prediction studies were carried out to describe the reactor dynamics for Cr^{VI} removal under a variety of process conditions. The model was modified to include only biodegradation for the bioactive column with MR-1, and only adsorption for the column charged with IOCS. The experimental data were shown to accurately describe the dynamics of each system within a small margin of error. A sensitivity analysis revealed the bioactive column was dependent on primarily the Monod rate parameters, μ_{max} and K_s, the yield coefficient, Y_a, and the biomass density X. The IOCS system was highly sensitive to the Freundlich adsorption parameter K_F as well as the diffusivity coefficient, D_s, and the film transfer coefficient, k_f.

7.2 Conclusions

Electrokinetic transport offers the advantage of transporting ionic species through groundwater, however laboratory evaluations into its application to clay soils highlights the transport-inhibitive effects caused by pH gradient formation. Nonetheless, an evaluation of integrating technologies capable of rapidly reducing Cr^{VI} in sandy soils proved to be beneficial for electrokinetic transport as well as treatment. The application of nZVI can be optimized by transporting contaminants by electrokinetic phenomena to the point of nZVI injection. This reduces the amount of nZVI required for a remediation effort, and maximizes its efficiency. Similarly, using electrokinetic transport to concentrate Cr^{VI} before integration with an MFC has been shown in this study to increase power production, and reduce the treatment time required for this *ex situ* approach.

Natural organic matter, represented by humic acid in the experimental work, was found to be significant for both biological reduction, and for chemical reduction of Cr^{VI} by nZVI. Biological treatment systems were sustained for longer periods of time with humic acid present. Humic acid can enhance Cr^{VI} reduction by *Shewanella oneidensis* MR-1 by serving two primary functions: a) acting as an extracellular redox mediator, shuttling electrons to terminal electron accepts, and b) limiting the bioavailability of Cr^{III} to microorganisms, reducing the toxic effects of Cr^{III} complexation in cellular DNA.

In Cr^{VI} remediation systems using nZVI, humic acid was found to inhibit reduction due to electrostatic repulsive forces between Cr^{VI} and humic acids prompting the competition for reactive sites on the nZVI surface. Furthermore, humic acids will complex with nZVI corrosion by-products, namely Fe^{2+} species, which are also capable of driving Cr^{VI} reduction reactions. It was found that Cr^{VI} treatment was severely effected by high concentrations of dissolved oxygen in water. Dissolved oxygen caused rapid corrosion of nZVI in water, which reduced the amount of Fe^0 available for reaction with Cr^{VI} species.

The reduction and transport of Cr^{VI} in dynamic sand columns were shown to be accurately modeled Cr^{VI} transport through an aquifer in the presence of *Shewanella oneidensis* MR-1, as well as chemical adsorption processes in an IOCS reactive barrier. Cr^{VI} reduction by *Shewanella oneidensis* MR-1 biofilm growth in sand media was reflected well by the model, which was modified to consider the reduction of Cr^{VI} as a biodegradation-only process. Reduction of Cr^{VI} in the biological columns indicated that biodegradation in soils is a very slow process. Reduction of Cr^{VI} by IOCS was shown to be an economic method for heavy metal removal from drinking water as a permeable reactive barrier or in a granular media filter in water treatment applications. This process was accurately predicted by the model, which was tailored to represent a system limited to adsorption as the sole Cr^{VI} removal mechanism.

It is important to observe that all environmental systems are different due to the incredible variability observed in nature. The chemistry of groundwater is no exception, as it is dictated by local environmental conditions such as temperature, pH, precipitation, oxidation-reduction potential, the geochemistry of subsurface formations, and many more. Therefore when considering environmental remediation, a person must have an understanding of the dynamic phenomena occurring on a microscale dimension. There are no universal solutions to maintaining or restoring the environment, which is reflected by this dissertation. This work highlights emerging remediation technologies, significant environmental factors that affect their performance, and the application optimization of these technologies through integration. The world is facing many complex environmental problems, and just as is emphasized in this work, the solutions will not come in the form of a singular concept. Multi-disciplinary collaboration and a global view will lead the environmental revolution the world needs, and bridge the gaps in understanding and perspective between academia, industry, and politics to find real, sustainable solutions.

7.3 Recommendations

The studies presented here provided insight into fundamental processes involved in the areas of electrokinetic transport, and the use of nZVI or MFCs for Cr^{VI} remediation. Additionally, introducing humic acids into these systems and quantifying their effect on Cr^{VI} transport and treatment are highlighted in this research. These technologies are presently in their infancy, and future studies are anticipated to continually fill in the existing gaps of knowledge. Some specific recommendations for future work being considered are as follows.

Electrokinetic Transport

- The present state of groundwater contamination in the United States offers a wide variety in options for implementing pilot-scale studies. Environmental conditions at any contamination site will be different, necessitating lab-scale research investigations.
- Electrokinetic transport application to dynamic groundwater systems for specific applications such as contaminant containment should be investigated. While this technology can transport contaminants, it may also be used to keep plumes from spreading in flowing groundwater systems.
- Biological treatment can be very important for many groundwater remediation projects, which highlights the importance of investigating the effects of electrokinetic application on soil microorganisms.

Zero-Valent Iron Nanoparticles

- Many research groups are currently investigating means of stabilizing nZVI particles with stabilizer compounds to reduce their affinity to aggregate. This has been attempted with humic acid, however different size fractions of humic acid may yield very different results. Smaller humic acid fractions tend to be more hydrophilic in character, potentially enhancing the interactions and removal of ionic contaminants.
- Fabricating iron nanoparticles with a functionalized surface coating to target specific contaminants has the potential of making nanoparticle use in groundwater remediation applications more efficient and cost effective. This has been attempted to

some extent with bimetallic nanoparticles for oxidation of organic contaminants but needs to be investigated for heavy metal removal.

Microbial Fuel Cells

- Operating MFCs with a single bacteria species may not be practical, as small shifts in conditions can have adverse effects on MFC performance, and for scaling considerations the cost becomes much higher. Mixed cultures such as those found in wastewater treatment plants will be much less sensitive to reactor conditions and can utilize the organic matter found in wastewater as a substrate. Mixed culture MFCs will be a significant aspect in MFC scaling design.
- Biofilm optimization on the electrodes may also significantly enhance the performance of MFCs. Factors such as development time, carbon source, and flow conditions can be investigated to optimize an MFC system through biofilm development.
- One of the biggest uncertainties regarding the future of MFCs is system scale-up. State-of-the-are lab-scale MFC devices are destined to be inefficient if directly scaled up as they currently exist. Original designs to optimize electrode surface area and minimize activations and ohmic losses will be needed for MFCs to compete with other renewable energy sources, and groundwater treatment strategies. It is important to address the following before any scale-up design would be contemplated: i) reducing proton-exchange membrane fouling, ii) different electron donors and acceptors in conjunction with a specific species of bacteria or consortium thereof, iii) genome modifications to enhance the microbial electron transport chain, and iv) the choice of suitable electrode material, among others.

Bibliography

Acar, Y.B. and A.N. Alshawabkeh (1993). “Principles of Electrokinetic Remediation.” Environmental Science and Technology, 27(13): p. 2638.

Ahammed, M.M., and V. Meera (2010) Metal oxide/hydroxide-coated dual media filter for simultaneous removal of bacteria and heavy metals from natural waters. *Journal of Hazardous Materials,* 181:788-793.

Al-Hamdan, A. Z., & Reddy, K. R. (2006). Geochemical reconnaissance of heavy metals in kaolin after electrokinetic remediation. *Journal of environmental science and health. Part A, Toxic/hazardous substances & environmental engineering*, *41*(1), 17–33.

Al-Hamdan, A. Z., & Reddy, K. R. (2008). Transient behavior of heavy metals in soils during electrokinetic remediation. *Chemosphere*, *71*(5), 860–71.

Al-Hamdan, A.Z. (2002) Speciation, Distribution, and Mobility of Heavy Metals in Soils During Electrokinetic Remediation, *Ph.D. Thesis, 73-75.*

Alowitz, M.J., Scherer, M.M. (2002) Kinetics of nitrate, nitrite, and Cr(VI) reduction by iron metal. *Environ. Sci. Technol.* 36, 299-306.

Baalousha, M., Manciulea, A., Cumberland, S., Kendall, K., & Lead, J. R. (2008). “Aggregation and surface properties of iron oxide nanoparticles: influence of pH and natural organic matter.” *Environmental Toxicology and Chemistry*, *27*(9), 1875–1882. Wiley Online Library.

Bailey, R.P., T. Bennet, and M.M. Benjamin (1992), Sorption onto and Recovery of Cr(VI) using Iron oxide-Coated Sand, *Wat. Sci. Tech.,* 26(5-6):1239-1244.

Bartlett, R.J., and J.M. Kimble (1975) Behavior of Chromium in Soils: II. Hexavalent Forms, *Journal of Environmental Quality,* 5(4):383-386.

Belchik, S.M., Kennedy, D.W,, Dohnalkova, A.C., Wang, Y., Sevinc, P.C., Wu, H., Lin, Y., Lu, H.P., Fredrickson, J.K., and Shi, L. (2011). Extracellular reduction of hexavalent chromium by cytochromes MtrC and OmcA of Shewanella oneidensis MR-1. Applied and Environmental Microbiology, 77 (12), 4035-404 (June issue, 2001).

Beliaev, A., and Saffarini, D. (1998). Shewanella putrefaciens mtrB encodes an outer membrane protein required for Fe(III) and Mn(IV) reduction. Journal of Bacteriology, 180 (23), 6292-6297.

Beliaev, A.S., Saffarini, D.A., McLaughlin, J.L., and Hunnicut, D. (2001). MtrC, an outer membrane decahaem c cytochrome required for metal reduction in Shewanella putrefaciens MR-1. Molecular Mirobiology, 39 (3), 722-730.

Bencheikh-Latmani, R., A. Obraztsova, M. Mackey, M. Ellison, and B.M. Tebo (2007): Toxicity of Cr(III) to *Shewanella* sp. Strain MR-4 during Cr(VI) Reduction, *Environ. Sci. Technol.*, 41:214-220.

Benjamin M.M. and Bloom N.S. (1981) Effects of strong binding of anionic adsorbates on adsorption of trace metals on amorphous iron oxyhydroxide. In *Adsorption from aqueous solution* (Edited by Tewari P.), pp 41-60. Plenum Press, New York.

Benjamin, M.M., R.S. Sletton, R.P. Bailey, T. Bennet (1996), Sorption and filtration of metals using iron oxide-coated sand, *Water Resources*, 30(11)2609-2620.

Bhattacharyya, K. G., & Sen Gupta, S. (2006). Adsorption of Chromium(VI) from Water by Clays. *Industrial & Engineering Chemistry Research*, *45*(21), 7232–7240.

Blowes, D.W., W. Ptacek, C.J., and Jambor, L.J. (1997). In site remediation of Cr(VI)-contaminated groundwater using permeable reactive walls: Laboratory Studies. *Environ. Sci. and Technol.,* 31(12), 3348-3357.

Bond, D.R., Holmes, D.E., Tender, L.M., Lovley, D.R., 2002. Electrode- reducing microorganisms that harvest energy from marine sediments. Science 295 (5554), 483–485.

Bowers, A.R., C.A. Ortiz and R.J. Cardozo, Iron processes for treatment of Cr(VI) wastewater, Metal Finishing, 84, 37-41 (1986).

Brutinel, E.D., J. Gralnick (2012), Shuttling Happens: soluble flavin mediators of extracellular electron transfer in Shewanella. *Appl Microbiol Biotechnol. 93: 41-48.*

Buffle, J., Greter, F.L., Haerdi, W. "Measurement of complexation properties of humic and fulvic acids in natural waters with lead and copper ion-selective electrodes." *Anal. Chem.* **1977**, 49:216-222.

Cabaniss, Steve, Greg Madey, Patricia Maurice, Yingping Zhou, Laura Leff, Olacheesy head Bob Wetzel, Jerry Leenheer, and Bob Wershaw, comps, Stochastic Synthesis of Natural Organic Matter, part II: molecular property distributions. *Biogeochemistry,* 86(3): 269-286.

Cantrell, K.J., Kaplan, D.I., Wietsma, T.W. (1995). Zero-valent iron for the in-situ remediation of selected metals in groundwater. *J. Hazard. Mat.* 42, 201-212.

Cernik, M. (2010) Chemically supported in situ remedial technologies. VSCHT Praha.

Chang, M.K., Voice, T.C., and Criddle, C.S. (1993). Kinetics of competitive inhibition and cometabolism in the biodegradation of benzene, toluene, and p-xylene by two Pseudomonas isolates. Biotechnology and Bioengineering, 41 (11), 1057-1065 [May 1993 issue].

Chen, J. M., & Hao, O. J. (1998). Microbial Chromium (VI) Reduction. *Critical Reviews in Environmental Science and Technology*, *28*(3), 219–251.

Chen, J., Gu, B., Leboeuf, E. J., Pan, H., & Dai, S. (2008). Spectroscopic characterization of the structural and functional properties of natural organic matter fractions, *48*(2002), 59–68.

Chen, J., Z. Xiu, G.V. Lowry, and P.J.J. Alvarez (2010) Effect of natural organic matter on toxicity and reactivity of nanoscale zero-valent iron, *Water Research*, 45:1995-2001.

Cheng, S., H. Liu and B.E. Logan. (2006). Increased performance of single-chamber microbial fuel cells using an improved cathode structure. *Electrochem. Comm.* 8:489-494

Cheung, K.H., and Gu, J.D. (2007). Mechanism of hexavalent chromium detoxification by microorganisms and bioremediation application potential: A review. International Biodeterioration and Biodegradation, 59 (1), 8-15, (January 2007 issue).

Chowdhury, A.I.A., D.M. O'Carroll, Y. Xu, and B.E. Sleep (2012) Electrophoresis enhanced transport of nano-sclae valent iron, *Advances in Water Resources*, 40:71-82.

Christian, P., Von der Kammer, F., Baalousha, M., & Hofmann, T. (2008). Nanoparticles: structure, properties, preparation and behaviour in environmental media. *Ecotoxicology (London, England)*, *17*(5), 326–43.

Clarke RL, Kimmel S, Lageman R, Smedley SI. (1996). Electrokinetic remediation of soils, sludges, and groundwater. *Proceedings of the American Power Conference 1996,* April 9-11, Chicago, pp. 347-352.

Comber, S., M. Gardner (2003), Chromium redox speciation in natural waters, *Journal of Environmental Monitoring*, 5(3):410-413.

Cook, S. M. (2009). Assessing the Use and Application of Zero-Valent Iron Nanoparticle Technology for Remediation at Contaminated Sites. *Jackson State University*, (August). Retrieved from http://cluin.org/download/studentpapers/zero-valent-iron-cook.pdf

Davis, A. and R. Olsen (1995). "The geochemistry of chromium migration in the subsurface." *Ground Water*. 33(5): 759-767.
Davis, J.A. and Leckie J.O. (1978) Effect of adsorbed complexing ligands on trace metal uptake by hydrous oxides. *Environ. Sci. and Technol.* 12, 1309-1315.

Deng, B., & Stone, A. T. (1996). Surface-Catalyzed Chromium(VI) Reduction: Reactivity Comparisons of Different Organic Reductants and Different Oxide Surfaces. *Environmental Science & Technology*, *30*(8), 2484–2494.

Dries, J., L. Bastiaens, D. Springael, S. Kuypers, S.N. Agathos, and L. Diels (2005) Effect of humic acids on heavy metal removal by zero-valent iron in batch and continuous flow column systems, *Water Research,* 39:3531-3540.

Ecology, T., & April, R. (2005). Sorption of Cu and Pb to kaolinite – fulvic acid colloids□: Assessment of sorbent interactions. *Geochimica*, *69*(7), 1675–1686.

El-Naggar, M.Y., Y.A. Gorby, W. Xia, and K.H. Nealson. The molecular density of states in bacterial nanowires, *Biophysical Journal*, 95 (1), L10-L12, 2008.

El-Shazly, A.H., A.A. Mubarak, A.H. Konsowa, Hexavalent chromium reduction using a fixed bed of scrap bearing iron spheres, *Desalination*, Volume 185, Issues 1–3, 1 November 2005, Pages 307-316.

Eykholt GR, Daniel DE. (1994). "Impact of system chemistry on electro-osmosis in contaminated soil." *ASCE Journal of Geotechnical Engineering* **120**(5):797-815.

Fang, Z., Xiuqi Qiu, Ruixiong Huang, Xinhong Qiu, Mingyu Li, Removal of chromium in electroplating wastewater by nanoscale zero-valent metal with synergistic effect of reduction and immobilization, Desalination, Volume 280, Issues 1–3, 3 October 2011, Pages 224-231.

Fiúza, A., A. Silva, G. Carvalho, A.V. de la Fuente, C. Delerue-Matos, Heterogeneous kinetics of the reduction of chromium (VI) by elemental iron, Journal of Hazardous Materials, Volume 175, Issues 1–3, 15 March 2010, Pages 1042-1047.

Fredrickson, J.K., Romine. M. F., Beliaev, A.S., Auchtung, J.M., Driscoll ,M.E., Gardner, T.S., Nealson, K.H., Osterman, A.L. , Pinchuk, G., Reed, J. L., Rodionov, D.A., Rodrigues J. L.M., Saffarini, D.A., Serres, M.H., Spormann, A.M., Zhulin, I.B., and Tiedje, J.M. (2008). Towards environmental systems biology of Shewanella. Nature Reviews in Microbiology, 6 (8), 592-603.

Fukushima, M. A., Nakayasu, K., Tanaka, S., & Nakamura, H. (1997). Speciation analysis of chromium after reduction of chromium (VI) by humic acid. *Toxicological & Environmental Chemistry*, *62*(1), 207–215.

Furukawa, Y., J.-W. Kim, J. Watkins, R.T. Wilkin (2002) Formation of Ferrihydrite and Associated Iron Corrosion Products in Permeable Reactive Barriers of Zero-Valent Iron, *Environ. Sci. Technol.,* 36:5469-5475.

Gaspard, S., Vasquez, F., and Holliger, C. (1998). Localization and solubilization of the iron (III) reductase of Geobacter sulfurreducens. Applied and Environmental Microbiology, 64 (9), 3188-3194.

Gent, D. B., Bricka, R. M., Alshawabkeh, A. N., Larson, S. L., Fabian, G., & Granade, S. (2004). Bench- and field-scale evaluation of chromium and cadmium extraction by electrokinetics. *Journal of hazardous materials*, *110*(1-3), 53–62.

Gheju, M., & Balcu, I. (2010). "Hexavaelnt chromium reduction with scrap iron in continuous-flow system. Part 2: Effect of scrap iron shape and size." *Journal of Hazardous Materials,* 182, 484-493.

Giasuddin, A. B. M., Kanel, S. R., & Choi, H. (2007). Adsorption of humic acid onto nanoscale zerovalent iron and its effect on arsenic removal. *Environmental science & technology*, *41*(6), 2022–7.

Gil, G.C., I.S. Chang, B.H. Kim, M. Kim, J.K. Jang, H.S. Park, H.J. Kim, Operational parameters affecting the performance of a mediator-less microbial fuel cell. *Biosens. Bioelectron.* 18 (2003) 327–334.

Gorby, Y. A., Yanina, S., McLean, J. S., Rosso, K. M., Moyles, D., Dohnalkova, A., Beveridge, T. J., Chang, I. S., Kim, B. H. & other authors (2006). Electrically conductive bacterial nanowires produced by Shewanella oneidensis strain MR-1 and other microorganisms. *Proc Natl Acad Sci U S A* 103, 11358–11363.

Gordon, E., Pike, A., Hill, A., Cuthbertson, P., Chapman, S., and Reid, G. (2000). Identification and characterization of a novel cytochrome c3 from Shewanella frigidimarina that is involved in Fe(III) respiration. Biochemical Journal, 349 (2), 153-158.

Grim, RE. 1968. Clay minerology. New York: McGraw hill. 596 p.

Gu, B., & Chen, J. (2003). Enhanced microbial reduction of Cr(VI) and U(VI) by different natural organic matter fractions. *Geochimica et Cosmochimica Acta*, *67*(19), 3575–3582.

Gu, B., Schmitt, J., Chen, Z., Liang, L., & MaCarthy, J. F. (1994). Adsorption and desorption of natural organic matter on iron oxide mechanisms and models. Environ- mental Science & Technology, 28, 38–46.

Guha, H., Jayachandran, K., and Maurrasse, F. (2003). Microbiological reduction of chromium(VI) in presence of pyrolusite-coated sand by Shewanella alga simidu ATCC 55627 in laboratory column experiments. Chemosphere, 52, 175-183.

Guha, H., K. Jayachandran, F. Maurrasse (2001) Kinetics of chromium (VI) reduction by a type strain *Shewanella alga* under different growth conditions, *Environmental Pollution*, 115:209-218.

Hamid, R.Y., S.M. Carver, A.D. Christy, O.H. Tuovinen (2008) Cathodic limitations in microbial fuel cells: An overview. *Journal of Power Sources* 180:683-694.

Han, R., Geller, J.T., Yang, L., Brodie, E.L., Chakraborty, R., Larsen, J.T., and Beller, H.R. (2010). Physiological and transcriptional studies of Cr(VI) reduction under aerobic and denitrifying conditions by an aquifer-derived pseudomonad. Environmental Science and Technology, 44 (19), 7491-7497.

Hau, H.H., and Gralnick, J.A. (2007). Ecology and biotechnology of the genus *Shewanella*. Annual Review of Microbiology, 6, 237-258. [Review, October 2007].

He, F., Zhao, D., 2005. Preparation and characterization of a new class of starch-stabilized bimetallic nanoparticles for degradation of chlorinated hydrocarbons in water. Environ. Sci. Technol. 39, 3314–3320.

Heidelberg, JF, Paulsen IT, Nelson KE, Gaidos EJ, Nelson WC *(2002)* Genome sequence of the dissimilatory metal ion-reducing bacterium Shewanella oneidensis, *Nat Biotechnol.,* 20:1118-23.

Hizal, J., & Apak, R. (2006). Modeling of copper(II) and lead(II) adsorption on kaolinite-based clay minerals individually and in the presence of humic acid. *Journal of colloid and interface science*, *295*(1), 1–13.

Holtz, R.D. and Kovacs, W.D. (1981). *An Introduction to Geotechnical Engineering*, Prentice Hall. (Chapter 4).

Hsu, J.-C., C.-J. Lin, C.-H. Liao, and S.-T. Chen (2008) Removal of As(V) and As(III) by reclaimed iron oxide coated sands. *Journal of Hazardous Materials*, 153:817-826.

Hsu, L. (2011), Evaluation of Chromium Remediation in Groundwater: Investigations Using Microbial Fuel Cells and Electrokinetic Systems, *Dissertation Document*, Chapter 3, pp. 48-50.

Hsu, L., S. Masuda, K. Nealson, and M. Pirbazari (2012) Evaluation of microbial fuel cell *Shewanella* biocathodes for treatment of chromate contamination. *RSC Advances,* 2:5844-5855.

James, B. (1996). "The Challenge of Remediating Chromium-Contaminated Soil." Environmental Science and Technology **30**(6):248-251.

Jardine, P. M., Fendorf, S. E., Mayes, M. a., Larsen, I. L., Brooks, S. C., & Bailey, W. B. (1999). Fate and Transport of Hexavalent Chromium in Undisturbed Heterogeneous Soil. *Environmental Science & Technology*, *33*(17), 2939–2944.

Jones, E. H., Reynolds, D. A., Wood, A. L., & Thomas, D. G. (2009). Use of Electrophoresis for Transporting Nano-Iron in Porous Media. *Ground Water*, 1-12.

Joshi, A., and M. Chaudhuri (1996) Removal of Arsenic from Ground Water by Iron Oxide-Coated Sand, *Journal of Environmental Engineering*, 122(8):769-771.

Kamolpornwijit, W., L. Liang, OR West, GR Moline, and AB Sullivan. 2003. Preferential flow path development and its influence on long-term PRB performance: Column study. Journal of Contaminant Hydrology 66, (3-4): 161-78.

Kaya, A., & Yukselen, Y. (2005). Zeta potential of soils with surfactants and its relevance to electrokinetic remediation. *Journal of hazardous materials*, *120*(1-3), 119–26.

Keane, E. (2010). *Fate, Transport and Toxicity of Nanoscale Zero-Valent Iron (nZVI) Used During Superfund Remediation*. Duke University.

Khan, LI. (1991). “Study of Electroosmosis in Soil: A Modified Theory and Its Applications in Soil Decontamination. PhD Dissertation, Department of Civil and Environmental Engineering, Lehigh University, Bethleham, PA.

Kim, B.H., Kim, H.J., Hyun, M.S., Park, D.H., 1999. Direct electrode reaction of Fe(III)-reducing bacterium, Shewanella putrifaciens. Microbiol. Biotechnol. 9, 127–131.

Kim, S.-O., Kim, K.-W., & Stu□ben, D. (2002). Evaluation of Electrokinetic Removal of Heavy Metals from Tailing Soils. *Journal of Environmental Engineering*, *128*(8), 705.

Kim, S., Moon, S., & Kim, K. (2001). Removal of heavy metals from soils using enhanced electrokinetic soil processing. *Methods*, 259–272.

Kim, J.R., S.H. Jung, B.E. Logan, and J. Regan. (2007). Electricity generation and microbial community analysis of alcohol powered microbial fuel cells. *Bioresource Technol.* 98(13): 2568-2577.

Kotaś, J., & Stasicka, Z. (2000). Chromium occurrence in the environment and methods of its speciation. *Environmental pollution (Barking, Essex□: 1987)*, *107*(3), 263–83.

Kozuh, N., J. Stuper et al. (2000). "Reduction and Oxidation Processes of Chromium in Soils." Environmental Science and Technology **34**: 112-119.

Kyziol, J., Twardowska, I., & Schmitt-Kopplin, P. (2006). The role of humic substances in chromium sorption onto natural organic matter (peat). *Chemosphere*, *63*(11), 1974–82.

Lee, T., Lim H., Lee, Y., Park, J. (2003) Use of waste iron metal for removal of Cr(VI) from water. *Chemosphere* 53, 479-485.

Leita, L., A. Margon, A. Pastrello, I. Arcon, M. Contin, D. Mosetti (2009) Soil humic acids may favor the persistence of hexavalent chromium in soil. *Environmental Pollution* 157,1862-1866.

Li, X., Elliott, D. W., & Zhang, W. (2006). Zero-Valent Iron Nanoparticles for Abatement of Environmental Pollutants□: Materials and Engineering Aspects. *Critical Reviews in Solid State and Material Sciences, 31:* 111–122.

Li, Y., Yue, Q.-Y., & Gao, B.-Y. (2010). Effect of humic acid on the Cr(VI) adsorption onto Kaolin. *Applied Clay Science*, *48*(3), 481–484.

Lies DP, et al. (2005) *Shewanella oneidensis* MR-1 uses overlapping pathways for iron reduction at a distance and by direct contact under conditions relevant for biofilms. *Appl Environ Microbiol* **71**:4414–4426

Littlejohns, J.V., and Daugulis, A.J. (2008). Kinetics and interactions of BTEX compounds during degradation by a bacterial consortium. Process Biochemistry 43 (1), 1068-1076.

Liu, T., & Lo, I. M. C. (2010). Influences of Humic Acid on Cr(VI) Removal by Zero-Valent Iron From Groundwater with Various Constituents: Implication for Long-Term PRB Performance. *Water, Air, & Soil Pollution*, *216*(1-4), 473–483.

Liu, T., & Tsang, D. (2008). Chromium (VI) reduction kinetics by zero-valent iron in moderately hard water with humic acid: Iron dissolution and humic acid adsorption. *Environmental science & technology*, *42*(6), 2092-2098.

Lo, I.M.C., C.S.C. Lam, K.C.K. Lai (2005) Competitive effects of trichloroethylene on Cr(VI) removal by zero-valent iron, *Journal of Environmental Engineering,* 131:1598-1606.

Lo, I.M.C., C.S.C. Lam, K.C.K. Lai (2006) Hardness and carbonate effects on the reactivity of zero-valent iron for Cr(VI) removal, *Water Resources,* 40:595-605.

Logan, B.E. 2008. *Microbial Fuel Cells***.** John Wiley & Sons, New York.

Logan, B.E., S. Cheng, V. Watson, and G. Estadt. (2007). Graphite Fiber Brush Anodes for Increased Power Production in Air-Cathode Microbial Fuel Cells. *Environ. Sci. Technol.*, 41(9):3341-3346.

Lojou, E., Bianco, P., Bruschi, M. (1998). Kinetic studies on the electron transfer between bacterial c-type cytochromes and metal oxides. Journal of Electroanalytical Chemistry, 452 (2), 167-177.

Lovely, D., J. Coates, E. Blunt-Harris, E. Phillips, J. Woodward (1996) Humic substances as electron acceptors for microbial respiration. *Nature* 382:445-448.

Lovely, D.R., D.E. Holmes, K.P. Nevin (2004) Dissimilatory Fe(II) and Mn(IV) reduction. *Adv. Microb Physiol.* 49, 219-286.

Lumsdon, D.G., and Fraser, A.R. (2005). Infrared Spectroscopic Evidence Supporting Heterogeneous Site Binding Models for Humic Substances. *Environmental Science and Technology,* **39** (17), 6624-663.

MacDonell M.T., and Colwell, R.R. (1985). Phylogeny of the *Vibrionaceae*, and recommendation for two new genera, *Listonella and Shewanella*. Systematic and Applied Microbiology, 6 (2), 171–82.

Mak, M.S.H., P. Rao, and I.M.C. Lo (2010), Zero-valent iron and iron oxide coated sand as a combination for removal of co-present chromate and arsenate from groundwater with humic acid, *Environmental Pollution*, 159:377-382.

Mak, Mark S.H., Irene M.C. Lo, Influences of redox transformation, metal complexation and aggregation of fulvic acid and humic acid on Cr(VI) and As(V) removal by zero-valent iron, Chemosphere, Volume 84, Issue 2, June 2011, Pages 234-240.

Malvankar, N. S. *et al*. Tunable metallic-like conductivity in microbial nanowire networks. *Nature Nanotech.* 7 Aug 2011.

Marsili, E., Baron, D.B., Shikhare, I.D., Coursolle, D., Gralnick, J.A., and Bond D R. (2008). *Shewanella* secretes flavins that mediate extracellular electron transfer. PNAS (Proceedings of the National Academy of Sciences), 105 (10), 3968-3973.

Meyer, T.E., Tsapin, A.I., Vandenberghe, I., de Smet, L., Frishman, D., Nealson, K.H., Cusanovich, M.A., and van Beaeumen, J.J. (2004). Identification of 42 possible cytochrome c genes in the *Shewanella oneidensis* genome and characterization of six soluble cytochromes. Omics (A Journal of Integrative Biology), 8 (1), 57-77 (January 2004 issue).

Miller, C.T., and Weber, W.J., 1985. Sorption of Hydrophobic Organic Pollutants in Saturated Soil Systems. *Journal of Contaminant Hydrology* 1:243-261.

Mueller, N.C., J. Braun, J. Bruns, M. Cernik, P. Rissing, D. Rickerby, B. Nowak (2012) Application of nanoscale zero valent iron (NZVI) for groundwater remediation in Europe, *Environ Sci Pollut Res,* 19:550-558.

Myers, C.R., and Myers, J.M. (1993). Ferric reductase is associated with the membranes of anaerobically grown Shewanella putrefaciens MR-1. FEMS Microbiology Letters, 108 (1), 15-22.

Myers, C.R., and Myers, J.M. (1997). Outer membrane cytochromes of Shewanella putrefaciens MR-1: spectral analysis, and purification of the 83-kDa c-type cytochrome. *Biochimica et Biophysica Acta*, 1326 (2), 307-318.

Myers, C.R., and Myers, J.M. (1992). Localization of cytochromes to the outer membrane of anaerobically grown Shewanella putrefaciens MR-1. *Journal of Bacteriology,* 174 (11), 3429-3438

Myers, J.M., and Myers, C.R. (2000). Role of the tetraheme cytochrome CymA in anaerobic electron transport in cells of Shewanella putrefaciens MR-1 with normal levels of menaquinone. *Journal of Bacteriology*, 182 (1), 67-75.

Myers, J.M., and Myers, C.R. (2001). Role for outer membrane cytochromes OmcA and OmcB of Shewanella putrefaciens MR-1 in reduction of manganese dioxide. *Applied and Environmental Microbiology*, 67(1), 260-269.

Nealson D.L., and M.M. Cox, *Lehninger Principles of Biochemistry*, Worth Publishers, New York, NY, 2000.

Nealson, K., and Saffarini, D. (1994). Iron and manganese in anaerobic respiration: environmental significance, physiology, and regulation. Annual Review of Microbiology, 48, 311-343. (Review article of microbial metal reduction providing mechanisms and enzymics).

Nealson, K., and Scott J., 2006. The prokaryotes. Springer Science, New York.

Noubactep, C., & Schoner, A. (2010). "Metallic iron for environmental remediation: Learning from electrocoagulation." *Journal of Hazardous Materials,* 175, 1075-1080.

OEHHA.ca.gov., *Final Technical Support Document on Public Health Goal for Hexavalent Chromium in Drinking Water*, http://oehha.ca.gov/water/phg/072911Cr6PHG.html, Updated 7/29/11.

Ottosen LM, Christenson IV, Rorig-Dalgaard I, Jensen PE, Hansen HK. (2008). "Ulitization of electromigration in civil and environmental engineering. Processes, transport rates and matrix changes." *Journal of Environmental Science and Health Part A* **43**(8):795-809.

Ottosen LM, Pederson AJ, Ribiero AB, Hansen HK. (2005). "Case study on the strategy and application of enhancement solutions to improve remediation of soils contaminated with Cu, Pb, and Zn by means of electrodialysis." *Engineering Geology* **77**(3-4):317-329.

Page, M. M., & Page, C. L. (2002). Electroremediation of Contaminated Soils. *Journal of Environmental Engineering*, *128*(3), 208.

Palmer, C. D., & Puis, R. W. (1994). EPA Ground Water Issue: Natural Attenuation of Hexavalent Chromium in Groundwater and Soils. *Environmental Research.*

Pamukcu, S., A. Weeks, J.K. Whittle (2004). Enhanced Reduction of Cr(VI) by Direct Electric Current in a Contaminated Clay. *Environ. Sci. Technol.* 38:1236-1241.

Park, D.H. and Zeikus, J.G. (1999) Utilization of electrically reduced neutral red by *Actinobacillus succinogenes:* physiological function of neutral red in membrane driven fumurate reduction and energy conservation. *Journal of Bacteriology* 181, 2403-2410.

Park, D.H. and Zeikus, J.G. (2002) Impact of electrode composition on electricity generation in a single-compartment fuel cell using *Shewanella putrefaciens. Applied Microbiology and Biotechnology* 59, 58-61.

Park, D.H. and Zeikus, J.G. (2003) Improved fuel cell and electrode designs for producing electricity from microbial degradation. *Biotechnology and Bioengineering* 81, 348-355.

Paul A. Siracusa, P. Somasundaran, The role of mineral dissolution in the adsorption of dodecylbenzenesulfonate on kaolinite and alumina, Colloids and Surfaces, Volume 26, 1987, Pages 55-77.

Pennell, Abriola, and Weber, 1993. "Surfactant Enhanced Solubilization of Residual Dodecane in Soil Columns". *Env. Sci. and Technol.* 27:2332-2340**.**

Phenrat, T., & Saleh, N. (2007). Aggregation and Sedimentation of Aqueous Nanoscale Zerovalent Iron Dispersions. *Environmental Science & Technology*, *41*(1), 284–290.

Phenrat, T., Saleh, N., Sirk, K., Kim, H. J., Tilton, R. D., & Lowry, G. V. (2008). Stabilization of aqueous nanoscale zerovalent iron dispersions by anionic polyelectrolytes: adsorbed anionic polyelectrolyte layer properties and their effect on aggregation and sedimentation. *Journal of Nanoparticle Research*, *10*(5), 795–814. Springer.

Phillips, D. H., B. Gu, D. B. Watson, Y. Roh, L. Liang, and S. Y. Lee. (2000). Performance evaluation of a zerovalent iron reactive barrier: Mineralogical characteristics. Environmental Science & Technology 34, (19): 4169-76.

Ponder, S. M., Darab, J. G., & Mallouk, T. E. (2000). Remediation of Cr(VI) and Pb(II) aqueous solutions using supported, nanoscale zero-valent iron. *Environmental Science & Technology*, *34*(12), 2564–2569.

Ponder, S. M., Darab, J. G., Bucher, J., Caulder, D., Craig, I., Davis, L., Edelstein, N., et al. (2001). Surface Chemistry and Electrochemistry of Supported Zerovalent Iron Nanoparticles in the Remediation of Aqueous Metal Contaminants. *Electroanalytical Chemistry*, (250), 479–486.

Ponnamperuma, F.N. (1972). The Chemistry of Submerged Soils. *Advances in Agronomy,* 24:29-95.

Powell, R.M., Puls, R.W., Hightower, S.K., Sabatini, D.A. (1995). Coupled iron corrosion and chromate reduction: mechanisms for subsurface remediation. *Environ. Sci. Technol.* 29, 1913-1922.

Powers, S., Abriola, L., and Weber, W., 1994. An experimental investigation of nonaqueous phase liquid dissolution in saturated subsurface systems: Transient mass transfer rates. *Water Resources Research.* 30(2):321-332

Powers, S., Abriola, L., Dunkin, J., and Weber, W., 1994. Phenomenological models for transient NAPL-water mass-transfer processes. *Journal of Contaminant Hydrology.* 16:1-3

Probstein, R.F. and R.E. Hicks, *Removal of Contaminants from Soils by Electric Fields.* Science, 1993. 260(5107): p. 498-503.

Puls, R.W., and R.M. Powell (1997). Permeable Reactive Subsurface Barriers for the Interception and Remediation of Chlorinated Hydrocarbon and Chromium (VI) Plumes in Ground Water, 1–4. *U.S. EPA Remedial Technology Fact Sheet.*

Quinn, J., Geiger, C., Clausen, C., Brooks, K., Coon, C., O'Hara, S., Krug, T., et al. (2005). Field Demonstration of DNAPL Dehalogenation Using Emulsified Zero-Valent Iron. *Environmental Science & Technology*, *39*(5), 1309–1318.

Rabaey, K., Willy Verstraete, Microbial fuel cells: novel biotechnology for energy generation, *Trends in Biotechnology*, Volume 23, Issue 6, June 2005, Pages 291-298.

Rabaey, K., and Verstraete, W. (2005) Microbial fuel cells: novel biotechnology for energy generation. *Trends in Biotechnology* 23, 291-298.

Rai, D., Eary, L. E., & Zachara, J. M. (1989). Environmental chemistry of chromium. *Science of The Total Environment*, *86*(1-2), 15–23.

Reardon, E. (1995) Anaerobic corrosion of granular iron: Measurement and interpretation of hydrogen evolution rates, *Environ. Sci. and Technol.,* 29:2936-2945.

Reddy KR, Karri MR. (2007). Electrokinetic delivery of nanoscale iron particles for in-situ remediation of pentachloraophenol-contaminated soils. *Proceedings of International Symposium* *on Geo-Environmental Engineering for Sustainable Development.* Oct 22-24, 2007, Xuzhou, China, pp.74-79.

Reddy, K. (2003). Effects of initial form of chromium on electrokinetic remediation in clays. *Advances in Environmental Research*, *7*(2), 353–365.

Reddy, K. R., & Chinthamreddy, S. (2003). Sequentially Enhanced Electrokinetic Remediation of Heavy Metals in Low Buffering Clayey Soils. *Journal of Geotechnical and Geoenvironmental Engineering*, *129*(3), 263.

Reddy, K. R., Xu, C. Y., & Chinthamreddy, S. (2001). Assessment of electrokinetic removal of heavy metals from soils by sequential extraction analysis. *Journal of hazardous materials*, *84*(2-3), 279–96.

Reddy, K.R., and Cameselle, C., *Electrochemical Remediation Technologies for Polluted Soils, Sediments and Groundwater*, John Wiley & Sons, Inc., Hoboken, New Jersey, 2009.

Reeder RJ, Schoonen MAA. (2006) Metal Speciation and Its Role in Bioaccessibility and Bioavailability, *Reviews in Mineralogy and Geochemistry,* 64, 59-113.

Richard, F., Bourg, A. (1991). "Aqueous Geochemistry of Chromium: A Review" *Wat. Res.* **25**(7): 807-816.

Ribiero AB. (1994). Electrokinetic removal of heavy metals from a polluted soil. *Comett Course – Pollution Control and Removal of Pollutants (Nitrates, Nitrites, Heavy Metals) from surface and groundwaters.* March 21-23, Lisbon, Portugal: Instituto Superior Technico.

Ringeisen, B. R., Henderson, E., Wu, P. K., Pietron, J., Ray, R., Little, B., Biffinger, J. C., et al. (2006). High Power Density from a Miniature Microbial Fuel Cell Using Shewanella oneidensis DSP10. *Environmental Science & Technology*, *40*(8), 2629–2634.

Rismani-Yazdi, H., S.M. Carver, A.D. Christy, and O.H. Tuovinen (2008) Cathodic limitations in microbial fuel cells: An overview, *Journal of Power Sciences*, 180:683-694.

Romanenko, V.I. and V.N. Koren'kov, (1977). A Pure Culture of Bacterial Utilizing Chromates and Bichromates as Hydrogen Acceptors in Growth Under Anaerobic Conditions. *Mikrobiologiya*, 46(3):414-417.

Rozendal, R.A. , Hamelers, H.V.M., Euverink, G.J.W., Metz, S.J., and Buisman, C.J.N. (2006). Principle and perspectives of hydrogen production through biocatalyzed electrolysis. International Journal of Hydrogen Energy, 31 (12), 1632-1640.

Sukovich, D.J., Seffernick, J.L., Richman, J.E., Hunt, K.A., Gralnick, J.A., and Wackett, L.P. (2010). Structure, function and insights into the biosynthesis of a head-to-head hydrocarbon in *Shewanella oneidensis* strain MR-1. Applied and Environmental Microbiology, 76 (12), 3842-3849.

Sachs, S., G. Bernhard (2011) Humic acid model substances with pronounced redox functionality for the study of environmentally relevant interaction processes of metal ions in the presence of humic acid, *Geoderma,* 162(1-2):132-140.

Sawada, A., Mori, K., Tanaka, S., Fukushima, M., & Tatsumi, K. (2004). Removal of Cr(VI) from contaminated soil by electrokinetic remediation. *Waste management (New York, N.Y.)*, *24*(5), 483–90.

Scherer, M. M., Richte. S., Valentine, R. L., Alvarez, P.J., 2000. "Chemistry and microbiology of permeable reactive barrier for in situ groundwater clean up." *Crit. Rev. Environ. Sci. Technol.* 30, 363-411.

Schmitt, D., Taylor, H. E., Aiken, G. R., Roth, D. a, & Frimmel, F. H. (2002). Influence of natural organic matter on the adsorption of metal ions onto clay minerals. *Environmental science & technology*, *36*(13), 2932–8.

Sengall, B.A., CE O'Bannon, JA Matthias (1980) Electro-osmosis chemistry and water quality. *Journal of Geotechnical Engineering Division* 106:1148-1152.

Shang JQ, Lo KY, Inculet II. (1995). "Polarization and conduction of clay-water-electrolyte systems." *Journal of Geotechnical Engineering* **121**(3):243-248.

Shariatmadari, N., Weng, C., Daryaee, H., Engineering, C., & Iust, T. (2009). Enhancement of Hexavalent Chromium [Cr(VI)] Remediation from Clayey Soils by Electrokinetics Coupled with a Nano-Sized Zero-Valent Iron Barrier. *Environmental Engineering Science*, *26*(6).

Shi, Z., Nurmi, J. T., & Tratnyek, P. G. (2011). Effects of Nano Zero-Valent Iron on Oxidation-Reduction Potential. *Environmental science & technology*. ACS Publications.

Sposito G. (1989). *The Chemistry of Soils.* New York: Oxford University Press

Stams, A.J., F.A. de Bok, C.M. Plugge, M.H. van Eekert, J. Dolfing, G. Schraa (2006) Exocellular electron transfer in anaerobic microbial communities. *Envrion Microbiol.* 8:371-382.

Stepniewska, Z., K. Bucior, and M. De Boodt, 2000. Chromium and its forms in soils in the proximity of the old tannery waste lagoon. *Int. Agrophysics*, 15:121-124.

Stevenson F.J., *Humus Chemistry: Genesis, Composition, Reactions*. Wiley, New York (1982)

Straub, K.L., Schnik, B. (2004) Ferrihydrite-dependent growth of *Sulfurospirillum deleyianum* through electron transfer via sulfur cycling. Appl Environ Microbiol. 70:5744-5749.
Strycharz-Glaven, S. R. Snider, A. Guiseppi-Elie, L. Tender (2011) On the electrical conductivity of microbial nanowires and biofilms. *Energy Environ. Sci.,* 4:4366-4379.

Tebo, B.M, and Obraztsova, A.Y. (1998). Sulfate-reducing bacterium grows with Cr(VI), U(VI), Mn(IV), and Fe(III) as electron acceptors. FEMS Microbiology Letters, 162 (1), 193-198. (Federation of European Microbiological Societies).

Thormann, K.M., Saville, R.M., Shukla, S., Pelletier, D.A., and Spormann, A.A. (2004). Initial phases of biofilm formation in *Shewanella oneidensis* MR-1. Journal of Bacteriology, 186 (23), 8096-8104.

Thurman, E.M., 1985. "Organic Geochemistry of Natural Waters." Martnum Nijhoff/Dr. W. Junk. Publishers, Dordrecht.

Tipping, E. *Cation Binding by Humic Substances;* Cambridge University Press: Cambridge, 2002.

Tipping, E., 1981. "The adsorption of aquatic humic substances by iron oxides". *Geochim. Cosmochim. Acta* 45, 191-199.

Tony R. Lee, Richard T. Wilkin, Iron hydroxy carbonate formation in zerovalent iron permeable reactive barriers: Characterization and evaluation of phase stability, *Journal of Contaminant Hydrology*, Volume 116, Issues 1–4, 30 July 2010, Pages 47-57.

USGS Water Science School, USGS.gov. 29, Oct. 2010. *<http://ga.water.usgs.gov/edu/wugw.html>*

US EPA, *Cost Analysis for Selected Groundwater Cleanup Projects: Pump and Treat Systems and Permeable Reactive Barriers,* Solid Waste and Emergency Response, EPA 542-R-00-013.

Vega, A., Fiuza, A., & Guimarães, F. (2010). Insight into the Phenomenology of the Cr(VI) Reduction by Metallic Iron Using an Electron Probe Microanalyzer. *Langmuir*, *26*(14), 11980–11986.

Venkateswaran, K., Moser, D.P., Dollhopf, M.E., Lies D.P., Saffarini, D.A., MacGregor, B.J., Ringelberg, D.B., White, D.C., Nishijima, M., Sano, H., Burghart, J., Stackebrandt, E., and Nealson, K.H. (1999). Polyphasic taxonomy of the genus Shewanella and description of *Shewanella oneidensis sp. nov*. International Journal of Systemic Bacteriology, 49 (2), 705–24.

Viamajala, S., Peyton, B. M., & Petersen, J. N. (2003). Modeling chromate reduction in Shewanella oneidensis MR-1: development of a novel dual-enzyme kinetic model. *Biotechnology and bioengineering*, *83*(7), 790–7.

Virkutyt, J., Sillanpää, M., & Latostenmaa, P. (2002). Electrokinetic soil remediation--critical overview. *The Science of the total environment*, *289*(1-3), 97–121. Retrieved from

von Canstein, H., J. Ogawa, S. Shimizu, J.R. Lloyd (2008) Secretion of flavins by *Shewanella* species and their role in extracellular electron transfer. *Appl Environ Microbiol.* 74:615-623.

Waller, R. (2013). *Groundwater and the Rural Homeowner*, USGS.gov, http://pubs.usgs.gov/gip/gw_ruralhomeowner/.

Wang, C.-B., and W.X. Zhang (1997) Nanoscale metal particles for dechlorination of PCE and PCBs. *Environ. Sci and Technol.* 31(7), 2154-2156.

Wang, Q., Cissoko, N., Zhou, M., & Xu, X. (2011). Effects and mechanism of humic acid on chromium (VI) removal by zero-valent iron (Fe 0) nanoparticles. *Physics and Chemistry of the Earth, Parts A/B/C*, *36*(9), 442–446.

Wang, Q., Qian, H., Yang, Y., Zhang, Z., Naman, C., & Xu, X. (2010). Reduction of hexavalent chromium by carboxymethyl cellulose-stabilized zero-valent iron nanoparticles. *Journal of Contaminant Hydrology*, *114*(1-4), 35–42.

Weng CH, Takiyama LR, Huang CP. (1994). Electroosmosis for the in-situ treatment of chromium-contaminated soil. *Hazardous and Industrial Wastes* 26:496-505.

Wieczorek S, Weigand H, Schmid M, Marb C. (2005). Electrokinetic remediation of an electroplating site: Design and scale-up for an in-situ application in the unsaturated zone. *Engineering Geology*, 77:203-215.

Wilkin, R.T., Su, C., Ford, R.G. and Paul, C.J. (2005). Chromium-removal processes during groundwater remediation by a zero-valent iron permeable reactive barrier. *Environ. Sci. Technol.,* 39(12), 4599-4605.

Williams, D. (1978). Electrophoresis and zeta potential of kaolinite. *Journal of Colloid and Interface Science*, *1977.*

Wilson DJ, Rodriguez-Maroto JM, Gomez-Lahoz C. (1995a). Electrokinetic remediation. I. Modeling of Simple Systems. *Separation Science and Technology* 30(15):2937-2961.

Wittbrodt, P. R., & Palmer, C. D. (1995). Reduction of Cr(VI) in the Presence of Excess Soil Fulvic Acid. *Environmental science & technology*, *29*(1), 255–63.

World Health Organization, *Guidelines for drinking-water quality, 3rd edition incorporating 1st and 2nd addenda,* 2006.

X.C. Jiang, J.S. Hu, L.A. Fitzgerald, J.C. Biffinger, P. Xie, B.R. Ringeisen, and C.M. Lieber (2010) Probing electron transfer mechanisms in *Shewanella oneidensis* MR-1 using a nanoelectrode platform and single cell imaging, *Proc. Natl. Acad. Sci. U.S.A.,* 107:16806-16810.

Xu, D., Zhu, S., Chen, H., and Li, F. (2006). Structural Characterization of Humic Acids Isolated from Typical Soils in China and their Adsorption Characteristics to Phenanthrene. *Colloids and Surfaces, Part A: Physicochemical and Engineering Aspects,* **276**, 1–7.

Xu, Y.H., Zhao, D.Y., 2007. Reductive immobilization of chromate in water and soil using stabilized iron nanoparticles. Water Res. 41, 2101–2108.

Y.A. Gorby, S. Yanina, J.S. McLean, K.M. Rosso, D. Moyles, A. Dohnalkova, T.J. Beveridge, I.S. Chang, B.H. Kim, K.S. Kim, D.E. Culley, S.B. Reed, M.F. Romine, D.A. Saffarini, E.A. Hill, L. Shi, D.A. Elias, D.W. Kennedy, G. Pinchuk, K. Watanabe, S.i. Ishii, B. Logan, K.H. Nealson, J.K. Fredrickson, Electrically conductive bacterial nanowires produced by Shewanella oneidensis strain MR-1 and other microorganisms, Proc. Natl. Acad. Sci. U. S. A. 103 (2006) 11358–11363.

Yamazaki, H., S. Gohda et al. (1980) "Chemical Forms of Chromium in Natural Water - Interaction of Chromium(III) and Humic Substances in Water." Journal of Oceanographical Society of Japan **35**:233-240.

Yang, G. C. C., Tu, H.-chuan, & Hung, C.-hsiung. (2007). Stability of nanoiron slurries and their transport in the subsurface environment. *Test*, *58*, 166-172.

Yeung AT. (1994). Electrokinetic flow processes in porous media and their applications. *Advances in Porous Media,* Vol. 2 (ed. MY Corapcioglu). Amsterdam, the Netherlands: Elsevier, pp. 309-395.

Yukselen, Y. and Kaya, A. (2003). Zeta potential of kaolinite in the presence of alkali, alkaline earth and hydrolyzable metal ions. *Water, Air, & Soil Pollution*, 155-168.

Zachara, J.M., C.E. Cowan *et al.* (1988). "Chromate adsorption by kaolinite." *Clay and Clay Minerals.* 36(4): 317-326.

Zhang, W. (2003). Nanoscale iron particles for environmental remediation: An overview. *Journal of nanoparticle Research*, *5*(3), 323–332.